ABSTRACT

Title of Document:	MOLYBDENUM ISOTOPE SYSTEMATICS IN NATURAL AND EXPERIMENTAL SETTINGS
	Kathleen Dwyer Scheiderich, Ph.D. 2010
Directed By:	Professor Richard J. Walker, Department of Geology

Molybdenum isotopes have a broad potential applicability for paleoenvironmental analysis, particularly with respect to questions of eutrophication history, development of anoxia, and sedimentation under conditions of varying oxygenation. Using a double-spike method, the Mo isotope proxy was applied to sediments and water samples from the Chesapeake Bay, where the severity of seasonal anoxic episodes has been increasing over the last century. It was discovered that isotopic fractionation is occurring in the estuary, as indicated by the large differences between the δ^{98}Mo of Mo dissolved in the water and authigenic Mo in the sediments. Increased variability of δ^{98}Mo values and increased authigenic Mo deposition were likely related to the onset of coastal anoxic episodes in the Bay. Sediment samples from the Eastern Mediterranean were also analyzed for δ^{98}Mo, along with redox-sensitive element concentrations (Re, Mo, V, Ba, and

Fe). Over the past 5 million years, climatic shifts have driven cyclic oceanographic changes in the Mediterranean, specifically basin-wide anoxic episodes, which are visible in the sedimentary sequence as layers that are highly enriched in redox-sensitive elements and organic matter (sapropels). I investigated whether δ^{98}Mo values, in conjunction with other proxies, could be used to infer the degree to which the deep basin was affected by anoxic conditions, and how this may have changed between individual anoxic episodes. There were clear temporal differences in the apparent severity of anoxia in the Mediterranean, as reflected by the proxies in the sapropels. The amount of Mo in Mediterranean seawater did not change during sapropel deposition, and therefore, the basin likely remained open to circulation. I collaborated in a project to determine whether Mo isotopes could be fractionated at high temperature and pressure in an experimental system, designed to mimic natural hydrothermal-type porphyry systems. It was found that Mo isotopes are fractionated between a melt and vapor phase under the experimental conditions, and in a manner consistent with equilibrium exchange processes. Molybdenum entering the melt phase undergoes a coordination change to higher coordination number, thus preferentially enriching the vapor phase in the heavier Mo isotopes.

MOLYBDENUM ISOTOPE SYSTEMATICS IN NATURAL AND EXPERIMENTAL SETTINGS

By

Kathleen D. Scheiderich

Dissertation submitted to the Faculty of the Graduate School of the
University of Maryland, College Park, in partial fulfillment
of the requirements for the degree of
Doctor of Philosophy
2010

Advisory Committee:
Professor Richard J. Walker, Chair
Professor Emeritus George R. Helz
Associate Professor James Farquhar
Associate Professor Michael Evans
Dean's Representative Professor Russell Dickerson

Dedication

For Mom and Dad and Hobbes.

Acknowledgements

I would not have been able to finish the project without the assistance of Aaron Pietruszka and Jasper Konter, who collaborated in developing the double spike. Many thanks to the Maryland Department of Natural Resources for water samples, the Maryland Geological Survey and Elizabeth Canuel (VIMS) for sediment samples for the Chesapeake Bay project. The Ocean Drilling Program is gratefully acknowledged for providing the samples for the Mediterranean project. I thank Michael Mengason, who entertained a crazy idea and set up the experiments that are described in Chapter 5. Aubrey Zerkle taught me about sulfur isotopes, and also got me involved with analyzing Mo isotopes in nitrogen-fixing organisms. Richard Ash and Bill McDonough have always been ready to help with analytical questions and have been great about all aspects of the struggle with the Nu. Jen Obernier provided me with timely life advice and general lifting of spirits. Rich and George have been excellent mentors, and I hope to live up to their high standards.

Table of Contents

List of Tables

List of Figures

Chapter 1: Molybdenum: An Introduction

The Basics

Molybdenum is a highly refractory, moderately siderophile, group VIB transition metal with seven stable isotopes (Fig. 1.1, Table 1.1). These seven isotopes are produced by various nucleosynthetic processes (p, r, and s, Table 1.1). In common with many transition metals, Mo can occur in a variety of oxidation states (2+, 3+, 4+, 5+, 6+). The electron configuration is $[Kr]4d^5 5s^1$: five unpaired electrons, one in each of the five 4d orbitals, and one unpaired electron in the 5s orbital. This electron configuration permits the wide range of possible oxidation states. In terrestrial systems, (IV), and (VI) are most common.

Common compounds (Fig. 1.2) of Mo include $Mo(VI)O_3$ (molybdenum trioxide, trigonal planar co-ordination), $Mo(VI)O_4^{2-}$ (aqueous tetrahedrally co-coordinated molybdate), and $Mo(VI)S_4^{2-}$ (aqueous tetrahedral thiomolybdate). The principal ore of Mo is molybdenite, $Mo(IV)S_2$, a hexagonal, heavy mineral with perfect cleavage (Fig. 1.3). It is found in high-temperature hydrothermal veins and in porphyry-type deposits, disseminated in quartz veins (e.g., Climax, Colorado and Butte, Montana). Molybdenum is an important element in low-temperature systems. Molybdenum-containing enzymes are found in all aerobic organisms (Hille, 2002), where they catalyze a variety of reactions (e.g., aldehyde oxidation, sulfite oxidation, nitrate reduction, and dimethyl sulfoxide reduction; Frausto da Silva and Williams, 2001; Mendel and Bittner, 2006). Some organisms (diazotrophs) have the capability to reduce N_2 to

ammonia; one of the enzymes that is necessary for this process is an Fe-Mo protein (dinitrogenase), which contains the site of N_2 binding (Georgiadis et al., 1992). Except for dinitrogenase (Rajagopalan and Johnson, 1992), all the known molybdoenzymes contain a cofactor (molybdopterin), whose biosynthetic pathway is universally conserved, implying that the pathway must have appeared early in the history of life (Mendel and Schwarz, 1999).

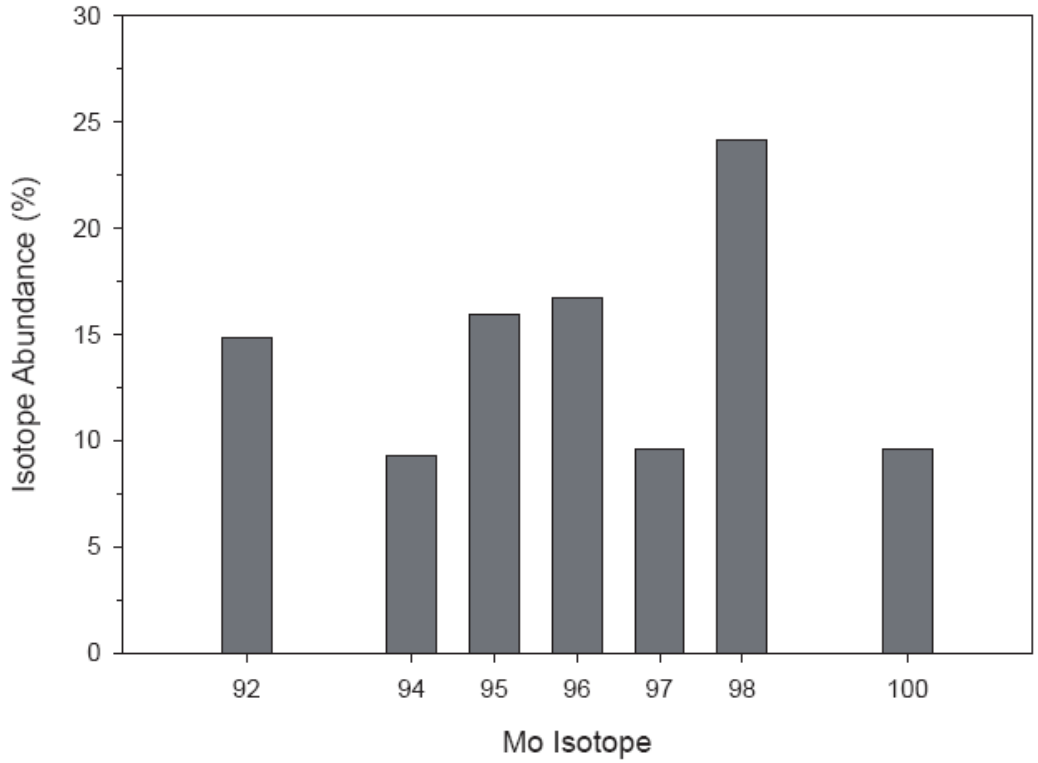

Figure 1.1: Relative abundances of stable molybdenum isotopes.

Table 1.1: Terrestrial Mo isotope composition

Mo Isotope	Nuclidic mass[a]	Mole fraction[a]	Process[b]
92	91.905810(4)	0.148362(148)	p
94	93.9050867(20)	0.092466(92)	p
95	94.9058406(20)	0.159201(159)	s,r
96	95.9046780(20)	0.166756(167)	s
97	96.9050201(20)	0.095551(96)	s,r
98	97.9054069(20)	0.241329(241)	s,r
100	99.907467(6)	0.096335(96)	r

[a]Coplen et al., 2002. (IUPAC Technical Report, and references therein).
[b] Wieser and De Laeter, 2007.

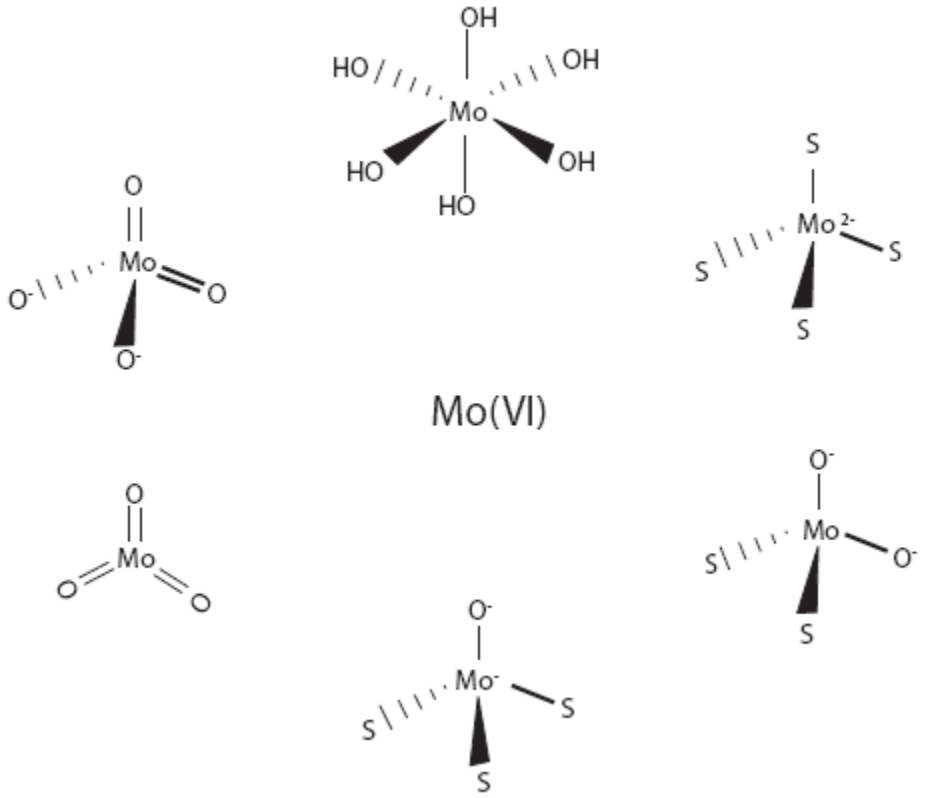

Figure 1.2: Molecular forms of Mo(VI). Clockwise from top middle: octahedral molybdenum hexahydroxide, tetrahedral thiomolybdate, tetrahedral oxythiomolybdate, tetrahedral oxy-trithiomolybdate, trigonal molybdenum trioxide, tetrahedral molybdate.

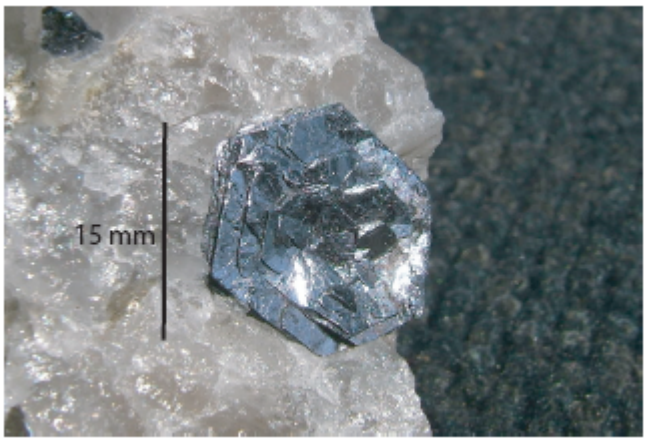

Figure 1.3: Euhedral hexagonal molybdenite in quartz, Molly Hill Mine, Quebec, Canada. 2008, John Chapman (Gnu Free Documentation license).

Molybdenum geochemistry in water and sediments

The Mo concentration in ocean waters is relatively constant with salinity (conservative, 10.5 µg/L; e.g., Bruland, 1983; Collier, 1985). This concentration and the conservative nature of Mo are unusual for a biologically essential trace element (Tribovillard et al., 2006). The residence time, (τ), 800,000 y, of Mo in seawater is also unusually long for a trace element (Morford and Emerson, 1999). The long residence time of Mo suggests that its highly soluble aqueous anion, molybdate, ($Mo(VI)O_4^{2-}$) is relatively unreactive in seawater. The main source of dissolved Mo to the oceans is continental weathering products delivered through rivers, so the Mo concentration of the input probably varies depending on the material being weathered at any one time (e.g., Bertine and Turekian, 1973). For example, where streams drain the area around the Climax molybdenite deposit (Colorado), Mo concentrations in stream water are very high (10 mg/L; Kaback and Runnells, 1980). In contrast, the Ottawa River, which flows through granitic bedrock, has a very low Mo concentration (~0.2 µg/L; Archer and Vance, 2008). Molybdenum concentrations in rivers draining regions with black shales tend to be relatively high (2.3-10 µg/L; Colodner et al., 1993).

The paucity of processes that can remove Mo from seawater are reflected in its generally long residence time in the ocean. In oxygenated seawater, at marine pH, Mo is not adsorbed by many of the most common constituents of oceanic sediments, such as clay particles, $CaCO_3$, or Fe-oxyhydroxides (Goldberg et al., 1998). The typical Mo concentration range of these types of sediments is only 0.05-2 µg/g, similar to the concentrations in

average shale and average continental crust (Taylor and McLennan, 1985; Rudnick and Gao, 2003). The major exceptions to limited removal are hydrogenous Mn-oxyhydroxides, which form as nodules or crusts in oxic, hemipelagic sediments, and have a high affinity for Mo (e.g., Calvert and Price, 1977; Shimmield and Price, 1986). These types of sediments accumulate at rates between a few mm per million years to hundreds of mm per million years. Molybdenum concentrations in nodules range between 0.03 to 0.05 wt. % (Cronan, 1976). The nature of this sink, however, leads to an important question regarding the mass balance of Mo in the oceans. Although up to 90% of the ocean floor is oxic by some estimates, with manganese deposits covering as much as 50% of some ocean basins (Glasby, 2000), the flux of Mo to oxic sediments is estimated to be between only 20% (Morford and Emerson, 1999) to 75% (Arnold et al., 2004) relative to river influx. Consequently, the general steady-state with respect to Mo inputs and removals likely requires an additional important sink. That sink is most likely sediments formed under anoxic conditions. Indeed, anoxic sedimentary regimes appear to sequester a quantity of the dissolved Mo influx that is disproportionate to their extent in the oceans (only about 0.3% of the ocean floor, Helly and Levin, 2004). Algeo (2004) calculated that in the Devonian, the greater extent of anoxia in the oceans, coupled with a greater burial flux accompanying formation of black shales could have drawn down the Mo concentration of seawater and lowered its residence time to ~470,000 y. Estimates for the removal of Mo to anoxic sediments range from 10-40% of

dissolved Mo in the oceans (Bertine and Turekian, 1973; Emerson and Huested, 1991; Morford and Emerson, 1999). Any additional imbalance (10-20%) might be accounted for by sedimentation in aqueous regimes that are O_2 depleted but not strictly anoxic (e.g., under oxygen minimum zones, such as may be found under regions with strong coastal upwelling), so-called 'suboxic' sediments.

The putative disproportionate removal of Mo to anoxic sediments leads to the importance of the geochemical behavior of Mo during anoxic sediment deposition. As noted above, Mo in *oxygenated* seawater exists as a fully soluble anion. The corollary is that in anoxic water there is a change in the solubility, and perhaps ionic state, of Mo, that this is reflected in an increased concentration of Mo in sediments that underlie such waters. Under anoxic conditions, Mo may be more susceptible to scavenging by organic matter (Helz et al., 1996; Zheng et al., 2000; Adelson et al., 2001; Nameroff et al., 2002), or more readily incorporated into pyrite, although for that step it must be reduced to Mo(IV) by sulfide (Huerta-Diaz and Morse, 1992; Morse and Luther, 1999; Bostick et al., 2003). Scavenging of Mo by any of these mechanisms likely does not take place within the water column, but in pore waters that underlie O_2-depleted water (Crusius et al., 1996; Zheng et al., 2000).

Anoxia, however, may not be entirely sufficient at inducing a change in Mo solubility. For example, low O_2 conditions (<5 μmol/L) in a modern oxygen minimum zone was observed to have no effect on dissolved Mo

concentrations (Nameroff et al., 2002). In order for Mo to become particle-reactive, the presence of sulfide appears to be necessary, possibly as a direct reactant in the formation of thiomolybdates, or Fe-Mo-S clusters that can be easily scavenged (Helz et al., 1996; Erickson and Helz, 2000; Vorlicek et al., 2004). Within the water column of the Black Sea, the concentration profile of dissolved Mo with depth is approximately the opposite of the H_2S profile (e.g., Emerson and Huested, 1991; etc), suggesting that removal is taking place within the water column. However, in euxinic water columns, it has been argued that there is no systematic relationship between sedimentary Mo and H_2S (e.g., Algeo and Lyons, 2006). In well-studied, seasonally anoxic, semi-enclosed settings such as the Cariaco Basin, Saanich Inlet, and Framvaren Fjord, profiles of the concentration of dissolved Mo show a tendency for Mo concentration to decrease with depth (possibly at the interface between O_2 and H_2S), and the sediments that form to become enriched in Mo (Emerson and Huested, 1991; Algeo and Lyons, 2006). This counter intuitively implies that scavenging within the water-column does not take place, rather Mo removal occurs at the sediment-water interface or in the sediments (Emerson and Huested, 1991). Measurements of sulfide and Mo in pore waters suggest that a sulfide threshold must be reached before Mo is removed (Colodner et., 1993; Zheng et al., 2000), although behavior of Mo in pore water is complicated by the cycling of MnO_x at the redox boundary in the sediments (Shimmield and Price, 1986; Calvert and Pedersen, 1993; Crusius et al., 1996). The process of MnO_x cycling has been shown re-deliver Mo to pore

waters below the redox boundary (e.g., Crusius et al., 1996; McManus et al., 2002; Morford et al., 2005), at which point it can be fixed in a solid (sulfide) phase (e.g., Calvert and Pedersen, 1993; Morford et al., 2009). Tribovillard et al. (2004) emphasized the importance of sulfurized organic matter in trapping Mo in the sediments. The concentration of aqueous H_2S has been shown to exert a control on the stepwise conversion of $Mo(VI)O_4^{2-}$ through a series of thiomolybdate intermediates with the formula $MoO_xS_{4-x}^{2-}$, beginning at a geochemical switch point of 11 μM (Erickson and Helz, 2000). It is these intermediates, and the final substituted thiomolybdate ($Mo(VI)S_4^{2-}$), thought to be the particle-reactive species, that are scavenged (Helz et al., 1996). Within the sediments, these stepwise reactions probably proceed through 6-coordinate, rather than 4-coordinate intermediates, and may be catalyzed by clay mineral surfaces (Vorlicek and Helz, 2002). The thiomolybdates are likely to be scavenged by pyrite (Bostick et al., 2003; Vorlicek et al., 2004), organic carbon, and particularly, sulfurized organic matter (Tribovillard et al., 2004). Furthermore, the trithio- and tetrathio-molybdate reactions may be kinetically irreversible on short time scales, which has been shown by the survival of MoS_4^{2-} for long periods in oxygenated water (Erickson and Helz, 2000). However, acidifying such a solution would serve to increase the rate of conversion from MoS_4^{2-} to MoO_4^{2-} (Erickson and Helz, 2000).

The relationship between Mo content and organic carbon (C_{org} or TOC) is also somewhat contentious. Because of the positive correlation between the two parameters in anoxic settings (Brumsack, 1986; Nijenhuis et al.,

1999; Warning and Brumsack, 2000; Werne et al., 2002; Algeo, 2004), Mo concentration has been used as a redox proxy. However, Tribovillard et al. (2004) showed high degrees of correlation only between Mo/Al and one particular subtype of organic matter, specifically sulfurized (orange) organic matter. In contrast, Wilde et al. (2004) argued that Mo/Al could be used as a proxy for original TOC content, based on the high degree of correlation. Lyons et al. (2003) found only a weak correlation between C_{org} and Mo/Al in Cariaco Basin sediments that were deposited under euxinic conditions. Algeo and Lyons (2006) proposed that the uptake of Mo at the sediment-water interface is dominated by organic 'host phases', and that this explains the Mo-TOC covariation in anoxic environments. However, there are limits to Mo and TOC enrichment, which include the Mo drawdown, deepwater renewal time, and amount of stagnation (Algeo and Lyons, 2006). As an example, if an anoxic setting did not receive a periodic renewal of oxygen and dissolved Mo, its degree of stagnation would increase, and the drawdown of Mo to the sediments would eventually lead to a long-term trend towards lower Mo/TOC ratios. Thus, Mo/TOC has been proposed to be a better proxy for degree of water mass restriction, as opposed to Mo alone being a straightforward proxy for redox state in the water column (Algeo and Lyons, 2006; Algeo et al., 2007; Scott et al., 2008).

Covariation of Mo with pyrite has also been a subject of debate. On one hand, there is some evidence that Mo is positively correlated with the pyrite content of host sediment (Huerta-Diaz and Morse, 1992; Crusius et al.,

1996; Tribovillard et al., 2008). Further, a modicum of data suggest that Mo readily enters Fe-S phases (Bostick et al., 2003), and a second study suggests that pyrite framboids may sequester Mo from overlying oxic water, during formation in shallow 'suboxic' sediments (Tribovillard et al., 2008). Other studies, however, have presented opposing evidence, e.g., for a lack of correlation between pyrite and Mo (Lyons et al., 2003). A key point with respect to correlations between Mo and pyrite may be the C_{org} concentration of the sediments, as this parameter appears to control the capacity for H_2S generation (Lyons et al., 2003). Microbially-mediated degradation of accumulated organic matter generates sulfide (from sulfate reduction), which reacts with Fe^{2+} to form pyrite (e.g., Passier et al., 1996). This has led to proposals that pyrite formation may be controlled by the availability of reactive Fe phases (FeO_x), rather than organic carbon (Raiswell and Canfield, 1998). As mentioned above, sulfurized organic matter strongly correlates with Mo content. However, sulfurized organic matter can only form when H_2S begins to accumulate, because H_2S formation has outstripped the supply of reactive Fe (Tribovillard et al., 2004). This, in turn, can only occur after FeO_x has been consumed (Raiswell and Canfield, 1998). Thus, pyrite formation appears to occur before organic matter is sulfurized (Tribovillard et al., 2004, and references therein).

Summary

The geochemistry of Mo in sediments appears to be controlled by the dichotomous behavior in aqueous environments: soluble under oxic

conditions, but becoming increasingly labile as the water column looses oxygen. Thus, Mo has potential for use as a proxy for organic carbon, for water column anoxia, and in conjunction with other parameters, for degree of water-mass restriction. However, full realization of the potential strengths of Mo as a proxy has been somewhat constrained by incomplete understanding of the mechanisms by which Mo is sequestered into sediments, the exact form in which it exists in the sediments, and in what sedimentary component it resides (e.g., pyrite versus sulfurized organic matter). These and similar topics continue to foster discussion and new research. In recent years, the use of Mo isotopes has been added to the tools for addressing these topics.

Molybdenum isotopes

Measurement of Mo isotopes in meteorites is fairly common (Murthy 1962, 1963; Wetherill, 1964; Qi-Lu and Masuda, 1992; Lee and Halliday, 2003; Nicolussi et al., 1998; Yin and Jacobsen, 1998; Dauphas et al., 2004). However, the goal of these studies was to identify mass-independent (nucleosynthetic) isotopic anomalies, as well as evidence for Tc decay in ^{97}Mo. The internal normalization used to correct for instrumental fractionation in such studies precludes measurement of natural, mass-dependent differences. Additionally, Mo isotopes have also been used to study Mo metabolism in the body (e.g., Turnlund et al., 1993; Turnlund et al., 1995; Sievers et al., 2001; Keyes and Turnlund, 2002). The first of these (Turnlund et al., 1993) utilized chromatographic separation (nearly identical to that

currently in use by geologists), combined with a triple-spike method and analysis by TIMS.

The geochemistry of Mo, and specifically its sensitivity to environmental reducing conditions, result in its utility as a proxy for the general redox state of a water column. In the search to refine redox interpretations of ancient sediments, Anbar et al. (2001), performed experiments of chromatographic separation of Mo and MC-ICP-MS (Multi-collector inductively -coupled plasma mass spectrometry) measurement of Mo isotopes using external fractionation correction. This was done in the hope that mass dependent variations might: 1) be found, and 2) be related to environmental conditions during deposition. A short time later, a different research group published a double-spike method for internal fractionation corrected Mo isotope analysis by MC-ICP-MS (Siebert et al., 2001). Both groups tested their respective methods on molybdenites (MoS_2; porphyry versus hydrothermal), and obtained positive results, in the sense that isotopic fractionation was observed (±0.3‰ in $\delta^{98}Mo$[1]). The two methods, however, differed in the external standard reproducibility associated with the measurements. The external fractionation correction method had a published 2σ of ±0.2‰ for standards, while the double-spike method was able to produce standard data with 2σ ±0.06‰, a significant improvement.

[1]Generally, in the remainder of this work, all Mo isotopic compositions will be reported as $\delta^{98}Mo$. This is done to introduce consistency in the nomenclature, as some working groups use different isotopes in the ratio. Conversion between $^{97}Mo/^{95}Mo$ and $^{98}Mo/^{95}Mo$ is achieved by dividing by 2/3, thus, no attempt will be made to identify where the original published data were reported using a different notation.

As an important side note, comparison of Mo isotope data from different labs suffers from the lack of a true recognized isotopic standard. The majority of researchers use SpecPure® Mo, or a similar material, as a normalizing standard, and define the isotopic composition of this material to be 0‰. It is not known how individual batches of this Mo solution might vary isotopically. Thus, data normalized using one batch would be internally consistent, but might not be consistent with data normalized using a different batch.

Once it was established that mass-dependent variations exist in a geological materials, and could be adequately resolved for some purposes, the next step was to determine the isotopic composition of Mo reservoirs and sinks (Fig. 1.4). In order to be able to make any interpretive statement about ancient sediments, the modern system needed to be quantified. Barling et al. (2001) showed that there was a large fractionation between the seawater molybdate reservoir (δ^{98}Mo=+2.3‰) and Mn oxyhydroxide (MnO_x) nodules (δ^{98}Mo average -0.8‰), which were noted in the preceding section to be a quantitatively important Mo sink on long time scales. The isotopically heavy nature of seawater was demonstrated to extend to three major oceans, and be constant with depth (Siebert et al., 2003). Siebert et al. (2003) confirmed removal of isotopically light Mo to MnO_x in two nodules, and the constant offset from seawater over a 60 Ma 'transect' in the nodules was taken as evidence that the δ^{98}Mo of seawater had not changed significantly in that time period. Samples of basalt, granite, and clastic sediment were measured and

found to have δ^{98}Mo values ranging from 0‰ to 0.3‰, suggesting that the net effect of transport and weathering processes does not affect δ^{98}Mo (Siebert et al., 2003).

Euxinic Black Sea sediments were shown to have δ^{98}Mo from +1.6 to +2.4, from which it was inferred that a highly efficient removal process from overlying sulfidic water acted on this system (Barling et al., 2001). Anoxic sediments were shown to display a fairly constant offset from seawater by -0.7‰ (McManus et al., 2002; Poulson et al., 2006). These observations have been frequently applied to the idea that the extent of anoxic/euxinic sedimentation in the past can be calculated if the isotopic compositions of the Mo input and oxic Mo sink are known (Arnold et al., 2004; Siebert et al., 2005; Wille et al., 2007; Pearce et al., 2008; Wille et al., 2008; Lehmann et al., 2007). Estimates of anoxic sedimentation made in this way have been used to assess the oxygenation state of the ancient ocean/atmosphere. However, as the Mo isotope data set has broadened, this type of calculation has been shown to be too simplistic to well describe natural systems. There are several important complications inherent to this type of modeling. The first is that 'suboxic' authigenic Mo formation constitutes an important sink for Mo (10-20%), and the δ^{98}Mo values that have been measured in 'suboxic' sediments span a large range (-0.5 to +1.3‰), with no constant offset from seawater (Siebert et al., 2006; Poulson-Brucker et al., 2009).

Secondly, recent measurements of δ^{98}Mo in rivers (Archer and Vance, 2008) have shown that rivers are isotopically disparate (+0.2 to +2.4‰), and

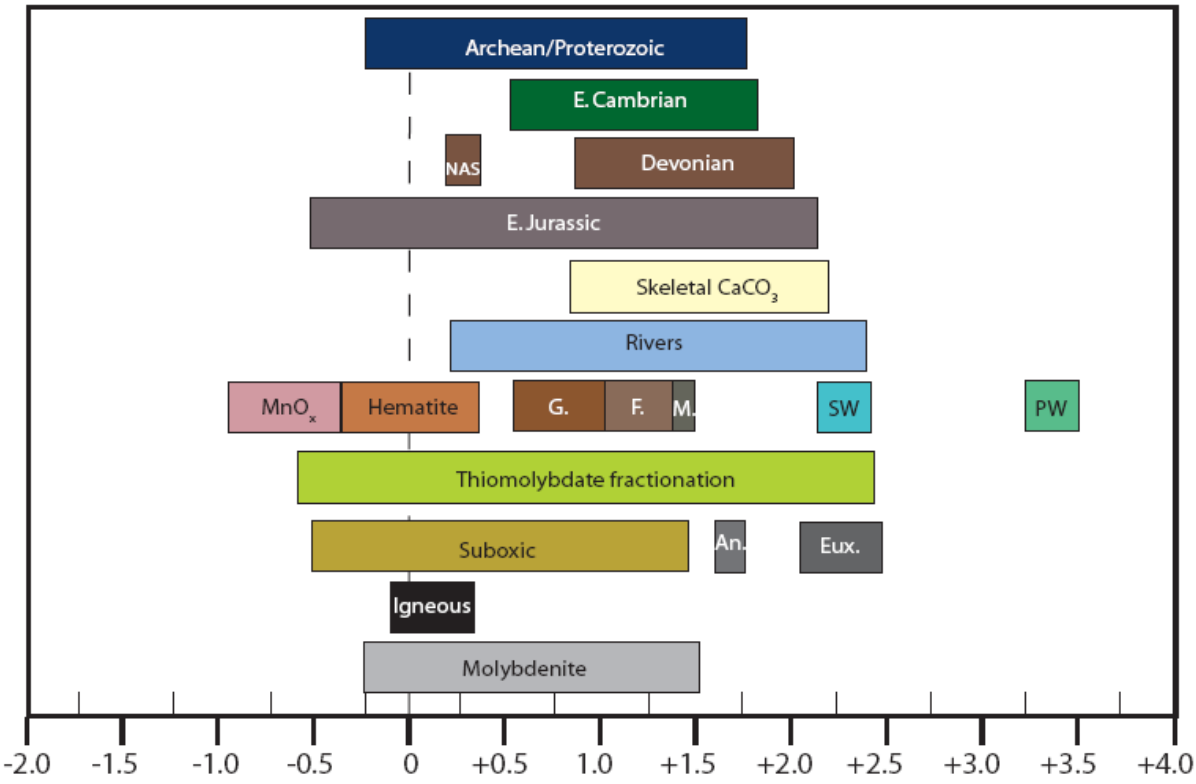

Figure 1.4: The range of measured Mo isotope values in a variety of settings and geological materials. Data references: *Archean/Proterozoic shales:* Siebert et al., 2005; Wille et al., 2007. *Early Cambrian:* Lehmann et al., 2007. NAS is a Devonian aged shale used at UMD as a rock reference material (see Chapter 2 for details). *Devonian:* Gordon et al., 2009. *Early Jurassic:* Pearce et al., 2008. *Skeletal carbonates:* Voegelin et al., 2009. *River water:* Archer and Vance, 2008. *MnO_x*: Barling and Anbar, 2004; Siebert et al., 2003; Wasylenki et al., 2008. *Hematite, goethite (G.), ferrihydrite (F.) and magnetite (M), all FeO_x:* Goldberg et al., 2009. *Seawater:* Siebert et al., 2003, Nakagawa et al., 2008. *Porewater (PW)*, McManus et al., 2002. *Thiomolybdate fractionation:* Neubert et al., 2008. *Suboxic sedimentation:* Siebert et al., 2006. *Anoxic sediments:* Poulson et al., 2006. *Euxinic sediments (Black Sea):* Nägler et al., 2005; Arnold et al., 2004; Barling et al., 2001. *Igneous rocks*: Siebert et al., 2003. *Molybdenites*: Malinovsky et al., 2007; Hannah et al., 2007.

in the case of the Nile, there are seasonal differences in δ^{98}Mo (+0.2 to +0.8‰). In this work (Chapter 3), the δ^{98}Mo of the Susquehanna River was measured and found to fall within this range (1.1‰). The apparent range of positive δ^{98}Mo values for river input has several implications: 1) it cannot be assumed that transport and erosion have no effect on the δ^{98}Mo of materials being weathered, and 2) it cannot be assumed that weathered materials start with a δ^{98}Mo near zero. Indeed, evidence from molybdenite deposits indicates that a large range in δ^{98}Mo can be generated via relatively high-temperature processes (-0.3 to +1.5‰, Hannah et al., 2007; Malinovsky et al., 2007). Furthermore, the δ^{98}Mo of molybdenite was shown to effect the δ^{98}Mo values of sediments in lakes close to the molybdenite occurrence (Malinovsky et al., 2007). While molybdenites are unlikely to be a major source of Mo to the oceans, several studies have demonstrated that continental materials formed by high temperature igneous or metamorphic processes can have significant, non-zero δ^{98}Mo values (Wieser and DeLaeter, 2003; Pietruszka et al., 2006; Hannah et al., 2007; Malinovsky et al., 2007). A comprehensive survey of δ^{98}Mo in igneous rocks is needed to determine if the isotopic range observed in rivers is the result of source or alteration/weathering processes.

Yet a third complication to the simple idea that the δ^{98}Mo value of a euxinic sediment reflects the δ^{98}Mo value of seawater is evidence from the Black Sea itself, which is arguably the best modern example of sedimentation under a euxinic water column. In the Black Sea, the H_2S_{aq} concentration is

near zero at the surface, begins to rise at the chemocline (~100 m depth), and is high and fairly constant below ~400 m depth (Neretin et al., 2001). This systematic variation was used to calculate the speciation of molybdate to thiomolybdate with depth (i.e., increasing H_2S_{aq}), from which came the concept of the geochemical 'switch point' at 11μM H_2S_{aq}, where water column scavenging of Mo becomes dominant (Erickson and Helz, 2000). In a study of δ^{98}Mo values in Black Sea sediments deposited under different H_2S_{aq} conditions, a wide range of values (-0.1 to +2.5‰) was found (Neubert et al., 2008). Combining the calculated δ values between individual Mo species (Tossell, 2005) with the model of Erickson and Helz (2000), Neubert et al. were able to provide support for the calculations of Tossell (2005), who predicted that large fractionations might result from a 'partial' removal by equilibrium fractionation.

The fractionation of Mo isotopes during adsorption to Mn-oxides has now been shown to be insensitive to pH changes (Barling and Anbar, 2004), ionic strength, and is not greatly affected by temperature (0.3‰ difference over 50℃; Wasylenki et al., 2008). The formation of MnO_x and adsorption of light Mo has been proposed to be the cause of isotopically heavy pore water (McManus et al., 2002). However, MnO_x are readily dissolved when buried to the redox boundary in sediments. The release of isotopically light Mo to the pore water (McManus et al., 2002), and subsequent uptake in authigenic sediments is thought to overprint the δ^{98}Mo values of any existing authigenic minerals (Reitz et al., 2007; Chapter 4, this work). Recently, evidence of Mo

fractionation during adsorption to Fe-oxy(hydroxides) has been reported, and the range of δ^{98}Mo values of Mo adsorbed to these minerals overlaps with the suboxic range (Goldberg et al., 2009). Since FeO_x forms are important components of aqueous sediments (Poulton and Raiswell, 2002), and can adsorb Mo (Goldberg et al., 1998), they may provide an additional important sink for Mo.

Finally, uptake of Mo has been shown to produce a range of δ^{98}Mo values in carbonates, although the amount of Mo that is sequestered in most carbonates is very small, <0.1µg/g (Voegelin et al., 2009). Skeletal carbonate phases, which dominate some marine sediments, have generally heavy δ^{98}Mo values, from gastropods of +0.7‰ to coral of +2.2‰ (Voegelin et al., 2009). These authors proposed that there is no effect of local redox conditions on Mo uptake to carbonates, but there is a biological effect in skeletal samples. Thus, non-skeletal ooids might be useful as a proxy for the δ^{98}Mo of the ambient seawater (Voegelin et al., 2009).

Additionally, it has been proposed, but not empirically proven, that Mo isotopes may be fractionated during adsorption to sinking or in-situ organic matter (Poulson-Brucker et al., 2009). Small fractionations (-0.5‰) have been shown to occur during uptake to the soil bacterium Azotobacter vinelandii (Wasylenki et al., 2007; Liermann et al., 2005), which requires Mo for N_2 fixation, and there is reason to believe that similar fractionations may be evidenced by aqueous N_2-fixing organisms, which share a biosynthetic pathway for the enzyme nitrogenase. Thus, if aqueous cyanobacteria were

abundant, under the appropriate conditions, microbial fractionation of Mo from the water column might be observable. This would probably require an anoxic water column, so that active nitrogen fixation could occur. If the flux of cyanobacterial biomass and fractionated Mo was large enough, it might be possible to see evidence for it in a sediment sample.

The contributions of this work

Several projects have been completed that will contribute to the understanding of Mo and Mo isotopes in geochemical systems. The first of these projects was to assess the behavior of Mo in the sediments and waters of Chesapeake Bay and its main tributary, the Susquehanna River (Chapter 3). The original idea behind this study was to determine whether Mo isotopes could track the onset, and document the severity of, coastal eutrophication and anoxia in the Bay. The Mo isotope data did not show a strong signal of anoxic deposition, but there was a trend towards increasing variability of δ^{98}Mo values, that was interpreted to indicate an increase in the incidence of coastal anoxia. It was also demonstrated that Mo isotopic fractionation was occurring within the Susquehanna river basin, and that Mo removal from the water column is taking place within the Chesapeake Bay. This work has been accepted for publication by Earth and Planetary Science Letters, and is co-authored by George Helz and Rich Walker.

The second large project was to investigate Mo isotope signatures in Pliocene-Pleistocene-aged core samples from the Mediterranean Sea (Chapter 4). The Mediterranean sediments include numerous organic-rich

layers that are called sapropels. These unusual sediments are thought to form when fresh water influx to the sea surface prevents convective mixing, leading to an episode of anoxia in the deep water, possibly combined with an increase in surface productivity. The project ultimately included not only Mo isotopes and Mo concentrations, but Re concentrations, major elements, and a small number of sulfur isotopic analyses. The main result of the study is that the conditions under which sapropels can form seem to vary significantly from episode to episode. These variations are apparent in all of the proxies that were examined, including Mo isotopes. This work is currently being prepared for submission.

The publication of molybdenite δ^{98}Mo data with a large and non-systematic range of values provided the impetus for a collaboration with Michael Mengason of the Laboratory for Mineral Deposits Research (UMD). Michael performed a number of experiments that were designed to determine whether fractionation of Mo takes place between a vapor phase and a melt phase at high temperature and pressure. The resultant run products were processed and analyzed for Mo isotopes. There appears to be a fairly systematic fractionation between the two phases, with the vapor phase being isotopically heavier. These results are presented in Chapter 5. We intend to publish a short paper that describes these data. Michael contributed the experimental products and knowledge of porphyry Mo deposits, while I contributed the Mo concentration and isotope measurements and background information in these topics.

Chapter 2: Method development at UMD

First attempts

The development of high sensitivity, high resolution multi-collector inductively coupled plasma mass spectrometry in 1992 (MC-ICP-MS) instigated a tide of research into the isotopic compositions, fractionation mechanisms, and behavior of the heavy transition elements (e.g., Cr, Fe, Cu, Zn, Mo), and other, 'non-traditional' stable isotopes (e.g., Li, Mg, Ca; see Johnson, Beard and Albarede, Eds., 2004, for a review). The first attempts at analyzing mass-dependent Mo isotope variations by MC-ICP-MS came in 2001 (Anbar et al,. 2001 and Siebert et al., 2001), and proved feasibility for future developments in the methodology, as discussed in Chapter 1. On a historical note, Murthy (1962, 1963) and Wetherill (1964) both attempted to measure Mo isotope variations in meteorites (stony and iron), but were hampered by analytical uncertainties, despite Wetherill's use of a double spike. This usage was one of the first practical applications of a double spike method. The primary difficulty of assessing the natural fractionation of Mo isotopes lies in precisely compensating for mass bias imparted during processing and analysis, because the total measured range of variation in δ^{98}Mo in earth materials is typically less than 4‰ (Anbar et al., 2001).

The groundwork for Mo isotope measurements at UMD was laid by Aaron Pietruszka, circa 2003-2004, who developed the preliminary chromatographic methods, and performed several series of Mo isotope measurements on solution standards, and sample material with simple matrices (molybdenites) using the UMD Nu-Plasma MC-ICP-MS (Pietruszka

et al., 2006). This work was the first to identify a large range in molybdenite Mo isotopic composition (-0.75 to +1.05‰). These measurements also determined that matrix effects for solution standards could be controlled with careful analytical techniques (Pietruszka et al., 2006). The path from these initial successful measurements to the high-precision measurement of more complex matrices has been lengthy. A discussion of the steps taken is presented here, as well as a summary of the methods currently in use.

Brief overview of MC-ICP-MS

The Nu-Plasma MC-ICP-MS instrument is double-focusing (electrostatic analyzer and a magnetic sector analyzer, in Nier-Johnson geometry), equipped with variable zoom optics for beam focusing, and 12 faraday detectors (Belshaw et al., 1998). In the simplest terms, mass spectrometry relies on the behavior of ions accelerated through a potential into a magnetic field, where the deflection of the ion's flight path through the field is determined by its mass to charge ratio (M/Z). The accelerated, deflected ions impact detectors, which record the number of ions per unit time as current. The current passes through a resistor with known specific resistivity (10^{11} Ω), which generates a voltage that is measured (V = I * R). Mass spectrometers differ in two fundamental aspects: how ions are created at the sample-input end, and the way in which the mass and number of ions is determined. The former must take into account the first ionization potential of the element; for elements with low to intermediate ionization potentials, gas-source or thermal ionization (TIMS) can be used, but elements with high

ionization potentials require a higher energy method such as a plasma. Although Mo can be ionized by thermal processes, its high first ionization potential of 684 kJ/mol means it is well suited for ionization by ICP. At the ionization temperature, 98% of Mo is ionized (Houk, 1986). The latter aspect takes into account whether the user wishes to measure element or isotope abundances, or element or isotope ratios. For precise isotope ratios, an instrument with multiple detectors is best, while for element abundances, a single-detector is better. This relates to issues with magnet hysteresis when analyzing over a large mass range. Here the discussion will focus on MC-ICP-MS, as the majority of the present work has focused on high precision and accurate isotope ratios.

In instruments that utilize ICP as the ion source, argon gas is generally used as the carrier gas as well as the 'source' gas. A cylindrical (induction) coil is wound around a quartz torch; a time-varying electrical current, supplied by a radio-frequency generator (at 27 MHz), is passed through the coil, which induces variable magnetic fields in the gas. A spark plug supplies the first electrons to interact in the magnetic field. Argon atoms are ionized and create a plasma with temperatures between 6000 and 10000 K. Samples are introduced as aerosols, and are indiscriminately ionized in the plasma. The ions created have a range of kinetic energies, which necessitates the use of an electrostatic filter (Albarede and Beard, 2004).

The Plasma Laboratory possesses several devices for sample introduction. The two nebulizers used for Mo work (ESI Apex and CETAC

Aridus) both operate on the same principle of desolvation. A liquid sample is introduced to the apparatus at a flow rate of ~40 µl/min, which is assessed before each analytical session. The liquid sample, passes through a heated membrane or chamber, where the solvent evaporates. The remaining solute is passed into the torch in a stream of sampling gas.

Mass bias and instrumental fractionation

Mass bias, or instrumental mass fractionation, refers to the variable transmission of the ion beam into the mass spectrometer. It is a significant drawback of ICP-MS, where there is a strong preferential transmission of heavier ions (Wombacher and Rehkämper, 2003). The majority of mass bias occurs in the source or source-mass analyzer interface, as opposed to within the mass analyzer, flight tube, or collectors (Albarede and Beard, 2004). For example, changes in the geometry of the skimmer cone can have a large effect on the mass bias; distance of the torch from the sample cone; or matrix effects. In ICP-MS, the degree of mass fractionation is significantly larger compared to TIMS, but is nearly time-invariant (Wombacher and Rehkämper, 2003). These effects can have major implications for stable Mo isotope measurements.

Three types of laws are commonly used to describe and correct for mass bias (linear, exponential, and power laws). Fractionation in ICP-MS can best be described with the exponential law. Here, the exponential law is given, using two Mo isotopes (^{98}Mo and ^{95}Mo) as an example.

(2.1) $$98/95_{true} = 98/95_{measured} * (98_{mass} / 95_{mass})^{\beta}$$

$$1.52445 = 98/95_{measured} *(97.905408/94.905842)^{\beta}$$

$$\beta=(\log(1.52445/98/95_{measured}))/(\log(97.905408/94.905842))$$

In MC-ICP-MS, the fractionation factors (β) are generally less than -2, and remain fairly constant for a given element (at UMD, $\beta_{Mo} = -1.718 \pm 0.009$). A correction in the measured ratio of a sample based solely on the exponential mass bias law is called 'internal normalization'.

Matrix effects can also be a source of significant mass bias and must be carefully eliminated. The term 'matrix effect' encompasses two main types of phenomena. The first is the range of isobaric or spectral effects: direct (e.g., ^{96}Zr at ^{96}Mo); oxides or nitrides (e.g., $^{84}Kr^{16}O$ at ^{100}Mo); and doubly charged species (e.g., $^{190}Os^{2+}$ at ^{95}Mo). The non-spectral effects are due to the presence of other elements in the purified sample, which can cause changes in the sensitivity of the element of interest. This change in sensitivity can alter the mass bias, and significantly affect the accuracy of measurements (Albarede and Beard, 2004). To illustrate this, the effect of a variety of elements (Mn, Fe, Al, V, Zn) on the accuracy of Mo isotope measurements was tested, by adding these elements to a standard reference material (Fig. 2.1). The standard used was a gravimetrically prepared solution made from a Mo wire. For this experiment, the wire standard was

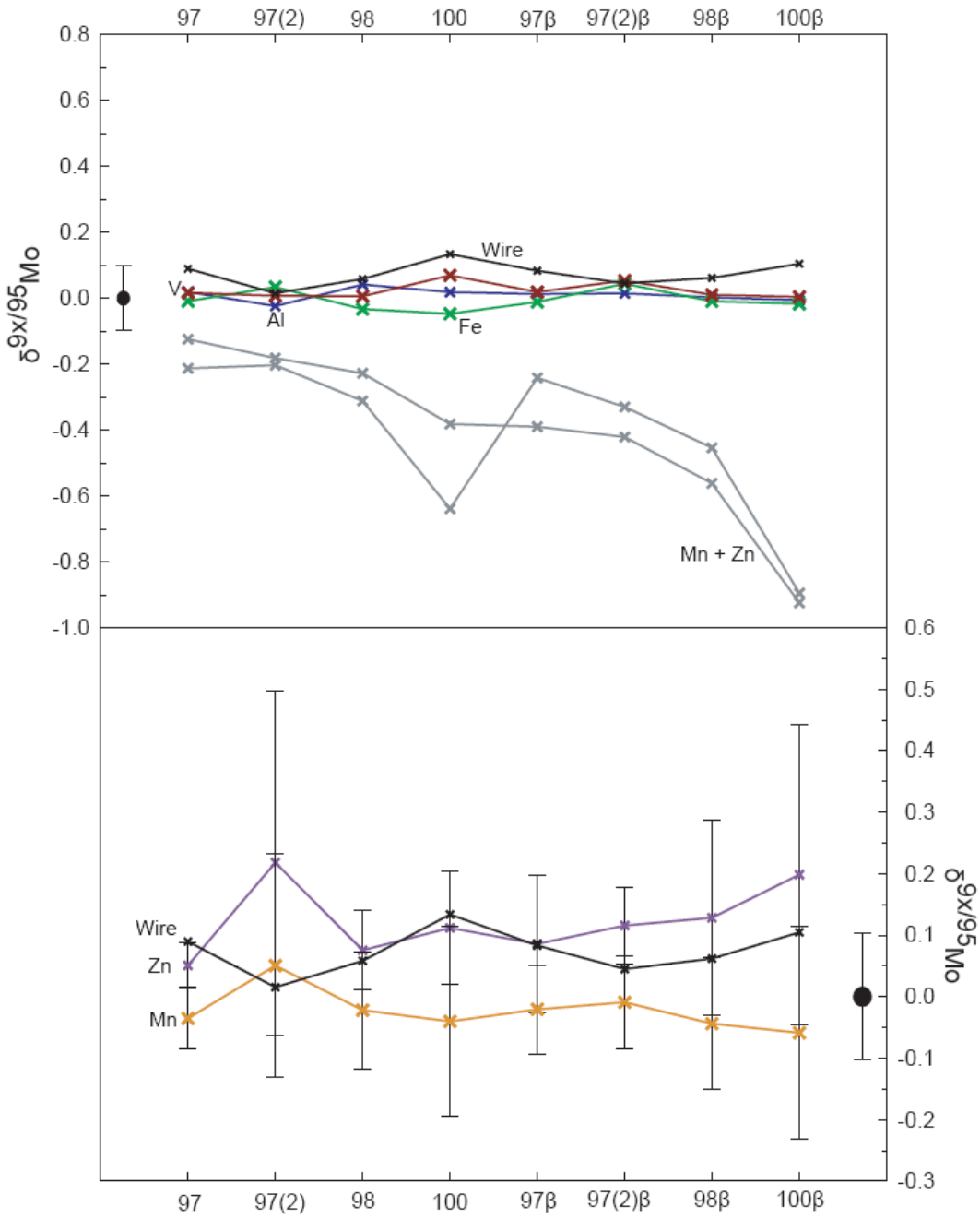

Figure 2.1: The matrix effect on $\delta^{9x/95}$Mo of the UMD wire standard (black), using V (red), Al (blue), Fe (green), Mn and Zn (grey), Zn (purple), and Mn (orange). All samples had Zr added for external normalization. For Zn and Mn, the error bars are the standard deviation of the number of measurements (3 and 7, respectively). A single measurement was made for the other elements. The 2σ error of a typical $\delta^{9x/95}$Mo value is shown for reference. B refers to ratios corrected with the fractionation factor β obtained using Zr. 97(2) uses the ratio taken during cycle 2 of the analysis.

Diluted to 800ng/g Mo, 200 ng/g Zr was added and the elements were added to separate aliquots. The elements were added in the following quantities: V, 0.01ng; Al, 0.01ng; Fe, 0.078ng; Zn, 12 ng; Mn, 0.078 ng and 200 ng; Mn + Zn, 12 ng + 0.078 ng. These experiments illustrate the negative effect of impurities in a sample on the accuracy of measured Mo isotope ratios. In many cases, the $\delta^{9x/95}$Mo value of the impure samples lies well outside the accepted standard deviation of these measurements. One problem is that these types of effects are not reproducible from sample to sample, as illustrated by the large range of values from repeated measurements of the standard plus Zn or Mn.

Both general types of matrix effect can be controlled to a large extent by ensuring that the separation/purification chemistry is effective at removing everything but the element of interest. The cleanliness of the chemistry can be checked for each sample measurement by scanning through the periodic table. For Mo measurements, scans from mass 50 (Cr) through mass 91 (Zr) and from mass 101 (Ru) to mass 120 (Sn) were checked for interfering elements.

Pietruszka and Reznick (2008) showed that a standard passed through an anion column was isotopically lighter than the same standard measured directly, likely as the result of an organic residue sourced in the anion resin itself, causing a matrix effect in the plasma. This 'column matrix effect' generated an isotope effect that encompassed ~25% of the natural variation in $\delta^{97/95}$Mo (Pietruszka and Reznick, 2008).

Methods for fractionation correction

The primary difficulty of assessing the natural fractionation of trace metal stable isotopes is compensating for mass bias during analysis. The natural equilibrium fractionation of elements tends to decrease with increasing temperature and increasing mass, as the relative mass difference between isotopes of an element becomes small (Urey, 1947). For example, the known range of variation in δ^{98}Mo in natural samples is only ~5‰, compared to ~60‰ for δ^{7}Li. Thus, correcting for the effects of analytical mass fractionation must be increasingly precise with higher-mass elements. Three commonly used techniques for fractionation correction will be discussed here, all of which were, or are, used at UMD for Mo isotope analysis.

Sample-standard bracketing

The first, and probably simplest, method for assessing and correcting for mass bias is termed sample-standard bracketing (SSB). The technique works on the assumption that mass bias is constant between samples and standards. In ICP-MS, the mass bias is large but is not subject to drift, so SSB can be used successfully. A standard with known mass bias is run before and after a sample with unknown mass bias, and the knowns are used to interpolate the mass bias in the sample (Albarede and Beard, 2004).

External fractionation correction

Instrumental mass bias is often corrected by external fractionation correction (FC). This refers to the addition, before analysis, of some amount of a different element with isotopic masses within the range of the element of interest (e.g., Belshaw et al., 1998). The principle behind external FC is that

the amount of mass bias for the element of interest can be calculated from mass difference measured in the added element (e.g., Walder et al.,1993; Marechal et al., 1999). However, the ability to measure accurate ratios for the isobaric isotopes may be compromised, and the fractionation of the two elements may not be identical. This method is applicable as long as the sample has been completely purified of the element that will be added, because its presence in the sample might alter the fractionation correction factor.

External FC can be combined with SSB to provide, in theory, an even better control on instrumental mass fractionation. However, 'automatrix' effects can result in two ways: by allowing the ratio of the sample element and added element to vary significantly between the bracketing standard and sample; and by allowing the concentration of the sample element to vary between standard and sample (Pietruszka et al., 2006).

Both SSB and external FC correct solely for instrumental mass bias, and cannot provide any correction for mass fractionation during sample processing. For example, it has been shown that ion exchange chromatography can isotopically fractionate heavy elements such as Fe and Cu, but that fractionation can be reduced if the elemental yield off the column is close to 100% (e.g., Anbar et al., 2001; Marechal et al., 1999).

Double-spiking

Double-spiking is another technique for precisely determining the true isotopic composition of an element in a sample, provided the element has

four or more isotopes. The technique involves the addition of two 'spike' isotopes with known concentrations and isotopic compositions, and provides a completely internal mass fractionation correction (Pietruszka et al., 2006). Double-spiking was first outlined mathematically by Dodson (1963) and has since been applied to many elements (Pb, Compston and Oversby, 1969; Galer 1999; Ca, Russell et al., 1978; Nägler et al., 2000; Ba, Eugster et al., 1969; Sr, Hofmann, 1971; Fe, Johnson and Beard, 1999, Dideriksen et al., 2006; Se, Johnson et al., 1999, Herbel et al., 2000; Cr, Schoenberg et al., 2008; Mo, Wetherill 1969, Siebert et al., 2001; S, Mann et al., 2008; Zn, Bermin et al., 2006; Ge, Siebert et al., 2006; U, Stirling et al., 2007; Cd, Ripperger and Rehkämper, 2007; Os, Markey et al., 2003).

The method can yield extremely precise fractionation-corrected values, but is subject to some of the same limitations as other measurement techniques; for example, clean sample separation and low blank are equally important in double-spiking, although quantitative yields are less so. Double-spiking may be more susceptible to memory effects in ICP-MS (Albarede et al., 2004). Finally, in order for double-spiking to be successful, the spike and sample must be equilibrated before any processing takes place, so that fractionation occurring after the equilibration step will affect the sample and spike to an equal degree (e.g., Johnson and Beard, 1999).

The principle that allows double spiking to work is geometrical in nature, and graphical presentations have frequently been used to illustrate this (e.g., Hofmann, 1971; Galer, 1999; Johnson and Beard, 1999; Siebert et

al., 2001; Albarede and Beard, 2004). For figures 2.2 and 2.3, each axis represents a ratio of two isotopes with all ratios having a common denominator. Only one possible mixing tie-line exists that connects the spike, the true mix (*M*), and the true sample (*S*) compositions (Hofmann, 1971; Galer, 1999; Johnson and Beard, 1999). The composition of *M* has been affected by instrumental mass fractionation, *f(m)*, to generate *m*, the measured mix. The composition of *S* is approximated by using a reference value (*s*) that has been affected by 'natural' fractionation, *f(s).* This is a valid approximation because, with heavier elements, the range of fractionation is relatively small (Albarede and Beard, 2004). The spike, *m*, and *s* do not share a common line (Fig. 2.2). However, a plane can be defined by the spike composition, the direction of the instrumental fractionation line, *f*(*m*), and *m*. Likewise, a plane can be defined by the spike composition, the natural fractionation line, *f*(*s*), and *s,* where the direction of *f*(*s*) is a function of the isotopic composition of *s* (Galer, 1999). These two planes will only intersect at the spike-*M*-*S* mixing line (Fig. 2.3). A unique solution for *S* is, therefore, given by the point where the spike-*M*-*S* mixing line intersects the natural fractionation line, *f*(*s*) (e.g., Hofmann, 1971; Galer, 1999).

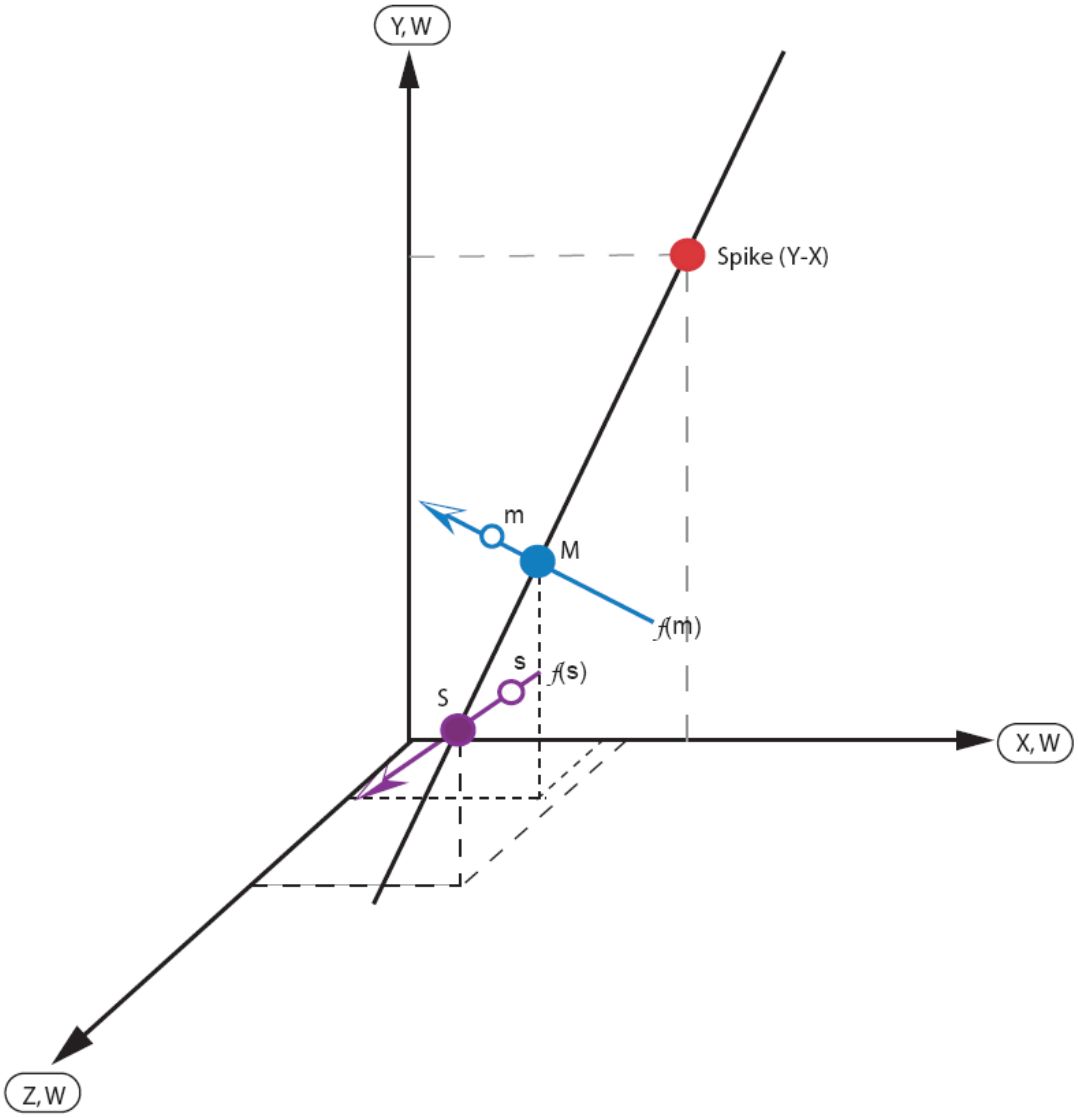

Figure 2.2: Graphical representation of double-spike geometry (Hofmann 1971; Galer 1999). Each axis in a three dimensional space represents one ratio, all with a common denominator (W). The spike has only Y and X. "True" values for the spike, mix (*M*), and sample (*S*) are closed circles. These values have been affected by fractionation, *f(m)* and *f(s)* (arrows) to yield the measured mix *m* and reference sample, *s* (open circles). The spike, M, and S must lie on a straight line.

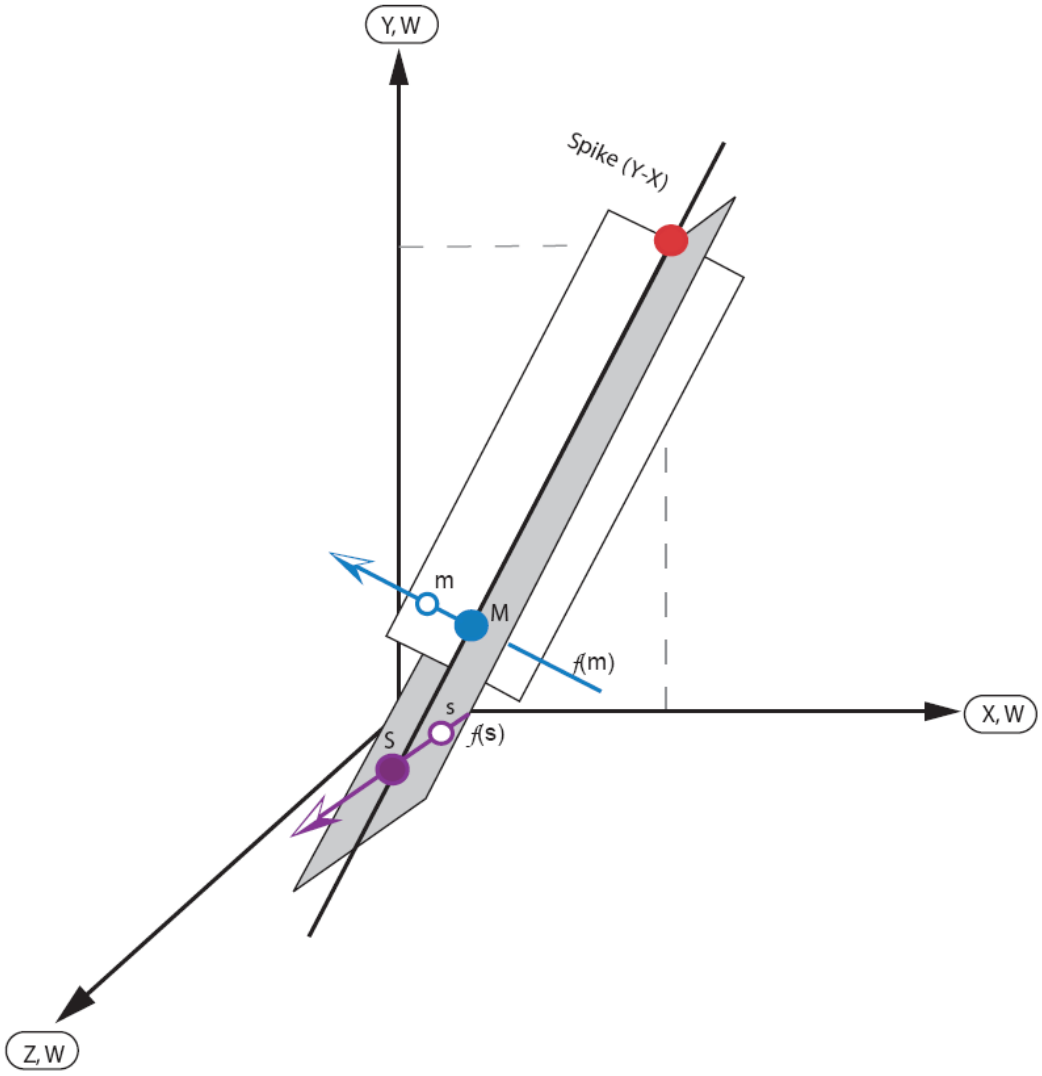

Figure 2.3: The two-plane solution to *S*. The grey plane contains the spike, the vector *f(s)* and s. The white plane is defined by the spike, the vector *f(m)*, and *m*. The intersection of the two planes is the mixing line of the spike, *M*, and *S*. *S* is given by the point where *f(s)* intersects the mixing line.

To find the solution for the intersection point, *S*-- that is, the "true" sample-- the data for the spike, *m*, and estimated *s* must be deconvoluted. This is done using a three-dimensional iterative approach that successively refines the true values for *S*, *f*(*s*), and *f*(*m*) from initial 'guesses' at these values (Siebert et al., 2001). Iteration is necessary because the geometric solution illustrated in Figures 2.2 and 2.3 is a linear approximation, whereas fractionation is best described by an exponential function (e.g., Johnson and Beard, 1999; Johnson and Bullen, 2004).

Attempts with SSB and external FC

Initially, the efforts at UMD centered on using the external FC method in conjunction with SSB. Zirconium and ruthenium have both been used for mass bias correction in Mo isotope measurements (e.g., Anbar et al., 2001; Pietruszka et al., 2006). Zirconium has isotopes of mass 90, 91, 92, 94 to 96, and has isobaric overlaps with Mo at masses 92, 94, and 96. Ruthenium has isotopes of mass 96, 98, 99, 100, 101, 102, and 104, and has isobaric overlaps with Mo at masses 96, 98, and 100. For these tests of the combined SSB and external FC methods, only Zr was used for external FC. In a Zr-spiked Mo isotope analysis, the fractionation factor (β) between ^{90}Zr and ^{91}Zr is calculated, based on a known ^{91}Zr/^{90}Zr, then applied to the measured Mo isotope ratios to correct for instrumental mass bias. Molybdenum isotope ratios, uncorrected for Zr, were also reported.

The bracketing standards that were used were dilutions of a 1000 mg/l Johnson-Matthey Company SpecPure® Mo plasma standard (Stock #35758, Lot #013186S). An appropriate amount of diluted Zr plasma standard was added to

the Mo bracketing standard, usually 800 ng/g Mo and 200 ng/g Zr. The acid used to dilute all samples and standards was 2% nitric acid, mixed using ultrapure nitric acid and 18mΩ deionized and distilled water. Care was taken to always use the same batch of acid for dilution of samples and standards, because small differences in acid strength can create matrix effects.

Using the combination of SSB and external FC methods introduced a number of technical difficulties. It was found necessary to keep the Zr and sample Mo signal intensities fairly constant from sample to bracketing standard (within 5%), and the voltage of Zr had to be no less than 10% of the Mo voltage, and the ratio of Mo/Zr needed to be fairly high. Deviation from these parameters resulted in significant automatrix effects, similarly described by Pietruszka et al. (2006). For the highest-quality data, the voltage of ^{98}Mo (the most abundant isotope) needed to be higher than 2v, and preferably as high as 5v. This was generally easily obtained with the 800 ng/g standard solution of Mo.

All published data of Mo isotope ratios in terrestrial materials use ^{95}Mo as the light isotope in the denominator because it is free of isobaric interference. Standard delta notation is used:

$$(2.2) \qquad \delta^{98}Mo_{sample} = 1000*(^{98/95}Mo_{sample}/^{98/95}Mo_{standard})-1)$$

In sample-standard bracketing, the $^{98/95}Mo_{standard}$ used to calculate a sample delta value was the average $^{98/95}$Mo of the two bracketing standards. Zirconium was added to purified samples, standard reference materials, and to the bracketing standard on the day of analysis. The δ values for a given sample were calculated

in two ways: 1) the 'uncorrected' Mo isotope ratios for sample and bracketing standards would be used to calculate the δ values; 2) the Zr(β)-corrected Mo isotope ratios for the sample and bracketing standards would be used. Ideally, the δ values for uncorrected-SSB and the Zr(β)-corrected SSB should be identical within error.

Two pure Mo standard reference materials (Mo wire and UMD-A, a ^{97}Mo-enriched solution) were analyzed several times during each run. These standards were measured to high precision during the attempts with SSB and external FC (Fig. 2.4, Table 2.1). In addition, the data could be compared to previously measured values for δ^{97}Mo, δ^{98}Mo, and δ^{100}Mo relative to the Mo plasma standard (Table 2.1; Pietruszka et al., 2006). For the presentation of these early data, δ^{97}Mo is used, because of the analytical routine that was in use at the time.

In addition to the solution standards, two different shale samples were obtained in large quantity to serve as matrix-matched standards for sample analysis. SDO-1 (Devonian Ohio Shale 1) is a U.S. Geological Survey certified geochemical reference material, and has known elemental concentrations. Its Mo concentration is 134 ± 21 μg/g (Kane et al., 1990). In addition, its Mo isotopic composition has been measured by several other labs. The second standard shale is NAS (New Albany Shale), which was obtained from the Indiana Geological Survey, and had a value for Mo concentration of 793 ug/g. Both of these shales were processed numerous times, and repeatedly measured (Fig. 2.5, Table 2.2). The results for the two shale standards showed initial promise,

but data acquired over a long period of time showed that mass-dependent instrumental fractionation was not being adequately corrected for by sample-standard bracketing and external FC. Problems primarily arose from the Zr addition, which were identified by large differences between SSB-δ values from Zr-fractionation corrected ratios (δ^{97}Mo-β), and SSB-Delta values (δ^{97}Mo), calculated using an Mo fractionation factor to correct for mass bias. Matrix effects from a number of sources probably added to the difficulties, although extensive efforts were made to ensure adequate sample cleanliness. Zirconium addition may have contributed to matrix effects by changing the sensitivity of Mo in the plasma. Ultimately, these problems required adoption of a double spike method to generate data of sufficient precision and accuracy.

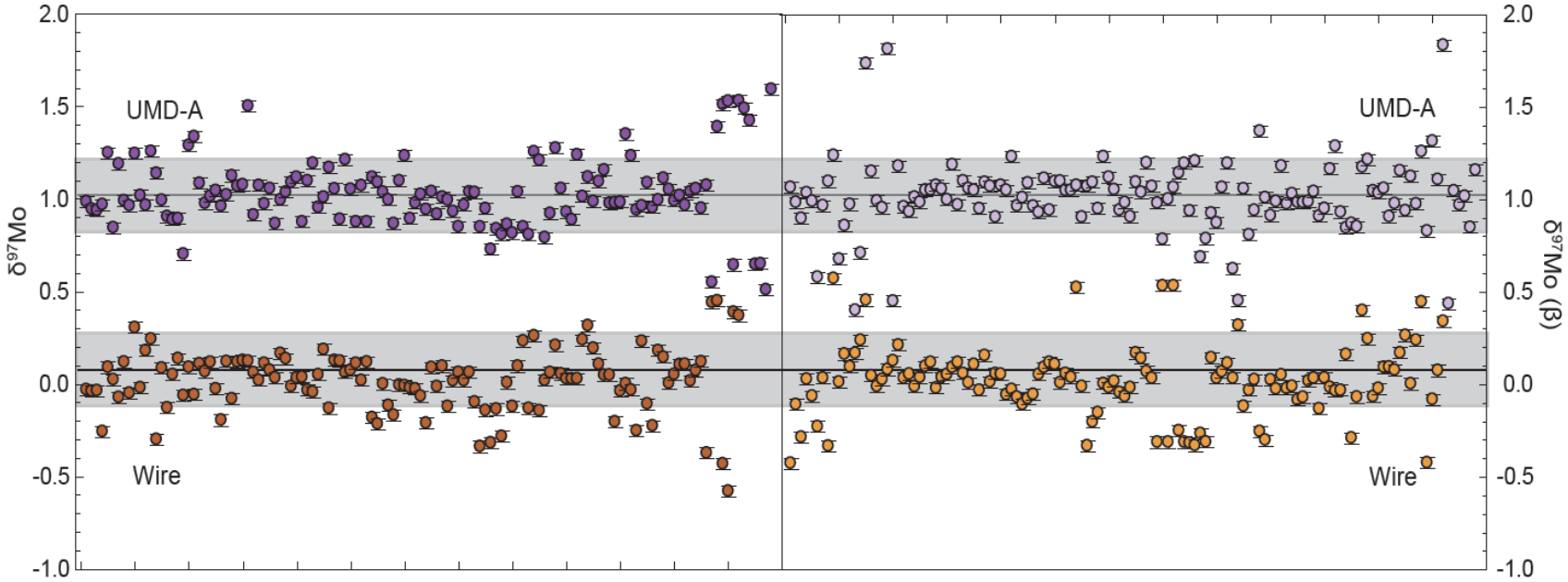

Figure 2.4: The δ^{97}Mo (left panel) δ^{97}Mo(β) (right panel) for UMD-A (purple) and the wire standard (orange). The average δ^{97}Mo value of UMD-A is +1.02‰ and of the wire +0.02‰ (table 2.1). The error bars are the $2\sigma_{mean}$ of the data sets, while the 1σ error is represented by the grey boxes (approximately ±0.2‰ in all cases).

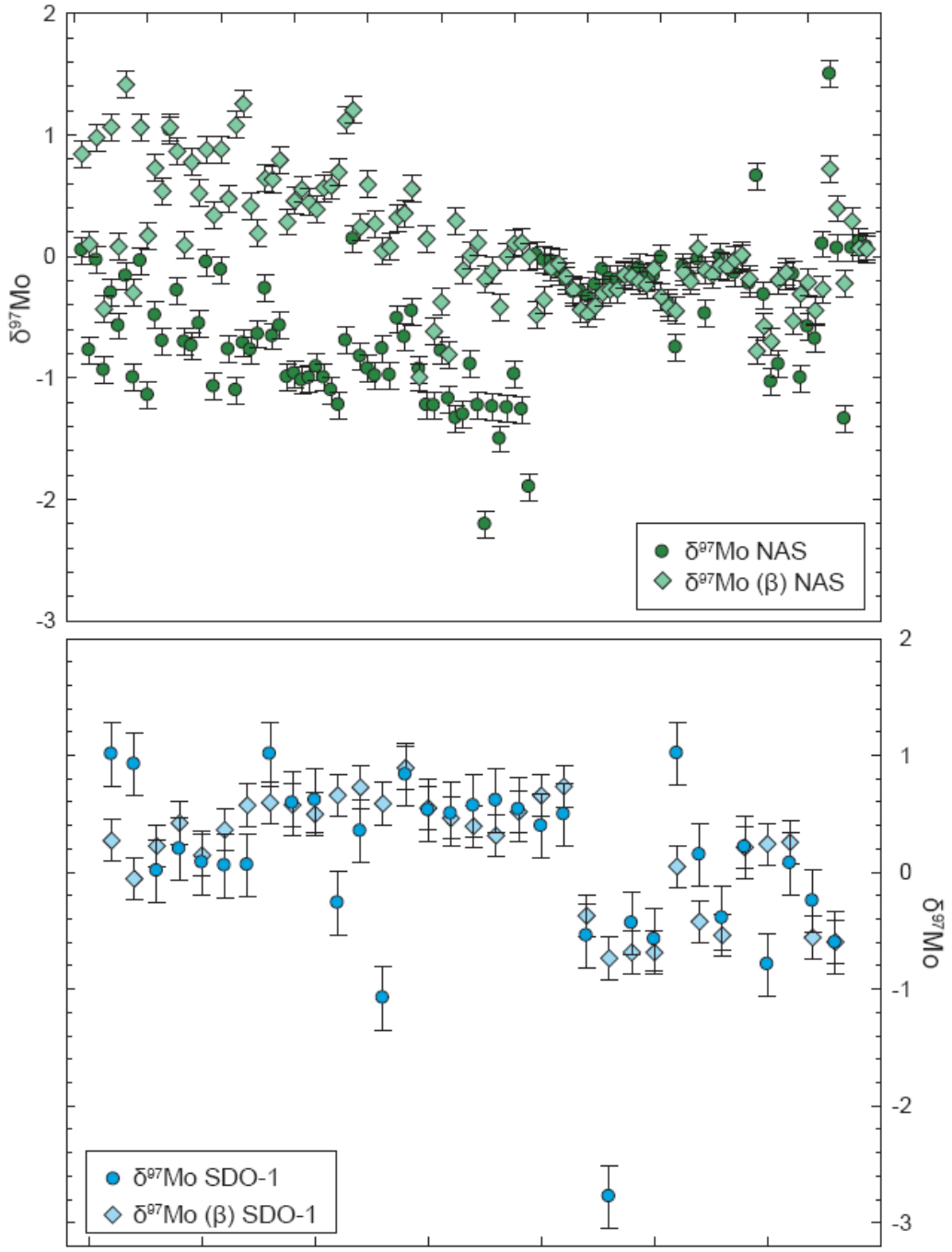

Figure 2.5: The δ^{97}Mo (circles) and δ^{97}Mo(β) (diamonds) values for NAS (top, in green) and SDO-1 (bottom, in blue). Error bars are values for $2\sigma_{mean}$ (table 2.2).

Table 2.1: Data for the two solution standards, 2005-2007.

UMD-A	$\delta^{97}Mo$	$\delta^{97}Mo$ (β)	**Wire**	$\delta^{97}Mo$	$\delta^{97}Mo$ (β)
Average	+1.03	+1.02	Average	+0.016	+0.017
2σ	0.38	0.41	2σ	0.34	0.39
2σ mean (n = 128)	0.034	0.036	2σ mean (n = 122)	0.030	0.035
2006[a] average	+1.086	+1.14	2006[a] average	+0.085	+0.15
2-σ	0.061	0.29	2σ	0.067	0.23
2σ mean (n = 10)	0.019	0.09	2σ mean (n = 11)	0.020	0.07

[a]Pietruszka et al., 2006.

Table 2.2: Data for two sediment reference materials; each material was processed through the column chemistry sequence numerous times and repeatedly measured.

NAS	$\delta^{97}Mo$	$\delta^{97}Mo$ (β)	**SDO-1[a]**	$\delta^{97}Mo$	$\delta^{97}Mo$ (β)
Average	-0.53	+0.17	Average	+0.09	+0.019
2σ	1.12	1.12	2σ	1.51	0.97
2σ mean (n = 108)	0.11	0.11	2σ mean (n = 31)	0.27	0.18

[a]Published value for δ^{97}Mo of SDO-1 is 1.02 (Barling et al., 2001).

Preparation and Calibration of a 97Mo-100Mo Double Spike

The ^{97}Mo-^{100}Mo double spike was prepared in collaboration with Drs. Aaron Pietruszka and Jasper Konter (San Diego State University). Enriched metal powders of ^{97}Mo (94.2%) and ^{100}Mo (92.6%) were dissolved and diluted gravimetrically to 6.3378 and 6.5156 µg/g, respectively. These concentrations were calibrated by mixing the spikes with variable amounts of a Mo-wire standard prepared gravimetrically to high precision.

In creating the double-spike, the ^{97}Mo-^{100}Mo isotopes were chosen because of their relatively low abundance in the Mo mass spectrum (9.55%, 9.63%, respectively; Figure 2.6), which leaves the more abundant ^{95}Mo (15.89%) and ^{98}Mo (24.23%) isotopes unspiked, and gives the best potential for high voltages on all ratios during measurement (Johnson and Bullen, 2004). Both ^{95}Mo and ^{97}Mo have no direct isobaric interferences, and ^{95}Mo is traditionally used as the denominator isotope. ^{96}Mo is avoided in the spike equations because of potential interferences from both Ru and Zr.

The optimal ratio of the two spikes was determined by assessing the error magnification that would result from different mixtures, as follows:

(2.3)

$$E(m)=\left[\left(\frac{97}{100}\right)_m\times\left(\left(\frac{97}{100}\right)_s-\left(\frac{97}{100}\right)_{sp}\right)\right]\div\left[\left(\left(\frac{97}{100}\right)_s-\left(\frac{97}{100}\right)_m\right)\times\left(\left(\frac{97}{100}\right)_m-\left(\frac{97}{100}\right)_{sp}\right)\right]$$

Where subscripts m, s, and sp refer to measured, sample, and spike ratios, respectively. A 1:1 mix results in an error magnification of 1.012 (Figure 2.7).

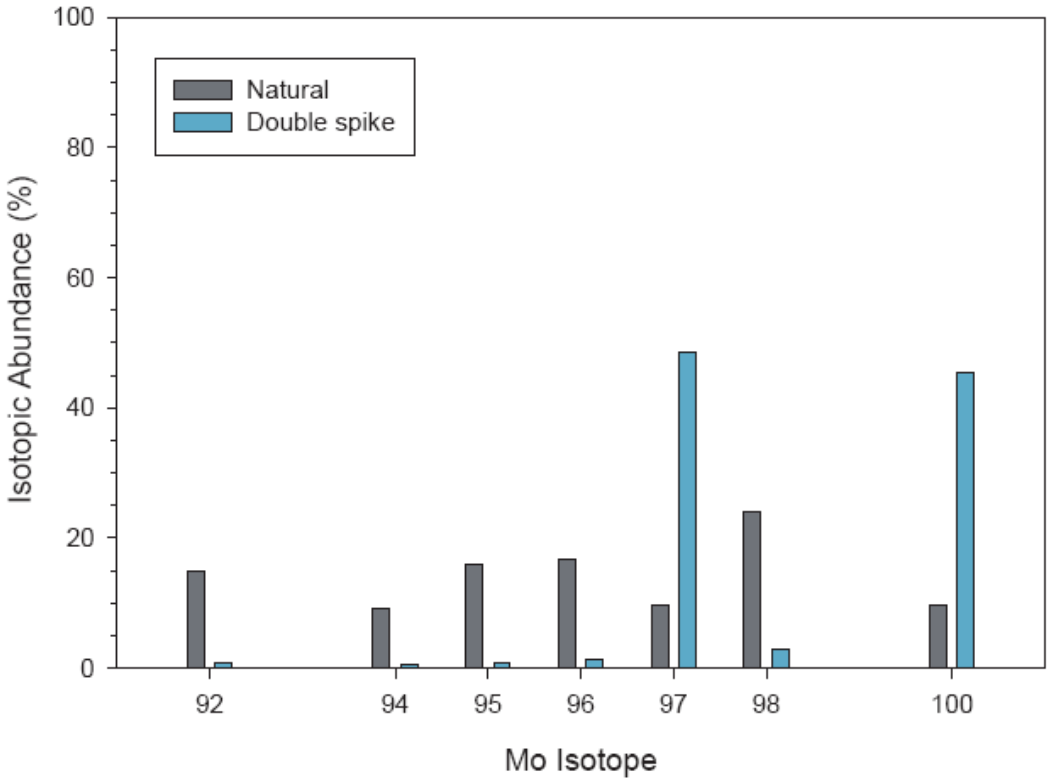

Figure 2.6: Natural Mo isotope abundances (grey) and the isotope abundances of the UMD double spike (blue).

Lower error magnification values (1.011) are possible with different mix ratios, but only a 1:1 mix minimizes the error for both $^{97}Mo/^{100}Mo$ and $^{100}Mo/^{97}Mo$ simultaneously. Further considerations that make a spike mix of 1:1 optimal are higher measurement precision of ratios close to 1, as opposed to very large or small ratios (Galer, 1999; Johnson and Bullen, 2004), and that such a ratio is close to the natural ratio (Siebert et al., 2001). The range of measured masses that results from this alternation of unspiked and spiked isotopes (^{95}Mo, ^{97}Mo, ^{98}Mo, ^{100}Mo) gives a minimum error multiplier of 0.47, according

to the formula given by Dodson (1969), as opposed to the error multiplier for ^{96}Mo, ^{97}Mo, ^{98}Mo, ^{100}Mo (0.6):

$$E(m)^2 = (\Delta Mass_{97,\ 100})^{-2} + (\Delta Mass_{95,\ 98})^{-2} \quad (2.4)$$

where the first difference term is for the spike masses, and the second for the non-spike masses. Double-spike schemes which utilize other spike isotopes (e.g., ^{92}Mo-^{98}Mo; Wieser and DeLaeter, 2009) can yield lower error multipliers (0.26), but the measurement program and instrumentation used for this study would make such a mix more difficult to measure, and prone to greater measurement errors.

After the optimal spike ratio was found, the best sample:spike ratio was calculated. It was determined that a small amount of underspiking quickly leads to large error amplification, but overspiking does not. The main problem with overspiking appears to be large additions of ^{95}Mo to the mix from the spike. The ideal mix was found to be around 1:1 spike to sample, which has an error magnification of 1.28 (Fig. 2.8). Ratios of 0.6 to 4 also have low error magnification (<1.4). However, a ratio of 4 leads to unacceptably high contributions to ^{95}Mo from the spike. Ideally, an optimal mix is attained when >90% of the spike isotopes come from the spike and >90% of the unspiked isotopes come from the sample (Johnson and Bullen, 2004). This can be easily demonstrated with an example: for a measured δ^{98}Mo value of 0.1‰,

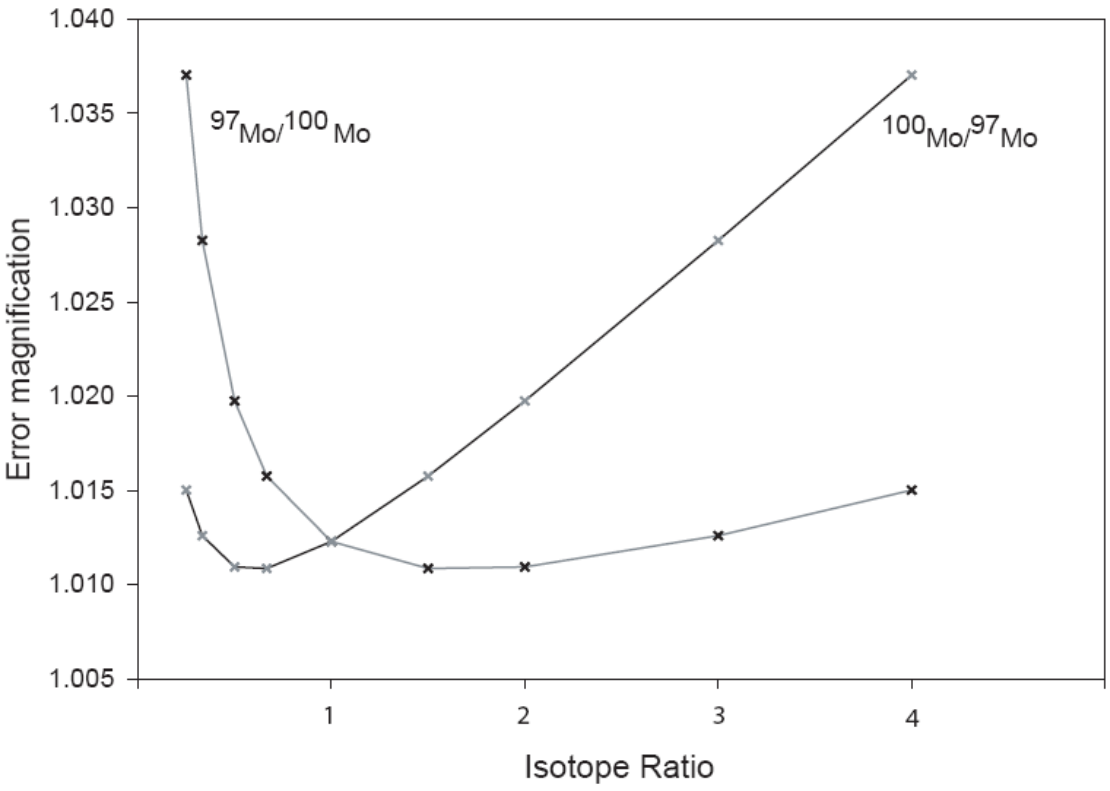

Figure 2.7: Error magnification due to changes in the ratio of ^{97}Mo to ^{100}Mo. The ideal ratio of the two spikes in the final mixed double spike is at the intersection of the two curves, at which point the error magnification is minimized for both curves (1.012). This results in a 1:1 mix of ^{97}Mo to ^{100}Mo.

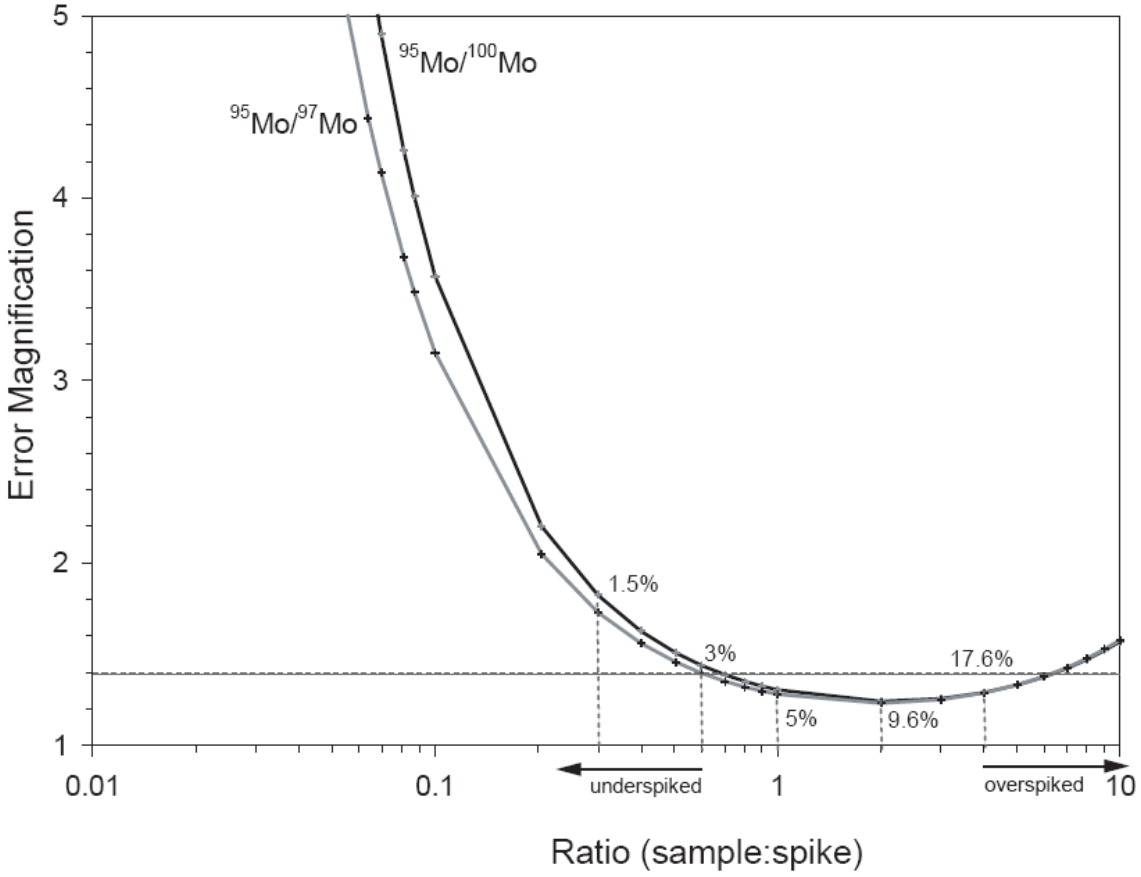

Figure 2.8: Error magnification for sample:spike mixes, where the spike is of the optimal 1:1 composition shown in Fig. 2.7. Vertical lines connect sample:spike ratios to the percent contributions of ^{95}Mo from the spike for that ratio. The horizontal line is an error magnification of 1.4. A sample:spike ratio of 1 is ideal, as this minimizes both the error magnification (1.28) and the contribution to ^{95}Mo from the spike (~5%). A ratio of 2 results in a lower error magnification (1.23) but has a 9.6% contribution to ^{95}Mo from the spike. Arrows indicate direction of, and location where, overspiking and underspiking occur.

an error magnification of 1.28 results in a value of 0.128‰, which changes the value by much less than the external reproducibility. An implication of this result is that in order to avoid over/underspiking the Mo concentration of the sample should be known to within 10%.This necessitates a preliminary concentration measurement for each sample.

The concentration of the final double spike was chosen in order to minimize the amount of spike needed for most samples, but also avoid having to measure out very small quantities of spike. Once this was determined, the two concentrated single spikes were mixed together and diluted to approximately one liter with ultra-pure, low-molarity nitric acid. All masses were precisely weighed with a timed evaporation correction and the balance was calibrated before weighing commenced. The mixed double spike was allowed to equilibrate for ~36 hours.

The composition and concentration of the double spike was determined by creating a series of mixes with varying proportions of double spike and wire standard with a known concentration of 1.922 µg/g (Table 2.3). Teflon beakers were carefully weighed 5 times, and then aliquots of the wire standard and double spike were added (separately) and weighed accurately to 5 decimal places by timed evaporation correction. These mixes covered a range from pure double spike to pure wire (Fig. 2.9). The Mo concentration of the double spike was determined by calculating its concentration in each mix using isotope dilution calculations, treating the wire standard as the ‘spike’ and the double spike as the ‘unknown’. Thus the Mo concentration of the

double spike was determined to be 29.3944 (± 0.035, 2 s.d.). The fractionation-corrected composition of the final double spike is given in Table 2.4. This was determined by correcting the measured ratios for each isotope pair of each mix, to the expected value of the ratio based on the proportions in the mix and the previously established compositions of the single spikes and the wire standard. The data acquisition routine designed to perform the Mo isotope measurements using the UMD Nu-Plasma MC-ICP-MS is shown in Table 2.5. The three ratios used are $^{95}Mo/^{98}Mo$, $^{97}Mo/^{98}Mo$, and $^{100}Mo/^{98}Mo$. The geometric approach (described on pages 43-45, illustrated in Figures 2.2 and 2.3) was refined specifically for Mo by Siebert et al. (2001). The Siebert et al. solution requires nested iterations to refine initial the starting values for coefficients for natural and instrumental fractionation, and sample and standard values, until there is convergence upon a "true" value for the sample isotopic composition. This approach was converted to a MATLAB program by Jasper Konter. This program performs 1000 nested iterations and incorporates the 1 s.e. measurement errors for each ratio. The 'assumed' parameters used are the ratios for the wire standard, and estimates of the degree of natural and instrumental fractionation (0.5 for both).

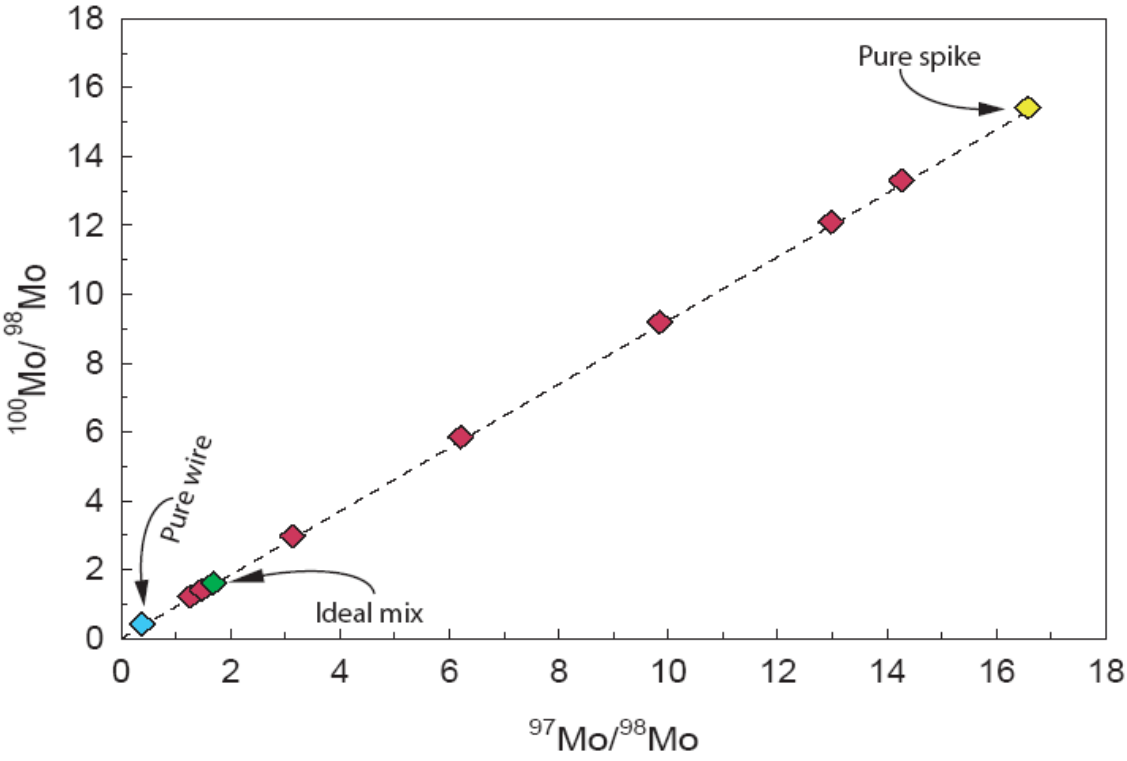

Figure 2.9: The composition of the final double spike, the pure wire standard, and mixes in ^{97}Mo/^{98}Mo and ^{100}Mo/^{98}Mo space. The ideal mix (1:1 spike Mo to sample Mo) is also shown.

Table 2.3: Fractionation-corrected ratios for the mixes of double spike and Mo wire. Mix D is the ideal sample:spike ratio. The instrumental background noise has been subtracted from the ratios. The 1 s.e. is the instrumental error on that ratio during measurement.

Mix (spike µg:wire µg)	92/98	1 s.e.	94/98	1 s.e.	95/98	1 s.e.	96/98	1 s.e.	97/98	1 s.e.	100/98	1 s.e.
Pure wire	0.52901	2.8E-05	0.34680	1.2E-05	0.61261	1.6E-05	0.65556	9.8E-06	0.38619	4.1E-06	0.41836	7.6E-06
Mix A (0.7)	0.58830	1.7E-05	0.36731	7.0E-06	0.63526	1.0E-05	0.67197	8.3E-06	1.27031	9.2E-06	1.21711	1.7E-05
Mix B (0.9)	0.58376	3.7E-06	0.36434	1.9E-06	0.63035	3.0E-06	0.66918	3.0E-06	1.48045	6.3E-06	1.41333	7.6E-06
Mix D (1.1)[a]	0.57901	5.5E-06	0.36123	2.8E-06	0.62538	3.4E-06	0.66581	3.0E-06	1.68754	6.2E-06	1.60699	5.8E-06
Mix E (2.5)	0.54462	5.6E-06	0.33916	3.5E-06	0.58999	3.9E-06	0.64136	4.6E-06	3.13855	1.8E-05	2.97007	2.1E-05
Mix F (6.9)	0.47765	6.3E-06	0.29520	3.5E-06	0.51855	5.9E-06	0.59353	7.2E-06	6.21223	5.9E-05	5.85091	7.6E-05
Mix G (17.2)	0.40669	7.0E-06	0.24614	4.8E-06	0.43827	7.8E-06	0.53759	6.8E-06	9.84649	1.3E-04	9.18503	1.2E-04
Mix H (43.0)	0.33888	7.8E-06	0.20120	6.6E-06	0.36544	7.4E-06	0.48834	1.1E-05	12.98074	2.9E-04	12.09771	2.3E-04
Mix J (73.9)	0.31077	1.0E-05	0.18265	8.0E-06	0.33537	9.6E-06	0.46784	9.3E-06	14.26339	3.9E-04	13.29812	3.7E-04
Pure D.S.	0.26204	1.4E-05	0.14991	8.7E-06	0.28251	1.4E-05	0.43108	1.1E-05	16.57465	3.8E-04	15.41567	3.6E-04

[a]Ideal mix

Table 2.4: Isotopic composition of the single spikes and the final double spike.

Mo isotope	$^{97}Mo_{spike}$	$^{9x}Mo/^{98}Mo$ in $^{97}Mo_{spike}$[a]	$^{100}Mo_{spike}$	$^{9x}Mo/^{98}Mo$ in $^{100}Mo_{spike}$[a]	$^{97}Mo/^{100}Mo$	$^{9x}Mo/^{98}Mo$ in DS[b]
^{92}Mo	0.00189	0.05743	0.01145	0.48368	0.00758	0.26204
^{94}Mo	0.00175	0.05282	0.00622	0.26140	0.00435	0.14991
^{95}Mo	0.00448	0.12781	0.01088	0.45089	0.00821	0.28251
^{96}Mo	0.01214	0.34425	0.01211	0.49649	0.01246	0.43108
^{97}Mo	0.94203	26.52343	0.00761	0.31138	0.048463	16.57465
^{98}Mo	0.03442	1	0.02379	1	0.02927	1
^{100}Mo	0.00328	0.09079	0.92794	36.89286	0.45350	15.41567

[a] Measured ratios internally fractionation corrected for β = 1.7178.
[b] Double spike

Table 2.5: The Faraday detector arrangement for an Mo isotope measurement. The instrument measures each requested isotope ratio 15 times per block, for a total of 4 blocks, with zeroes at half-mass after every block. The program centers the axial peak (Ax) before each block. A gain calibration was run on each day that measurements were made. After a minimum two hours of warm-up time, the instrument was tuned to at least 2v on ^{98}Mo for all measurements. Zirconium and Ru, which overlap the Mo mass spectrum, were monitored on one isotope each (90 and 99, respectively) to ensure that no direct interferences were occurring from these elements. All ratios were measured to internal precision better than 0.01% (2σ).

Detector	H6	H5	H4	H3	H2	H1	Ax	L1	L2	L3	L4	L5
Zero 1	99	98	97	--	96	--	95	--	94	93	92	91
Zero 2	97.55	96.55	95.55	--	94.55	--	93.55	--	92.55	91.55	90.55	89.55
Cycle 1	99.55	98.55	97.55	--	96.55	--	95.55	--	94.55	93.55	92.55	91.55

Long term result for standards with the double spike method

A summary of the data acquired for our in-house reference materials illustrates the performance of the double spike over the two years of its use. The baseline for double spike measurements is a mix of the plasma standard and the double spike. This is measured every session, and long-term reproducibility of its delta value is, as expected, very high (Table 2.6). This procedure also provides a fractionation-corrected $^{98/95}$Mo ratio for the standard. Delta values were calculated by comparing the reduced sample $^{98/95}$Mo ratio to the $^{98/95}$Mo ratio for an in-house Johnson-Matthey Company SpecPure® Mo plasma standard (Stock #35758, Lot #013186S). The SpecPure® Mo plasma standard is frequently used in the literature as the standard reference to calculate a delta value for seawater (+2.3‰, Siebert et al., 2003).

This procedure provided an additional check on long-term instrument performance with respect to Mo isotopes, through comparison of δ^{98}Mo values for the Mo standard. Similarly, a mix of a proposed NIST Mo solution standard (Table 2.7) and the double spike was measured in two different sessions a year apart, and have very high reproducibility (Table 2.8).

The performance of the Nu- plasma is monitored in part by an internal fractionation correction measured with an the Mo plasma standard. An internal fractionation factor is calculated for $^{98/95}$Mo which is then used to calculate corrected values for $^{92/95}$Mo, $^{97/95}$Mo, and $^{100/95}$Mo. Epsilon values are then calculated for these fractionation corrected ratios. While the value that is used as the standard in the epsilon equation is arbitrary, the

expectation exists that the instrument be able to obtain results within half an epsilon unit of the nominal value. If this is not the case, additional tuning is performed.

In addition to SDO-1 and NAS, multiple aliquots of Fairhaven sediment and a Mediterranean sapropel sample (969D 4H-2, 131) have been processed. Long-term external reproducibility of two in-house rock reference standards is ±0.2‰ for δ^{98}Mo at the 2σ level (Fig. 2.10, table 2.9). Five separate analyses of the Fairhaven sample yield variance of 15.5 ±0.1 µg/g in concentration and δ^{98}Mo +0.94‰ ±0.09 (2σ). One of the rock standards, USGS SDO-1, has published Mo isotope values of δ^{98}Mo +1.16‰ ± 0.1 (2σ) and +1.2 ± 0.3 (2σ) (Wasylenki et al., 2008; Poulson-Brucker et al., 2009). Our δ^{98}Mo value of +0.88‰ ± 0.19 (2σ, n = 54) is offset to a slightly lower value by ~0.3‰, which is just within the published errors. The offset, if real, could be due to isotopic differences between batches of SpecPure® Mo, or, more unlikely, to heterogeneity in the SDO-1 standard. Inter-lab comparison of results is stifled by the lack of a true isotopic standard, and the differences in isotopic values of a rock standard emphasizes the need to establish a bona-fide isotopic reference material.

The results for these reference materials appear to have better reproducibility over the relatively short periods of time, for example in a three-day measurement session, as opposed to month to month. This can be seen in Fig. , where clusters of analyses with similar δ^{98}Mo values are apparent. These clusters often are indicative of data collected within a short span of time.

Table 2.6: Data for measurements of the mix of double spike plus Mo plasma standard. 1 s.e. are instrumental errors. All measurements made with the Apex unless otherwise noted. The average δ^{98}Mo is -0.07‰ (±0.05, $2\sigma_{mean}$).

	100/98	1 s.e.	97/98	1 s.e.	95/98	1 s.e.	95/98 (reduced)	δ^{98}Mo
Ds/Ps[a]	1.84702	3.2E-5	1.84331	2.2E-5	0.58847	1.1E-5	0.65596	-0.28
Ds/Ps	1.84860	3.1E-5	1.84243	2.2E-5	0.58747	7.7E-6	0.65568	0.16
Ds/Ps	1.84893	3.7E-5	1.84251	1.6E-5	0.58742	7.5E-6	0.65572	0.09
Ds/Ps	1.84508	3.7E-5	1.84371	4.0E-5	0.58926	1.6E-5	0.65600	-0.34
Ds/Ps[b]	1.83860	1.1e-4	1.84727	7.1e-5	0.59234	5.0e-5	0.65571	0.11
Ds/Ps[c]	1.86194	3.8E-5	1.86481	2.0E-5	0.58994	1.4E-5	0.65581	-0.04
Ds/Ps	1.86223	4.0E-5	1.86470	2.3E-5	0.58982	1.8E-5	0.65582	-0.06
Ds/Ps	1.86205	3.0E-5	1.86473	1.6E-5	0.58989	1.3E-5	0.65582	-0.06
Ds/Ps	1.86220	4.7E-5	1.86464	2.3E-5	0.58988	1.8E-5	0.65591	-0.20
Ds/Ps	1.86254	4.1E-5	1.86455	2.1E-5	0.58974	1.5E-5	0.65591	-0.19
Ds/Ps	1.86267	7.8E-5	1.86444	3.7E-5	0.58961	3.3E-5	0.65583	-0.08
Ds/Ps	1.86140	2.7E-5	1.86510	1.8E-5	0.59018	1.2E-5	0.65576	0.03
Ds/Ps[d]	1.86336	4.0E-5	1.86425	2.0E-5	0.58931	1.6E-5	0.65582	-0.07
Ds/Ps	1.86413	5.0E-5	1.86382	2.6E-5	0.58899	2.5E-5	0.65591	-0.2
Ds/Ps	1.86476	2.4E-5	1.86359	1.7E-5	0.58864	1.0E-5	0.65581	-0.05
Ds/Ps	1.86350	3.1E-5	1.86442	1.4E-5	0.58937	1.0E-5	0.65591	-0.2
Ds/Ps[e]	1.86327	5.2E-5	1.86302	4.8E-5	0.58891	2.3E-5	0.65574	0.07
Ds/Ps	1.86090	6.9E-5	1.86474	4.0E-5	0.59025	2.3E-5	0.65578	-0.01
Ds/Ps	1.86324	7.3E-5	1.86373	4.3E-5	0.58908	2.5E-5	0.65565	0.20
Ds/Ps	1.85682	8.4E-5	1.85549	6.3E-5	0.58872	3.3E-5	0.65567	0.17
Ds/Ps[f]	1.85206	5.2E-5	1.85458	4.5E-5	0.59013	2.3E-5	0.65582	-0.06
Ds/Ps	1.85755	3.9E-5	1.85369	3.3E-5	0.58808	1.6E-5	0.65589	-0.18
Ds/Ps[g]	1.86682	1.7E-4	1.85679	1.6E-4	0.58594	1.2E-5	0.65588	-0.15
Ds/Ps	1.86948	5.0E-5	1.85929	4.0E-5	0.58584	7.2E-6	0.65590	-0.18
Ds/Ps	1.87022	2.1E-5	1.86014	2.3E-5	0.58583	8.0E-6	0.65587	-0.14
Ds/Ps[h]	1.86741	4.3E-5	1.86165	2.3E-5	0.58718	1.8E-5	0.65580	-0.04
Ds/Ps	1.86742	4.8E-5	1.86188	2.4E-5	0.58724	2.0E-5	0.65581	-0.06
Ds/Ps	1.86764	4.7E-5	1.86133	2.4E-5	0.58717	1.1E-5	0.65584	-0.09

[a]April 29, 2008, [b]May 14, 2008, [c]June 2, 2009,
[d]June 4, 2009, [e]July 8, 2009, [f]July 31, 2009,
[g]Aug 14, 2009 (Aridus), [h]September 7, 2009
$^{98/95}$Mo to calculate δ^{98}Mo: 1.524905

Table 2.7: Data for the potential NIST 3134 Mo standard. Note the high precision of the epsilon values (parts in ten thousand difference). Epsilon calculated with the ratios given in the footnotes.

	97/95	**1 s.e.**	98/95	**1 s.e.**	100/95	**1 s.e.**	β98/95	97/95 fc	$\varepsilon^{97}Mo$[a]	100/95 fc	$\varepsilon^{100}Mo$[b]	92/95 fc	$\varepsilon^{92}Mo$[c]
N-1	0.62501	1.3E-05	1.61164	4.2E-05	0.66861	2.9E-05	-1.787495	0.60214	-3.04	0.60998	-1.50	0.92692	7.91
N-2	0.62501	1.6E-05	1.61164	5.9E-05	0.66860	3.9E-05	-1.787364	0.60214	-3.12	0.60997	-1.71	0.92712	10.12
N-3	0.62500	1.3E-05	1.61162	4.6E-05	0.66861	3.0E-05	-1.787022	0.60212	-3.33	0.60995	-1.94	0.92706	9.41
N-4	0.62500	1.1E-05	1.61167	3.9E-05	0.66861	2.6E-05	-1.788021	0.60213	-3.28	0.60996	-1.79	0.92713	10.16
N-5	0.62502	1.5E-05	1.61168	5.0E-05	0.66863	3.3E-05	-1.788254	0.60213	-3.16	0.60995	-2.06	0.92715	10.44

[a] $^{97/95}$Mo: 0.602324
[b] $^{100/95}$Mo: 0.610072
[c] $^{92/95}$Mo: 0.926184

Table 2.8: Data for NIST 3134 Mo, mixed with the double spike during two different measurement sessions. Average δ^{98}Mo for the entire data set is +0.114 (±0.2, 2σ). However, for measurements *a-e*, the average is +0.03 (±0.06, 2σ), and for *f-k*, the average is 0.22 (±0.06, 2σ).

	100/98	**1 s.e.**	**97/98**	**1 s.e.**	**95/98**	**1 s.e.**	**95/98 (reduced)**	**δ^{98}Mo**
Nist + DS (a)[a]	2.08420	5.4E-05	2.08325	4.1E-05	0.58258	1.5E-05	0.65566	0.182
Nist + DS (b)	2.08454	3.2E-05	2.08343	2.4E-05	0.58252	1.3E-05	0.65564	0.217
Nist + DS (c)	2.08459	3.8E-05	2.08343	2.9E-05	0.58251	1.3E-05	0.65565	0.194
Nist + DS (d)	2.08457	3.8E-05	2.08346	2.3E-05	0.58251	1.3E-05	0.65562	0.238
Nist + DS (e)	2.08443	6.8E-05	2.08345	3.5E-05	0.58254	2.0E-05	0.65562	0.249
Nist + DS (f)[b]	2.10689	7.2E-05	2.10092	6.3E-05	0.58072	1.2E-05	0.65577	0.018
Nist + DS (g)	1.72219	1.7E-05	1.71042	1.6E-05	0.58917	7.2E-06	0.65578	0.004
Nist + DS (h)	1.72230	2.2E-05	1.71038	1.8E-05	0.58909	6.1E-06	0.65574	0.053
Nist + DS (i)	1.72227	2.4E-05	1.71030	2.1E-05	0.58906	8.1E-06	0.65573	0.079
Nist + DS (j)	1.72202	2.1E-05	1.70984	1.6E-05	0.58904	7.1E-06	0.65578	-0.003
Nist + DS (k)	1.72195	2.0E-05	1.70988	2.0E-05	0.58906	8.8E-06	0.65577	0.019

[a] NIST 3134 *a-e*, June 9, 2008, Apex.
[b] NIST 3134 *f-k,* Aug 14, 2009, Aridus.

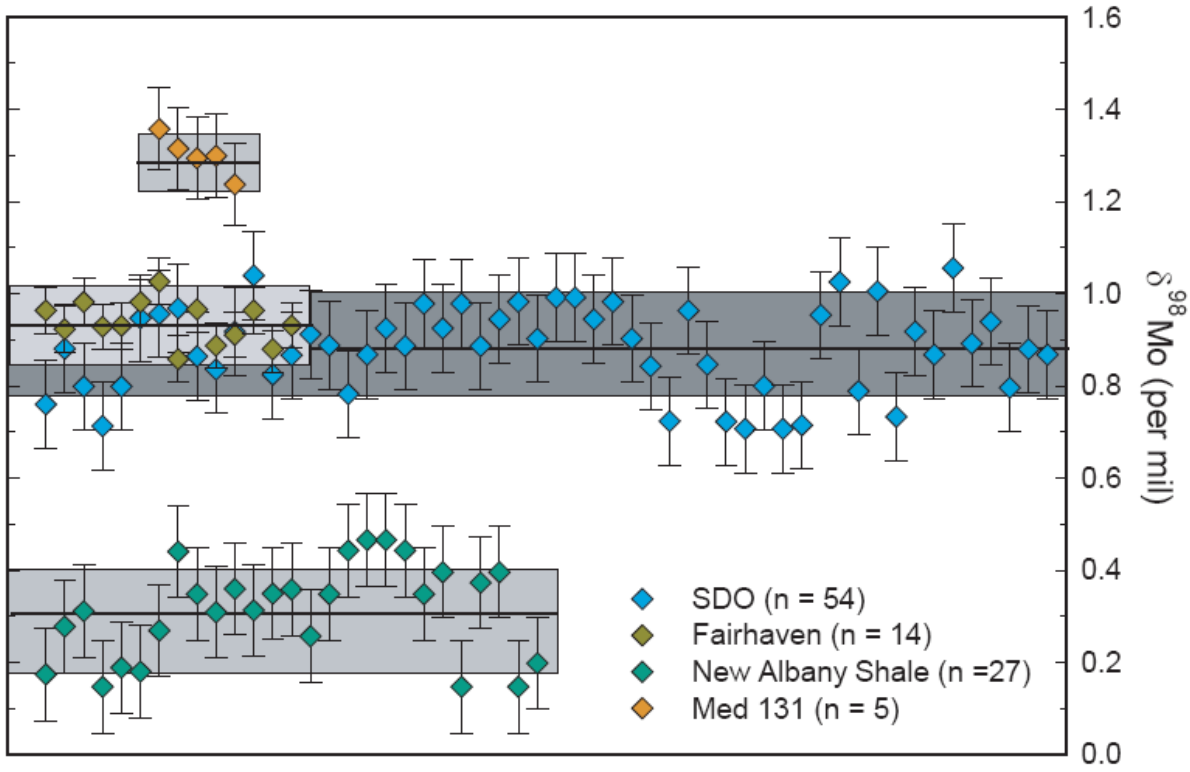

Figure 2.10: δ^{98}Mo values for two sediment reference materials and two sample materials. Each material was processed several times. The grey boxes are the 2σ standard deviation of the data (Table 2.9). The black lines are the average of the data. For the Med 131 data, see chapter 4.

Table 2.9: Long-term external reproducibility for sediment reference materials using the Mo double spike. NAS was digested 10 times, SDO-1 was digested 11 times,and the Fairhaven sediment was digested 5 times.

NAS	$\delta^{98}Mo$	**SDO-1**	$\delta^{98}Mo$	**Fairhaven**	$\delta^{98}Mo$
Average	+0.31	Average	+0.88[a]	Average	+0.94
1σ	0.103	1σ	0.094	1σ	0.046
2σ	0.20	2σ	0.19	2σ	0.09
2σ mean (n = 27)	0.040	2σ mean (n = 54)	0.025	2σ mean (n = 14)	0.024

[a]Compare the reproducibility and average for SDO to Table 2.2.

Column chemistry and sample preparation

Column Chemistry

A two-column chromatographic separation consisting of anion-exchange and cation-exchange steps, was used to purify samples containing complex matrices of organic matter, clay and silicate (Pietruszka et al., 2006). The anion chemistry accomplishes stepwise separation of such matrix elements as Fe^{3+}, Al, K, and Zr from retained Mo, while the cation column retains the matrix elements and does not retain Mo in the correct acid strength. Initially, the Teflon columns used for anion separate were 34 cm long with a 0.6 cm i.d. The teflon columns used for cation separation were 12 cm long with a 0.6 cm i.d. Each type of column was fitted with a frit and Teflon dripper. These columns held ~10 ml and ~3.5 ml of resin, respectively. To ensure low blank, the anion resin was batch-cleaned thoroughly prior to use, using 8M HNO_3, 6M HCl, and 1M HCl, sequentially, with 2 rinse steps in distilled de-ionized water between each acid. A second cleaning of the anion resin was performed in the column just prior to sample addition by rinsing with three different strengths of HCl. Acid strengths were checked at room temperature using a densitometer.

To ensure complete separation from other elements and high Mo yield off the anion column (to avoid fractionation on the column), large volumes of acid were used during the processing (e.g., 120 ml of 1M HCl and 50 ml of 5M HNO_3 were used to elute Mo). This method was altered after it was found that almost all the Mo is eluted with the first 30 ml of 1M HCl, making the use of 5M HNO_3 as an Mo eluent superfluous (Fig 2.11 and table 2.10). The anion

resin was discarded after each sample, but the cation resin was cleaned with 250 ml of 6M HCl, and reused. Using this procedure, a set of 6 samples took more than a week to prepare for analysis, because of the long time each acid took to drip through the column, and the time needed to reduce 170 ml of eluent to dryness on a 90℃ hot plate, in order to pr oceed to the next step.

Eventually, the need to process a large number of samples in shorter time necessitated changing the column chemistry. The size of column used was the main alteration; the overall sequence of acids was not changed. In lieu of the Teflon columns, Biorad polyproplyene (Poly-prep™) disposable columns with a 2 cm resin bed and 10 ml sample reservoir and porous 20 μm hydrophilic polymer frit were employed for both the anion and cation chemistry. Accordingly, the volumes of acid needed to achieve a quantitative Mo yield were much less (Tables 2.11 and 2.12). The small quantity of resin used (~2-3 ml) meant that saturating the resin with ions might be a problem. However, the small sample quantities that were generally dissolved and passed through the column were well under the resin capacity

A second change was the addition of a third column. This last column was a scaled-down version (1/10 the size) of the starting anion column, and its purpose was to remove the last traces of Fe, Zr, and other elements remaining after the cation separation. The sequence of acids used to accomplish the separation was not changed significantly in the 3 column procedure compared to the two-column procedure . The time required for the

three-column process was ~4 days from start to finish, and up to 20 samples could be processed simultaneously.

After the Mo was separated and dried, a small amount of aqua regia was added. This was done to destroy any organic residue that may have been added to the sample from the resin (Pietruszka and Reznick, 2008). Just prior to analysis, the separated Mo was dissolved in an appropriate amount of 2% nitric acid and refluxed on a hot plate. Digestion and column blanks were assessed by passing a known amount of ^{97}Mo spike through the digestion and column separation chemistry. Blanks for the 3-column chemistry ranged between 2 and 6 ng Mo, comprising less than 1% of the total Mo for any sediment samples.

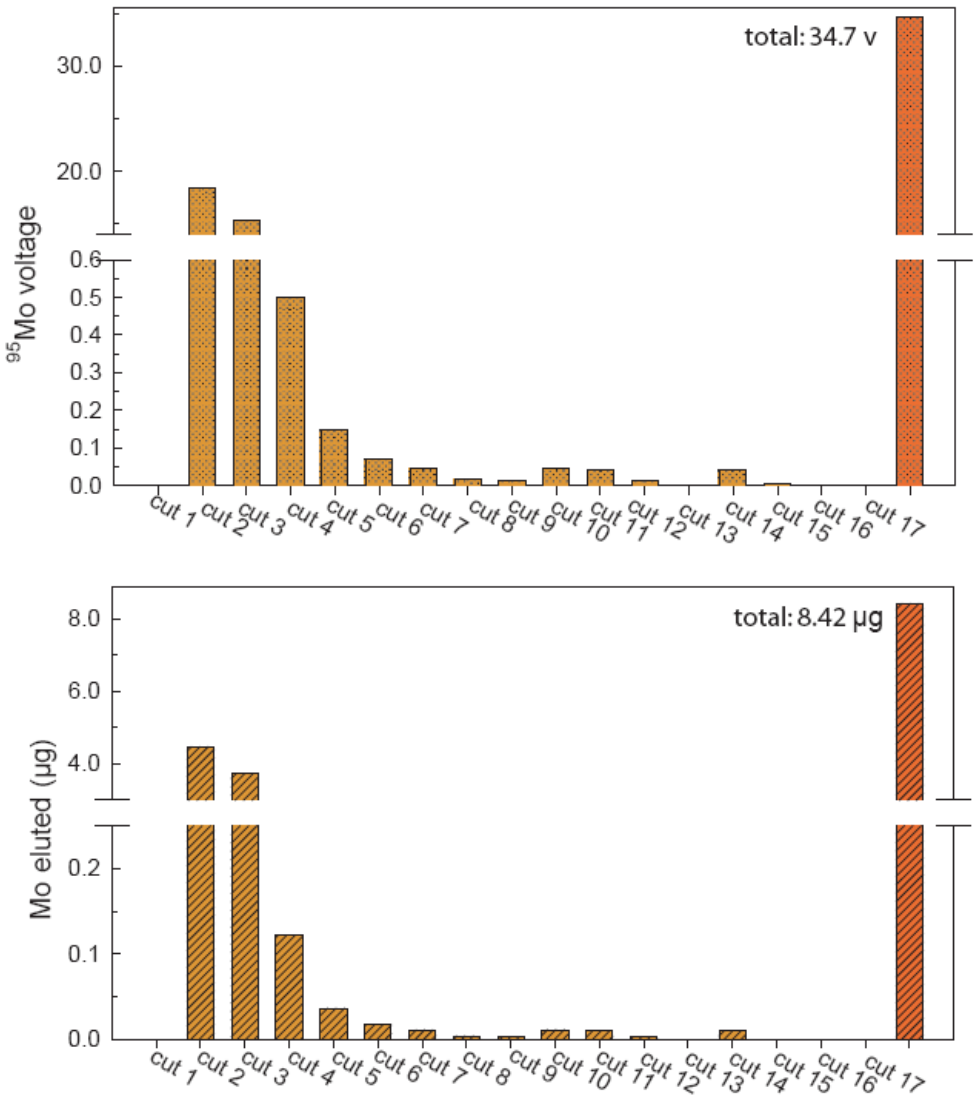

Figure 2.11: Test of Mo elution in the anion column. The test used 0.01452g of NAS, resulting in 8.4216 ug of Mo in the sample. Cuts 1-12 are 1M HCl, while cuts 13-17 were 5M HNO_3. Each cut was 10 ml.

Table 2.10: Test of Mo elution in the first anion column. Over 90% of the Mo was eluted in the second and third cuts.

Cut[a]	Volts ^{95}Mo	% volt.	ug	% ug
cut 1	0	0	0	0
cut 2	18.4	53.02	4.465	53.017
cut 3	15.4	44.28	3.729	44.278
cut 4	0.5	1.441	0.121	1.441
cut 5	0.15	0.432	0.036	0.432
cut 6	0.07	0.202	0.017	0.202
cut 7	0.045	0.130	0.011	0.130
cut 8	0.016	0.046	0.004	0.046
cut 9	0.012	0.035	0.003	0.035
cut 10	0.047	0.135	0.011	0.135
cut 11	0.04	0.115	0.010	0.115
cut 12	0.013	0.037	0.003	0.037
cut 13	0	0.000	0.000	0.000
cut 14	0.043	0.124	0.010	0.124
cut 15	0.0023	0.007	0.001	0.007
cut 16	0	1.441	0	0
cut 17	0	0.432	0	0
Total	34.695	99.9994	8.4216	100

[a]Cuts 1-12 were 1M HCl, cuts 13-17 were 5M HNO_3.

Table 2.11: Anion column chemistry sequence. A third column repeats this sequence with one-tenth of the resin volume.

Anion column	Acid strength/volume
Load Resin	Pre-cleaned 2 ml AG 1x8 (200-400 mesh, Cl-)
Condition	0.01M HCl (10 ml)
Condition	1M HCl (10 ml)
Condition	6M HCl (10 ml)
Load sample	6M HCl (1-4 ml)
Rinse Zr, etc.	6M HCl (18 ml)
Rinse Fe, etc.	0.01M HCl/0.1M HF (18 ml)
Elute Mo	1M HCl (14 ml) → evaporate to dryness
Reconstitute dried sample	6M HCl (4 ml)

Table 2.12: Cation column chemistry sequence.

Cation column	Acid strength/volume
Load resin	2 ml AG 50Wx8 (200-400 mesh)
Load sample	1.4M HCl (2 ml)
Elute Mo	1.4M HCl (12 ml)

Sediment sample preparation

Sediment samples were prepared by grinding to a fine powder in a ceramic mortar. Organic-rich powders were combusted at 500℃ in a muffle furnace for 5-6 hours. It was determined that Mo is not lost during the combustion process and does not alter the isotopic composition of samples, based on comparative tests of combusted and non-combusted rock standards. After combustion, ~200-500 mg of sample were weighed into 15 ml Teflon Savillex screw-cap beakers, and a ^{97}Mo-^{100}Mo double spike solution (29.39 µg/g Mo in 2% nitric acid) was weighed and added. Digestion proceeded sequentially at 90-120° on a hotplate, using first aqua regia, then HNO_3 plus concentrated HF, and lastly concentrated HCl, drying the sample between each step. The dissolution steps were repeated until the solution in the beaker was clear and free of visible particles. All acids except for HF were quartz distilled. The HF was Seastar™ Baseline®, which typically has Mo impurities of <5 pg/g.

Preparation of water samples

Due to the saline nature of the water samples that were collected from the Chesapeake Bay (Chapter 3), additional treatment was required before the samples could be processed via the standard column sequence (T. Dahl, personal communication). Chelating resin (Biorad Chelex-100) was stirred with 1 L of acidified sample, plus spike, for 24 hours (Table 2.13). In the case of the Susquehanna River, 5 L of water was used in order to obtain a

maximum amount of Mo for analysis. The resin was decanted, and Mo and other metals were eluted using NH_4OH. The sample was then passed through the standard column chemistry, as already described. A test of the sample yield revealed that the method was successful at removing close to 97% of the spike and sample Mo from the water, and that 90% of this Mo could then be retrieved from the chelating resin. The blank for one liter of distilled water was 0.22 µg, or approximately 4% of the sample Mo for the estuarine samples, but ~20% of the Mo in the river water.

Water samples from the Chesapeake Bay were collected in 1-gallon HDPE jugs by the Maryland Department of Natural Resources, during a research cruise August 18-19, 2008. The jugs were purchased sealed and filled with distilled water. Aboard ship, the distilled water was emptied, the jug was filled and emptied 3 times with the ambient water, and then filled and closed. It was determined that acid-leaching the jugs prior to the water collection was unnecessary, because there was no measurable Mo in the distilled water, or in a sample of 5% HNO_3 used to leach the plastic for ~24 hours. These two assessments were made using a Thermo E2 single-collector ICP-MS.

Water from the Susquehanna River was collected by the author on March 20, 2009, below the Conowingo Dam outflow. A 5-gallon HDPE carboy was used; this carboy was acid-leached for 4 days in 5% HNO_3, because it had previously been used for water sampling. The carboy was filled by

wading into the river, submerging the jug and emptying it 3 times, and then filling it.

Table 2.13: Chelating Resin chromatography sequence for water samples.

Chelating Chemistry	Treatment
Acidify 1L sample to pH 1	Conc. HNO_3
Add double spike	Low heat, equilibrate 36 hours
Buffer solution to pH 4.8-5.5	CH_3COONH_4
Add 6 ml Chelex-100	Stir 24 hours, then decant resin to a clean column
Elute Mo (and other metals)	4M NH_4OH (50 ml stepwise)
Dry, redissolve, proceed to anion column	2-4 ml 6M HCl

Chapter 3: Century-long record of Mo isotopic composition in sediments of a seasonally anoxic estuary (Chesapeake Bay)[2]

Abstract

A double-spike method was used to obtain Mo isotope data for sediments and waters of the seasonally anoxic Chesapeake Bay, and its primary tributary, the Susquehanna River. The dissolved Mo distribution in the estuary is non-conservative, reflecting minor Mo loss to the sediments, although removal of Mo to the sediments does not have a large influence on the isotopic composition of the water column. The δ^{98}Mo of dissolved Mo in most of the estuary is dominated by seawater. Six samples with salinity >15 have an average δ^{98}Mo = +2.17‰ (± 0.12), which agrees well with a δ^{98}Mo value for the CASS-4 seawater standard of +2.23‰. A single sample of Susquehanna River water has a δ^{98}Mo of +1.02‰, consistent with recent findings of positive δ^{98}Mo in rivers worldwide. Susquehanna river sediments, in contrast, have δ^{98}Mo ~ -0.1‰. The difference between the river water and sediment values implies that isotopic fractionation occurs within the river basin. The δ^{98}Mo values for estuarine sediments are offset from values in the overlying water. Most samples deposited before 1925 have δ^{98}Mo less than 0‰, similar to the Susquehanna sediments. Subsequently, there is an increase in the variability of δ^{98}Mo, with values ranging up to +0.8‰. The transition to increased variability coincides with the onset of authigenic Mo deposition, which was previously attributed to escalating summertime anoxia.

[2]This chapter has been published in Earth and Planetary Science Letters as Scheiderich, K., Helz, G.R. and Walker, R.J., 2010.

Authigenic Mo concentrations correlate poorly with δ^{98}Mo in core samples, suggesting that independent mechanisms influence the two parameters. Authigenic Mo concentrations may be controlled by shifting pore water H_2S levels, while δ^{98}Mo may be primarily affected by annual variations in Mn refluxing.

Introduction

Dissolved Mo in seawater, present almost entirely as MoO_4^{2-}, has an isotopic composition (δ^{98}Mo) that is believed to be as much as 2‰ heavier than Mo delivered from continental sources, such as clastic sediments and igneous rocks (Barling et al., 2001; Siebert et al., 2003). Manganese oxyhydroxides (henceforth MnO_x) are a major sink for Mo in oxygenated seawater (Bertine and Turekian, 1973), and it has been shown that the Mo adsorbed onto MnO_x is isotopically light relative to dissolved MoO_4^{2-} in the source solution (Barling et al., 2001; Barling and Anbar, 2004; Siebert et al., 2003; Wasylenki et al., 2008). This supports the idea that fractionation of Mo isotopes during adsorption to MnO_x is primarily responsible for the heavy isotopic composition of seawater (Barling et al., 2001; Barling and Anbar, 2004; Siebert et al., 2003).

This simple model has been used to interpret the oxygenation histories of ancient and modern oceans (e.g., Poulson et al., 2006; Wille et al., 2007), and freshwater systems (e.g., Malinovsky et al., 2007). Formation of MnO_x from dissolved Mn(II) requires a high oxidation potential and is, therefore, believed to have always required free O_2. Consequently, the history of free O_2

availability in the ocean can be potentially assessed with the aid of Mo isotopes in sedimentary rocks (Arnold et al., 2004; Pearce et al., 2008; Wille et al., 2007).

Complicating such interpretations is the discovery that authigenic Mo deposited in suboxic (O_2 < 10μM) environments is 1 to 2‰ lighter than seawater (Siebert et al., 2006). Since MnO_x is not deposited under suboxic conditions, at least one additional process for selectively removing light Mo isotopes from seawater must exist. This process probably contributes to the modern, heavy δ^{98}Mo value of seawater, and will have contributed to past seawater δ^{98}Mo values.

Fractionation during thiomolybdate formation is a second process that might influence δ^{98}Mo values in sediments from suboxic zones. Quantum mechanical calculations indicate that negative equilibrium isotopic fractionations on the order of -2 to -5‰ occur in the presence of sulfide, and could be detected if removal of Mo from seawater were incomplete (Tossell, 2005). In support of this idea, fractionation of up to -3‰ between dissolved and particulate Mo is observed under mildly sulfidic, but euxinic conditions in the Black Sea (Neubert et al., 2008).

The potential for using Mo isotopes to monitor paleoredox conditions may also be further complicated by the report of isotopic compositions heavier than 0‰ in a number of rivers (Archer and Vance, 2008). It has been assumed that the continents deliver material with Mo isotopic compositions close to 0‰, but this now appears to be overly simplistic. Generation of

isotopically heavy Mo in seawater can no longer be assumed to be a result of processes wholly internal to the ocean; continental weathering regimes are probably contributing through as-yet unidentified mechanisms. Therefore, to better understand Mo isotopes in the ocean, isotopic fractionation processes within estuaries and river basins must be investigated.

Estuaries represent the geochemical transition zone between river basins and the ocean. It is unknown what Mo isotopic fractionation processes might occur in estuaries, and how such processes might affect the isotopic composition of the ocean. This study provides the first survey of Mo isotopes in both the sediments and waters of an estuarine system. We report Mo concentrations and isotopic data from one of the largest and most extensively studied North American estuaries, Chesapeake Bay, located on the east coast of the United States (Fig. 3.1). During the 20th century, Chesapeake Bay underwent a change from a well oxygenated to a seasonally anoxic estuary (Adelson et al., 2001; Cronin and Vann, 2003; Hagy et al., 2004; Zimmermann and Canuel, 2002), making the historic pattern of Mo isotopes in Chesapeake Bay sediments of particular interest.

Sample descriptions

Water samples

Eight water samples from six stations in the main stem of the Chesapeake Bay were obtained (Fig. 3.1). The samples were collected August 12-13, 2008 by the Maryland Department of Natural Resources. At all stations, water was collected in distilled water leached 1-gallon HDPE jugs at mid-depth

(Table 3.1). At the two end-member stations, water was also collected within one meter of the bottom. Temperature, pH, salinity, and dissolved O_2 measurements were taken at depth during sampling. All Mo concentrations were determined the day after sampling, and Mo for isotopic composition measurements was processed 3-4 months later. No reagents were added before processing began. Water from the Susquehanna River was obtained March 19, 2009, in an acid-leached 5-gallon HDPE carboy. The water was collected from shore, below the outflow of the Conowingo Dam. Processing for Mo isotopes proceeded on the same day.

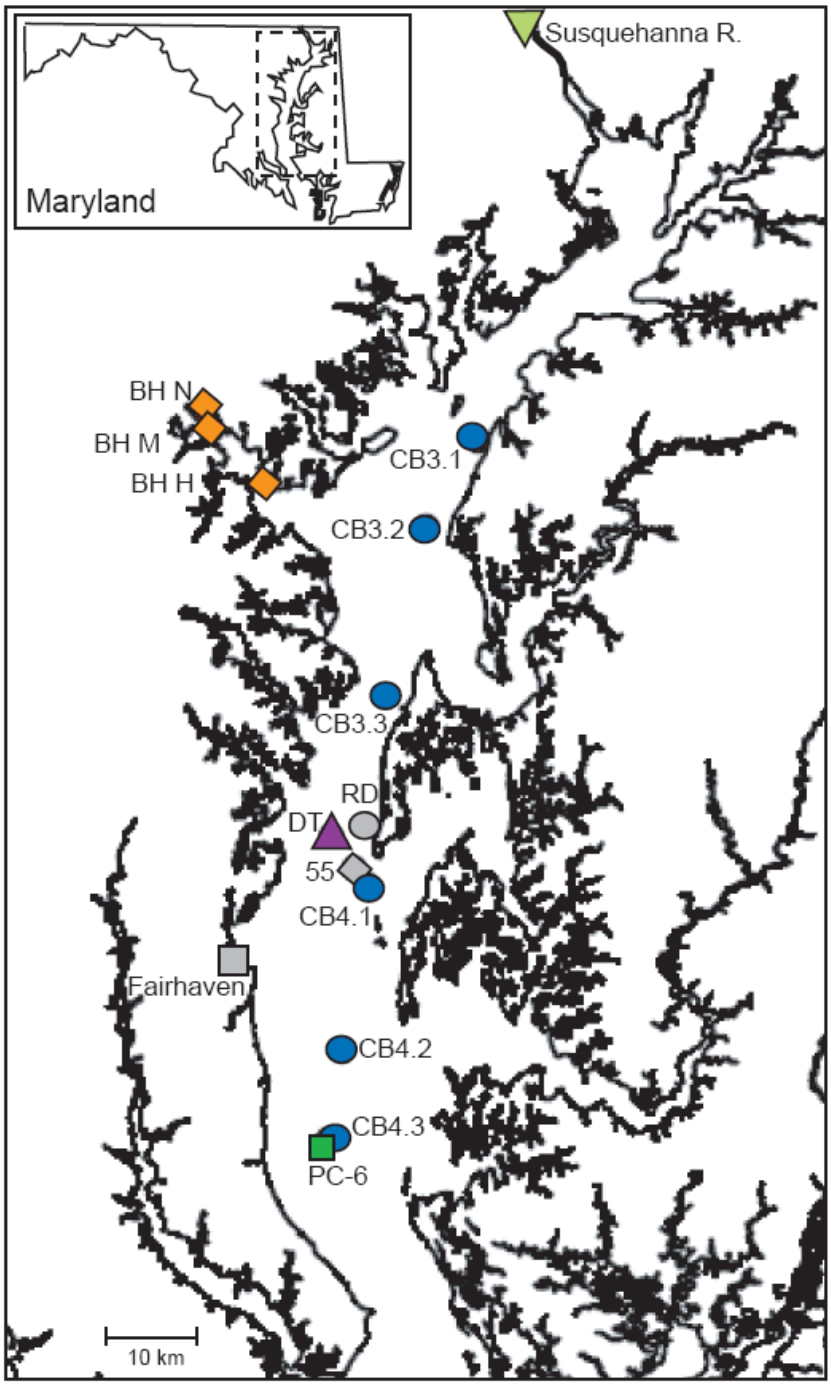

Figure 3.1: Chesapeake Bay and environs. Site locations for Chesapeake Bay water samples (blue circles), and sediments are shown. The green triangle is the location of both the Susquehanna River water sample and sediments. Other symbols are (North to South): orange diamonds- Baltimore Harbor; grey circle- Core RD; purple triangle- Depth Traverse; grey diamond- Core 55; grey square-- Fairhaven; green square- PC-6. The upper left inset map provides location of Chesapeake Bay in the state of Maryland.

Sediment samples

A total of forty sediment samples from seven sites (Fig. 3.1) in the Chesapeake Bay were analyzed for their Mo concentration and isotopic composition. All sediments are from archived collections that have been the subject of previous publications (Dolor et al., 2009; Helz et al., 1985a, 1985b; Marcantonio et al., 2002; Officer et al., 1984; Sinex and Helz, 1981; Sinex and Helz, 1982; Zimmermann and Canuel, 2002), and additional information on the sites is available in the Electronic Supplement. The data are intended to establish the historical extent of seasonal anoxia by analyzing samples from two long cores (Table 3.2) covering the entire 20th century, and supplementing the core data with small sample sets (Table 3.3) representing sources and processes within and around the Bay.

Table 3.1: Data for Chesapeake Bay water samples, Susquehanna River water, and a seawater standard.

Station ID	Lat./Long.	Sample depth (meters)	Salinity	Temp. (℃)	Diss. O_2 (mg/L)	pH	Mo (µg/L)	δ^{98}Mo
CB 3.1 (intermediate)[a] Gunpowder Neck	39.14'54º/ 76.14'16º	7	11.6	25.3	2.2	7.4	3.07	1.81
CB 3.1 (bottom)[b] Gunpowder Neck	39.14'54º/ 76.14'16º	13	15.9	25	0.2	7.4	4.35	2.25
CB 3.2 (intermediate) Swan Point	39.9'48º/ 76.18'22º	3	8.7	24.8	5.6	8.1	2.36	1.99
CB 3.3 (intermediate) Bay Bridge	39.59'42º/76.21'34º	17	19.7	25.1	0.2	7.4	5.57	2.26
CB 4.1 (intermediate) Kent Point	38.48'30º/76.23'58º	17	20.1	25.4	0.2	7.4	6.04	2.18
CB 4.2 (intermediate) Mid-Bay, Tilghman Is.	38.38'41º/76.25'3º	17	20.8	25.8	0.2	7.5	5.93	2.19
CB 4.3 (intermediate) Dares Beach	38.33'23º/76.26'4º	17	22	26	0.3	7.5	6.3	2.01
CB 4.3 (bottom) Dares Beach	38.33'23º/76.26'4º	25	22	26	0.3	7.5	6.42	2.16
Susquehanna River Conowingo Dam	39.39.36′76.10.25°	surface	0				0.27	1.02
CASS-4[c] seawater Halifax Harbor	44.51′63.11°	12	30.7				8.84	2.23

[a, b] Intermediate and bottom refer to the water column depth at which the sample was taken. Intermediate samples were taken approximately half-way to the bottom, while bottom samples were taken within 1 m of the sediment surface.
[c] Seawater standard from the National Research Council of Canada.

The deep, main channel of the Chesapeake Bay often experiences the most intense seasonal anoxia. Cores RD and 55 (Table 3.2) are located less than 10 km apart in this region of the Bay. Mass accumulation rates were determined by the Pb-210 method, and corroborated by other time markers (Helz et al., 1985a; Helz et al., 2000; Officer et al., 1984; Zimmermann and Canuel, 2002). Core RD, collected by the USGS in 1998, spans 53 years of sedimentation at a mass accumulation rate of 1.2g/cm^2 per year (1944 to 1997; Zimmermann and Canuel, 2002). It was collected in a water depth of 26.5 m. Core 55 was collected by the Maryland Geological Survey in 1979, and spans ~78 years of sedimentation with a mass accumulation rate of 0.4g/cm^2 per year (~1900 to 1978; Helz et al., 1985a). It was taken in ~25 m water depth. These cores were sectioned at 2 cm intervals, which is too coarse to resolve annual depositional features. Therefore, the focus of this study is on broader geochemical trends over the 20th century, as opposed to year-to-year variations.

The sample set includes three samples from a core in the Conowingo Reservoir, in the lower part of the Susquehanna River. The Susquehanna is the principal tributary to the Chesapeake Bay; therefore these samples are representative of the lithogenic material being delivered to the Chesapeake Bay.

Three samples from Baltimore Harbor were selected to look for Mo isotopic anomalies that could be associated with anthropogenic Mo. The Baltimore area is the site of historical smelting operations, and these

particular harbor sediments are contaminated with various metals used in commerce and industry (e.g. 500-1800 μg/g Cu, 320-640 μg/g Pb; Dolor et al. 2009; Sinex and Helz, 1982).

Three core samples from PC-6 capture pre-agricultural sediment conditions in Chesapeake Bay. The oak/ragweed pollen horizon in the core is used to establish the arrival of European agriculture in the region, sometime before ~1700 (Cooper and Brush, 1993; Helz et al., 2000).

One sample (Fairhaven) is taken from a shoreline outcrop of the Miocene-aged Fairhaven member of the Calvert group. Erosion of these bluffs contributes a significant amount of sediment to the Bay (Biggs, 1970).

Samples from the sediment surface (DT) were collected near Cores RD and 55. These three samples, deposited under increasing water depths (3.4 to 26.2 m) are used to assess the possibility of a relationship between Mo isotopic composition and water depth.

Table 3.2: Data for core samples. Iron and Mn data from Dolor et al. (2009). Calculation of authigenic Mo and depositional flux are discussed on pages 89 and 93, respectively.

Sample Name (cm core depth)	Age	Mo (µg/g)	δ98Mo[a]	Auth. Mo	% auth.	Depo. Flux (µg/cm^2/yr)	Fe (%)	Mn (µg/g)
RD 3 (4)		2.3	0.18	1.4	59	1.6	3.6	600
RD 10 (18)	1998	1.9	-0.01	0.8	41	0.9	4.2	980
RD 15 (28)	1995	7	0.05	5.7	82	6.9	4.8	840
RD 20 (38)	1992	2	0.24	0.9	46	1.1	4.1	940
RD 27 (52)	1990	1.6	-0.11	0.3	21	0.4	4.8	1220
RD 30 (58)	1986	1.5	0.09	0.3	18	0.3	4.7	1210
RD 35 (80)	1985	1.8	0.41	0.9	50	1.1	3.4	690
RD 45 (120)	1972	2.1	-0.22	1.0	50	1.3	4.0	750
Core 55 (0)	1945	4.3	-0.07	3.3	76	1.7	3.8	540
Core 55 (8)	1979	2.7	0.38	1.7	61	1.1	3.9	720
Core 55 (10)	1970	2.3	0.00	1.2	51	0.9	4.3	940
Core 55 (12)	1968	4.4	0.40	3.3	75	1.8	4.2	820
Core 55 (16)	1966	1.5	-0.28	0.2	15	0.6	4.8	790
Core 55 (20)	1964	1.7	0.27	0.4	26	0.7	4.7	870
Core 55 (26)	1963	1.8	0.80	0.8	43	0.7	3.9	840
Core 55 (28)	1957	9.5	0.34			3.8		
Core 55 (32)	1955	2.4	0.48	1.4	58	1.0	3.8	810
Core 55 (38)	1951		0.25					
Core 55 (44)		2.4	0.40	1.3	54	1.0	4.1	980
Core 55 (50)	1940	1.4	0.21	0.3	21	0.6	4.2	730
Core 55 (54)	1935	1.5	-0.21	0.5	35	0.6	3.7	650
Core 55 (58)	1932	2.2	0.49	1.1	51	0.9	4.1	710
Core 55 (68)	1929	1.3	-0.15	0.3	20	0.5	3.9	700
Core 55 (76)	1921	1.3	-0.11	0.1	9	0.5	4.4	720
Core 55 (94)	1917	1.1	-0.12	0.1	6	0.4	3.9	430
Core 55 (96)	1907	1.7	0.28	0.6	36	0.7	4.1	550
Core 55 (100)	1906	1.4	-0.21	0.3	24	0.6	4.0	530

[a] External reproducibility <0.1 ‰ (2σ).

Table 3.3: Data for Susquehanna River sediments and additional Chesapeake Bay sediments. Iron and Mn data from Dolor et al. (2009). For calculation of authigenic Mo, see page 90.

Sample Name (cm core depth)	Age	Mo (µg/g)	Auth. Mo	% auth.	δ^{98}Mo	Fe (%)	Mn (µg/g)
Susquehanna (8)		2	0.0	0.0	-0.07	7.5	2700
Susquehanna (28)		1.5	0.6	40	-0.13	3.4	1800
Susquehanna (44)		2.8	1.3	46	0.06	5.7	1800
Balt. Harbor H (22)		8.5	5.7	67	-0.09	10.0	650
Balt. Harbor M (104)		5.9	3.9	67	-0.11	7.4	4800
Balt. Harbor N (20)		3.2	1.4	44	0.11	6.8	860
DT 0902[a] (3.4 m)	1977	1.9	0.2	12	0.04	6.3	3000
DT 0903 (6.7 m)	1977	2.4	0.9	37	0.17	5.7	2200
DT 0907 (26.2 m)	1977	2.2	1.1	50	-0.09	4.1	1000
PC-6 (369)	~1300	1.8	0.8	43	-0.39	3.9	520
PC-6 (424)	~800	4.1	3.0	73	0.20	4.1	510
PC-6 (482)	~300	1.8	0.8	46	0.07	3.7	510
Fairhaven[b] (n = 1)	Miocene	15.5	14.8	96	0.96	2	110
Fairhaven 2 (n = 3)	Miocene	15.6			0.95		
Fairhaven 3 (n = 6)	Miocene	15.4			0.94		
Fairhaven 4 (n = 3)	Miocene	15.5			0.92		
Fairhaven 5 (n = 1)	Miocene	15.4			0.93		

[a] DT samples were collected from the sediment surface at the specified *water* depth.

[b] Numbers for the Fairhaven indicate individual digestions; n refers to number of measurements for each digestion. External reproducibility for the Fairhaven is < 0.1 ‰, and for the other standards 0.2‰ (2σ).

Methods

Sample preparation and measurement

Complete details for all methods are provided Chapter 2, but a brief overview is provided here. Finely powdered sediments (0.2 to 0.5 g) and acidified water samples (1 to 5 L) were spiked with a ^{97}Mo-^{100}Mo double spike solution (29.39 µg/g Mo in 2% nitric acid), to correct for analytical mass bias (e.g., Siebert et al., 2001). Sediment samples were then digested with concentrated, high-purity acids. Trace metals from water samples were pre-concentrated using a chelating resin, according to the method of T. Dahl (personal communication). Chromatographic separation, using anion and cation exchange resins, was used to purify Mo from all samples (Pietruszka et al., 2006). Blanks for the 3-column chemistry ranged between 2 and 6 ng Mo, comprising less than 1% of the total Mo for all sediment samples. The blank for processing one liter of distilled water was 0.22 µg, or approximately 4% of the water-sample Mo for the estuarine samples. This quantity of blank contributes ~20% of the Mo to the Susquehanna River sample, because of its lower Mo concentration, leading to the possibility that the isotopic ratio for this sample is slightly biased.

Measurements were made using a Nu Instruments multi-collector ICP-MS at the University of Maryland. Raw isotope ratios were reduced using a modified version of the iterative scheme introduced by Siebert et al. (2001). Delta values were calculated using the standard notation: δ^{98}Mo = (($^{98/95}$Mo sample/ $^{98/95}$Mo standard)-1)*1000, where the standard is an in-house Johnson-Matthey Company SpecPure® Mo plasma standard (Lot # 013186S),

and its $^{98/95}$Mo ratio is fractionation-corrected by measuring double-spiked aliquots and reducing the raw data.

Maximum long-term external reproducibility of two in-house rock reference standards is ±0.20‰ for δ^{98}Mo at the 2σ level (Chapter 2). Five separate digestions of the Fairhaven sample, and multiple analyses of each processed digestion, have a 2σ of ±0.09‰. Concentration data derived from the double-spike data for the Fairhaven have approximate uncertainties of ±1% (15.5 ±0.1 µg/g), which likely includes some sample heterogeneity.

In order to facilitate comparison with published results from other institutions, a widely available seawater standard (CASS-4, National Research Council Canada) was processed and analyzed. The sample had a Mo concentration of 8.84 µg/L, compared to the certificate value of 8.78 ± 0.86 µg/L. This concentration is ~10% lower than that of open-ocean seawater (e.g., Collier, 1985), possibly because the CASS-4 water was collected in a harbor, and has a salinity of 30.7. The Mo isotopic value was +2.23 ± 0.09‰ (2σ), within the analytical uncertainty for one published measurement of seawater (+2.3 ± 0.1‰; Siebert et al., 2003), but outside the uncertainty of another measurement (+2.45 ± 0.11‰; Nakagawa et al., 2008). The lower δ^{98}Mo, compared to previous results, could be a result of either the lower salinity or lower Mo concentration relative to open-ocean seawater, or a consequence of normalizing to different batches of SpecPure® Mo used by the other researchers.

Calculation of authigenic Mo

Conventionally, Mo in bulk sediment digestates is regarded as consisting of lithogenic Mo and authigenic Mo, the latter being ultimately derived from dissolved Mo in the water column. A quantity termed Mo_{auth} can be calculated in order to characterize the authigenic component of Mo present in a sample (e.g., Adelson et al., 2001). This calculation mathematically removes the lithogenic Mo component from a sample by normalizing to an element whose concentration is largely lithogenic in nature. In this study, normalization is done with Fe for analytical reasons (Dolor et al., 2009), rather than the commonly preferred, diagenetically immobile Al. As shown by the extensive study of Daskalakis and O'Connor (1995), either element may be used in estuarine and near-shore waters, because deposition rates of Fe are much faster than the diagenetic mobility of Fe. Thus, its vertical distribution is not measurably affected by diagenesis.

Normalizing removes concentration variations that are due to changes in grain size within cores, and allows different sediment types from disparate localities within the Bay, such as the Susquehanna River (mostly sand) and PC-6 (homogenous clay), to be compared. The operational definition (Adelson et al., 2001) for Mo_{auth} is:

$$(3.1) \qquad Mo_{auth} = Mo_{meas} - [Fe_{meas} * (Mo/Fe)_{lith}]$$

In this formulation, the lowest Mo/Fe ratio in the sample set is used to define the $(Mo/Fe)_{lith}$, because such a sample would imply the greatest crustal

content, and be representative of the local background with respect to Mo. The Susquehanna River sample from 8 cm satisfies this definition (2.7 x10^{-5}); the oldest sample from Core 55 (96 cm, ~1900) also has a similarly low Mo/Fe ratio (2.8 x10^{-5}).

Results

Chesapeake Bay and Susquehanna River water

Dissolved Mo concentrations for six mid-depth and two near-bottom water samples show a non-linear distribution with salinity, indicating a small degree of Mo removal from the water column within the estuary (Fig. 3.2a). Non-conservative behavior of Mo has previously been reported by van den Berg (1993), who also proposes removal within mesohaline regions (salinity of 7-20 psu) to explain the contrast to conservative behavior of Mo in the ocean. The Mo concentration versus salinity distribution is similar to that found by Kingston et al. (1983). Bottom samples fall on the same concentration versus salinity curve as mid-depth samples (Fig. 3.2a).

Susquehanna River water has a measured Mo concentration of 0.27 µg/L (Table 3.1). This is roughly one-half of the amount estimated or measured for rivers globally (e.g., Archer and Vance, 2008; Martin and Maybeck, 1979). The regression of Mo concentration in the Bay vs. salinity (Fig. 3.2a) extrapolates to a similar, but slightly lower, Mo concentration for the river (0.2 µg/L). Susquehanna River water has a relatively long residence time after it enters the northern, oligohaline Bay (~6 months). Therefore, the

extrapolated value may be a better estimate of the time-averaged Mo concentration in water derived from the Susquehanna River.

The measured δ^{98}Mo of the river water, +1.02‰ (± 0.09, 2σ), is within the range of values measured in other rivers by Archer and Vance (2008). The isotopic composition of dissolved Mo in the Bay (Fig. 3.2b) appears to be dominated by seawater. This can easily be attributed to the much higher concentration of Mo in seawater than in river water. For the six samples with salinity >15 psu, where little Mo is being contributed by river water, the average δ^{98}Mo is +2.17 ± 0.12, in good agreement with values for seawater. In the vicinity of cores 55 and RD, the seasonal range of salinity is 5 to 15 psu, and δ^{98}Mo in this water is not greatly different from that in seawater. This establishes that dissolved Mo in Chesapeake Bay, the source of authigenic Mo at these sites, is isotopically heavy.

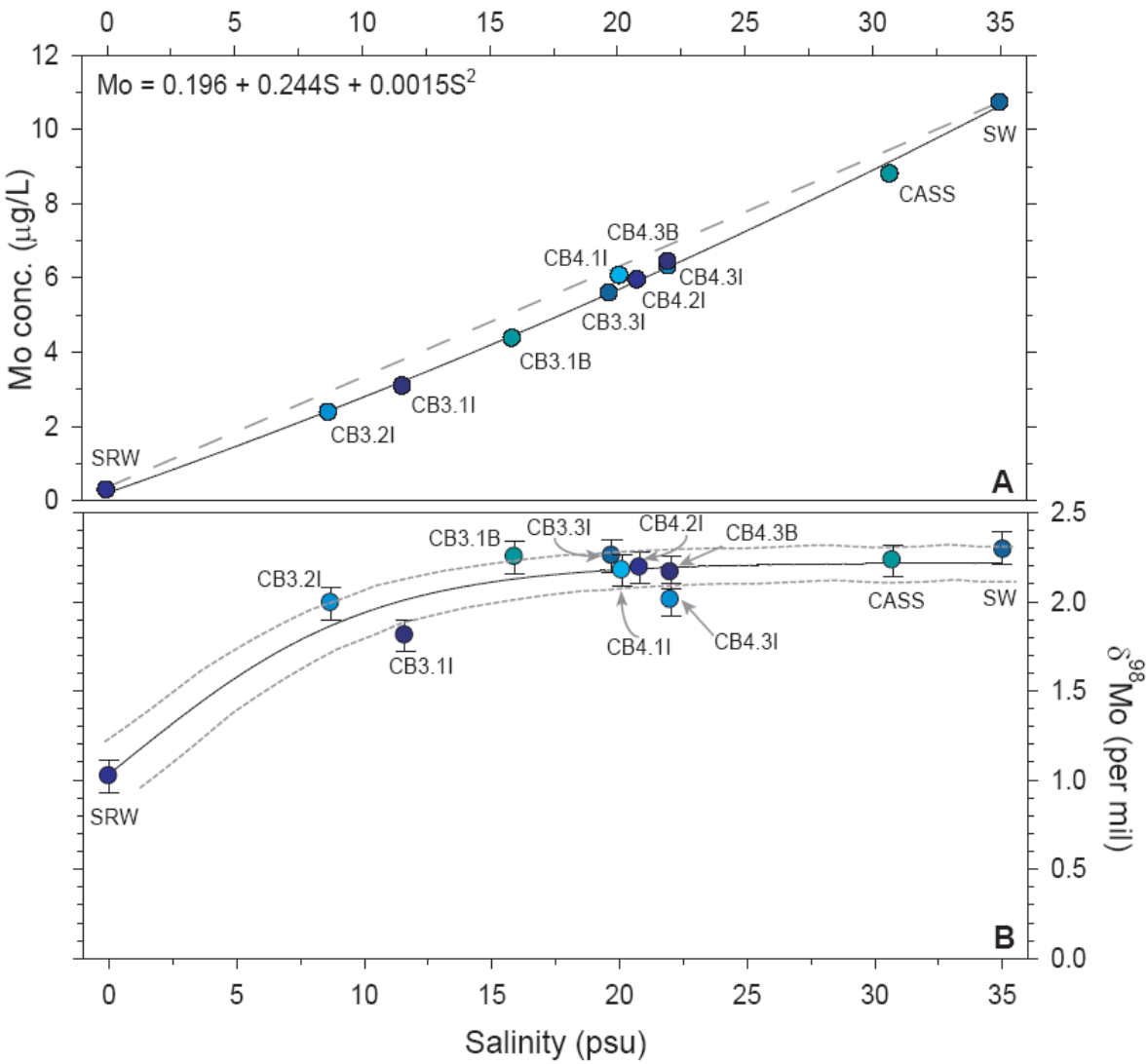

Figure 3.2a: Molybdenum concentration (µg/L) versus Salinity (psu). The solid line is a 3rd-order polynomial regression between Susquehanna River water (SRW) and salinity-normalized seawater (Collier, 1985). The relationship between Mo concentration and salinity is non-linear, as shown by the deviation from a linear trend (dashed line). This implies that removal of Mo is taking place in the Chesapeake Bay, particularly between salinities of 7-20 psu. Water with that range of salinities overlies the seasonally anoxic main channel.

Figure 3.2b: Molybdenum δ^{98}Mo (µg/L) versus Salinity (psu). The solid line is a sigmoid curve fit to the data with 95% confidence intervals (dotted lines). The δ^{98}Mo value of Chesapeake Bay water is dominated by seawater.

Chesapeake Bay and Susquehanna River sediments

Molybdenum concentrations for cores RD and 55 are presented in Figure 3.3a and Table 3.2. In Figure 3.3b, the depositional flux of Mo_{auth} is presented. To obtain these values, the calculated Mo_{auth} (Eq. 3.1) is multiplied by the appropriate sediment mass accumulation rate (Fig. 3.3b, Table 3.2). In the first two decades of the 20th century, very little Mo_{auth} accumulated in the deep channel of Chesapeake Bay, similar to the results of Adelson et al. (2001). Subsequently, Mo_{auth} fluxes increased, although inter-annual variability remained high throughout the century.

Molybdenum isotopic data for cores RD and 55, versus deposition date, are presented in Figure 3.4. In samples from the first two decades of the century, four of the five δ^{98}Mo values are < 0‰. Subsequently, the number of positive δ^{98}Mo values increases. The 3-fold higher deposition rate in core RD, compared to core 55, implies that the RD site receives significantly more sediment input, which seems to dilute the impact of Mo_{auth} formation on the Mo isotopic composition of the bulk sediment. The Susquehanna River sediments (Table 3.3) have low Mo concentrations, and an average δ^{98}Mo value of -0.05‰ (± 0.09) (Fig. 3.5). Similarly, surface samples from the depth traverse (DT) also have low Mo concentrations, with no trend related to water depth or Mn concentration (Table 3.3). The average δ^{98}Mo value for the three DT samples is +0.04‰ (± 0.13), not analytically distinct from the Susquehanna River sediment samples. Based on these samples, the Mo isotopic composition of the lithogenic material delivered to the Bay by the

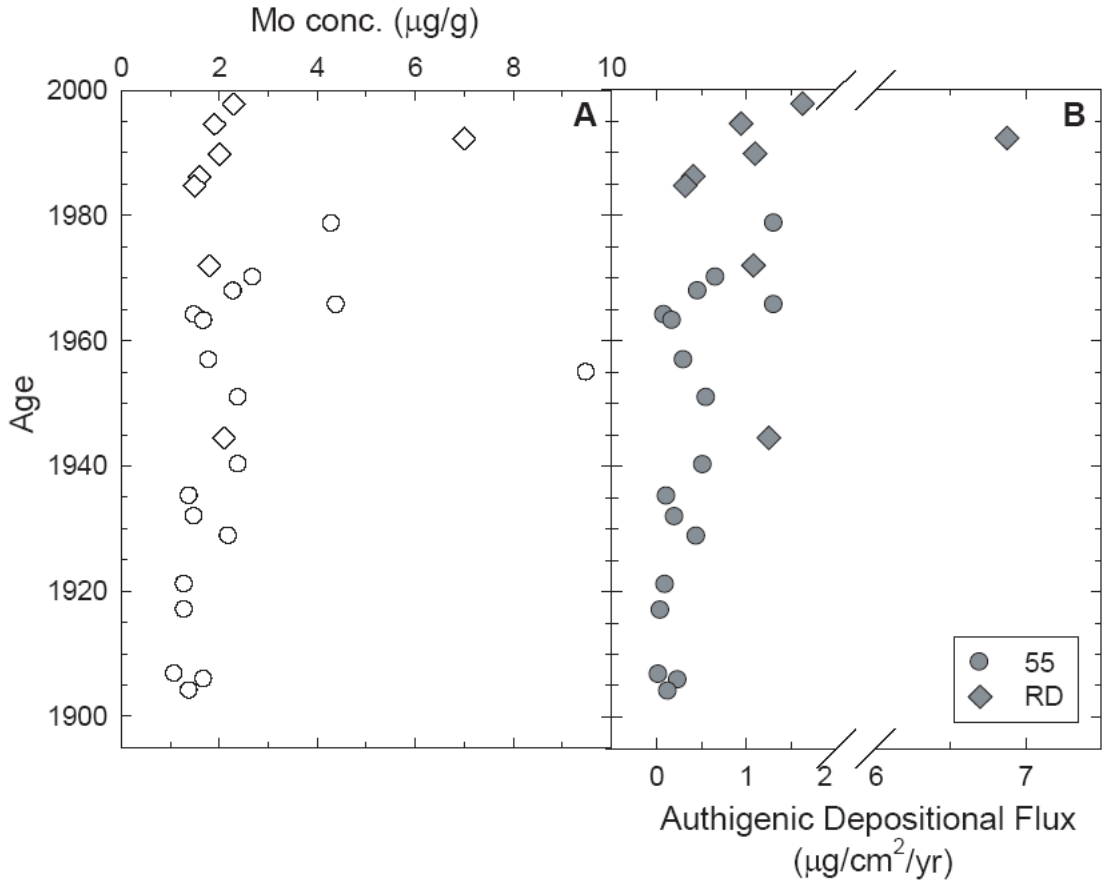

Figure 3.3a: Molybdenum concentration (μg/g) versus age/depth for cores RD and 55. On the y-axis, depth has been translated to date of deposition (age) using the deposition rates given by Helz et al. (1985a) and Zimmerman and Canuel (2002).

Figure 3.3b: Depositional flux of authigenic Mo versus age/depth for cores RD and 55. Note a break in scale between 2 and 6 μg/cm^2/yr. For discussion of depositional flux, see page 93.

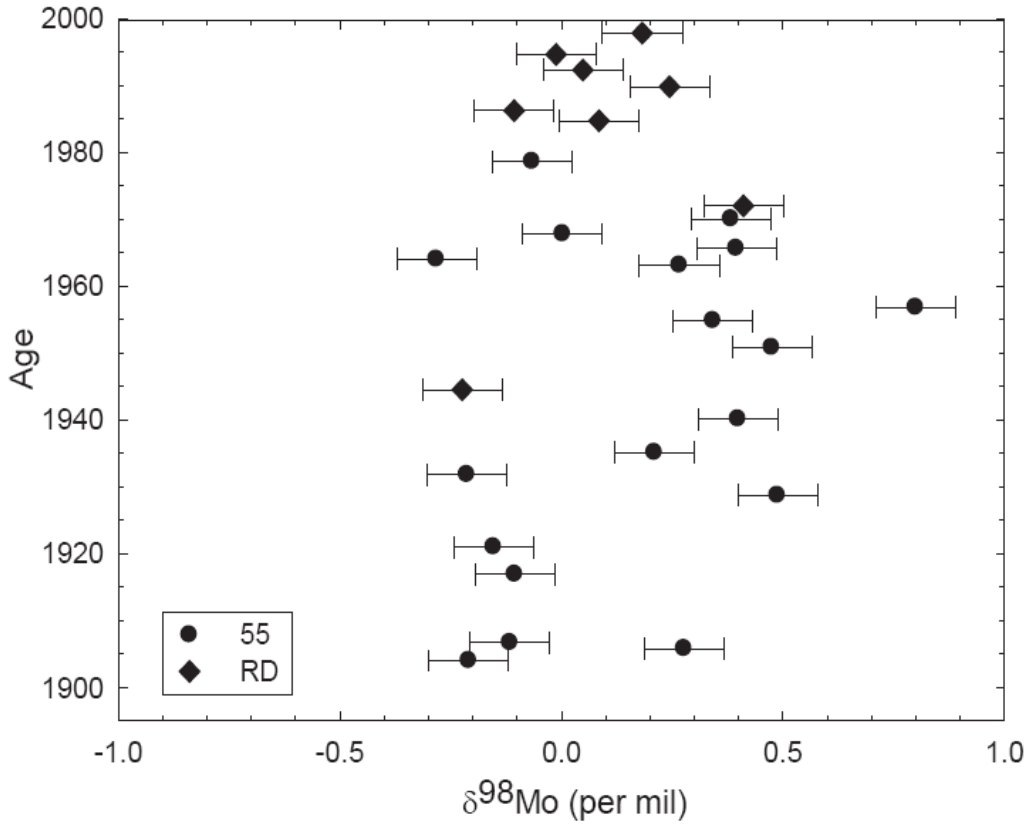

Figure 3.4: Molybdenum isotopic composition versus age/depth for cores RD and 55.

Susquehanna River appears to be indistinguishable from the presumed global continental crust value of ~0‰ (Siebert et al., 2003).

Baltimore Harbor sediments differ from the preceding samples in having higher Mo concentrations, from 3.2 to 8.5 µg/g (Fig. 3.5), but are similar in Mo isotopic composition (Table 3.3). The elevated Mo concentrations could be anthropogenic, or a result of microbial sulfate reduction. The isotopic similarity of these contaminated sediments to uncontaminated sediments elsewhere in the Bay suggests that anthropogenic Mo contamination does not impose a distinctive isotopic signature that could be used as a contaminant tracer (in contrast with $^{187}Os/^{188}Os$; Helz et al., 2000).

The three samples from core PC-6 predate the arrival of European agriculture (1675-1775), and therefore provide insight to historical Mo behavior in the Bay. In this context, they can be compared with the early 20th century, pre-eutrophication core samples. Two of the three PC-6 samples have Mo concentrations averaging 1.8 µg/g, while one sample (~800 ybp) has a higher concentration of 4 µg/g. The topmost sample (~1300 ybp) is isotopically light (-0.39‰), possibly a reflection of greater MnO_x formation. The other two samples are not resolvable from 0‰, the presumed signature of lithogenic Mo derived from the Susquehanna Basin. The Mo in the PC-6 samples is similar in concentration and isotopic composition to the Mo in Susquehanna River sediments. This could be an indication that most of the

Mo in these samples was derived from bed load, as opposed to authigenic processing of Mo derived from the water column.

A Mo-rich (15 μg/g) sediment sample from the Miocene Fairhaven cliffs has the highest Mo concentration and heaviest Mo isotopic composition (+0.97‰) measured for the entire Chesapeake Bay suite. The isotopic composition and relative enrichment in Mo of this formation suggest it may have been deposited in a suboxic basin or lagoon. Shoreline erosion of the Mo-rich Fairhaven outcrop has been hypothesized as a source of Mo enrichment in PC-6 sediments (Adelson et al., 2001), but the outcrop lies too far to the south for it to be a likely sediment source at the Core 55 and RD sites.

Discussion

Authigenic Mo formation in the Chesapeake Bay

In the absence of anoxic conditions, it might be expected that the Mo concentration and δ^{98}Mo values of Bay sediments would be similar to the concentration and δ^{98}Mo values of Susquehanna River sediments, based on the simple paradigm that Mo in river-transported detrital bed load is deposited within the Bay, while Mo dissolved in river water and seawater transits the estuary unaltered. In the modern day, the dissolved Mo distribution in the waters of Chesapeake Bay is not conservative (Fig. 3.2a), implying that Mo_{auth} is forming in the Bay. Additionally, core samples deposited after 1925 have higher Mo concentrations and more Mo_{auth}, compared with samples deposited

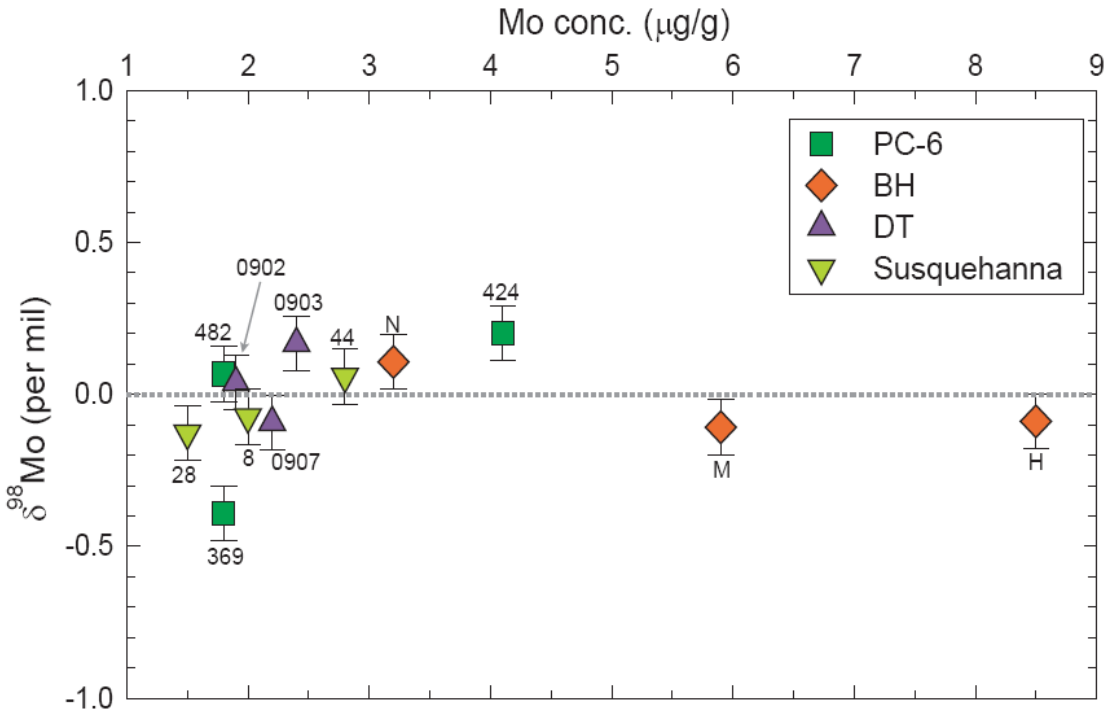

Figure 3.5: Mo isotopic composition versus Molybdenum concentration (μg/g) for the Susquehanna River sediments, PC-6, Baltimore Harbor (BH), and depth traverse (DT). A δ^{98}Mo = 0‰ line is shown for reference.

before 1925 (Figures 3.3a and 3.3b). The implication is that a persistent change in deep water sedimentation took place sometime after 1925. This change likely involved an increase in intensity and occurrence of seasonal anoxia (Cooper and Brush, 1993, Adelson et al., 2001). In 1960, a period of decreased Mo_{auth} is likely the result of low river flow during a prolonged drought. Recent monitoring of the Bay has shown that low river flow tends to reduce the extent and severity of coastal eutrophication (Hagy et al., 2004).

The considerable scatter in the Mo concentrations of the core samples after 1925 might be due to the great variation in the extent of seasonal anoxia from year to year, heavily influenced by spring runoff and nitrate loading (Hagy et al., 2004). For example, between the summers of 1985 and 1986, the volume of moderately hypoxic water (dissolved O_2 < 2 mg/L) changed from 4.4 x 10^9 m^3 to 11.0 x 10^9 m^3, but between 1959 and 1960 only changed from 4.9x10^9 m^3 to 4.2x10^9 m^3 (Hagy et al., 2004). Therefore, we conclude that the Mo_{auth} profile for cores RD and 55 most likely reflects super-annual variations in anoxia.

The core RD and 55 data display a wide range of both isotopic values and amounts of Mo_{auth} (Fig. 3.6). Although there is a general trend relating heavier $\delta^{98}Mo$ values with more Mo_{auth}, the scatter is large, and R^2 is low (+0.18). This indicates that the processes controlling Mo_{auth} and $\delta^{98}Mo$ are substantially independent of one another (Fig. 3.6). The regression line indicates that a lithogenic end member (Mo_{auth} = 0%) should have $\delta^{98}Mo$ = -0.11‰, while the authigenic end member has $\delta^{98}Mo$ = +0.45‰. The upper

and lower dotted lines represent mixing of lithogenic Mo with seawater Mo and MnO_x-derived Mo, respectively. Within error, these lines enclose all the data for cores RD and 55, suggesting that the samples can be derived by mixing Mo_{auth} from MnO_x with dissolved Mo from seawater, plus lithogenic Mo. The regression line (Fig. 3.6) suggests that the most common Mo isotopic composition of the Mo_{auth} mixing end- member is approximately +0.45‰, implying that Mo_{auth} in a typical year is derived 60% from MnO_x and 40% from seawater Mo. However, the scatter of the data implies that the proportions of Mo_{auth} derived from MnO_x and seawater vary greatly from year to year. It is important to note that sediment deposition rates in Chesapeake Bay are on the order of 10^3 times faster than typical deep-sea rates. The implication for Mo_{auth} is that, in order to avoid dilution of the signal, the process delivering Mo_{auth} to the sediments must be very robust indeed.

In many settings, organic carbon is the most important carrier of Mo, and sediments often show a high degree of correlation between organic carbon contents and Mo (Tribovillard et al., 2004). However, when the organic matter has not been sulfurized and the S is in the pyrite form, this correlation disappears (Tribovillard et al., 2004). In Chesapeake Bay, low organic carbon contents (1.8 to 3.3%) show no relationship to amount of Mo_{auth}, similar to the latter example (Appendix 1). This suggests that, in this estuary, organic carbon plays a more limited role in influencing Mo_{auth} than in other environments.

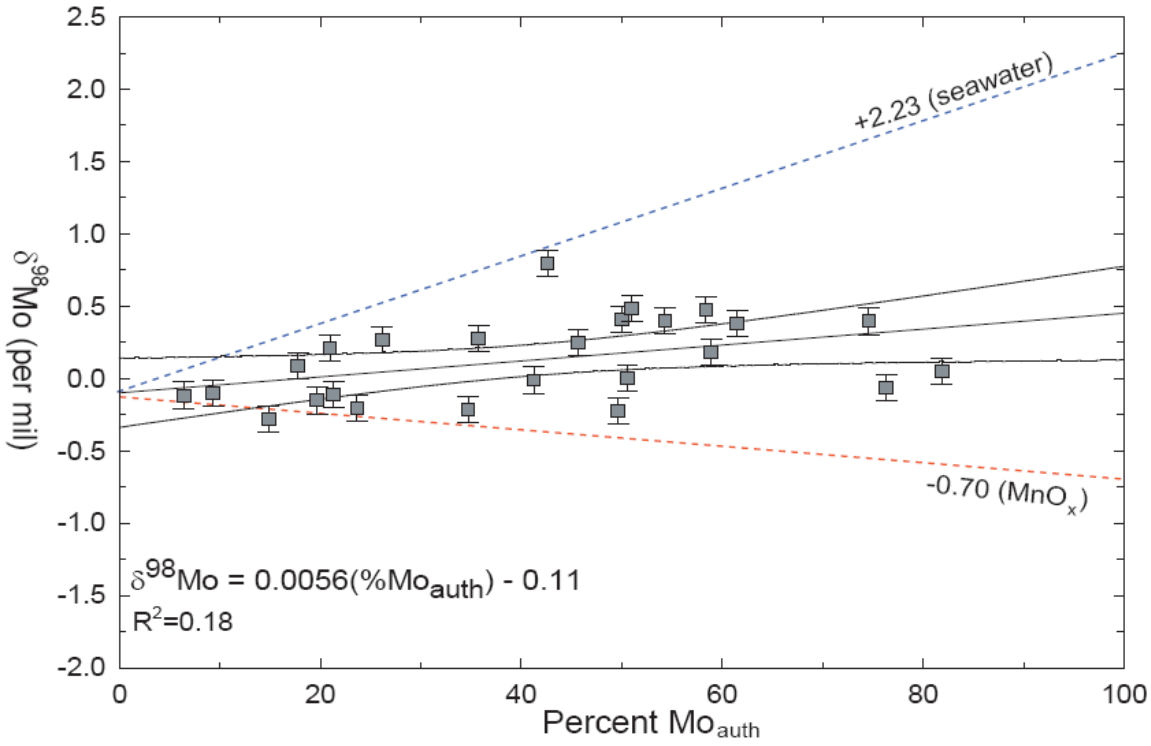

Figure 3.6: Percent of authigenic Mo versus Mo isotopic composition for the data of cores RD and 55 (all grey squares, not differentiated by core). Solid lines are a linear regression through the data with 95% confidence intervals. Upper dotted line represents a mixing line for lithogenic Mo with seawater, lower dotted line represents a mixing line for MnO_x-derived Mo with lithogenic Mo. The regression equation yields an estimate for the isotopic composition of continental material contributed by the Susquehanna Basin (-0.11‰), and an upper value for a hypothetical sample with 100% authigenic Mo of approximately +0.45‰.

Molybdenum isotope fractionation in Chesapeake Bay sediments

Molybdenum in sediments from the main channel of Chesapeake Bay is, in most cases, isotopically heavier than lithogenic Mo, but lighter than dissolved Mo (as MoO_4^{2-}) in the overlying water (Fig. 3.6). A feasible mechanism must explain both the variability in isotopic composition and the range of Mo_{auth} content. Many processes that result in Mo isotopic fractionation have been identified, for example, microbial metabolism (Wasylenki et al., 2007), carbonate deposition (Voegelin et al., 2009), and Fe oxide precipitation (Malinovsky et al., 2007; Goldberg et al., 2009). Two processes result in fractionations that are both large and distinct, MnO_x precipitation and thiomolybdate formation. Many of the other recently identified fractionation mechanisms result in isotope values within the brackets established by MnO_x and thiomolybdate (Fig. 3.6), and therefore may not be easily distinguishable from one another in a complex system.

When H_2S reacts with MoO_4^{2-}, thiomolybdates are formed. If theoretical calculations are correct (Tossell 2005), thiomolybdate should be isotopically light relative to the starting MoO_4^{2-}. If H_2S_{aq} exceeds ~11 μM, the conversion can become quantitative, given sufficient time for the reaction to take place (Erickson and Helz, 2000). In this case, no fractionation will be detected, as the thiomolybdate product will have the same isotopic composition as the starting MoO_4^{2-}. Where H_2S_{aq} values are below the switch-point, selective scavenging of thiomolybdate, from a mixture of MoO_4^{2-} and thiomolybdate, might occur. Such a process has been proposed to explain the

isotopic composition of surface sediments from varying water depths in the Black Sea (Neubert et al., 2008).

Invoking fractionation associated with thiomolybdate formation to form authigenic Mo that is lighter than the MoO_4^{2-} in the water column is problematic for Chesapeake Bay. In contrast to the Black Sea (e.g., Neubert et al., 2008), a thiomolybdate-based mechanism probably never operates in the Chesapeake Bay water column because the requisite H_2S_{aq} levels rarely obtain (Lewis et al., 2007). One model for Mo_{auth} formation in estuaries proposes that MoO_4^{2}- diffuses from the water column into the pore water, where it eventually reaches the H_2S_{aq} = 11 µM isopleth (Adelson et al., 2001; Boothman and Coiro, 2009). At that horizon, thiomolybdate formation is activated. In this model, seasonal fluctuation of the 11 µM isopleth depth within the sediments exerts control on the rate of Mo_{auth} formation. Although Mo geochemistry in pore water is not well understood, several studies suggest that Mo is nearly quantitatively removed from pore water at this horizon (Colodner et al., 1993; Morford et al., 2007; Zheng et al., 2000). However, quantitative removal from pore water would produce Mo_{auth} with δ^{98}Mo values identical to the overlying water. This appears to be inconsistent with Figure 3.6.

Alternatively, delivery of isotopically light Mo to the pore waters can be easily accomplished by dissolution of MnO_x particles. During episodes of water column anoxia in Chesapeake Bay, Mn refluxing takes place (Eaton, 1979; Helz et al., 1985b). Refluxing involves reduction of surface-sediment

MnO_x to Mn^{2+}, which can be transported upwards through the anoxic zone, until it encounters oxic near-surface waters. In this zone, MnO_x particles can re-form, fractionating Mo during adsorption (e.g., Wasylenki et al., 2008). The MnO_x particles eventually sink back to the sediment surface, carrying Mo that is isotopically lighter than that in the overlying water. This Mo is released as the Mn cycle is repeated. At sites near Core RD, Shaw et al. (1994) show that dissolved Mn^{2+} rises 1000-fold in bottom waters during spring, reaching summertime peaks of several μM after O_2 disappears. Eaton (1979) found that in summer, Mn is solubilized from surface sediments fast enough to replace the dissolved Mn concentration in 20 m of bottom water in less than two weeks. Furthermore, Moffett (1994) showed that Mn^{2+} diffusing into oxic surface water is oxidized to particulate MnO_x at rates exceeding 2000% per day. These findings imply that Mn can be recycled many times during the summer months, and each cycle has the potential to release isotopically light Mo into the water near the sediment-water interface. Once isotopically light Mo builds up, it can be subsequently fixed as Mo_{auth} after diffusing to the 11μM H_2S_{aq} horizon. This is similar to the scheme proposed by Reitz et al. (2007).

A key difference between the thiomolybdate and MnO_x mechanisms is the location in which the fractionation from isotopically heavy dissolved Mo to isotopically light Mo occurs. In the first mechanism, fractionation occurs near the 11μM H_2S horizon in the sediments (e.g., Neubert et al., 2008). This would result in an isotopically heavy MoO_4^{2-} 'residue' in the pore water, but it

is not obvious how this residue could be selectively returned to the water column. In the second mechanism, fractionation occurs in the water column, removed from the site of Mo_{auth} formation.

The MnO_x mechanism is attractive because the processes that control Mo_{auth} formation (pore water H_2S_{aq}) and $\delta^{98}Mo$ (MnO_x) are separate, even though both are influenced by seasonal oxygen stress in the estuary. This is consistent with the positive relationship, but low correlation coefficient, between $\delta^{98}Mo$ values and percentage of Mo_{auth} in the core data (Fig. 3.6).

Isotopic mass balance in the Chesapeake Bay watershed

The average sediment discharge from the Susquehanna Basin to the Bay is 5×10^{12} g/y (Gross et al., 1978). The composition of this sediment is estimated at 1.4×10^{-6} g Mo/g sed, giving a Mo flux from the watershed of 7.0×10^{6} g Mo/y as solid material. Freshwater discharge averages 34.7×10^{9} m^3/y or 3.47×10^{16} g H_2O/y (Schubel and Pritchard, 1987). Based on the Mo concentration of the Susquehanna River, the dissolved Mo in river water is about 0.2×10^{-9} g Mo/g H_2O, making the mass of dissolved Mo leaving the basin about 6.9×10^{6} g Mo/y. The mass of Mo leaving the Susquehanna basin in solid versus dissolved form appears to be roughly equal, in agreement with findings for the world's large rivers (Martin and Meybeck, 1979).

This simple Mo budget indicates that an isotopic mass balance problem might exist for the Susquehanna watershed. Pre-1925 sediment samples from Core 55, as well as sediments from the Susquehanna River

itself, suggest that δ^{98}Mo in sediments from the watershed is about -0.1‰. In contrast, δ^{98}Mo in the water is +1.02‰. Although this latter value is based on only one measurement, it is consistent with the broader findings of Archer and Vance (2008). Assuming those isotopic values are typical of solid-phase and dissolved Mo, then either the average δ^{98}Mo of rocks that are undergoing weathering in the basin is closer to +0.5‰, as opposed to the generally assumed 0‰, or weathering and erosion in the basin are not in steady state. Release of water with δ^{98}Mo = +1.02‰ from a basin averaging 0‰ would require that either a reservoir of isotopically light solid material is forming somewhere in the basin, or that isotopically heavy rocks are presently being selectively weathered. A plausible hypothesis based on the latter possibility posits that black shale associated with extensive coal deposits in the basin is being leached at an accelerated rate by acid mine drainage. Investigation of Mo isotopes in the Susquehanna River basin is a topic for future study.

Conclusions

The Chesapeake Bay sediments display a range of δ^{98}Mo that is ~1.2‰. All samples are offset from the water-column isotopic composition by at least ~1‰. The δ^{98}Mo range is somewhat smaller than that of the suboxic regimes described by Siebert et al. (2006), and is much larger than would be expected of a pure anoxic system (Poulson et al., 2006). In common with previous research, Mn-rich sediments in Chesapeake Bay contribute isotopically light Mo, but this signature is diluted by mixing with other components and low total amounts of $Mo_{auth.}$

There is significant evidence that fractionation of Mo isotopes is occurring during sedimentation in the Chesapeake Bay, and that the isotopic composition of these sediments is distinctly different from the composition of major Mo sources to the Bay. We propose a mechanism that provides a satisfactory explanation for the observed trends in the Mo isotope data and Mo_{auth} concentrations from core samples in the seasonally anoxic main stem of the Bay. Sediment samples from the past century show a distinct change in sedimentation since 1925, as inferred from Mo isotope values, indicating an increase in the severity of coastal eutrophication, and increased efficiency of the Mo_{auth} formation mechanism.

Chapter 4: Molybdenum isotopic signatures in Pliocene-Pleistocene aged Mediterranean sapropels[3]

Abstract

In the sediments of the Mediterranean Basin, unusual organic carbon-rich layers, known as sapropels, occur at regular intervals that correspond to orbital insolation cycles. These layers are enriched in trace metals that are sensitive to low-O_2 conditions, such as Re and Mo. Sapropel deposition is, most likely, the result of a highly specific set of conditions that include hydrographic changes that encourage development of anoxic conditions. Molybdenum isotopes have the potential to discriminate between a variety of scenarios for sapropel deposition, such as localized or basin-wide anoxia, 'suboxic' conditions, or euxinia.

The Mediterranean evidently switched rapidly and often from an oxic state to an anoxic state. δ^{98}Mo values for sapropels and spatially associated hemipelagic sediments vary greatly, ranging from -0.6 to +3.5‰. The heaviest isotopic values are primarily found in the hemipelagic sediments and rarely within the sapropel layers. However, it might be expected that if anoxic conditions prevailed during sapropel deposition, a seawater isotopic composition (~+2.3‰) would be evident in the layer. Comparison between Mo isotopic compositions of sapropel layers and compositions present in normal marine sediments suggest that low-O_2 conditions sometimes prevailed during the 'normal' segment of the depositional cycle, and are responsible for heavy

[3] This research used samples and/or data provided by the Ocean Drilling Program (ODP). ODP is sponsored by the U.S. National Science Foundation (NSF) and participating countries under management of Joint Oceanographic Institutions (JOI), Inc.

isotopic compositions during those times. Given the very high amounts of organic carbon present, it also may be possible that sinking organic matter was an important carrier of Mo in this environment.

Introduction

Beginning in the earliest Pliocene, and continuing into the Holocene, the Mediterranean Basin saw the onset of deposition of sapropels, which are cyclic, laminated, organic-rich (>2% TOC) sedimentary layers (Sakamoto et al., 1998). Numerous studies using a variety of lines of evidence have concluded that sapropel deposition occurred as a result of anoxic conditions that prevailed in the Mediterranean Sea during this period (e.g., Rossignol-Strick et al., 1982; Passier et al., 1999; Emeis et al., 2000; Larrasoana et al., 2003; Scrivner et al., 2004). Anoxic conditions, coupled with high primary productivity, appear responsible for many of the unique features observed in the sapropel layers, including high organic carbon contents (e.g., Cramp and O'Sullivan, 1999; Sancetta, 1999), and enrichments in elements that are redox sensitive, such as V, Mo, and Re, relative to both continental crust and average shale (Nijenhuis et al., 1998; Warning and Brumsack, 2000; Wehausen and Brumsack, 1998).

There is considerable evidence that the anoxic conditions were instigated by vast inputs of fresh water that diluted the normally hypersaline (38 psu) Mediterranean Sea surface waters (Thunell and Williams, 1989; Kroon et al., 1998). A freshening event would likely prevent sinking of surface water, which currently keeps the bottom waters of the Eastern Mediterranean

aerated to the level of about 60% of the air saturation value appropriate for their temperature and salinity. Freshening, therefore, would weaken formation of new, oxygen-rich deep water masses (Rossignol-Strick et al., 1982), and weaken the normal anti-estuarine circulation pattern. In this situation, deep water ventilation would be low, and result in suboxic conditions (Stratford et al., 2000). Alternatively, it has been suggested that, with a fresh water cap, the circulation would reverse to an estuarine type, and intermediate water would enter from the Western Mediterranean basin over the 300 m deep sill at the Strait of Sicily (Stratford et al., 2000). In this mode, deep waters would become anoxic. Under any set of conditions in which deep waters are not being quickly renewed, oxygen utilization will quickly outstrip the supply in the deep waters (Rohling, 1994), resulting in suboxic or anoxic conditions. Sapropels could, therefore, form under either weak anti-estuarine or estuarine circulation, but those formed under the estuarine circulation (anoxic mode) would be the most organic-carbon rich (Stratford et al., 2000).

The delivery of fresh water needed to repeatedly limit deep-water ventilation has been linked to the direct influence of high-latitude insolation maxima, through eccentricity-modulated precessional minima (e.g., Hilgen, 1991). Eccentricity minima influence low-latitude (African) monsoon cycles, and the Mediterranean is affected by increased Nile River flow (Rossignol-Strick, 1983; Tuenter et al., 2003).

Despite this conceptual understanding, many issues remain unresolved regarding sapropel deposition in the Mediterranean, especially

considering that conditions likely varied for individual sapropels. For example, although the effects of diagenesis during basin re-oxygenation have been studied (Jung et al., 1997; Thomson et al., 1995), many aspects of this process remain poorly understood. Also, the high trace metal contents in the sapropels require a renewable source. While this source is likely to be seawater (e.g., Nijenhuis et al., 1998), mechanisms and rates of replacement, as well as possible changes in the amount of exchange between the Eastern and Western Mediterranean during anoxic episodes remain little explored. The thickness of the oxygen-deprived deep layer is also debated (e.g., Casford et al., 2003).

Redox-sensitive trace elements, such as Fe, V, Mo, and Re, in oceanic sediments/sedimentary rocks have commonly been used as proxies for paleoredox and paleoproductivity (e.g., Bertine and Turekian, 1973, Emerson and Huested, 1991; Calvert and Pedersen, 1993; Colodner et al., 1993; Crusius et al., 1996; Zheng et al., 2000; Wilde et al., 2004; Tribovillard et al., 2004, 2006, Morford et al., 2005, 2009; Algeo and Lyons, 2006). The dramatic changes in solubility of these elements under different degrees of oxygen depletion may be reflected in their relative and absolute concentrations recorded in sediments (Tribovillard et al., 2006). Molybdenum isotopes can also be used to provide complementary information regarding paleoredox conditions (e.g., Reitz et al., 2007; Neubert et al., 2008; Pearce et al., 2008; Gordon et al., 2009; Poulson-Brucker et al., 2009). Dissolved MoO_4^{2-} is relatively inert, while MoS_4^{2-}, which forms under sulfidic conditions,

is readily scavenged by sinking particles (Vorlicek et al., 2004). This dichotomous behavior, coupled with isotopic fractionation resulting from adsorption to sedimentary particles, sets the framework for the utility of Mo isotopes. Seawater has been shown to have a relatively uniform δ^{98}Mo of +2.3‰ (e.g., Siebert et al., 2003; Nakagawa et al., 2008), so sediments deposited in fully euxinic conditions (H_2S_{aq} > 11 µM; Erickson and Helz, 2000) tend to record the δ^{98}Mo of seawater as a result of quantitative Mo removal (e.g., Neubert et al., 2008). Conversely, sediments that form in oxic seawater are more likely to have δ^{98}Mo lighter than seawater as a result of processes such as Mn-oxide formation, which preferentially adsorbs light Mo isotopes (Barling and Anbar, 2004; Wasylenki et al., 2008).

Here, we examine absolute and relative abundances of V, Mo, Re, in conjunction with Mo isotopes, to discern amongst the complex depositional signals that are likely recorded in Mediterranean sapropels. These include climatic signals, water column processes, and possible diagenetic overprinting. We address, primarily, the question of the state of the water column during sapropel deposition, and the conditions that obtained during hemipelagic sedimentation. We discuss how this type of dynamic system differs fundamentally from the type locality for euxinic deposition (the Black Sea), and from oxic, 'suboxic' and anoxic regimes. However, some similarities with all these depositional types will be identified and discussed.

Background

Mediterranean hydrography

The Mediterranean Sea consists of the Eastern Mediterranean and Western Mediterranean, two large basins that are separated by an ~330 m deep sill in the Strait of Sicily, and from the Atlantic Ocean by the 280 m sill in the Strait of Gibraltar. Circulation is characterized by relatively free eastward exchange of surface water, including inflow from the Atlantic Ocean, and westward exchange of subsurface water (Rohling, 1994). This anti-estuarine flow pattern is driven by the excess of evaporation over precipitation (Bethoux, 1980). Evaporation and warming takes place in the surface water as it flows eastward, altering the density and salinity parameters (Millot and Taupier-Letage, 2005). This warm, very salty water sinks during localized convective cooling episodes, and oxygen-rich intermediate and deep water masses are formed (Millot and Taupier-Letage, 2005). The main mass of Mediterranean intermediate water forms in the Levantine basin, and Eastern Mediterranean deep water forms in the Adriatic Sea as a result of intense winter cooling (Robinson et al., 2001; Rohling 1994). Deep convective mixing, which presently keeps the deep parts of both basins well oxygenated, is encouraged by net buoyancy loss (Rohling 1994). Complete renewal of the deep water below 1500 m is estimated to take between 80 (Schlitzer et al., 1991) and 150 years (Roether and Well, 2001). During sapropel deposition, influx of fresh water to the surface layer likely prevented normal convective mixing, weakened the circulation pattern, and possibly led to stratification of the water column, on the scale of ~1000 years (e.g., Rossignol-Strick et al.,

1982). The set-up of the estuarine circulation pattern, where the Western Mediterranean supplies a limited quantity of deep water beneath the buoyant surface layer, has also been suggested (Stratford et al., 2000; Nijenhuis et al., 1999; Warning and Brumsack, 2000). The surface buoyancy maintains stratification until the density deficiency of the surface water is reversed (Rohling, 1994).

Tectonics

The Mediterranean is considered to be a remnant of the Tethys Sea, and the Mediterranean Ridge has been proposed to be a growing accretionary prism, resulting from the convergence of the African and European Aegean plates, where the African plate is subducting beneath the European Aegean plate (e.g., Ryan et al., 1982; Camerlenghi, 1990, Fig. 4.1). The ridge is, therefore, composed of compressional features: folded and faulted sediments, and a 'cobblestone' topography is formed by alternating basins and ridges (Kastens, 1981). The topography is accentuated by dissolution and collapse of the Messinian deposits (karst) and salt doming (Camerlenghi and Cita, 1987). Some of the basins are currently brine filled and anoxic, while others no longer have brine present (Jongsma et al., 1983).

Messinian Salinity Crisis

Beginning at 5.96 Ma, desiccation of the Mediterranean Basin began, and isolation from the Atlantic Ocean occurred between 5.59 and 5.33 Ma (Krijgsman et al., 1999). This allowed for the deposition of as much as 3 km of evaporite sediments typical of sabkha facies and playas (dolomite, gypsum,

anhydrite, halite, and potash), whose upper bound is well delineated in seismic reflection profiles (the 'M' reflector; e.g., Ryan et al., 1971). These layers were definitively identified as such by Hsü et al. (1973), who also proposed a 'desiccation and isolation' model for their formation. Before cores were taken, the existence of Miocene-aged evaporites was known from on-shore sections. These evaporites were buried by 100 to 400 m of late Neogene to Quaternary hemipelagic sediments (Emeis et al., 2000). Evidence has shown that the initial driver of Mediterranean desiccation was not sea-level change, but rather tectonics (Krijgsman et al., 1999), specifically, uplift along the African and Iberian margins that closed the ocean gateway (Duggen et al., 2003).

Site Description

The Ocean Drilling Program's (ODP) Leg 160, conducted in 1995, drilled multiple cores in the Mediterranean Sea with the purpose of recovering extensive Pliocene-Holocene sedimentary sequences (Emeis and Sakamoto, 1998). Site 969 (33.5°N, 24.5°E) is located on the Me diterranean Ridge, ~100 km south of Crete (Fig. 4.1). The water depth at the site is 2192 m (Emeis et al., 2000). The site is located in a region whose surface water could be influenced by Nile runoff, and subsequent delivery of fluvial nutrients (Meyers and Arnaboldi, 2005). The site is bathed by Eastern Mediterranean Deep Water, and lies in the region of water exchange between the Ionian and Levantine basins.

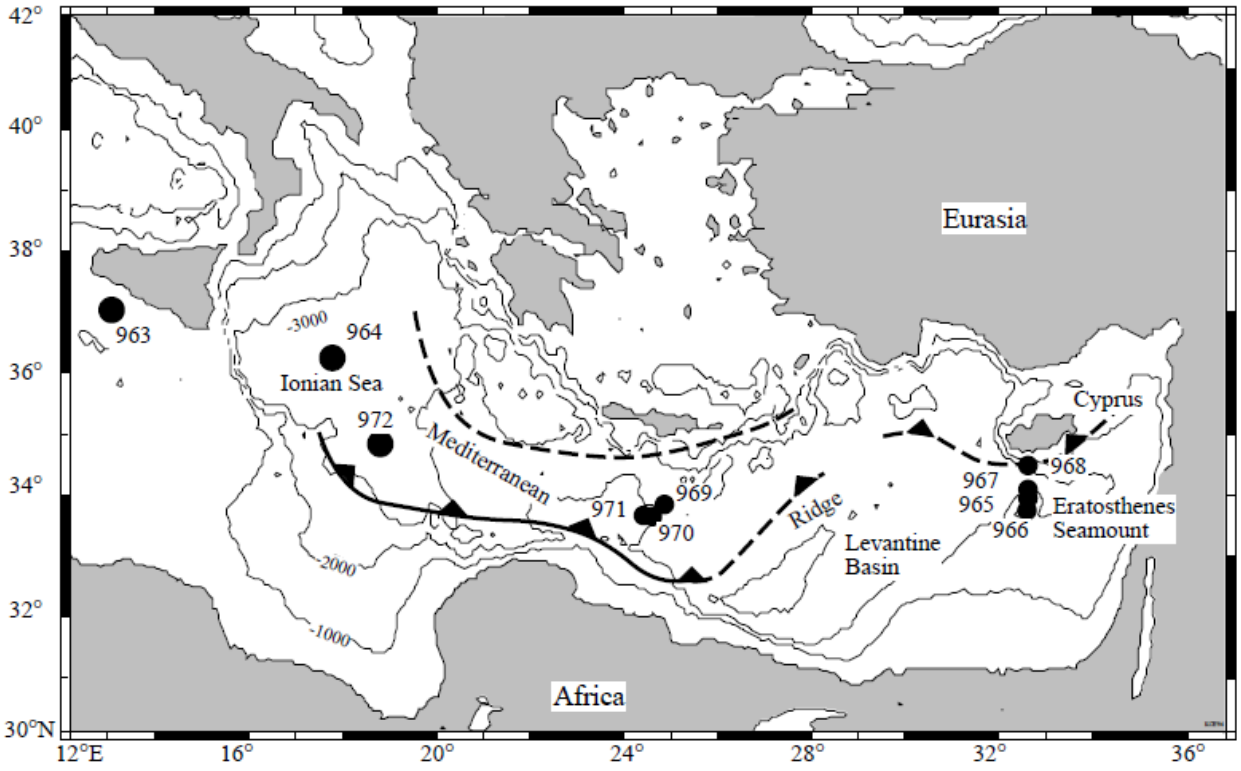

Figure 4.1: Map of the Eastern Mediterranean and ODP cores drilled during Leg 160 (Emeis and Sakamoto, 1998; used with the permission of the Ocean Drilling Program).

Site 969 consists of 6 separate holes (A through F); in this study, only samples from Hole D were examined. Site 969, Hole D was chosen for this study because of the excellent preservation of its sapropels. ODP shipboard procedures involved dividing each hole into ~10 m cores, which were further subdivided into 1.5 m sections. Two cores from Hole D, 4H and 5H, were sampled. The average sedimentation rate in these two cores was 22 m/My, though some intervals had different rates (Emeis et al., 1996; Table 4.1). The dominant lithology is a mix of moderately bioturbated nannofossil ooze, with sparse foraminifera and hemipelagic clay (henceforth referred to as 'hemipelagic' sediment). The hemipelagic sediment is intercalated with

organic-rich sapropel layers. The sapropel layers in both these cores display fine laminations and internal color gradations that can be seen in core photos (Emeis et al., 1996, Appendix 2). In some intervals of hemipelagic sedimentation, extensive reddish layers are apparent, which are though to be the oxidized remains of former sapropels, completely erased by 'burn-down' diagenesis (Emeis et al., 2000), but sometimes retaining a portion of the organic and trace-element rich nature of the precursors (Thomson et al., 1995).

Age model

Assuming the orbitally-driven nature of their deposition, age tuning to an eccentricity-modulated precessional index allows for good precision in ages (±500 yr, Emeis et al., 2000). The middle of each sapropel was assigned an age by Emeis et al. (2000), adapted from the orbital insolation (astronomical) age model of Lourens et al. (1998; Table 4.2). Those ages were determined based on the $La90_{(1,1)}$ summer insolation curve at 65°N (Laskar et al., 1993). The insolation ages themselves are based on cyclostratigraphic tuning to the Laskar et al. (1993) astronomical insolation record, with a 3000 year lag incorporated into the ages (Lourens et al., 1998; Emeis et al., 2000). In this work, the sapropel mid-point ages of Emeis et al., (2000), were used to linearly interpolate ages for the remaining samples (Fig. 4.2), using sedimentation rates from Emeis et al. (1996).

Sampling strategy

The samples record about 420 thousand years of deposition, and span the Pliocene-Pleistocene boundary (1.45 to 1.87 Ma, Table 4.2). More closely-spaced samples were taken in the interval between 1.44 and 1.47 Ma. This interval, thus, has much higher temporal resolution than the samples between 1.48 and 1.87 Ma. The strategy behind the high-temporal resolution samples was to investigate incremental changes in sapropel properties, and thus, in the depositional conditions, over a single sapropel. In contrast, the low temporal resolution samples were intended to provide details about the broader range of potential depositional modes for sapropels in the Mediterranean. All the samples are ~1 cm thick plugs, each of which samples ~500 years of deposition, which is less than the resolution of the age model.

Table 4.1: Sedimentation rates, in meters/million years (m/My) for intervals of core 969D used to calculate ages (Emeis et al., 1996).

Start	End	Sed. Rate (m/My)
4H-2, 40	4H-3, 20	33.6
4H-3, 20	4H-4, 27	29.6
4H-4, 27	4H-5, 95	21.7
4H-5, 95	5H-1, 50	6.4
5H-1, 50	5H-4, 20	22.1

Table 4.2: Core 969D sapropels, their number, insolation cycle, thickness, and duration (Emeis et al., 2000). The depth in the core section is given for the top and bottom of the sapropel. Mbsf: meters below sea floor, for the middle of the sapropel.

Sapropel #	Insol. cycle	Top (cm)	Bottom (cm)	Mbsf (middle)	Thickness (cm)	Time for deposition
25	140	51	86	30.09	35	9700
26	142	122	134	30.68	12	3300
27	152	82	93	33.28	11	5200
28[a]	156	35	51	34.33	16	--
29	160	140	7	35.39	17	28300
31	172	45	65	37.95	20	9100
32[a]	176	42	71	39.47	29	--
33	178	123	139	40.21	16	7300
34	180	38	69	40.94	31	14100
35	182	120	136	41.68	16	7300

[a]Not sampled

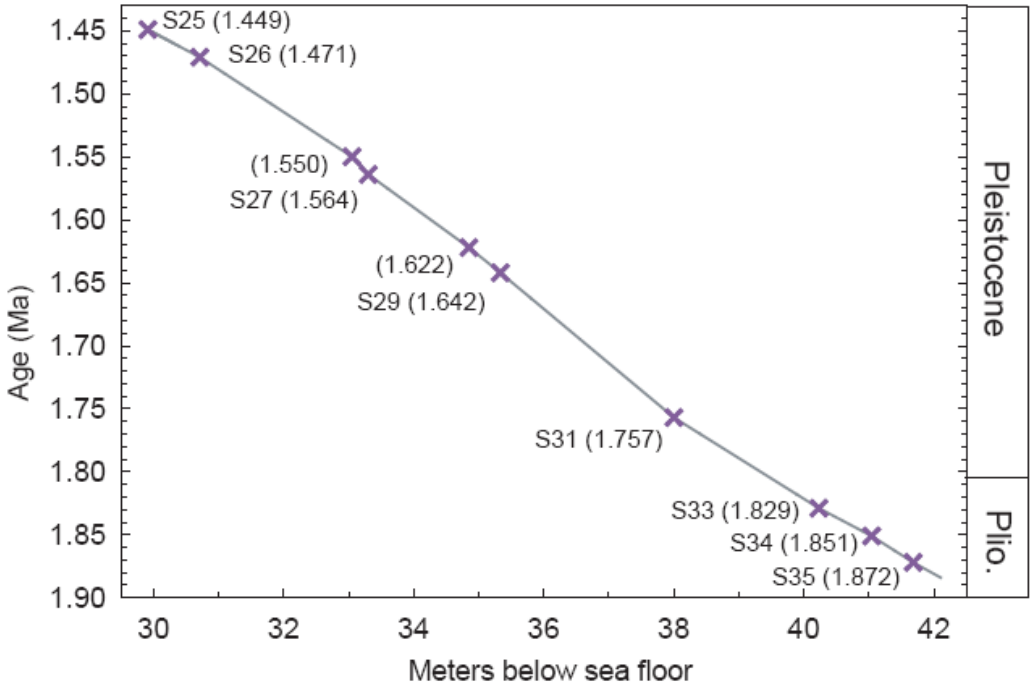

Figure 4.2: Age model for the Mediterranean samples. The cross marks indicate published age points for sapropels or sapropel ghosts (Emeis et al., 2000). These 'tie' points are used to linearly interpolate ages for the other sediment samples. Changes in the slope of the line indicate changes in the sedimentation rate (Table 4.1).

High temporal resolution sampling across a single sapropel (S25)

A single sapropel (I-140, Sapropel #25, samples 4H-2, 54 through 4H-2, 84), which is ~30 cm thick, was sampled at 2-cm intervals, with occasional 4-cm spacing.The deposition of the entire sapropel took ~9700 years (Table 4.2). The advent of sapropel deposition (4H-2, 98 through 4H-2, 88) and the return to hemipelagic sedimentation (4H-2, 40 and 51) were also closely sampled. The deposition of S25 was briefly interrupted after ~6500 years (20 cm), resulting in an ~2000 y (~7 cm) hiatus during which hemipelagic sediments were deposited. The hiatus has been interpreted to be the result of a brief renewal of convective mixing of sufficient intensity to overcome the chemical titration of oxygen by reduced compounds (Rohling et al., 2006; Scrivner et al., 2004). Convective mixing might have occurred as a result of a brief dry period that interrupted the monsoon maximum, resulting in cooling surface water conditions; an idea which is supported for Holocene-aged "interrupted" sapropels (e.g., Rohling et al., 2006; Scrivner et al., 2004). After the hiatus, sapropel deposition then continued for a further ~1200 y (3 cm) interval. Emeis et al. (2000), considered the total unit as a single sapropel.

Low temporal resolution samples

This aspect of the study examines samples from seven different sapropel layers. Two samples were taken adjacent to one another in two of these sapropels. Hemipelagic sediments were sampled at random intervals, and several were taken in areas of the core where reddish pigmentation was noted (Emeis et al., 1996). One sample (4H-6, 40) is a 'ghost' sapropel,

which is a former sapropel where the organic carbon has been completely oxidized.

Analytical Methods

All the samples were prepared by first crushing to a fine powder in a ceramic mortar, and then combusting at 500°C in a furn ace for ~5 hours, in order to rid the sample of organic carbon. Combustion at this temperature does not result in a loss of Mo or Re, nor does it change the Mo isotopic composition (Scheiderich et al., 2010). Small subsamples of powder were dissolved and spiked with a ^{97}Mo spike, in order to determine preliminary Mo concentrations. These measurements were made by single-collector ICP-MS. For determination of isotopic composition and final concentrations, the samples were weighed into Teflon Savillex beakers and an appropriate amount of a ^{97}Mo-^{100}Mo double spike solution was weighed and added. Dissolution was accomplished by adding concentrated distilled acids (HCl, HNO_3, $HCLO_4$, and HF) and heating to 90°on a hot plate. In the case of the hemipelagic samples, which are carbonate-rich, the spiked sample was transferred to a clean centrifuge tube, and shaken with 1-2 ml of 1M HCl until all the carbonate was reacted. 3-4 ml of distilled H_2O was added and the sample was centrifuged. This solution was drawn off, transferred to a clean beaker, dried, then reconstituted in 6M HCl. The remaining solid sample was then digested with HF. After the HF step, the solution was returned to the digested sample. This method circumvents the difficulty of using HF to accomplish a bulk dissolution of Ca-rich samples, where appreciable amounts

of insoluble CaF will form, and possibly sequester Mo. This method was tested by analyzing comparing it to the same samples processed via a bulk method (Chapter 2). Resulting isotopic values and concentrations were identical within analytical uncertainties. Once fully dissolved, Mo was separated from matrix using an anion exchange column, followed by a cation exchange column. Often a third column was necessary to complete the separation; this column was a small version of the initial anion column. Details of the bulk dissolution and chromatographic procedures are described in Chapter 2. For each set of samples, one of two in-house rock standard reference materials was also processed and analyzed. These data are provided in Chapter 2. Duplicate samples are shown in Appendix 2. The concentration errors from the double-spike method were a maximum of ~4%, and the 2-s.d. error for Mo isotope analyses is ±0.1‰, based on long-term reproducibility of the two in house reference materials. The Mo blank averaged 3 ng, which comprised less than a tenth of 1% of total Mo extracted from any sample, and was inconsequential for all samples.

Combusted powder was sub-sampled for Re concentration analysis via isotope dilution. This was accomplished by adding a ^{185}Re spike to small quantities (<0.1 g) of bulk sample, and dissolving them. The Re chromatographic separation procedure is described in Morgan and Walker (1989). The Re blank was <10 pg and was insignificant for all samples. Errors on Re concentrations are ±1% or better. All Mo and Re measurements were

performed using a Nu Plasma MC-ICP-MS, coupled with an ESI Apex desolvating nebulizer for sample introduction.

Major and select minor element analysis was performed on uncombusted sample material by X-ray fluorescence (Phillips 2402 XRF vacuum spectrometer) at Franklin and Marshall College, PA. Approximate uncertainties for XRF analysis in this lab are ±1% for major elements and ±5% for minor elements (Boyd and Mertzman, 1987). Detection limits for Co, Cr, and V are 1-2 µg/g, for Sr and Zr, 0.5 µg/g, and for Ba 5 µg/g. Detection limits for major elements are 0.02 g/kg (Marques et al., 2004).

Total organic carbon (TOC) was determined on µg quantities of uncombusted, carbonate-free sapropel. The carbonate was eliminated from the sample by reaction with 1M HCl. Once all the carbonate was dissolved, the sample was dried, and the requisite amount weighed into an aluminum boat. The analyses were performed on a Micromass Isoprime continuous flow mass spectrometer. Errors for TOC are ≤0.3%, based on reproducibility for repeated analyses of an organic carbon standard.

A small subset of sapropel and hemipelagic samples were processed and analyzed for multiple sulfur isotopes. The methods for separation of sulfur phases and subsequent analysis of sulfur isotopes are described in Appendix 2. All data are normalized to V-Canyon Diablo Troilite (V-CDT), and $\delta^{34}S$ is further normalized to Mediterranean seawater sulfate.

Results

Molybdenum isotope data, V, and Re concentrations, and Mo/Al, Fe/Al and Mn/Al ratios are plotted, relative to age, in Figures 4.3 and 4.4. The plots are separated into high-resolution (1.44 to 1.47 Ma) and low-resolution (1.48 to 1.90 Ma) for clarity. In these figures, Mo/Al ratios, Fe/Al, and Mn/Al are plotted in order to illustrate variations in an element relative to terrigenous concentrations. For these samples, Al is controlled by terrigenous input, so normalizing to Al eliminates the effects of trace element dilution by carbonate as well as opal (Nijenhuis et al., 1999; Lyons et al., 2003). The ranges of V, Re, Mo/Al, Fe/Al, Mn/Al, and δ^{98}Mo values, are illustrated for both hemipelagic and sapropel samples in Figs. 4.5 and 4.6. Noteworthy aspects of these parameters include the large range of δ^{98}Mo values (4‰) in hemipelagic material, and the smaller range present in the sapropels (1.8‰).

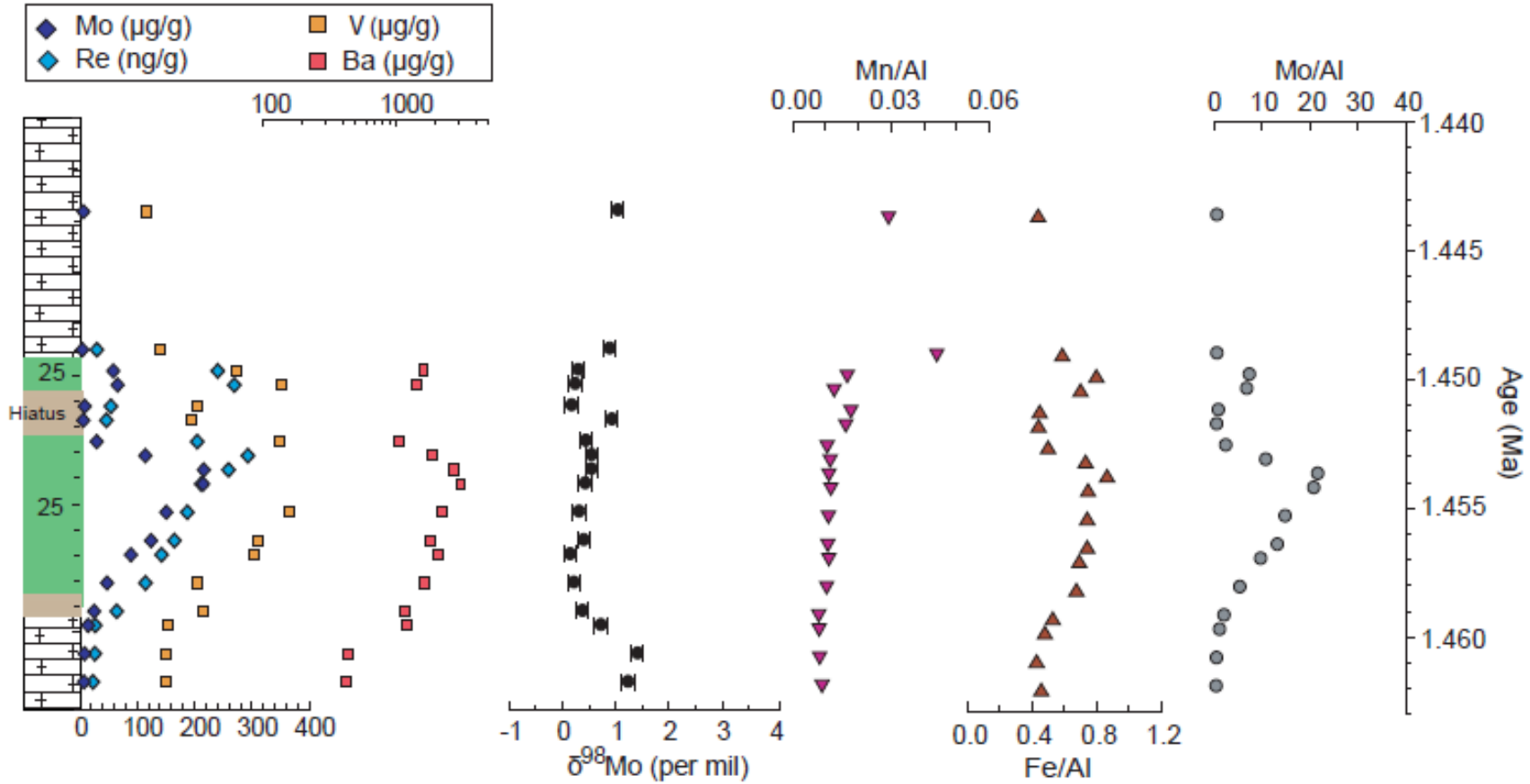

Figure 4.3: The high-temporal resolution sampling across S25. The green layer represents the sapropel, whereas the brown layers encompass samples whose geochemistry is most likely influenced by proximity to the sapropel. Hemipelagic intervals are indicated by the blocked background.

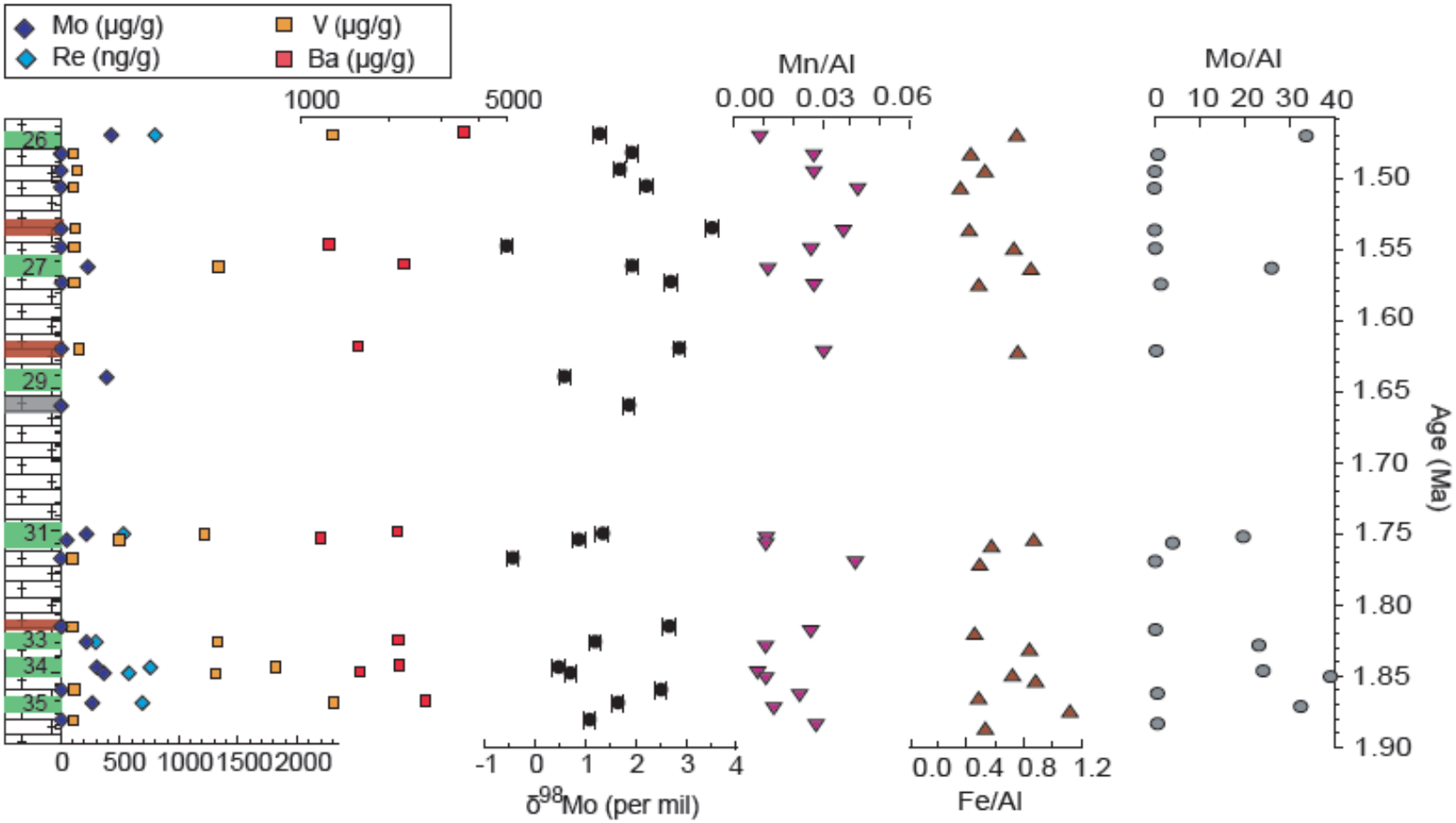

Figure 4.4: Low temporal resolution sampling in older sediments. Red-brown layers indicate regions that may be affected by oxidative diagenesis (Emeis et al., 2000). The grey bar is a ghost sapropel. The thickness of the colored bands is not a true representation of the time-duration of the layers, because of compression of the time axis.

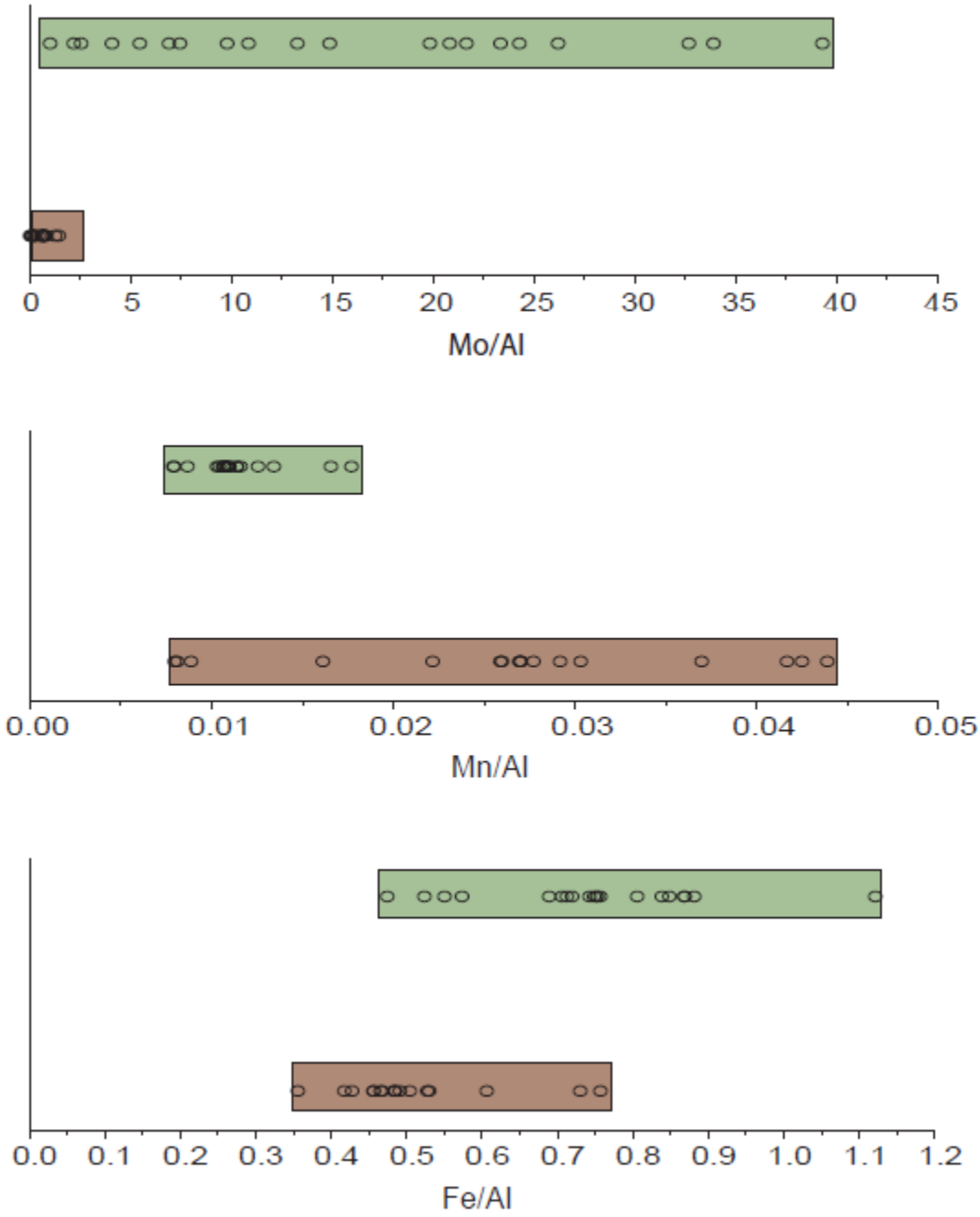

Figure 4.5: Range plots for Mo/Al, Mn/Al and Fe/Al. Green boxes are sapropels, brown boxes are hemipelagic sediments. Sample values are shown as circles within each range.

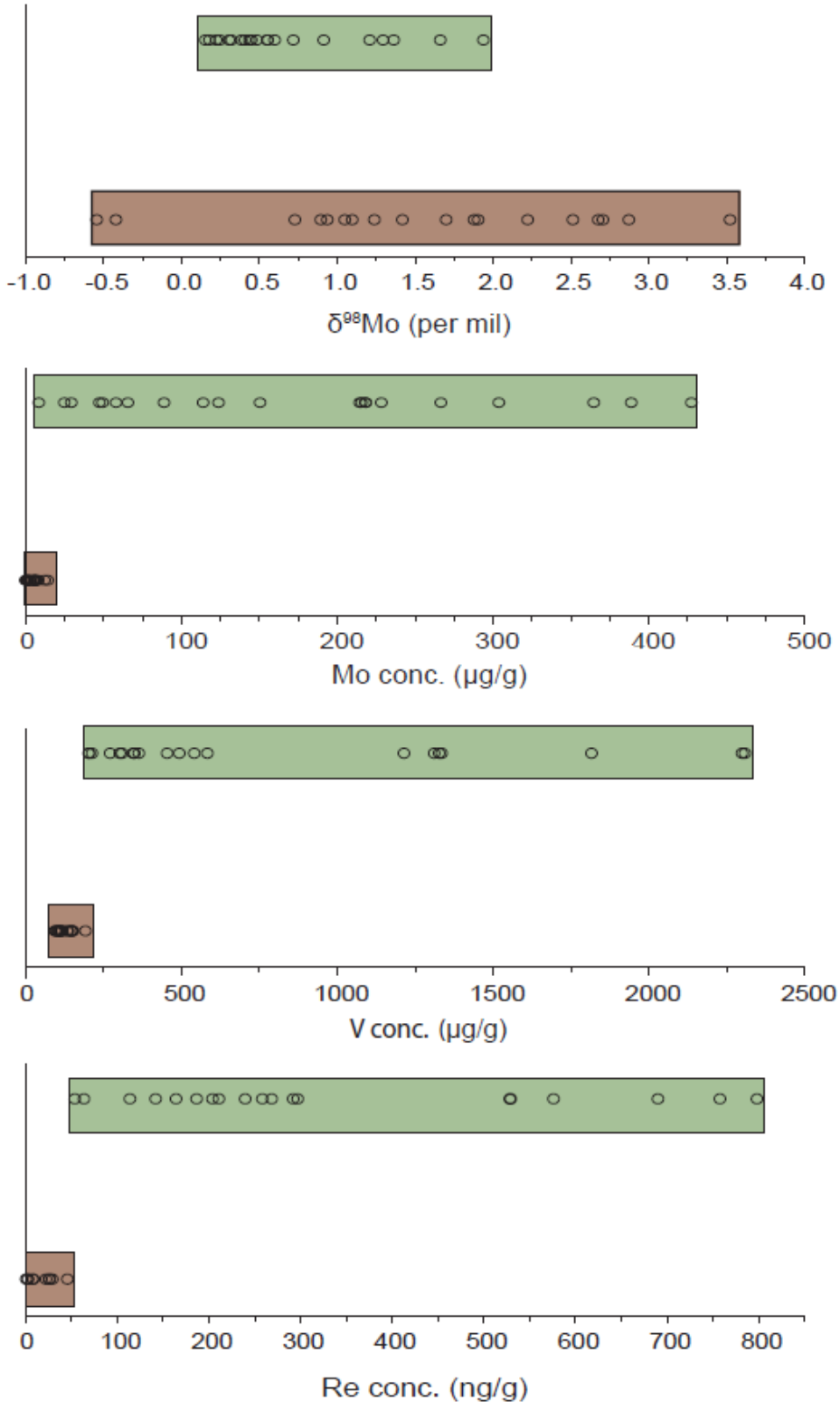

Figure 4.6: Range plots for δ^{98}Mo, and Mo, V, and Re concentrations. Green boxes are sapropels, brown boxes are hemipelagic sediments. Sample values for each parameter are indicated as circles within the range.

Table 4.3: Trace element concentrations and major element ratios (weight %) for redox-sensitive elements, and Mo isotope data for the entire data set. Molybdenum isotope data are relative to the UMD plasma standard (~0‰).

969D Samples	Sap. #	Age	Mbsf[a] (top)	δ^{98}Mo ‰	V conc. µg/g	Mo conc µg/g	Re conc ng/g	Re/Mo	Mo/Al	Mn/Al	Fe/Al
4H-2, 40		1.444	29.80	1.05	116	6.82			0.77	0.029	0.47
4H-2, 51		1.449	29.91	0.90	139	4.92	30.2	6.1	0.77	0.044	0.61
4H-2, 54	25	1.450	29.94	0.31	274	58.7	241	4.1	7.5	0.017	0.81
4H-2, 56	25	1.450	29.96	0.25	352	66.3	270	4.1	7.0	0.013	0.71
4H-2, 59		1.451	29.99	0.19	206	9.05	54.7	6.0	1.1	0.018	0.48
4H-2, 61		1.452	30.01	0.94	195	6.56	46.7	7.1	0.71	0.016	0.47
4H-2, 64	25	1.453	30.04	0.45	348	29.9	205	6.8	2.6	0.010	0.52
4H-2, 66	25	1.453	30.06	0.56	457	115	293	2.6	11	0.011	0.74
4H-2, 68	25	1.454	30.08	0.56	544	216	259	1.2	22	0.011	0.87
4H-2, 70	25	1.454	30.10	0.44	586	215	212	1.0	21	0.012	0.76
4H-2, 74	25	1.455	30.14	0.33	366	151	188	1.2	15	0.011	0.75
4H-2, 78	25	1.456	30.18	0.41	312	124	165	1.3	13	0.011	0.75
4H-2, 80	25	1.457	30.20	0.16	305	89.4	143	1.6	10	0.011	0.71
4H-2, 84	25	1.458	30.24	0.23	206	48.0	115	2.4	5.5	0.010	0.69
4H-2, 88		1.459	30.28	0.39	216	25.4	65	2.5	2.2	0.0079	0.55
4H-2, 90		1.460	30.30	0.74	155	14.9	27.5	1.9	1.3	0.0080	0.51
4H-2, 94		1.461	30.34	1.42	150	8.62	26.6	3.1	0.70	0.0082	0.46
4H-2, 98		1.462	30.38	1.24	149	7.57	23.3	3.1	0.61	0.0089	0.48

[a]Meters below sea floor of the top of the sample.

Table 4.3: continued.

969D Samples	Sap. #	Age	Mbsf (top)	δ^{98}Mo ‰	V conc. µg/g	Mo conc µg/g	Re conc ng/g	Re/Mo	Mo/Al	Mn/Al	Fe/Al
4H-2, 131	26	1.471	30.71	1.30	2300	428	799	1.9	34	0.0087	0.75
4H-3, 20		1.484	31.10	1.91	110	6.82	1.56	0.23	0.88	0.027	0.43
4H-3, 55		1.496	31.45	1.71	136	1.46			0.16	0.027	0.53
4H-3, 90		1.508	31.80	2.23	103	0.479			0.073	0.043	0.36
4H-4, 27		1.537	32.67	3.53	120	1.12	3.41	3.1	0.14	0.037	0.42
4H-4, 65		1.550	33.05	-0.54	112	2.33			0.26	0.026	0.73
4H-4, 90	27	1.564	33.30	1.94	1340	229			26	0.011	0.85
4H-4, 120		1.575	33.60	2.71	116	12.8	8.61	0.67	1.5	0.027	0.49
4H-5, 95		1.622	34.85	2.88	152	3.82	3.22	0.84	0.46	0.030	0.76
4H-5, 143	29	1.642	35.33	0.60		389					
4H-6, 40		1.662	35.80	1.88		3.45					
5H-1, 50	31	1.753	37.90	1.37	1220	219	530	2.4	20	0.011	0.87
5H-1, 60	31	1.757	38.00	0.92	496	50.1			4.1	0.011	0.57
5H-1, 100		1.770	38.40	-0.42	97	1.58			0.26	0.042	0.49
5H-2, 99		1.818	39.89	2.68	100	2.08	9.51	4.6	0.28	0.026	0.46
5H-2, 133	33	1.829	40.23	1.22	1330	219	298	1.4	23	0.011	0.84
5H-3, 49	34	1.847	40.89	0.49	1820	304	759	2.5	24	0.0080	0.72
5H-3, 64	34	1.851	41.04	0.72	1310	365	577	1.6	39	0.011	0.88
5H-3, 100		1.863	41.40	2.52	117	6.30			0.74	0.022	0.49
5H-3, 128	35	1.872	41.68	1.67	2310	267	691	2.6	33	0.013	1.12
5H-4, 20		1.884	42.10	1.10	106	6.11			0.77	0.028	0.53

[a]Sapropel numbers, ages and Mbsf data from Emeis et al., 2000.

Table 4.4: Major and trace element data for sapropel samples. Major elements in weight %, trace elements in µg/g. Insufficient material was available to perform these analyses on 4H-5, 143.

969D	SiO_2	TiO_2	Al_2O_3	Fe_2O_3 T	MnO	MgO	CaO	Na_2O	K_2O	P_2O_5	SO_3	LOI[a]	Sr	Zr	Cr	Co	Ba
4H-2, 54	26.6	0.4	7.8	6.3	0.13	3.7	46.7	2.5	1.0	0.3	1.0	32.0	1220	140	120	53	1620
4H-2, 56	31.9	0.4	9.5	6.8	0.12	4.1	36.6	2.7	1.3	0.3	1.1	27.6	980	150	130	58	1440
4H-2, 59	29.9	0.4	8.5	4.0	0.15	3.6	50.7	1.8	1.0	0.1	0.3	30.2	1360	150	100	<2	
4H-2, 64	40.6	0.6	11.5	6.0	0.12	4.7	30.7	2.4	1.4	0.2	0.2	26.9	950	180	170	38	1050
4H-2, 66	37.1	0.5	10.5	7.8	0.12	4.4	29.3	2.8	1.5	0.2	0.4	29.0	820	190	180	79	1870
4H-2, 68	25.7	0.5	10.0	8.7	0.11	4.2	27.9	2.8	1.4	0.2	1.4	31.5	790	180	200	49	2700
4H-2, 70	37.6	0.5	10.3	7.8	0.12	4.3	28.7	3.2	1.5	0.2	0.1	31.7	840	200	190	31	3080
4H-2, 74	37.3	0.5	10.1	7.6	0.11	4.4	28.2	3.0	1.6	0.1	0.6	29.2	760	180	160	49	2260
4H-2, 78	35.2	0.5	9.3	7.0	0.10	4.2	31.8	3.2	1.6	0.1	0.6	28.7	790	170	160	30	1820
4H-2, 80	33.9	0.5	9.1	6.4	0.10	4.0	35.8	3.0	1.5	0.2	0.4	29.4	890	170	140	28	2100
4H-2, 84	32.8	0.4	8.7	6.0	0.09	3.9	38.2	2.5	1.2	0.1	0.9	27.6	900	150	130	36	1630
4H-2, 88	41.0	0.6	11.3	6.3	0.09	4.8	28.3	2.4	1.4	0.1	0.4	23.8	760	170	190	11	1170
4h-2, 131	42.4	0.6	12.6	9.5	0.11	6.3	10.6	5.0	2.3	0.2	1.3	36.3	540	200	310	75	3550
4H-4, 90	29.8	0.4	8.7	7.4	0.10	4.5	36.6	3.4	1.3	0.2	1.3	28.6	1230	150	190	49	2230
4H-5, 143												42.4					
5H-1, 50	38.1	0.5	11.0	9.6	0.12	5.5	22.1	3.6	1.7	0.2	0.4	38.1	830	170	250	110	2130
5H-1, 60	42.1	0.6	12.1	7.0	0.13	4.8	24.8	2.8	1.5	0.2	0.5	27.3	830	170	180	42	1170
5H-2, 133	36.7	0.5	9.4	7.9	0.10	5.3	29.1	3.4	1.3	0.2	0.9	44.3	990	170	220	57	2120
5H-3, 49	45.7	0.6	12.5	9.0	0.10	5.9	13.4	4.0	2.4	0.2	0.8	40.4	580	190	280	77	2160
5H-3, 64	32.2	0.4	9.3	8.2	0.10	4.6	33.7	3.2	1.2	0.2	1.2	41.3	1140	160	210	53	1590
5H-3, 128	28.5	0.4	8.2	9.2	0.11	4.4	32.6	3.9	1.4	0.2	1.8	46.3	1140	190	240	95	2630

[a]Loss on ignition

Table 4.5: Major and trace element data for hemipelagic samples. Major elements in weight %, trace elements in µg/g. Insufficient material was available to perform these analyses on 4H-6, 40.

969D	SiO_2	TiO_2	Al_2O_3	Fe_2O_3 T	MnO	MgO	CaO	Na_2O	K_2O	P_2O_5	SO_3	LOI[a]	Sr	Zr	Cr	Co	Ba
4H-2, 40	30.3	0.46	8.9	4.2	0.26	3.3	49.9	1.7	0.9	0.2	0.3	30.4	1570	180	79	<2	
4H-2, 51	22.3	0.28	6.4	3.9	0.28	2.9	62.1	1.3	0.6	0.2	0.2	34.4	1770	130	72	10	
4H-2, 61	32.7	0.44	9.3	4.4	0.15	3.8	45.3	1.8	1.2	0.1	0.2	28.3	1220	150	120	10	
4H-2, 90	40.6	0.56	11.2	5.7	0.09	4.6	29.6	2.1	1.3	0.1	0.4	22.4	820	170	160	8	1210
4H-2, 94	43.6	0.61	12.2	5.6	0.10	4.6	26.0	2.1	1.8	0.1	0.4	21.5	900	190	130	6	440
4H-2, 98	43.9	0.63	12.3	6.0	0.11	4.5	25.2	2.2	1.7	0.1	0.7	21.2	870	200	110	2	430
4H-3, 20	26.5	0.39	7.8	3.3	0.21	3.4	54.1	1.9	1.2	0.2	0.4	31.1	1680	160	63	<2	
4H-3, 55	31.9	0.42	8.9	4.7	0.24	4.0	44.0	2.1	1.3	0.1	0.4	28.1	1350	150	120	<2	
4H-3, 90	23.3	0.32	6.6	2.4	0.28	3.3	61.7	1.2	0.7	0.2	0.1	34.9	1750	140	61	<2	
4H-4, 27	27.8	0.38	7.8	3.3	0.29	3.7	54.0	1.4	0.9	0.2	0.2	32.4	1530	150	84	<2	
4H-4, 65	30.7	0.45	8.8	6.5	0.23	3.4	44.7	1.6	0.7	0.2	0.5	24.8	1430	170	94	<2	1240
4H-4, 120	31.1	0.42	8.5	4.1	0.23	3.7	48.8	1.8	0.9	0.2	0.5	29.9	1520	170	64	<2	
4H-5, 95	29.3	0.38	8.2	6.2	0.25	4.4	42.9	2.1	1.3	0.2	0.8	21.9	1150	120	110	3	1560
4H-6, 40												26.0					
5H-1, 100	22.8	0.30	6.0	3.0	0.25	3.4	62.1	1.6	0.7	0.3	0.1	28.6	1730	140	54	<2	
5H-2, 99	27.4	0.37	7.3	3.4	0.19	3.4	55.8	1.5	0.7	0.2	0.1	31.5	1690	160	82	<2	
5H-3, 100	31.5	0.43	8.6	4.2	0.19	3.4	47.9	1.8	1.0	0.2	0.2	29.2	1610	180	69	<2	
5H-4, 20	27.5	0.38	7.9	4.2	0.22	3.3	53.3	1.8	1.1	0.2	0.3	30.9	1440	180	65	<2	

[a]Loss on ignition

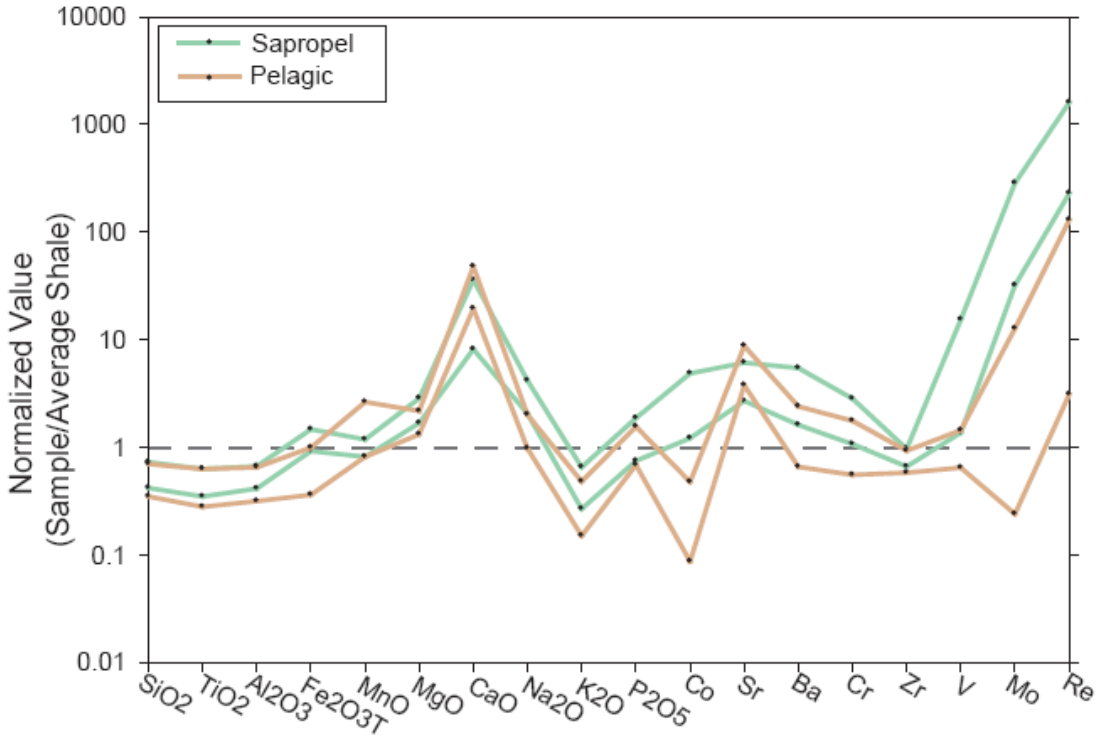

Figure 4.7: Sapropel (green) and hemipelagic sediment (brown) normalized to average shale. The lines represent the upper and lower bound for each sediment type. Values below the dashed line represent depletions relative to average shale; values above represent enrichments relative to average shale. Trace elements to the right are arranged in approximate order of increasing oxidation state. Calcium and Sr are probably enriched as a result of high carbonate concentrations.

Vanadium, Mo, and Re are in low concentrations in the hemipelagic material, compared to the sapropels. Mn/Al ratios tend to be lower in sapropels compared with hemipelagic sediment, while the opposite largely holds true for Fe/Al. Major and some trace element concentrations (V, Cr, Co, Sr, Zr, Mo, Ba, and Re) for both hemipelagic sediments and sapropels, have relative abundance patterns that are distinctly different from average shale (Taylor and McLennan, 1985). Further, for most major elements measured, the average-shale normalized

hemipelagic and sapropel trends are similar to each other (Fig. 4.7). Trends in the trace elements are especially different from average shale, and there are large differences between sapropels and hemipelagic sediment, particularly V, Co, and Ba. In contrast to other studies (e.g., Morford et al., 2005), V in these Mediterranean sediments does not appear to be highly correlated with Mn/Al, but does appear to be positively correlated to Fe/Al.

Total organic carbon (TOC) was determined for some of the sapropel samples in the low temporal resolution sample suite (Table 4.6). TOC contents range from 8 to 19.5%. TOC and V concentration are highly correlated ($r^2 = 0.87$), whereas TOC is only weakly correlated with Mo/Al ratios ($r^2 = 0.57$) (Fig. 4.8).

Table 4.6: Total organic carbon contents (in weight %) for some sapropel samples.

Sample	TOC, wt. %
4H-4, 90	14.73
4H-5, 143	8.18
5H-1, 50	13.31
5H-1, 60	8.03
5H-2, 133	12.37
5H-3, 49	13.93
5H-3, 64	13.75
5H-3, 128	19.48

Results in S25

Over the ~9700 years of S25 deposition, the δ^{98}Mo profile shows a trend to heavier values, starting at +0.23‰ and ending at +0.45‰ before the hiatus, with an average δ^{98}Mo value of +0.36‰ (±0.14, 1 s.d.). No simple correlation exists between redox-sensitive element concentrations and δ^{98}Mo. One of the

hemipelagic samples from the sapropel hiatus has a heavier δ^{98}Mo value than the associated sapropel, and most of these hemipelagic sediment samples have δ^{98}Mo values that are heavier than those in S25.

Beginning ~6 cm below the sapropel proper, concentrations of redox-sensitive elements start to increase above the sediment background. All of the redox-sensitive elements are most concentrated in the upper-middle part of S25. The relative enrichment for V concentrations is much less than for Re and Mo, but generally follow the same pattern. Barium is significantly enriched in the sapropel (Figs. 4.3 and 4.4). During the oxic hiatus, Fe/Al, Mo/Al, and Re concentrations return to background values before increasing again during the renewal of sapropel deposition. Mn/Al is relatively constant (0.01 to 0.02) throughout most of S25, but there is a marked increase to 0.04 just after S25 deposition ends. However, crustal ratios of 0.06 are not attained.

Results in the sediments between 1.48 and 1.90 Ma

The sapropels in this older sequence have δ^{98}Mo values that are much more variable than those in S25. Two sapropels (S34 and S29) have values that are within the range of S25, but other samples are generally heavier, with δ^{98}Mo between +0.9 and +1.9‰. The TOC data are loosely correlated with δ^{98}Mo values and Mo/Al. Many of the older sapropels have larger enrichments in V, Re, Ba, Mo/Al, and Fe/Al, compared with S25.

The hemipelagic samples exhibit mostly heavy δ^{98}Mo values, between +1.1 and +3.5‰. Two samples have very light δ^{98}Mo values (-0.4 and -0.5‰). All

the samples have relatively low concentrations of V, Mo, Re, and low Fe/Al. Most show enrichments in Mn/Al compared to the sapropel layers.

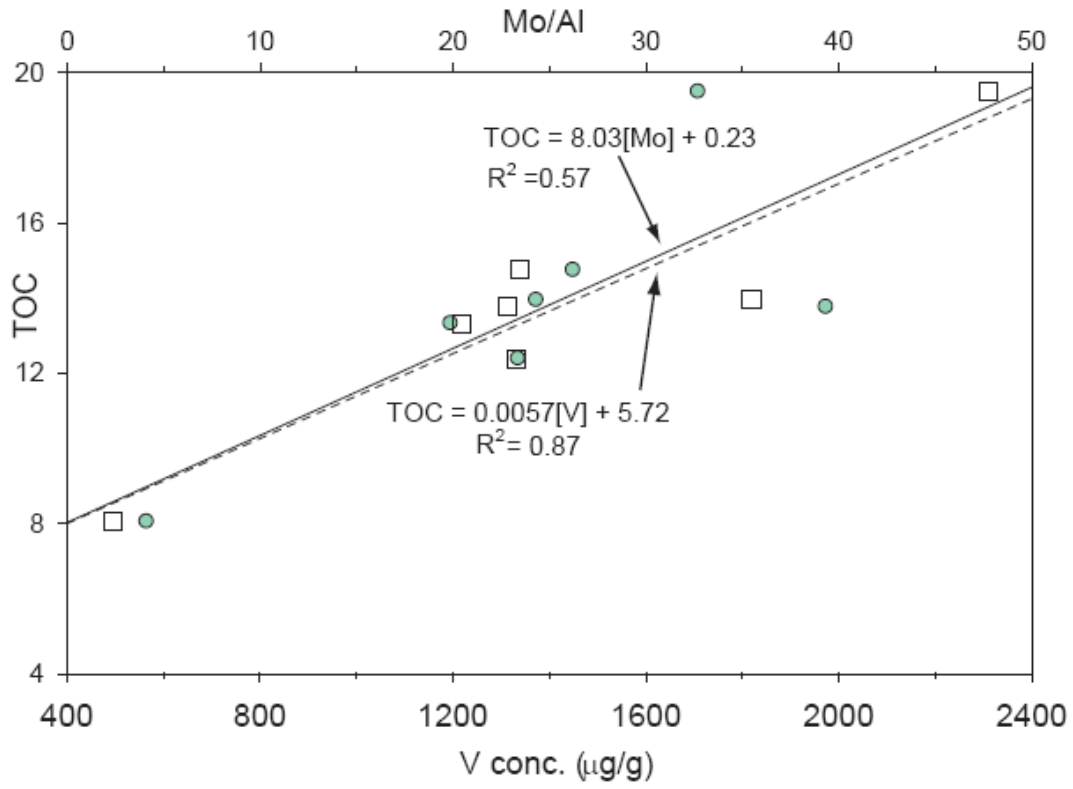

Figure 4.8: Positive correlation, in the older sapropels, between TOC and V concentration (squares), and between TOC and Mo/Al (green circles).

Discussion

The Eastern Mediterranean during sapropel deposition can be compared to the Black Sea, a 'type locality' for euxinic deposition. The Black Sea has been extensively studied with respect to the hydrologic controls operating in the basin, and the effects on redox-sensitive element behavior. Such a comparison provides a context in which to place the Mediterranean sediments. Hydrographically, the two basins differ in a number of features, the first being that

the Black Sea circulation is estuarine. This results from the much lower salinity of the surface waters (~18 psu, Colodner et al., 1995) relative to the hypersaline input from the Mediterranean. The Black Sea has been permanently euxinic below 100 m depth since ~7500 years ago (Ryan et al., 1997), while the modern Mediterranean is well ventilated at all depths (Malanotte-Rizzoli and Robinson, 1992), but experienced anoxic, possibly sulfidic conditions during sapropel events as recently as 7000 years ago.

In general, the Mediterranean sapropels are much richer in the redox-sensitive elements (V, Re, Mo, and Ba) than Black Sea sapropels (e.g., Brumsack 1989; Ravizza et al., 1991; Nägler et al., 2005), which has also been noted by other studies (Rinna et al., 2002; Warning and Brumsack, 2000). Fe/Al ratios in the Mediterranean sapropels and hemipelagic sediment are similar to those from euxinic and oxic Black Sea sediments (Lyons and Severmann, 2006). The average Re/Mo ratio in the Black Sea sapropels (Ravizza et al., 1991; Warning and Brumsack, 2000) is lower than the average in Mediterranean sapropels (1.5 vs. 3.7). Lastly, in the Black Sea, Mo isotope fractionation occurs along the gradient of H_2S_{aq} levels (-0.6 to +2.0‰; oxic sediments ~+0.2‰), until the switch point is reached, whereupon sediments reflect a δ^{98}Mo value close to seawater (~+2.3±0.2‰; Nägler et al., 2005; Neubert et al., 2008; Arnold et al., 2004). The consensus with respect to the Black Sea is that high sulfide levels in the water column, below 400 m, lead to nearly complete scavenging of redox-sensitive elements from the water column.

Redox-sensitive element concentrations

The V, Re, Mo, and Ba concentrations and Fe/Al ratios in S25 appear to track the slow onset of water-column conditions necessary for sapropel deposition (Fig. 4.3). These parameters all begin to increase above the background values at about 6 cm below the sapropel. This might indicate an increased degree of scavenging from the water column. Alternatively, diffusion of sulfide out of the sapropel after its deposition might have increased the diagenetic fixation of these elements (Rinna et al., 2002). These parameters reach a peak in the middle to upper portion of S25, which could reflect the most intense reducing conditions in

the water column. After the hiatus, V, Re, and Mo do not again reach as high concentrations as in the main portion of S25, suggesting that suboxic conditions dominated.

Many of the older sapropels (S26, S27, S34, S35) have all the indicators of high degrees of oxygen depletion: high Mo, Re, and V concentrations, and high TOC, Fe/Al, and Mo/Al. These examples have 2 to 4 times as much V as S25, and higher Re and Mo concentrations, suggesting that different depositional conditions may have obtained. Vanadium and TOC are highly correlated in these samples (Fig. 4.8), as a result of V being strongly associated with organic carbon (e.g., Emerson and Huested, 1991). Mo/Al and TOC are less well correlated (Fig. 4.8), possibly because Mo removal may be positively controlled by the amount of sulfide (HS^-) produced in organic carbon-rich sediments (Crusius et al., 1996; Helz et al., 1996; Erickson and Helz, 2000; Lyons et al., 2000).

Fe/Al in Mediterranean sediments

Fe/Al ratios are another proxy for the state of the water column during deposition, Fe/Al between 0.6 and 1.2 characterizes euxinic conditions, ratios between 0.5-0.6 indicate more oxic deposition (Lyons and Severmann, 2006). Iron deposited on oxic shelf environments will be remobilized, until it eventually moves into the deep euxinic water where it can be fixed as pyrite, enriching the euxinic sediments relative to the oxic sediments (Lyons and Severmann, 2006). Fe/Al can also reflect Fe enrichment through formation of Fe-oxyhydroxide phases, when euxinic conditions are not present (Lyons and Severmann, 2006). In sediments immediately surrounding sapropels, post-depositional diagenesis can result in formation of FeO_x phases can form from oxidized pyrite (Larrasoana et al., 2003).

The average Fe/Al of sapropels in this study is 0.75 (± 0.15, 1σ); by the Lyons and Severmann (2006) scheme these values are well within the euxinic range. However, the light δ^{98}Mo values differ from expectations for sediments deposited under such conditions (Fig. 4.9). The discrepancy may be related to higher Fe input to the basin during sapropel formation, consistent with hypotheses of increased nutrient fluxes (Rossignol-Strick et al., 1982; Rohling and Gieskes, 1989; Thomson et al., 1995). However, the Fe/Al ratios do indicate an overall O_2 depleted system.

δ^{98}Mo of Mediterranean sediments

There are two particularly striking features in this data set. The first is the wide range in δ^{98}Mo within organic-rich layers that presumably formed under low-

O_2 conditions, coupled with the fact that few of the values approach the presumed δ^{98}Mo of Mediterranean seawater (~+2.3‰). This is particularly striking when compared with the consistency of the sapropel δ^{98}Mo values from the Black Sea.

The second unusual feature in the sample set is the even larger range of δ^{98}Mo values that are evident in the hemipelagic ooze deposited between sapropel episodes, and the very heavy δ^{98}Mo in many of these samples. It might be expected that these sediments, deposited under oxic conditions, would have light δ^{98}Mo values consistent with any of the following processes: addition of detrital Mo (~0‰), removal to MnO_x (δ^{98}Mo = -0.8 to -0.‰, Barling and Anbar, 2004, Wasylenki et al., 2008), or removal to FeO_x (-0.4 to +1.3‰, Goldberg et al., 2009). MnO_x, in particular, is a significant carrier of Mo in oxic oceanic sediments (Bertine and Turekian, 1973). However, while many of these samples have Mn/Al ratios greater than those in the sapropels, only two samples have δ^{98}Mo values typical of MnO_x-rich sediments. FeO_x phases may dominate over MnO_x in marine sediments (Poulton and Raiswell, 2002), and can also adsorb large amounts of Mo (Gustafsson, 2003). Thus, the range of fractionation seen within the hemipelagic sediments may be partly a result of adsorption to FeO_x (Goldberg et al., 2009). Indeed, in the Black Sea, oxic hemipelagic sediments are significantly lighter (-0.1 to +0.3‰) than the sapropel above them (Nägler et al., 2005; Neubert et al., 2008). Thus, the

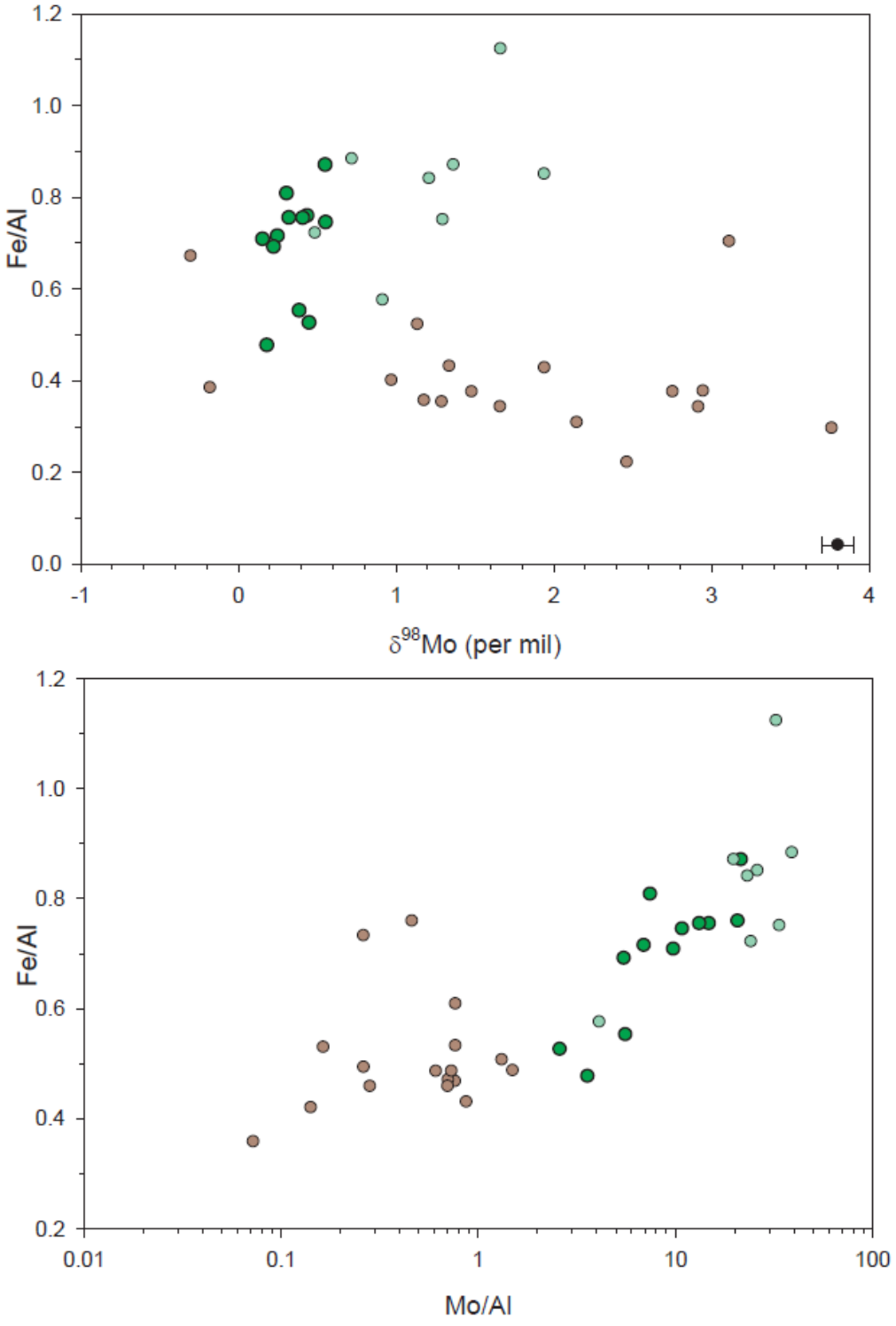

Figure 4.9: Top: Fe/Al versus Mo isotopic composition. **Bottom:** Fe/Al versus Mo/Al. Symbols as in previous figures (brown for hemipelagic sediments, dark green for S25 and pale green for older sapropels).

positive values in the Mediterranean oxic sediments are contradictory to the prevailing view about how δ^{98}Mo values are controlled in the oceans. In order to explain these two features, two general classes of mechanism are considered. The first class includes mechanisms that utilize a different source of Mo during sapropel versus hemipelagic deposition. The second class invokes variable fractionation mechanisms of Mo from the same source material, probably seawater, during the two times.

Variable Mo sources

Two possibilities for a Mo source other than seawater will be discussed. The first of these possibilities involves the upward diffusion of Mo-rich brine from buried Messinian salt deposits. Evaporative processes may enrich a brine in trace elements, particularly Mo, and result in δ^{98}Mo in brines similar to, or heavier than, seawater (Ryb et al., 2009). It has been argued that upward brine migration contributed to the salinity of the modern Mediterranean (van Santvoort, 1996). However, several observations are inconsistent with the idea that the Mo in sapropels was delived by an Mo-rich brine. An upward-migrating brine would have to move through ~70 m of sediment, through which other sapropels are distributed. It would likely lose any Mo that it carried as soon as it encountered sulfidic pore water. Secondly, and more importantly, an upward-moving front might be expected to yield the heaviest δ^{98}Mo values near the bottom of a profile, with values decreasing smoothly towards the top as a result of diffusive fractionation. However, the profile shows both light and heavy values in the lower and upper sapropels, probably ruling out a brine-related mechanism.

The second possibility for variably-sourced Mo is a change in the δ^{98}Mo of surface seawater during sapropel deposition, stemming from freshwater influx. The δ^{98}Mo of the sapropels could be set by scavenging of Mo in the highly productive surface waters. Both Mo isotope and trace-element mass-balance calculations provide arguments against a significant change in the δ^{98}Mo of seawater during sapropel deposition.

The dilution of ambient seawater with Nile freshwater of a different isotopic composition could affect the δ^{98}Mo of the Mediterranean, and thus, of sapropels forming under euxinic or anoxic conditions. To test this, a simple conservative linear mixing calculation was performed, using the Mo concentrations and δ^{98}Mo values of Nile river water (Archer and Vance, 2008). It is necessary to assume that Pliocene-Pleistocene oceanic δ^{98}Mo was similar to today's +2.3‰ (Siebert et al., 2003). Futher description of the calculation and a plot of the results of the calculation are given in Appendix 2. In order to significantly change the isotopic composition of the Eastern Mediterranean through freshwater addition alone, the mix would require >80% freshwater, because the Mo concentration in river water is low (<1.4 µg/L) compared to seawater.

It is possible to assess the likely sources of V, Mo, and Re to the sapropels, and to determine whether the Eastern Mediterranean was entirely restricted during sapropel deposition (Nijenhuis et al. (1999). The total amount of metal, in kg, in a sapropel deposited over an area of 2/3 of the Eastern Mediterranean is calculated (Table 4.7). Using the volume of the Eastern Mediterranean, the total amount of metal (in kg) available in the basin is also

calculated. Using the deposition rate of the sapropel, and metal concentration, the rate of removal of each element can be calculated. Different potential trace element sources are manipulated to determine the time required to satisfy the sapropel metal 'demand' with that source. These sources are: Nile river influx increased by factors of 1.5 and 10; Nile influx increased by 1.5 plus Black Sea water; and exchange with Western Mediterranean seawater. The concentration parameters for seawater, Nile river water and Black Sea water are given in Table 4.8. The flow parameters are further described in Appendix 2. In the calculations using river water and Black Sea water, the time to deliver the requisite metal quantities is many times longer than the duration of sapropel deposition (Table 4.7). However, seawater satisfies the trace element quantities, even at an exchange rate decreased by a factor of 10.

Furthermore, if seawater was the source, then circulation between the Eastern Mediterranean and Western Mediterranean cannot have shut down completely, or the effect would be seen as a sudden decrease in trace-metal concentration across the sapropel. The amount of time required to completely deplete the Eastern Mediterranean in V, Mo and Re, given isolation of the deep water, and removal at the calculated rates, is given in the last column. In most cases, the times are shorter than the duration of sapropel deposition, yet no sudden decrease is seen in the trace element profiles (Fig. 4.3).

Thus, either scavenging was incomplete (but probably high), or circulation continued between the two basins. A scenario of limited circulation is consistent with evidence for reduced ventilation during formation of some sapropels (e.g.,

Casford et al., 2003; Larrasoana et al., 2003), because the vast quantities of sinking organic matter would rapidly deplete the new deep water mass of O_2 (e.g., Rohling, 1994). Support for incomplete scavenging can be seen in the profile of δ^{98}Mo in S25. The near constant values suggest that the δ^{98}Mo of the source water was not changing during sapropel deposition.

V*ariable Mo fractionation mechanisms*

The degree of variability between sapropels and hemipelagic sediments suggests a fractionation process within the water column or pore water, or possibly a diagenetic resetting of the δ^{98}Mo values after burial, as was observed for Holocene Mediterranean sapropels (Reitz et al., 2007). Sapropels frequently experience post-depositional oxidative diagenesis (e.g., Thomson et al, 1995; Jung et al., 1996). During such a process, Mo could be fractionated during uptake to oxic authigenic phases such as MnO_x (Reitz et al., 2007) or FeO_x. Thus, it is important to determine whether the sapropels in this study were 'burned down'. It has been argued that Ba is the trace element that is least susceptible to this effect, and is, therefore, the best indicator of the original extent of a sapropel (Thomson et al., 1995; Wehausen and Brumsack, 2000). Profiles of Ba and Mo concentrations suggest that S25 did not experience an oxidation front (Figs. 4.3 and 4.4).

Previous studies have reported conditions under which isotopic fractionation of Mo relative to seawater could occur in the water column: 1) anoxic margins, where δ^{98}Mo of +1.6‰ have been reported (Poulson et al., 2006), 2) 'suboxic' water columns where δ^{98}Mo has been observed to range from

-0.5 to +1.6 (e.g., Siebert et al., 2006), 3) variably sulfidic water columns below, and up to, the quantitative switch point (Erickson and Helz, 2000), where δ^{98}Mo has been observed to range between -0.6 and +2.4‰ (Neubert et al., 2008), and 4) in oxic sediments, uptake of Mo by MnO_x and FeO_x can significantly fractionate Mo from seawater values (Barling and Anbar, 2004, Wasylenki et al., 2008; Goldberg et al., 2009).

In a previous study of Mo isotopes in a Mediterranean sapropel, it was found that the δ^{98}Mo values could be attributed to dissolution of MnO_x and delivery of light δ^{98}Mo to the pore water, which could then be fixed as thiomolybdates below the redox boundary (Reitz et al., 2007). Such a hypothesis seems less likely in this case, because there is a distinct difference: geochemical evidence suggests that the Eastern Mediterranean was intermittently ventilated during S1 deposition (Casford et al., 2003), whereas most of the evidence presented thus far indicates suboxic water column conditions during deposition of S25, and anoxic conditions for most of the older sapropels. Development of MnO_x layers during sapropel deposition is, thus, unlikely. As further support for the lack of a MnO_x role in the δ^{98}Mo values of S25, Mn/Al ratios are consistently low. A peak in Mn/Al just above the sapropel most likely indicates the depth of the redox boundary in the sediments at some time after sapropel deposition had ceased. The peak in the Mo profile is not coincident with the Mn peak, suggesting that Mn dissolution and Mo enrichment are not related.

Table 4.7: Mass balance calculations. All trace metals in quantities of µg/g (sapropel and background values) or µg/L (Seawater, Nile water, and Black Sea water). Calculations for S25 and S26 are shown. See Table 4.2 for sapropel thicknesses, deposition rates, and durations. Calculations from Column 4 onward are made using an excess quantity in the sapropel, over the background concentration for each element. Average density of the sapropel is 1.4 g/cm^3.

S25	**µg/g ave.**	**kg in sapropel**	**kg in SW in EM***	**Removal rate (kg/yr)**	**River * 1.5**	**River * 10**	**River + Black Sea**	**Seawater**	**Seawater/10**	**No SW input**
V	430	1.4×10^{11}	4.1×10^{9}	1.8×10^{7}	187,000	28,000	105,000	2200	21,900	230
Mo	100	4.5×10^{10}	3.4×10^{9}	5.6×10^{6}	83,000	12,400	23,000	80	830	6000
Re	0.2	9.0×10^{7}	1.8×10^{7}	11,300	293,000	44,000	39,000	300	3070	1600
S26	**µg/g**				*(years)*	*(years)*	*(years)*		*(years)*	*(years)*
V	2300	4.0×10^{11}	4.1×10^{9}	1.2×10^{8}	519,000	77,800	292,000	6090	60,900	30
Mo	430	7.8×10^{10}	3.4×10^{10}	2.4×10^{7}	145,000	21,800	40,400	150	1400	1400
Re	0.8	1.5×10^{8}	1.8×10^{7}	44,200	474,000	71,000	63,300	500	4900	400

***Eastern Mediterranean**

Table 4.8: Parameters for concentrations (Seawater, Nile river water, Black Sea water). Background concentrations are from the hemipelagic sediments.

	Seawater	**River water**	**Black Sea water**	**Background**
V	1.65[a]	1[a]	1.5[a]	116
Mo	13.6[b]	0.7[c]	3.5	2.4
Re	0.007[d]	0.0004[e]	0.005[e]	0.003

[a]Emerson and Huested, 1991.
[b]Van der Weijden et al., 1990.
[c]Archer and Vance, 2008.
[d]Anbar et al., 1992.
[f]Colodner et al., 1995.

Delivery of isotopically light Mo from MnO_x dissolution could, nonetheless, have affected the total isotopic composition of S25. In order to generate the observed values, assuming a euxinic water column and complete drawdown from seawater (+2.3‰) and a $\delta^{98}Mo_{MnOx}$ of -0.7‰, 60% of the Mo would need to be delivered from MnO_x. Other sapropels would need a smaller contribution from MnO_x in order to attain their isotopic compositions.

Overall, however, invoking mixing of diagenetic MnO_x-derived Mo is unsatisfying as a way to impart the observed isotopic compositions, because of the lack of Mn/Al enrichments in the sapropels that would indicate delivery of isotopically light Mo. There is no correlation between Mn/Al ratio and $\delta^{98}Mo$, nor between Mn/Al and Mo concentrations or Mo/Al. MnO_x reduction typically happens at such shallow sediment depths that much of the Mn, and presumably any released Mo, or V, can be lost to the bottom water (Morford et al., 2005).

Suboxic and anoxic deposition generate distinctive ranges of Mo isotopic compositions. In Fig. 4.10, these ranges are laid out with respect to the measured bottom water content (Siebert et al., 2006; Poulson et al., 2006), and the Mediterranean data are binned according to the ranges. The largest number of sapropel samples fall into ranges that are consistent with deposition under low, variable degrees of oxygenation. However, the majority of the hemipelagic samples also are encompassed by ranges consistent with lower oxygen, suggesting the possibility that the oxic water column of the Pliocene was less

oxic than the modern Mediterranean, and that therefore hemipelagic deposition was also occurring under a 'suboxic' water column.

A suboxic/anoxic mechanism for the δ^{98}Mo values in the sapropel is problematic in one respect. The observed enrichments in trace metals are at odds with previous studies identifying only small enrichments (<10 µg/g) under bottom water O_2 of 5 µM or less (e.g., Zheng et al., 2000; Nameroff et al., 2002). Fractionation of Mo during formation of thiomolybdate intermediates (Tossell, 2005) provides a possible explanation for the entire range of δ^{98}Mo values in the sapropels. This mechanism occurs under varying concentrations of H_2S_{aq} (Erickson and Helz, 2000), as suggested by Neubert et al. (2007), for Black Sea sediments. Such a process generates a similar range of values to those for suboxic deposition, as noted by Neubert et al., but high redox-sensitive element concentrations are more easily reconciled with a model where low oxygen coexists with low sulfide.

A scenario to generate sulfide and create low bottom water O_2 can be envisioned. Oxidation of high quantities of sinking organic carbon probably contributed to deep water O_2 depletion (e.g., Rohling and Hilgen, 1991), while bacterial sulfate reduction in the forming sapropel, and subsequent outward diffusion of the generated H_2S, may have created a sulfidic layer above the sediments (Passier et al., 1997). The concentration and thickness of the H_2S_{aq} layer above the sediments would be temporally variable, dependant on rates of deep water advection, and the balance between organic matter delivery, sulfate reduction, and reactive Fe supply. Molybdate in the water column, upon

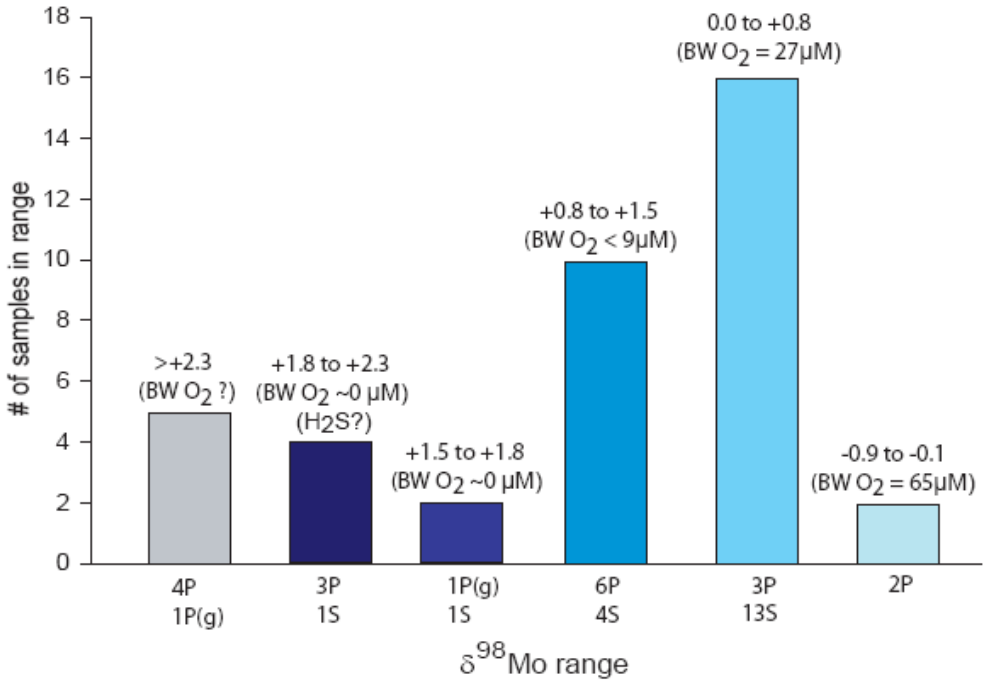

Figure 4.10: The number of samples from this study that fall into the specified δ^{98}Mo range. The corresponding number of hemipelagic (P) and sapropels (S) in each range is given below. P(g) refers to 'ghost' sapropels, samples that were sapropels, but have been diagenetically erased . These ranges correspond to bottom water (BW) oxygen contents (Siebert et al., 2006; Poulson et al., 2006).

exposure to the sulfidic layer, would commence formation of thiomolybdate, along the sequence dictated by [H_2S_{aq}] (Erickson and Helz, 2000). Thus, Mo would fractionatate from the initial seawater δ^{98}Mo (+2.3‰) according to the particular species of thiomolybdate formed (Tossell, 2005). Slow advection of WM bottom water with δ^{98}Mo = 2.3‰ might ensure that the isotopic composition of the source pool does not change significantly with time.

One possible complication in this concept is that molybdate reaching the sulfidic layer may already be fractionated, as a result of association with organic matter. Available evidence (Liermann et al., 2005; Wasylenki et al., 2007) suggests that biological utilization of Mo would result in net lighter Mo reaching the sulfidic layer, and budget calculations suggest an -0.1‰ offset from seawater (Poulson-Brucker et al., 2009). In such a case, the thiomolybdates that formed under higher [H_2S_{aq}] would necessarily appear lighter than seawater. Thus, organic matter fractionation prior to thiomolybdate formation does not present a difficulty with respect to the observed values in the sapropels.

A partial-fractionation model is successful at explaining the entire range of δ^{98}Mo data observed in the sapropel sediments, from 'suboxic' values to anoxic values, and some that approach 'euxinic'. The δ^{98}Mo data bear out previous hypotheses that the conditions for sapropel formation were different for each individual event. For sapropels with suboxic/ partially fractionated thiomolybdate signatures, the conditions may not have progressed beyond weakened circulation and lessened bottom water ventilation (e.g., Stratford et al., 2000), while for the anoxic sapropels, circulation reversal and isolation of the deep water may be more likely.

Sulfur isotope systematics in 969D

Sulfur isotopes from sapropels might be useful in determining whether the water column was euxinic during sapropel formation. Sulfur isotope data and uncertainties are listed in Table 4.9. The δ^{34}S results in sedimentary pyrite from this study are consistent with previous results (Passier et al., 1997). Modern

seawater sulfate in the Mediterranean has $\delta^{34}S$ = +20.6‰ (De Lange et al., 1990), thus the fractionation between seawater sulfate and sulfide in the sediments can be calculated (Table 4.9). Seawater sulfate and sulfide in hemipelagic sediments are fractionated from one another to the largest degree, up to $\delta^{34}S$ = -67‰. Fractionation between seawater sulfate and sulfide in the sapropels is less than $\delta^{34}S$ = -60‰ (Figure 4.11). In the sapropels, pyrite is thought to form as a result of reaction of Fe with HS- (e.g., Passier et al., 1996; Böttcher et al., 2003) produced by dissimilatory sulfate reducing prokaryotes.

During dissimilatory sulfate reduction, and sulfur disproportionation, prokaryotic organisms generate distinctive isotope signatures in both $\delta^{34}S$ and $\Delta^{33}S$ that have been the focus of recent studies (e.g., Farquhar et al., 2003; Johnston et al., 2005, 2007). These signatures result from the flow of sulfur through the specific steps in the metabolism (Farquhar et al., 2003, 2007), and provide additional information about fractionation at branch points between reactants and products during the flow of S through the network (Farquhar et al., 2003).

The structure of the sulfate reduction metabolism forms the basis for interpretation of these isotopic signatures, and the isotopic fractionation associated with sulfate reduction can be modeled using a metabolic network approach (e.g., Rees, 1973; Brunner and Bernasconi, 2005; Farquhar et al., 2007). Farquhar et al. (2007) calculated a field of $\delta^{34}S$ and $\Delta^{33}S$ values for sulfide produced during the sulfate reduction metabolism, using the network of Brunner and Bernasconi (2005) (Figure 4.12). This network expanded on the original

network of Rees (1973), allowing for the generation of much larger overall fractionations during the sulfate reduction metabolism. Thus, the field calculated by Farquhar et al. (2007) represents the extent of isotopic values that can reasonably be produced via the sulfate reduction metabolism alone (i.e., without additional oxidative sulfur cycling). This model provides a good fit for sulfur isotope data from lab-cultured sulfate reducers (e.g., Farquhar et al,. 2003; Johnston et al., 2005, 2007), while providing a means by which much larger fractionations measured in natural systems could be generated by sulfate reduction alone (e.g., Fry et al., 1991).

Table 4.9: Sulfur isotopic composition of pyrite in sapropels and hemipelagic sediments.

Sapropel	**$\delta^{34}S$**	**1σ**	**Normalized[a]**	**$\Delta^{33}S$**	**1σ**	**$\Delta^{36}S$**	**1σ**
4H-2, 56	-39.29	0.010	-58.69	0.101	0.016	-1.205	0.121
4H-2, 64[b]	-40.96	0.007	-60.32	0.109	0.011	-1.311	0.099
4H-2, 66	-39.92	0.005	-59.30	0.098	0.008	-1.266	0.095
4H-2, 70	-33.82	0.010	-53.32	0.122	0.007	-1.272	0.123
4H-2, 74	-36.62	0.005	-56.06	0.123	0.007	-1.259	0.180
4H-2, 78	-33.47	0.008	-52.98	0.098	0.012	-0.849	0.110
4H-2, 84	-38.80	0.017	-58.20	0.100	0.007	-1.309	0.026
5H-2, 133	-33.48	0.006	-52.99	0.115	0.019		
Hemipelagic							
4H-2, 59	-44.38	0.005	-63.67	0.114	0.016	-1.248	0.099
4H-2, 90	-45.11	0.002	-64.38	0.111	0.014		
4H-2, 94	-47.52	0.002	-66.75	0.130	0.004	-1.415	0.059

[a] $\delta^{34}S$ normalized to the $\delta^{34}S$ of Mediterranean seawater sulfate, +20.6‰ (Passier et al., 1996).
[b]Transitional sample.

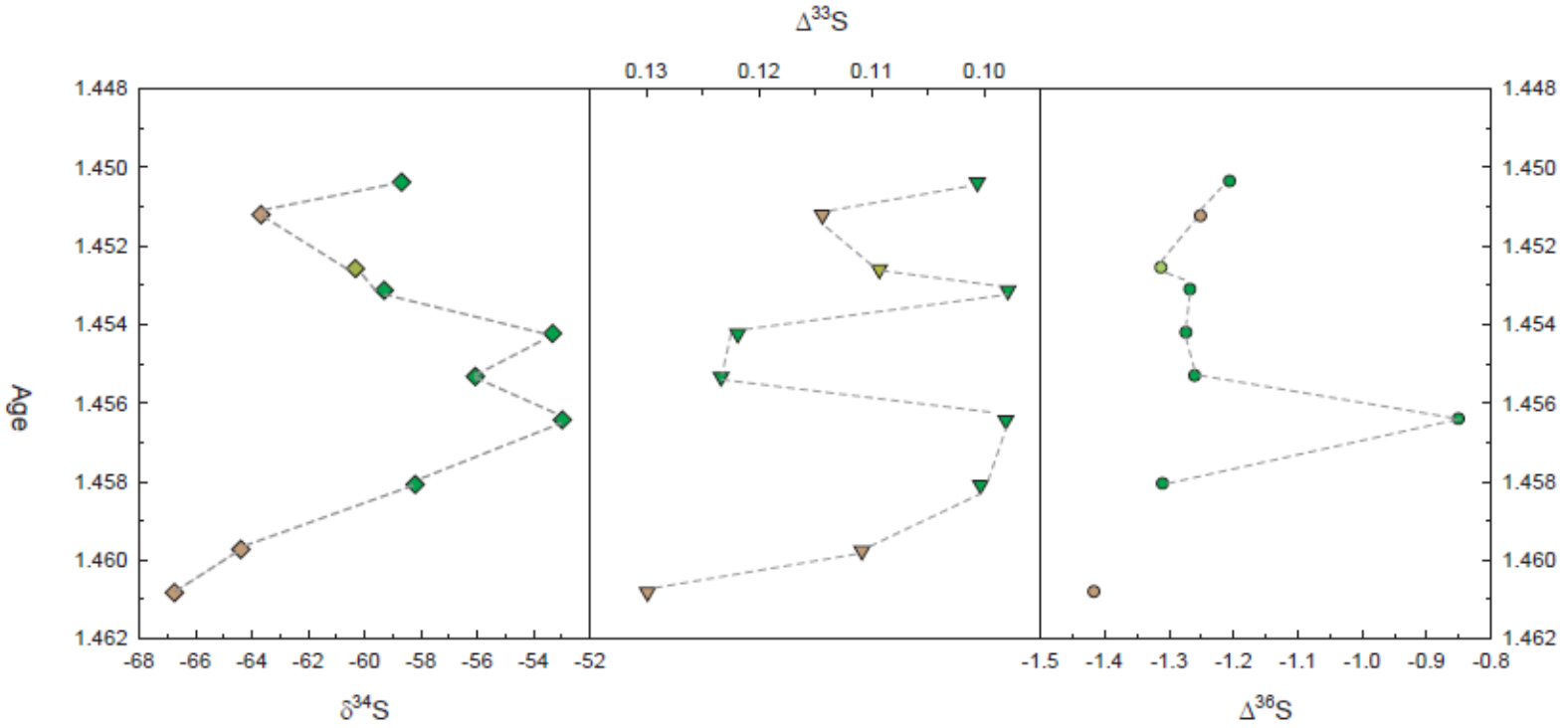

Figure 4.11: Profiles of $\delta^{34}S$, $\Delta^{33}S$, and $\Delta^{36}S$ relative to age. $\delta^{34}S$ has been normalized to seawater sulfate. Sapropels are in green, hemipelagic sediments in brown. In all figures, the error bars are smaller than the symbol size.

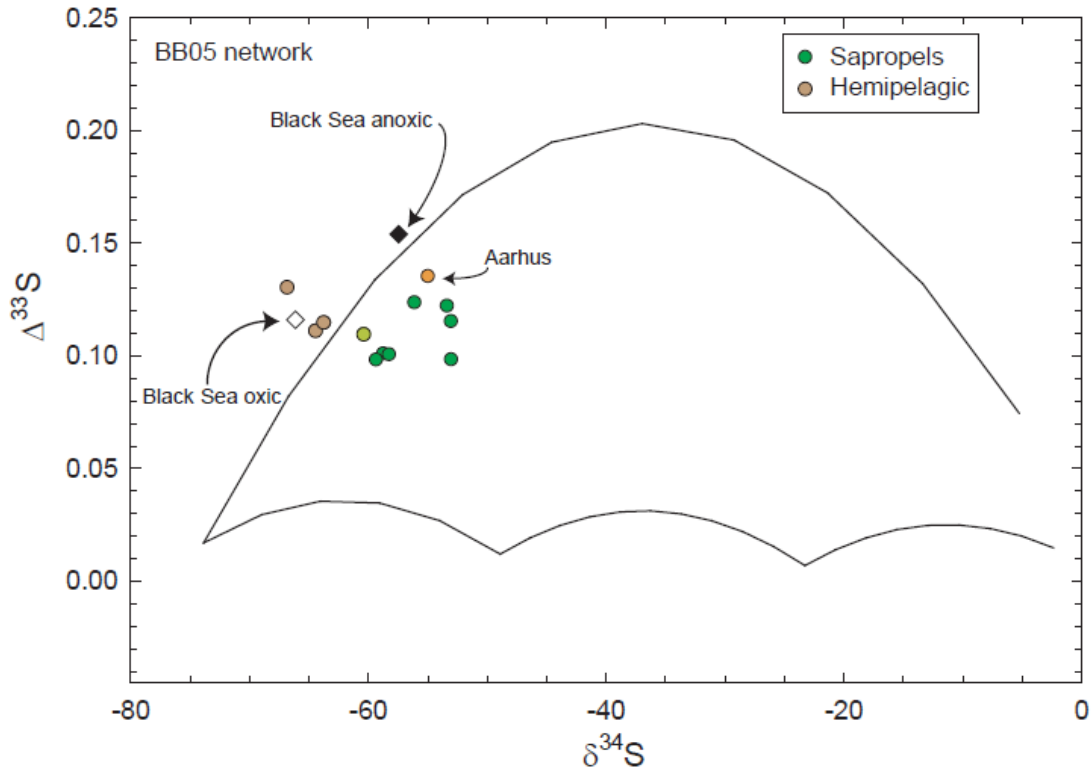

Figure 4.12: BB05 network for sulfur metabolisms (black line). Black Sea and Aarhus data from Johnston et al. (2008). The green circles are sapropel samples, the brown circles are hemipelagic sediment. The yellow circle is a sample that is transitional between sapropel and hemipelagic sedimentation.

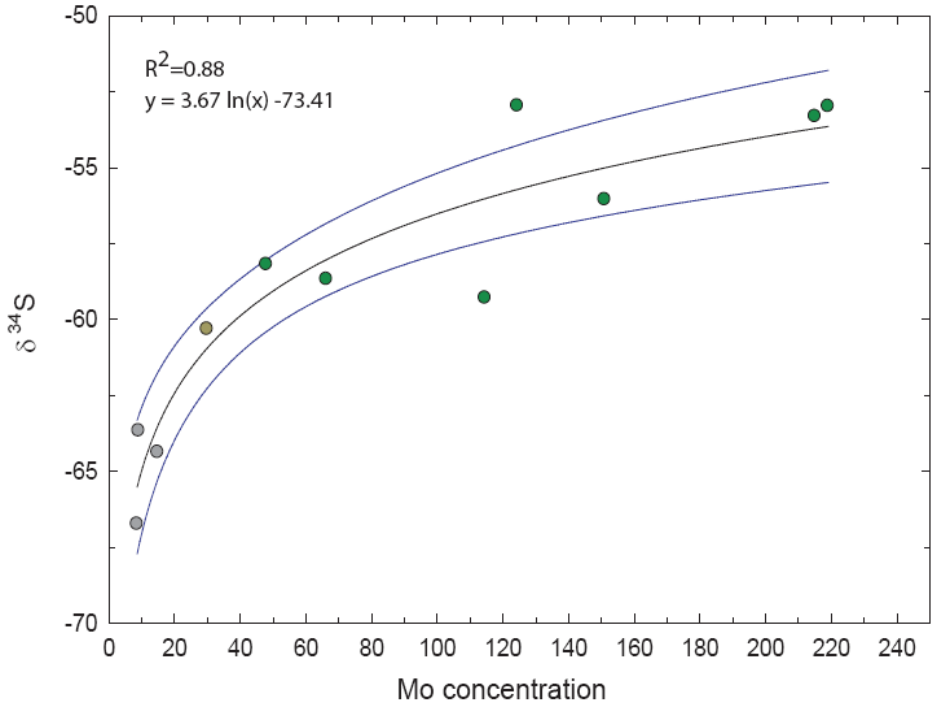

Figure 4.13: Correlation between Mo concentration and $\delta^{34}S$ (black line, blue lines are 95% confidence limit of the data fit). Green circles are sapropel samples, grey circles are hemipelagic samples. The yellow circle is a sample that is located at the transition between sapropel deposition and normal sedimentation.

The position of the sapropel data within the BBO5 network (Fig. 4.12) implies that the sulfur isotopic compositions in the sapropels can be satisfied by sulfate reduction, while the position of the hemipelagic sediments outside of the network requires an additional fractionation mechanism to produce heavier values. This process is most likely sulfur disproportionation of sulfur intermediates (e.g., Johnston et al., 2008). This disparity may suggest that the water column during sapropel deposition was different than during hemipelagic sedimentation. Sapropel deposition likely took place with a redox boundary located in the water column, while the redox boundary moved into the sediments

at other times. A redox boundary in the sediments allows for oxidation of sulfide to sulfur intermediates, which can be further fractionated by sulfur disproportionating organisms.

A good logarithmic correlation ($r^2 = 0.88$) exists between $\delta^{34}S$ and Mo concentration for all samples for which mutual data are available (Fig 4.13). The highest Mo concentrations are coincident with the lightest $\delta^{34}S$ values. Thus, high degrees of Mo removal correlate with $\delta^{34}S$ values that indicate an anoxic water column above the forming sapropel. This strong positive relationship suggests that Mo is related to $\delta^{34}S$ through the connection with organic carbon (Tribovillard et al., 2006, McManus et al., 2006; Lyons et al., 2003).

Molybdenum in hemipelagic sediments

An unexpected finding in the Mo isotope data is the predominant occurrence of $\delta^{98}Mo > 0.7‰$ in the hemipelagic samples (Figs. 4.6 and 4.11), which likely indicates deposition under low bottom water conditions. This supports the idea that, for many of these samples, the Pliocene 'oxic' bottom water was less oxygenated than the modern. Many of these also have Mo concentrations much greater than crustal or shale averages. Because of MnO_x precipitation and diagenetic cycling, and contribution of continental material with $\delta^{98}Mo$ ~0‰ (Siebert et al., 2003), it would be expected that oxic sediments would have little Mo, and be isotopically light. Indeed, oxic sediments from the Black Sea have 0.8 to 1.0 µg/g Mo, and $\delta^{98}Mo$ +0.1 to 0.3‰ (Nägler et al., 2005), while a hemipelagic sample from the Holocene Mediterranean has 2.4 µg/g Mo and $\delta^{98}Mo$ +0.2 (Reitz et al., 2007). Oxidized remnants of a Mediterranean Holocene

sapropel had light δ^{98}Mo values, down to -0.7‰ (Reitz et al., 2007). However, in our study, several very heavy δ^{98}Mo values (2.3 to 3.5‰), indicate an extreme loss of light Mo, such as might occur by removal to a phase such as MnO_x. These values are similar to measurements of δ^{98}Mo in pore-water, where Mo removal to isotopically light authigenic phases enriched the pore fluid in heavy Mo (McManus et al., 2002).

For almost all the hemipelagic samples, the proportion of detrital Mo appears to be low, based on Mo/Al ratios. The Mo/Al ratio of average crust is 0.07 (Rudnick and Gao, 2003), and of average shale 0.08 (Taylor and McLennan, 1985), and many of the hemipelagic samples have more than 10x these ratios. Thus, contribution of a continental δ^{98}Mo signature to the hemipelagic sediments is probably negligible.

Foraminiferal and nannofossil carbonate is a major component of these sediments. It was only recently recognized that carbonates can have a large range of δ^{98}Mo values (Voegelin et al., 2009). The inherent Mo concentration of skeletal carbonate phases is low (on the order of 0.05 µg/g, Voegelin et al., 2009), so carbonate-hosted Mo is unlikely to be significantly contributing to the δ^{98}Mo in the Mediterranean samples.

With the exception of two samples with δ^{98}Mo values of -0.4 and -0.5‰, contributions from MnO_x can be ruled out. A δ^{98}Mo signature similar to that of MnO_x adsorption can be generated through Mo adsorption to hematite, with a minimum δ^{98}Mo ~ -0.4‰ (Goldberg et al., 2009). The two hemipelagic samples with negative δ^{98}Mo values likely contain Mo that has been fractionated by

adsorption to MnO_x or hematite, or both. The presence of small amounts of magnetite in the background sediments and the oxidized layers above sapropels (Larrasoana et al., 2003) could also have an effect on the δ^{98}Mo of the hemipelagic sediments. Molybdate diffusion into pore water and subsequent adsorption to magnetite particles provides a possible explanation for some of the hemipelagic sediments, in terms of both Mo concentration and isotopic composition.

Pyrite is probably a carrier of Mo in sediments (Huerta-Diaz and Morse, 1992; Vorlicek and Helz, 2002). The fractionation of Mo during adsorption to or scavenging by pyrite is unknown, but has been proposed to be the source of the -0.7‰ offset of δ^{98}Mo from seawater to anoxic, non-sulfidic sediments (Poulson et al., 2006). Pyrite forms readily in the sapropels and adjacent sediments as a result of sulfide diffusion from sapropels (e.g., Passier et al., 1996), and could form in buried hemipelagic sediments that are below the redox boundary.
In the Black Sea, buried, formerly oxic sediments have Fe/Al <0.63 and low degrees of pyritization (Lyons and Severmann, 2006). The Fe/Al ratio in most 969D hemipelagic samples is <0.53; a few samples have higher ratios. The amount of Fe/Al suggests that pyrite, or certain FeOx phases forming in the hemipelagic sediment, could be responsible for the δ^{98}Mo values that are less than seawater.

The source of isotopically very heavy Mo for some hemipelagic samples remains to be identified. If the explanation for δ^{98}Mo values in the sapropels is partial fractionation during thiomolybdate formation, and suboxic/anoxic

conditions, then Mo remaining in pore water would become heavier. Diffusion of this pool of Mo out of the sapropel region and into the hemipelagic sediments satisfies the need for an isotopically heavy Mo source to form the observed sediments. Where isotopically heavy hemipelagic samples are well removed from a sapropel, diffusion of Mo into pore water, formation of isotopically lighter phases, and diffusion of the heavy Mo pool to the redox boundary, where it could be fixed, is a possible way to generate heavy δ^{98}Mo signatures.

Collectively, the δ^{98}Mo and trace metal evidence points to hemipelagic depositional conditions that were similar to continental shelves or upwelling zones (Siebert et al., 2006; Morford et al., 2005; Nameroff et al., 2002). Possibly, the Eastern Mediterranean basin was subject to variations in ventilation, and was on the whole less well-ventilated than it presently is during periods of hemipelagic sedimentation. This suggest that the difference between sapropel and hemipelagic episodes was the input of organic carbon, and not drastic shifts in the degree of bottom water oxygenation caused by changes external to the basin.

Rhenium/Molybenum ratios

The work of Crusius et al. (1996), presented the idea that the ratio of Re to Mo in sediments could be used as an indicator of anoxic versus 'suboxic' conditions. Samples with Re/Mo close to seawater (0.8×10^{-3}) are indicative of anoxic conditions, while higher ratios ($>9 \times 10^{-3}$) indicate suboxic deposition (Crusius et al., 1996). Using Re/Mo to distinguish between between an anoxic and a suboxic water column is theoretically possible because Re and Mo are

removed from seawater at different redox potentials (Crusius et al., 1996), resulting in preferential enrichment of Re, relative to Mo, in suboxic sediments. This implies that low levels of sediment oxidation (burn-down) might cause loss of Re (Crusius and Thompson, 2000), before causing loss of Mo. In the Black Sea, euxinic sediments have Re/Mo ratios from 0.7 to 2.1 (Ravizza et al., 1991).

If Re/Mo ratios of sapropel samples faithfully record information about the oxygenation state of the water column during deposition, then the low Re/Mo suggest that the sapropels examined here were likely deposited under relatively reducing conditions (Fig. 4.14), in agreement with previous results for this site (Warning and Brumsack, 2000; Rinna et al., 2002). For S25, Re/Mo ratios are higher (more oxic) below the sapropel, and then transition gradually to Re/Mo reflecting anoxic conditions in the center of the sapropel (Re/Mo = 1; Fig. 4.14). The water column then evolves towards a ratio consistent with 'suboxic' conditions, and during the hiatus, quite high ratios are present. The water column appears to be more oxic during sapropel deposition following the hiatus (Re/Mo = 4.1). In the older sediments, Re/Mo is consistent with strongly anoxic conditions in many of the sapropels (e.g., S33, Re/Mo = 1.4; S26 = Re/Mo 1.9). Within hemipelagic samples, there is little consistency in Re/Mo. Ratios range between 7.1 and 0.2, with only one sample (4H-3, 20) displaying an 'oxic' (crustal) ratio (~0.3; Zheng et al., 2000). This sample, however, has 3 times the abundance of Re and Mo compared to average shale. Thus, the Re/Mo suggests that the pelagic samples were also deposited under suboxic conditions, possibly under conditions similar to modern suboxic regimes that have reported Re/Mo up to 19

(Crusius et al., 1996). Alternatively, the high pelagic ratios could be a function of preferential Re addition to pore water during diagenetic oxygenation, while Mo is retained in the sediments (Colodner et al., 1993). A return to anoxic pore water conditions upon deeper burial could have preserved the diagenetic Re/Mo.

We suggest that Re/Mo indicates sapropel formation under both suboxic and anoxic regimes, and hemipelagic sedimentation under varying oxygen levels. However, there is a disconnect between the precise intervals that are designated as anoxic or suboxic using Re/Mo, and those so indicated by the other data. The δ^{98}Mo values, particularly for S25, are 'suboxic' but have, for some of the sequence Re/Mo ratios consistent with anoxic deposition. Conversely, the sapropels identified as 'suboxic' by Re/Mo have δ^{98}Mo values that are isotopically heavy (+1 to +2‰), usually taken as an indicator of more reducing conditions.

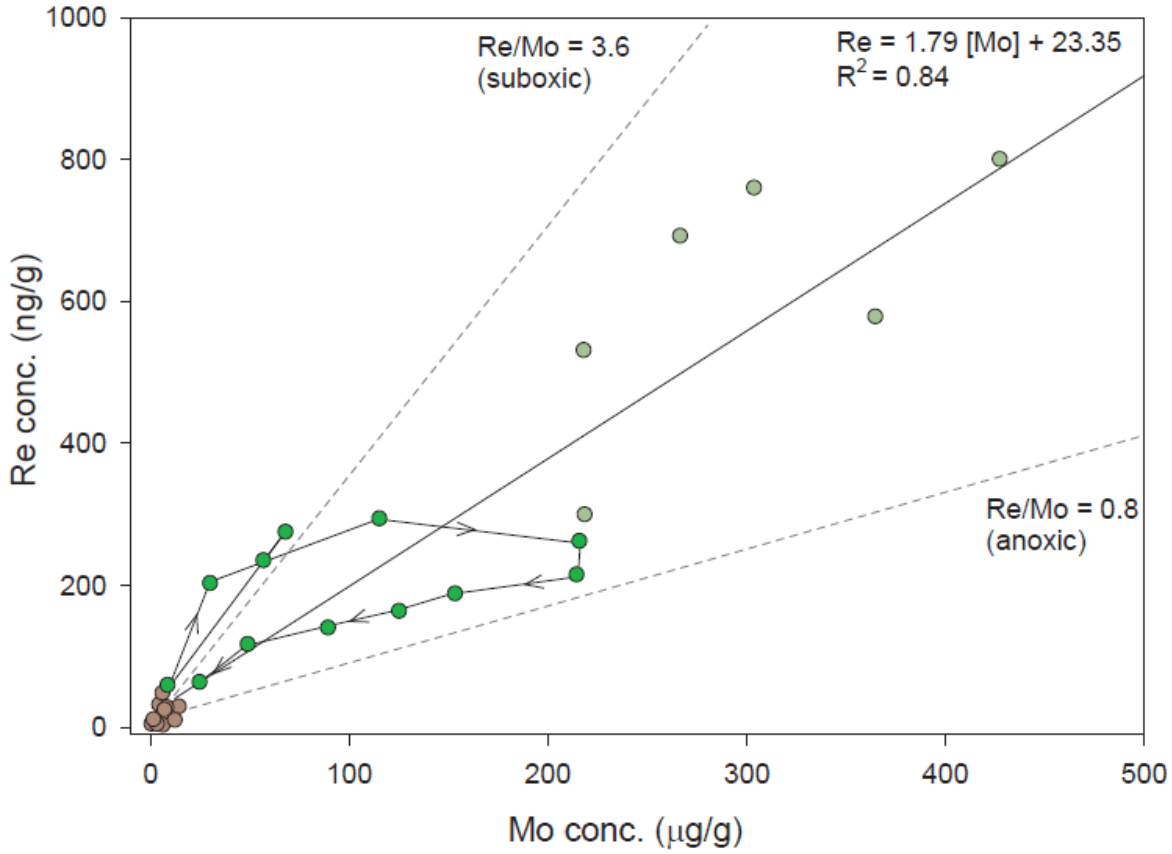

Figure 4.14: Re/Mo ratios in sapropels and hemipelagic sediment. S25 is shown as the darker green circles, while the older sapropels are light green circles. The line which connects the S25 samples indicates the sequence of deposition (counter-clockwise).

In order to resolve this apparent decoupling, the Re concentrations alone may be the key. If high Re alone is indicative of 'suboxic' conditions, then it might correspond with suboxic δ^{98}Mo values (Fig. 4.15). Rhenium concentrations in S25 are lower compared with sapropels with more clearly anoxic signatures, indicating that the Re concentrations and δ^{98}Mo are in agreement with respect to prevailing suboxic conditions during S25 deposition, and anoxic conditions in older sapropels.

Thus, it remains to be answered why the Re/Mo is not faithfully recording the state of the water column during sapropel formation. One possibility is that the Re/Mo of Mediterranean water was changing with time during sapropel deposition. Warning and Brumsack (2000) noted a decrease in average sapropel Re/Mo with increasing distance from the seawater source, possibly as a result of high Re and Mo removal rates to the sediments. This would affect Re more than Mo, because of its lower concentration in seawater.

Another explanation comes from a comparison with the Black Sea. Sulfidic conditions leading to incomplete scavenging of Mo might also lead to partial scavenging of Re, in the same proportion. Thus, the ratio will reflect seawater. In water column profiles from the Black Sea (Colodner et al., 1995), scavenging of more than 75% of Re and Mo does not appear to greatly change the dissolved Re/Mo ratio. Once sulfidic conditions are established in the water column, the underlying sediments will carry a ratio that resembles seawater regardless of the amount of scavenging. In the Mediterranean samples, then, incomplete removal of Re and Mo at seawater ratios could be consistent with partial isotopic fractionation of Mo during thiomolybdate formation. The larger basin size and direct source of seawater in the Mediterranean allow for an overall greater capacity to generate authigenic Re and Mo, compared to the Black Sea. Incomplete scavenging of the Eastern Mediterranean water column would still have the ability to deliver high quantities of trace elements to the sediments.

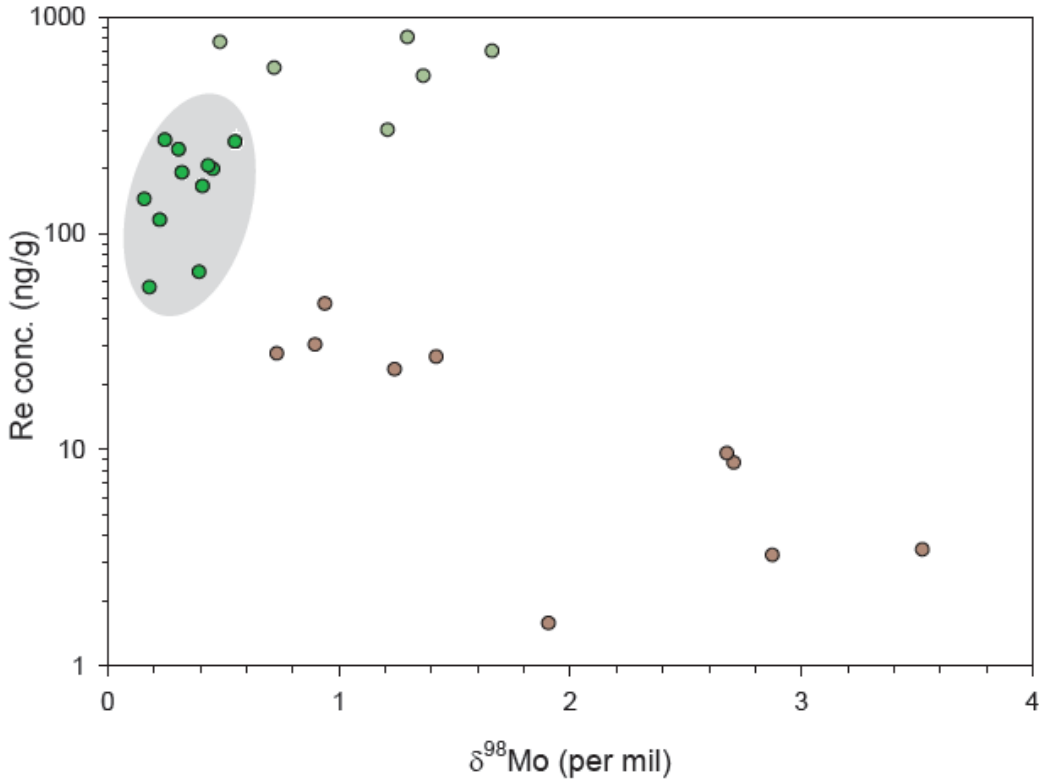

Figure 4.15: Rhenium concentrations compared to δ^{98}Mo. The grey circle encompasses the S25 samples (dark green). Pale green circles are the older sapropels. Brown circles are the hemipelagic sediments.

Conclusions

In this study of Mediterranean sapropels, hemipelagic sediments were found to exhibit a range of δ^{98}Mo values nearly equivalent to the entire natural range that has been previously observed. Sapropel formation, based on the results of the variety of redox-sensitive proxies applied, was clearly a process that took place under varying conditions. Thus, every sapropel represents a different balance of water-column, pore-water and diagenetic processes. For the most part, using δ^{98}Mo in conjunction with other proxies, it is possible to determine whether a sapropel formed under suboxic, anoxic, or partly sulfidic conditions. The Mediterranean sapropels have δ^{98}Mo values that are evidence

for incomplete (fractionated) Mo removal, trace metal contents and Re/Mo ratios that indicate high, but incomplete, degrees of scavenging from the water column. δ^{98}Mo values and other proxies from the hemipelagic samples indicate that the degree of oxygenation during the Pliocene-Pleistocene was also variable, but generally lower than in the modern Eastern Mediterranean.

The data for the sapropels suggest another important point: that Re/Mo ratios cannot be relied upon to be a strict indicator of anoxic versus suboxic depositional environment. We propose that high, but incomplete, degrees of removal can generate Re/Mo ratios similar to seawater. This allows for high Re, Mo and V concentrations and fractionated δ^{98}Mo values to be coincident with seawater Re/Mo, which could be misleading given the current paradigm.

Chapter 5: Experimental determination of Mo isotope fractionation at high temperature and pressure

Abstract

An experimental design that approximates a porphyry ore system at deep crustal temperatures and pressures (800℃ and 100 mPa) was used to assess the fractionation of Mo isotopes between a vapor phase and a melt phase. Molybdenum isotopic analysis of quenched run products was conducted using a double-spike technique and multi-collector ICP-MS analysis. Resolvable fractionation between vapor and melt was observed, with heavy Mo isotopes favoring the vapor phase. Distribution coefficients of Mo indicate that Mo favors the vapor phase, in agreement with previous results. A likely explanation for the observed fractionation is that Mo undergoes a coordination change in the vapor, which might explain the preference of heavy Mo isotopes for that phase.

Introduction

A number of early Mo isotope studies included analyses of molybdenite (MoS_2), for its ease of processing and simple matrix (e.g., Anbar et al., 2001; Barling et al., 2001). These studies reported a modest range in δ^{98}Mo (-0.47 to +0.27) for magmatic molybdenites, which might be expected for heavy element fractionation in relatively high temperature systems (Urey, 1947). Further studies, however, revealed a larger range with values from -0.77 to +2.27‰, that appeared unrelated to the temperature or age of the deposit (Wieser and DeLaeter, 2003; Pietruszka et al., 2006; Hannah et al., 2007; Malinovsky et al., 2007). Two studies have systematically surveyed MoS_2 deposits, and concluded that there may be differences in δ^{98}Mo that are related to the type of ore deposit

(Pietruszka et al., 2006; Mathur et al., 2009). Globally, porphyry systems exhibit the largest range of values (-0.39 to +0.80‰), with samples from different parts of the same deposit having highly variable δ^{98}Mo (-0.24 to +0.51‰; Mathur et al., 2009).

The use of Mo isotopes to study redox conditions of ancient ocean environments has been predicated on assumptions about the behavior of Mo and Mo isotopes in reduced and oxygenated environments, and about the isotopic composition of input Mo. The ocean Mo reservoir is isotopically heavy (2.3‰), and is though to reflect loss of isotopically light Mo to authigenic sediments under oxic conditions. However, constraints on the δ^{98}Mo of dissolved and particulate material being delivered to the oceans are not well-developed. Studies of various igneous rocks suggested the δ^{98}Mo of the input is likely to be near 0‰ (Siebert et al., 2001), but recent data for rivers show that δ^{98}Mo in river water is highly variable (Archer and Vance, 2008).

Input of large quantities of isotopically heavy molybdenite-derived Mo might have the potential to change the ocean δ^{98}Mo, introducing an uncertainty to paleoredox studies. Such an effect would be more likely in localized settings, such as enclosed seas, continental shelves proximal to uplifted areas, estuaries, or lakes. Indeed, one instance of molybdenite weathering affecting δ^{98}Mo and Mo concentrations in lake sediments has already been identified (Malinovsky et al., 2007).

Few laboratory studies have been conducted on Mo isotope behavior. Most of these have focused on identifying the fractionation associated with Mo

removal to Mn and Fe oxides (Barling and Anbar, 2004; Wasylenki et al., 2008; Goldberg et al., 2009), which are major components of sediments, and contribute significantly to Mo removal from the ocean. Other fractionation factors have been deduced from sediments themselves (McManus et al., 2002). The difficulty of identifying a fractionation factor for MoS_2 formation is the inability to link the available molybdenite δ^{98}Mo data with a specific mechanism, either temperature, pressure, or fO_2. One study has suggested that variations up to ~1‰ in MoS_2 samples from a single occurrence could be explained by Rayleigh fractionation from a vapor phase, but that the average isotopic composition of MoS_2 from such a deposit would be close to that of bulk continental crust (Hannah et al., 2007). Molybdenum isotope data for the few igneous samples that have been measured were interpreted to mean that high-temperature processes do not fractionate Mo isotopes (Siebert et al., 2001). However, variations in Mo isotopic compositions of a Hawaiian basalt, a MORB, and a Columbia river flood basalt suggests that this may not always be true. These three materials have δ^{98}Mo of -0.10, +0.08, and +0.26, respectively (Scheiderich and Walker, unpublished data). No experimental evidence has shown that Mo is fractionated during high-temperature and/or high crustal pressure processes, such as might be present in a hydrothermal ore system, where Mo(IV)S_2 might form.

The goal of this study, therefore, is to experimentally determine the magnitude and direction of Mo isotope fractionations among coexisting phases at equilibrium conditions under high crustal temperatures and pressures. The experimental system consisted of a vapor phase and a melt phase. Based on

equilibrium isotope fractionation theory (e.g., Schauble, 2004), the expectation was that the vapor phase would become isotopically heavier, while the melt phase would become lighter.

Molybdenite is a common sulfide mineral associated with porphyry-style deposits, which are thought to be the result of magmatic-hydrothermal activity. The source of the Mo in the magmas that give rise to some porphyry ore systems is thought to be lower crustal rocks (Candela and Piccoli, 2005). Porphyry deposits occur in a wide variety of tectonic settings, but the two main types of porphyry Mo are rift-related (Climax-type) and subduction- related (Endako-type; Sinclair, 2007). Ore metals are partitioned into a volatile phase within the magma chamber, which accumulates at the apex of the chamber (e.g., Candela, 1989). Vapor escapes into the overlying fractured rock, whereupon it cools to precipitate ore minerals (Sinclair, 2007). This type of mineralization forms the basis for the experimental design, which is a simple system consisting, at run conditions, of co-existing vapor and melt phases. Molybdenum has been shown to more favorable partition into the vapor phase relative to the melt (D_{Mo} >1, vapor-melt) (Candela and Holland, 1984). At high temperature and pressure, $Mo(VI)O_3$ has been experimentally shown to be highly soluble in water vapor, possibly as a result of hydration (Rempel et al., 2006), so in the vapor phase, Mo is likely present as $MoO_3 \cdot nH_2O$ (Rempel et al., 2009). At fO_2 above the iron-wüstite buffer, Mo(VI) is the dominant oxidation state in a silicate melt, and Mo is probably present as molybdate, and to a smaller degree as molybdenyl (MoO_6^{6-}) moieties (Farges et al., 2006).

Experimental Methods

The experimental design was as follows: 25 mm x 5 mm Au capsules were loaded with materials that, under the run conditions, created a melt phase and a Mo-containing vapor phase, allowing study of the fractionation of Mo isotopes between these reservoirs. The experiments were designed so that all had the same ratio of melt to vapor (0.4:1). 40 mg of a synthetic haplogranite glass (GR-1, Qz: 0.38, Ab: 0.33, Or: 0.29) was used to generate the melt. GR-1 is the minimum melt composition for 100 MPa and 800℃. This material was tightly packed into the capsule in order to minimize inclusion formation in the melt. Its initial Mo content was below the detection limit of solution analysis by single collector ICP-MS. The materials loaded to generate the vapor phase included distilled H_2O with NaCl eq 1.8 mol % (Na:K 1:1; Na:H 10:1), and 25 µg/g Mo from a $NaMoO_4$ solution. A total of 100 µL of solution was loaded into the capsule and weighed (Table 5.1). The loaded capsule was crimped shut and weighed, then frozen with dry ice and arc-welded shut to seal the capsule, then weighed again. After drying overnight in a 110℃ ove n, the capsule was weighed again to assess whether loss of liquid had occurred.

The experimental apparatus consisted of a cold-seal René-41 Ni-alloy pressure vessel, in which the capsule was placed. The vessel was then sealed and pressurized to 100MPa with H_2O. The vessel was then placed at a 12° angle to the horizontal (to suppress convection) inside a tube-style furnace. Temperature was raised, at constant pressure, to the run condition of 800℃, at which point the 'vapor' phase is a supercritical fluid. During a run, the temperature was constantly measured by means of a type-K thermocouple

inserted into a hole in the pressure vessel. Runs of durations from 7 to 38 days were performed. Oxygen fugacity was maintained at the Ni-NiO buffer, because at 800℃, H^+ can permeate the gold vessel freely.

At the termination of the run, the pressure vessel was removed from the furnace and cooled isobarically to 350℃ with a jet of ambient air. At 350℃, the quench was completed by placing the vessel in room-temperature water. Once cooled, the run capsule was removed, rinsed, and weighed. Removal of the liquid run product (i.e., the quenched vapor phase) proved to be challenging, and the product was occasionally lost. A syringe was used to puncture the Au capsule and retrieve the liquid into a Savillex beaker for weighing. The capsule was then cut open, the glass bead (i.e., quenched melt phase at run temperature and pressure) removed, rinsed in 1M HNO_3, and weighed. These glass beads were frequently blue in color. The inside of the capsule was rinsed with 1M HNO_3, and this wash liquid was retained in a Savillex beaker for processing and measurement.

Processing the run products and the starting $NaMoO_4$ (both crystalline and a 100 ppm solution) for Mo concentration and isotopes followed established procedures (Chapter 2). The crystalline $NaMoO_4$ was weighed, spiked, and then dissolved in 6M HCl. The liquid run products were dried down and re-dissolved in 6M HCl, while the glass products were dissolved with ~0.5 ml concentrated HF, then dried and dissolved in 6M HCl. A small aliquot of each sample was diluted in 2% HNO_3, and the solutions initially analyzed for Mo concentration by single-collector ICP-MS, using a standard addition calibration curve technique. Once

the Mo concentration was known, the double-spike was added to the sample in an appropriate amount, and weighed. A three-column ion chromatography procedure was used to separate Mo from other elements (Scheiderich et al., 2010). The purified Mo was then dissolved in 2% HNO_3 for analysis by MC-ICP-MS. A few samples were sufficiently enriched in Mo that more than one measurement could be made with the solution. A small number of samples had very small quantities of Mo and were over-spiked. The δ^{98}Mo data for these samples are not presented, because of large estimated uncertainties. Concentrations for all the samples were calculated from the double-spike data. Molybdenum concentrations, δ^{98}Mo, and run parameters are presented in Table 5.1.

Results

The crystalline $NaMoO_4$ had a δ^{98}Mo of -0.24‰, and the 100 ppm Mo solution of $NaMoO_4$ used for the experiments had a δ^{98}Mo of -0.20‰. These values are identical within the 2σ external reproducibility for Mo isotope measurements (±0.1‰). The melt products consistently displayed δ^{98}Mo values less than 0‰ (average δ^{98}Mo = -0.64‰ ± 0.21, 1σ; Fig. 5.1). The fluids (vapor) had δ^{98}Mo greater than 0‰, with one exception, with an average value of +0.36‰ ± 0.30, 1σ (Fig. 5.1). The δ^{98}Mo of the liquids used to wash the capsules after the experiment are highly variable (Table 5.1).

Table 5.1. Summary of Mo concentrations, isotopic compositions, and run times for the experiments. Italics indicate replicate isotope analysis.

Sample	Mo conc. µg/g	Total µg Mo	g sample	δ^{98}Mo ‰	95 voltage	Run time (h)
40b glass	3.05	0.0494	0.01623	-0.652	0.11	375
40b fluid	3.90	0.2114	0.05426	0.072	0.45	375
40c glass	5.92	0.0902	0.01525	-0.893	0.19	375
40c fluid	0.98	0.0165	0.01684	N/A	0.42	375
42b glass	6.91	0.1161	0.0168	-1.208	0.26	250
42b fluid	0.38	0.0131	0.03433	N/A	0.039	250
42c glass	5.40	0.0857	0.01587	-0.869	0.22	175
42c fluid	8.66	0.4430	0.05113	-0.056	0.66	175
42c fluid	--	--	--	-0.193	--	175
44 b glass	5.584	0.1656	0.02966	-0.696	0.63	857
44b fluid	1.809	0.1066	0.05893	0.747	0.44	857
44b wash	0.327	0.4091	1.24995	0.216	1.11	857
53a glass	7.715	0.2747	0.03561	-0.397	0.92	861.5
53a fluid	6.782	0.2307	0.03402	0.832	1.17	861.5
53a fluid	--	--	--	0.744	--	861.5
53a wash	0.191	0.4255	2.2284	0.329	1.01	861.5
54 glass	5.022	0.1680	0.03346	-0.411	0.78	910
54 fluid	17.957	1.0225	0.05694	0.146	0.96	910
54 fluid	--	--	--	0.168		910
54 wash	1.028	0.9461	0.91989	-0.069	1.43	910
56 glass	3.469	0.1298	0.0374	-0.546	0.31	341.5
56 fluid	11.778	0.3529	0.02996	0.598	0.539	341.5
56 wash	0.171	0.2720		0.151	0.55	341.5
61 glass*	2.485	0.0899	0.03618	-0.506	0.23	166.5
62b glass*	3.525	0.1213	0.03441	-0.509	0.28	
63 glass	4.299	0.1603	0.0373	-0.609	0.45	507.3
63 fluid	4.182	0.1605	0.03838	0.142	0.9	507.3
63 wash	0.290	0.5152		-0.455	0.36	507.3
68 glass	7.035	0.2564	0.03644	-0.455	0.72	333.5
68 fluid	5.980	0.5819	0.09731	0.374	1.32	333.5
68 wash	0.171	0.3111		-0.876	0.74	333.5
71 glass	3.648	0.1253	0.03433	-0.606	0.36	458
71 fluid	15.489	0.7610	0.04913	0.298	1.43	458
71 wash	0.242	0.2942		0.101	0.66	458
75 glass*	3.705	0.1242	0.03353	-0.614	0.26	263
78 glass	2.926	0.1064	0.03638	-0.674	0.314	165
78 fluid	9.171	0.5303	0.05782	0.548	0.69	165
78 fluid	--	--	--	0.517	--	165
78 wash	0.811	0.3602		0.294	1.03	165
$NaMoO_4$ [a]	54.36	54.89	1.00977	-0.199	1.11	--
$NaMoO_4$ [b]	1944099	486.02	0.00025	-0.241	0.98	--

*Glasses with no corresponding fluid phase.
[a]Liquid (100 ppm in 2% HNO_3).
[b]Crystalline.

The quantity of Mo in the melt phase was low, with little variance between runs (average 0.14 µg Mo ± 0.06, 1σ). The vapor phase averaged higher concentrations, albeit more variable (average 0.37 µg Mo ± 0.31, 1σ). The wash liquids had relatively low concentrations of Mo (Table 5.1). The Mo concentration of the wash is used to calculate the amount of Mo that is missing from the system (fugitive Mo, Table 5.2), assuming that the capsule did not leak. The fugitive Mo is calculated by summing the amount of Mo in the fluid, vapor, and wash phases, and including in the sum an estimate of the unrecovered Mo, obtained by subtracting the mass of recovered fluid from the starting fluid mass. The starting amount of Mo, less the recovered amount, is considered to be fugitive Mo.

Table 5.2: Starting Mo, total Mo recovered from the experiment, and the calculated α and D_{Mo} for experiments where both phases were recovered. Fugitive Mo is the amount of Mo missing from the system: the difference between the starting Mo and the Mo recovered, plus the estimated amount of Mo that was in fluid not recovered The amount of Mo in this difference was calculated by multiplying by the concentration of Mo in the recovered fluid. Experiments in italics used 60µL of a 100 ppm Mo starting solution, which was not weighed.

Experiment	µg Mo to start	µg Mo recovered[a]	Recovery %	Fugitive Mo[b] (µg)	α	D_{Mo}
40b	*~6*	0.2608	--	*5.7*	1.0007	1.28
42c	*~6*	0.5287	--	*5.5*	1.0008	0.60
44	2.4346	0.7509	31	1.68	1.0014	0.32
53a	2.6915	1.4304	53	1.26	1.0012	0.88
54	2.5428	2.4199	95	0.12	1.0006	3.58
56	2.5215	1.5897	63	0.93	1.0011	3.40
63	2.5395	1.1004	43	1.44	1.0008	0.97
68	2.5613	1.1801	46	1.38	1.0008	0.85
71	2.5490	1.9987	78	0.55	1.0009	4.25
78	2.6508	1.3918	53	1.26	1.0012	3.14

[a] Recovered Mo = vapor Mo + melt Mo + wash Mo + estimated Mo in lost fluid.
[b] Starting Mo - Mo recovered
Average α: 1.00096 ±0.00028
Average D_{Mo} : 1.93 ±1.48

Calculation of α (vapor-melt) and D_{Mo} (vapor-melt)

The fractionation factor, α, for Mo isotopes between vapor and melt can be calculated from the δ^{98}Mo values of these phases for each experiment where both were recovered (Fig. 5.3):

$$(5.1) \qquad (1000 + \delta^{98}Mo_{vapor})/(1000 + \delta^{98}Mo_{melt}) = \alpha$$

The average α for all the experiments is 1.00096 (0.96‰), ± 0.00028 (0.28‰, 1σ). Likewise, where both run products were recovered, D_{Mo}, the elemental partition coefficient between the vapor and melt, can be calculated from the concentration of Mo in these phases (Fig. 5.3). The average D_{Mo} for the ten paired products is 1.93 ±1.48, which is similar to previous studies (Candela and Holland, 1984). In calculating α and D_{Mo}, the Mo in the wash is not included, because there is uncertainty as to whether the Mo in the wash belongs to the fluid phase or to the melt phase.

Discussion

Possible problems

It is important to identify the potential pitfalls of the experimental setup and recovery procedure, as these might significantly affect the results. The first problem is that for most of the experiments, the efficiency of recovery of Mo from the total system (vapor + melt + wash) was generally less than 50% (Table 5.1). This implies that some to most of the initial Mo with which the system began was lost (fugitive Mo). One possibility is that the Au capsule adsorbed some of this

fugitive Mo. This effect, if present, was not related to run length (Fig. 5.4). If Mo uptake into a third phase involves a different isotopic fractionation of Mo, then it might be apparent in the α value (Fig. 5.4). There appears to be a small effect of Mo loss on the overall fractionation between the two phases. The R^2 of the trend between these two factors is 0.6, but it is a very shallow trend. It suggests that experiments with the least fugitive Mo might be more reflective of the true isotopic fractionation between vapor and melt. Small fragments of several Au run capsules have been dissolved in order to determine whether a significant quantity of Mo entered the capsule.

Partitioning of Mo between the melt and fluid might be dependent on the concentration of Mo in the system. Natural systems are likely to have much lower concentrations of Mo (1-2 μg/g). The blue color of the glass beads suggest the possibility that Mo in the glass is polymerized, and Mo polymers are likely to be more stable at high Mo concentrations. However, the similarity of the D_{Mo} value obtained here to previous results suggests that this may not be a primary concern.

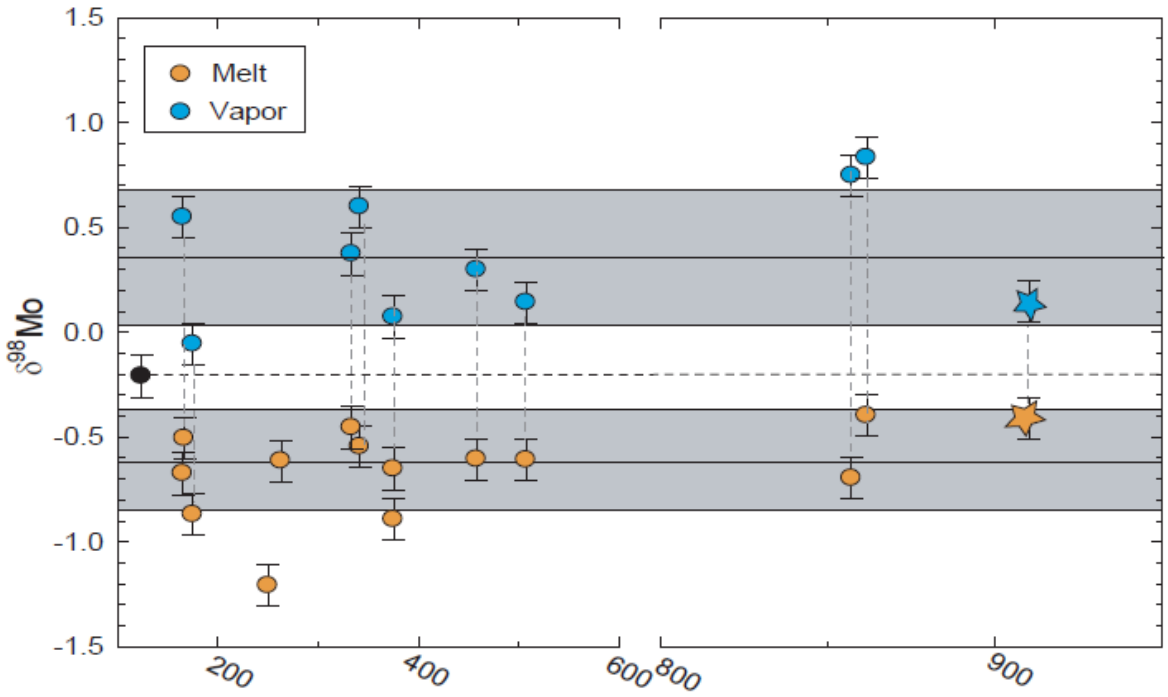

Figure 5.1: δ^{98}Mo of run products versus run time. Orange circles are melt, blue circles are vapor. The starred experiment (54) did not have an isobaric quench. Grey tie lines connect run products from the same experiment.

There is the possibility that inclusions of vapor were trapped in the melt upon quench. Data suggest that such inclusions contribute Mo that is less than 5% of the total present in the melt. A simple calculation shows that a 5% contribution from the vapor to the melt composition is not significant enough to shift its isotopic composition. Assuming that the vapor has an average δ^{98}Mo of 0.4‰, the isotopic composition of the melt would shift by only +0.02‰ for a 5% contribution of vapor. This is well within the external reproducibility of δ^{98}Mo measurements, and, thus, is not a significant source of error to the δ^{98}Mo values for the melt phase.

Interpretation of experimental results

The most important observation is that the average δ^{98}Mo values for the run products are isotopically distinct from the starting Mo composition. This is strong evidence that fractionation between the two phases has taken place. The vapor phase is consistently isotopically heavier than the coexisting melt, which was expected based on equilibrium fractionation theory.

No trend in δ^{98}Mo is apparent, in either phase, with run length. This time-independence suggests that the system has quickly reached equilibrium with respect to Mo isotopes (Fig. 5.1). At 320℃ and 10 M Pa, 6 days were required to reach equilibrium with respect to Mo solubility according to Rempel et al. (2006). Therefore, it is likely that the time to reach isotopic equilibrium is shorter than the shortest experiment, ~7 days. With respect to Mo concentration of the run products, again, no trend was apparent with run length (Fig. 5.2), which supports the assertion that the system reached equilibrium in less than 7 days. Molybdenum concentration and δ^{98}Mo are only poorly correlated for either phase (Fig. 5.5), but the amount of Mo captured in the glass shows more consistency. This could be related to incomplete collection of the vapor run product at the end of the experiment.

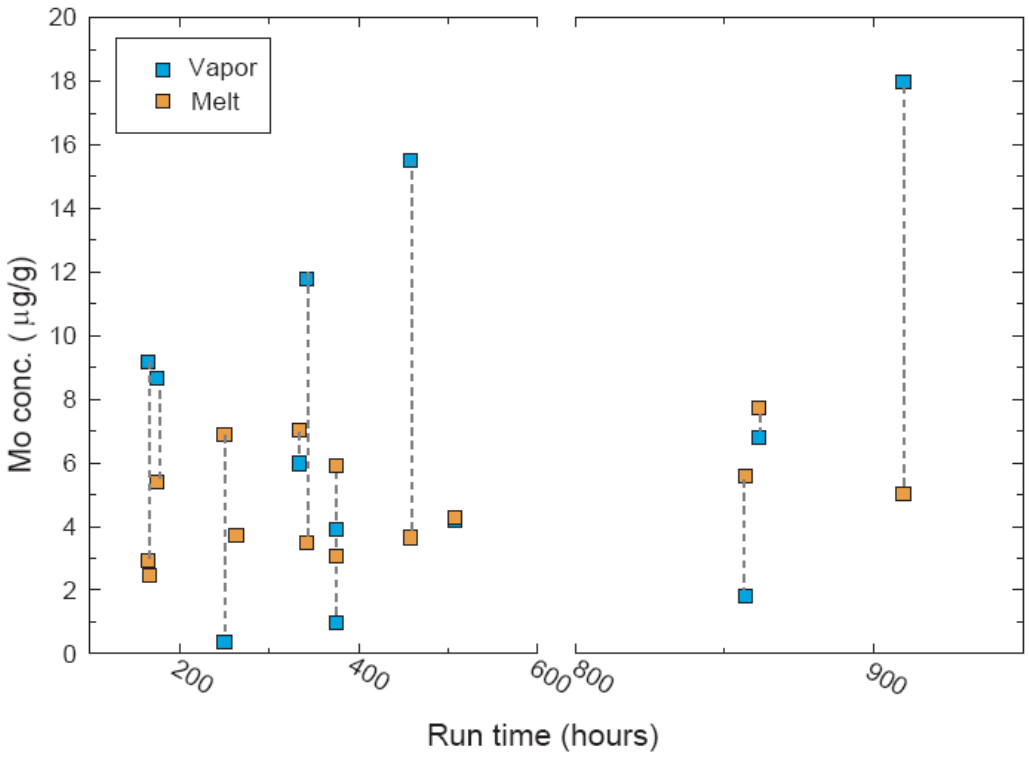

Figure 5.2: Mo concentration versus run time of the experiment. Tie lines connect vapor and melt concentrations for the same experiment. Some melts do not have corresponding vapor because it was lost upon opening the capsule.

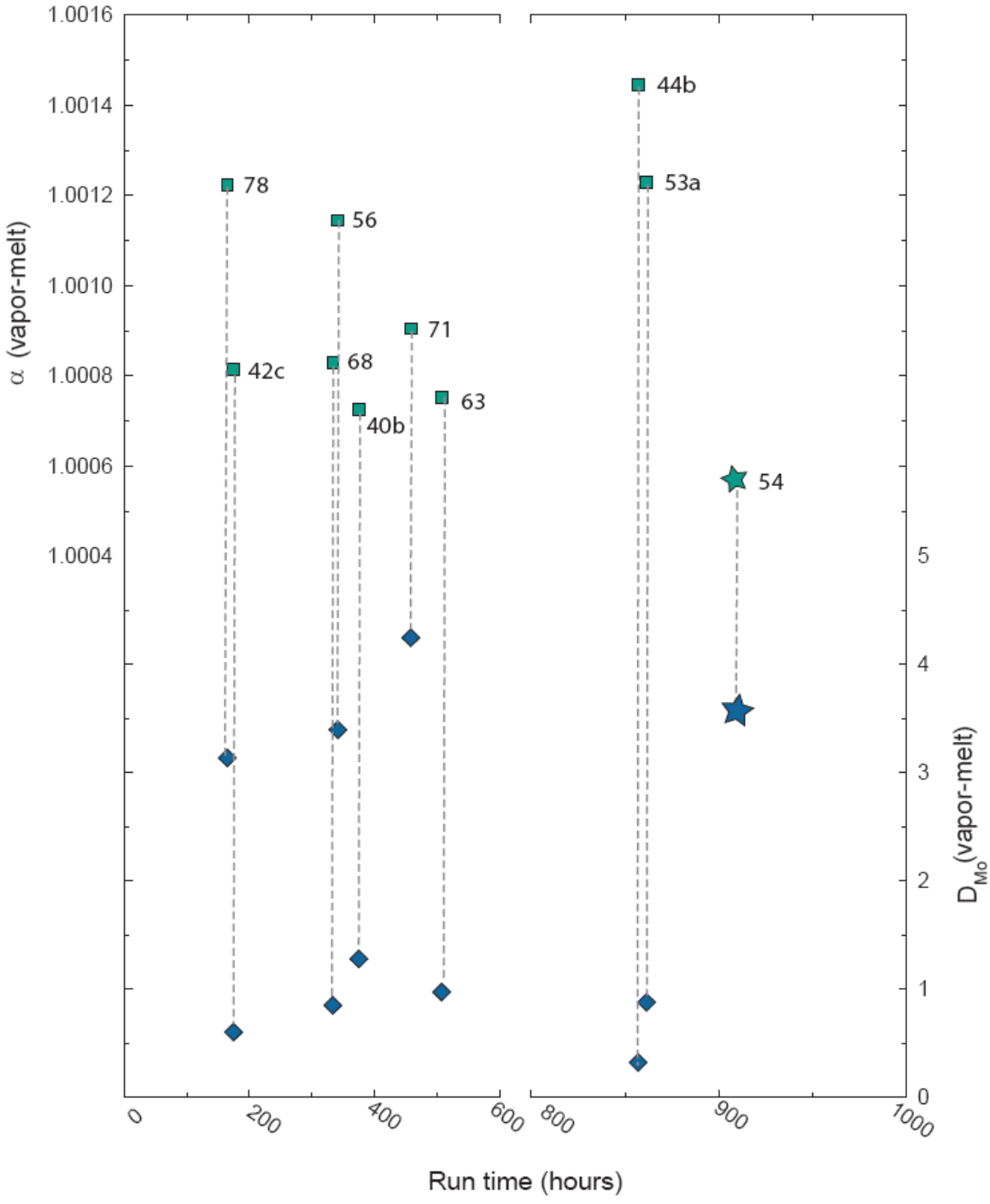

Figure 5.3: α(vapor-melt-) and D_{Mo} (vapor-melt) with respect to run time. There is no apparent trend in these parameters with time. Experiment 54 is starred because it is the sole experiment for which the quench was not isobaric. Tie lines connect α and D_{Mo} for the same experiment.

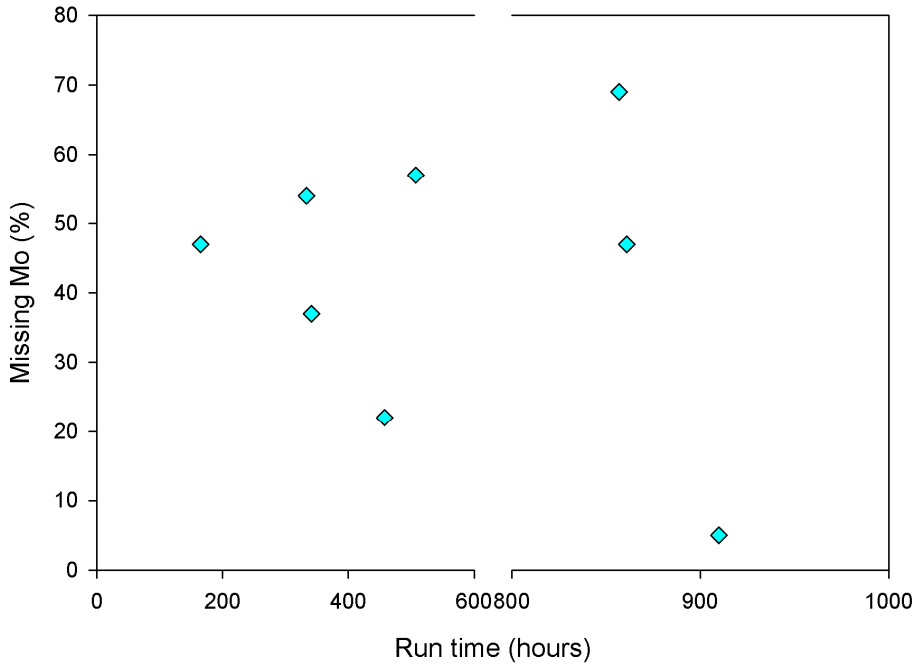

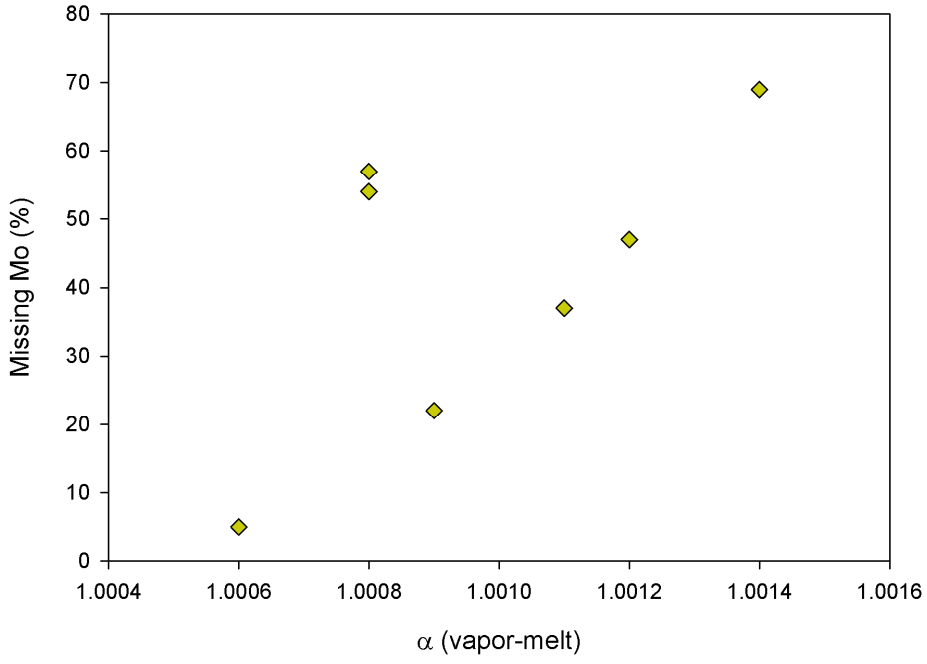

Figure 5.4: (Top): Fugitive Mo (µg) versus run time. **(Bottom):** Fugitive Mo (µg) as a function of α value. There appears to be a shallow trend towards more fractionation with increasing quantities of fugitive Mo.

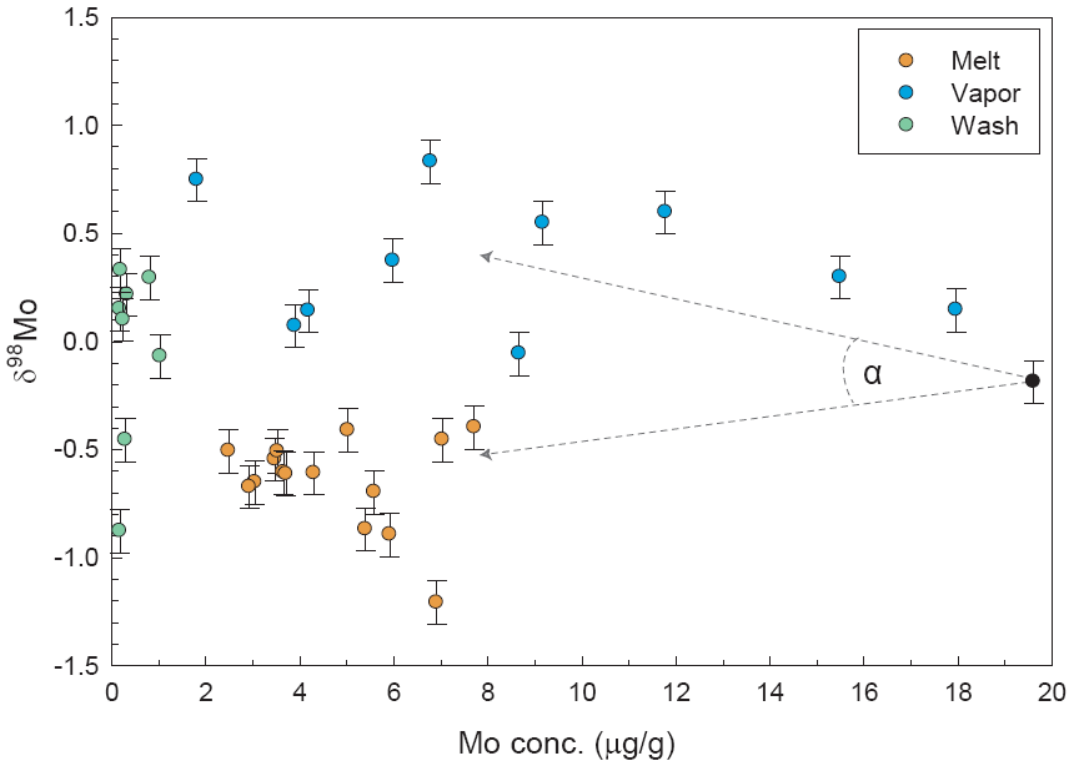

Figure 5.5: Molybdenum isotopic composition as a function of Mo concentration. The δ^{98}Mo of the starting material is shown at the right. 100µl (containing 25 µg/g Mo) of the material was placed in the capsule at the start.

When discussing possible causes for the observed fractionation between the melt and the vapor, we assume that the fractionation is an equilibrium isotope effect. Equilibrium stable isotope fractionation is a function of the vibrational energies of molecules containing atoms of different masses (Urey, 1947). For heavier elements with smaller overall fractionations, the most important processes governing stable isotope partitioning include oxidation state, coordination number, electron configuration, and bonding environment (e.g., to H, O or N), among others (Schauble, 2004). A phase with high bond strength and bond stiffness will tend to favor the heavier isotopes of an element. Thus, a phase with high oxidation state, low coordination number, or low-spin electron configuration compared to the phase with which it is in equilibrium, should be isotopically heavier.

In the system experimentally examined here, vapor phase Mo is (VI) in a trigonal planar coordination (Rempel et al., 2006; 2009), while in the melt it is (VI) with tetrahedral and octahedral coordination (Farges et al., 2006). Thus, heavier δ^{98}Mo values in the vapor phase may be a result of a coordination number change around Mo as it moves into the melt phase.

It is, however, possible that the oxidation state of Mo is different in the melt and vapor phases. One reason to suspect that this might be the case is the blue color of the quenched melt. The blue color might be indicative of polyoxometalate complexes or Mo polymers, in which Mo has been partially or wholly reduced from (VI) to (V) or (IV). In this case, fractionation theory predicts that the heavy isotopes will remain with the higher oxidation state. If the Mo in the

melt is reduced, its isotopic composition would become lighter, while the vapor became isotopically heavier. Based on the data, it does not seem possible to differentiate between these two candidates. If any of the Mo is (V), another problem presents itself. This is the possibility that the Mo(V) would not reach equilibrium with the double spike, or might not be captured efficiently by the existing column chemistry. The second instance could significantly fractionate Mo isotopes, which, if the first instance were true, could not be corrected by the double-spike process. Incomplete recovery of Mo(V) from the column chemistry could also be a reason that the Mo mass balance failed.

Geological implications

We have shown that there is well-resolved Mo isotopic fractionation in an experimental vapor-melt system that mimics how Mo may become enriched in a volatile phase in a magmatic-hydrothermal system. One major implication of this is that it suggests that separation of isotopically heavy Mo into a volatile phase should generate an isotopically lighter reservoir of Mo in the crust (relative to the starting Mo composition). Such an interpretation is probably generally applicable to oxidized systems. However, the presence of sulfur and other volatiles is likely to change the coordination environment and oxidation state of Mo (Farges et al., 2006). This would affect the Mo fractionation factor to an unknown degree, because of differences in the bond partners to Mo in each phase. It is still unknown what the fractionation associated with molybdenite formation is. Molybdenite may crystallize from the vapor phase as temperature falls, and hydrated MoO_3 reacts with H_2S. Hannah et al. (2007) suggested that

crystallization of molybdenite can be described as a Rayleigh distillation process. If the starting vapor Mo is isotopically heavy, then by Rayleigh fractionation, MoS_2 should evolve to even heavier values. While on balance the measured MoS_2 $\delta^{98}Mo$ values have been heavy, some light $\delta^{98}Mo$ values have also been reported. This could mean that the fraction of Mo removed from the vapor during distillation was small. The main problem with applying the experimental data is that, while the starting $\delta^{98}Mo$ of the Mo in the experimental system was known, this is rarely the case in a natural system. Nevertheless, these experiments provide the first estimate for the high temperature/high-pressure equilibrium isotope fractionation of Mo between a vapor phase and a melt phase.

Conclusions

In this work, a number of directions have been explored with respect to Mo isotopes, and suggest areas where further research could significantly strengthen the current understanding of the global Mo isotope system. Progress towards a more quantitative model of the cycling of Mo would improve the ability to use Mo isotopes as proxies of redox conditions.

The behavior of Mo in a seasonally anoxic estuary over the past century was studied. In the Chesapeake Bay, annual changes in nutrient runoff influence the intensity of O_2 depletion in the deep water. Molybdenum is enriched in Chesapeake Bay sediments, and appears to be lost from the water column. Estuaries are the interface between rivers and the ocean, and as such process weathered material arriving from the interiors of continents. This particular avenue would benefit from a more complete understanding of the processing of Mo in the watershed. Since most rivers that have been investigated (Archer and Vance, 2008), including the Susquehanna River in this dissertation, have Mo isotope values that are heavy, understanding the chemical or physical weathering processes that might impart this signature is very important. These heavy values might be purely indicative of the source material of Mo in the watershed, in which case study of the actual rocks and sediments in the drained basin would be important. This could then be used to determine the seasonal variation in degree and rate of processing that takes place during transport downstream.

The study of Mediterranean sediments illustrates the need to better understand Mo isotope behavior in the so-called suboxic regimes. In the literature, 'suboxic' has been used as a catch-all for most Mo isotope signatures that are not distinctly anoxic/euxinic, or derived from MnO_x adsorption. A wide range of values occur in low-O_2 settings, and it should be possible to distinguish processes that are imparting these isotope signatures. Sequential extraction of Mo from different sedimentary components might show that the array of signature is related to a mix of values derived from adsorption to FeO_x, pyrite, organic matter, or from conversion to partial-thiomolybdate species. Additionally, a better understanding of the diagenetic behavior of Mo isotopes in sediments and in pore water would be useful in differentiating between primary isotope signatures and those reset by diagenetic processing. More holistic studies of modern systems, that include sediments, porewater, trapped particles, and overlying water (e.g., Dahl et al., 2009), would contribute to a more complete modeling of Mo isotope cycling.

In the final chapter, we experimentally determined a Mo isotope fractionation factor between vapor and melt. The history of experimentally determining isotope fractionation factors is long (e.g., Urey, 1947; McCrea, 1950) and has led to the ubiquitous use of oxygen isotopes in paleoceanography, and in metamorphic systems. These factors are fundamental to understanding the measured isotope ratios in sediments, ore deposits, or other rocks. Thus, an important future direction is to expand the database of Mo isotope fractionation

factors, which should lead to the increased ability to understand the measurements made in natural systems.

Appendices

Appendix 1. Supplemental information to Chapter 3.

The northernmost samples are from a 1979 core in the Conowingo Dam reservoir on the Susquehanna River, the main tributary to the Chesapeake Bay (Helz et al., 1985). The Susquehanna River provides about half the total fresh water to the Bay, and dominates the sediment budget (Hobbs et al., 1992).

One sample from each of three separate cores (BH N, M, and H) taken in Baltimore Harbor were analyzed. Industrial activity in the Baltimore area has left the harbor sediments contaminated with Cu, Zn, and other metals. The Harbor is frequently dredged, disturbing any age-depth relationship (Mason et al., 2004; Sinex and Helz, 1982). Contamination is greatest in the inner harbor (Cores N and M), and eases eastward towards the Bay's main stem (Core H). For example, Cu concentrations are: 730 µg/g Cu in Core N, 1800 µg/g in Core M, and 500 µg/g in Core H (Dolor et al., 2009; Sinex and Helz, 1982).

Surface samples were obtained from a shallow to deep water traverse, close to the location of cores RD and 55. Increased Mn content in shallow-water sediments, compared to deep-water sediments, is the result of a process called refluxing. In this process, MnOx that has fallen out in deeper water as particles is dissolved when reducing conditions develop in summer (Helz et al., 1985). These surface samples (Depth Traverse, DT, 0902, 0903, and 0907) are characterized by high Mn concentrations that decrease with increasing water depth. DT 0902, at 3.4m water depth, has 3000 µg/g Mn, DT 0903 at 6.7 m has 2200 µg/g, and

DT 0907 at 26.2 m has 1000 µg/g Mn (Dolor et al., 2009). Only the fine fraction of these sediment samples (<63 µm) was available.

Core PC-6 is our most southerly sample site. It samples sediments approximately 30 km south of Core 55. The samples come from below the horizon that represents the regional introduction of European agriculture (~1700 ybp), as determined by ragweed pollen abundance (Helz et al., 2000). The ages of these three samples are approximately 1300, 800, and 300 ybp, interpolated from a sedimentation rate of 0.11 cm/yr (Helz et al., 2000).

In the vicinity of PC-6, shoreline bluffs of the Miocene-aged Fairhaven member of the Calvert Formation stand above the Chesapeake Bay. The Fairhaven member is characterized by enrichments in several redox-sensitive metals, including Mo. The Fairhaven was digested five separate times and each digestion was analyzed several times. These data are presented in table A1. Organic carbon content in weight percent (TOC) was measured on carbonate-free samples for the two cores, RD and 55. These data are presented in table A2.

Table A1: Data for individual analyses of the Fairhaven sediment.

Standard	Date analysed	δ^{98}Mo
Fairhaven 1	5/14/2008	0.964
Fairhaven 2	6/17/2008	0.923
Fairhaven 2	6/17/2008	0.982
Fairhaven 2	7/7/2008	0.929
Fairhaven 3	12/18/2008	0.931
Fairhaven 3	12/18/2008	0.982
Fairhaven 3	12/18/2008	1.026
Fairhaven 3	12/18/2008	0.858
Fairhaven 3	12/18/2008	0.966
Fairhaven 3	12/18/2008	0.888
Fairhaven 4	6/2/2009	0.911
Fairhaven 4	6/3/2009	0.964
Fairhaven 4	6/4/2009	0.880
Fairhaven 5	6/4/2009	0.931
	1 S.D.	**0.046**
	2 S.E.	**0.024**
	Average	**0.938**

Table A2: Organic carbon content of Chesapeake Bay core samples.

Sample Name (cm core depth)	TOC
RD 3 (4)	3.06
RD 10 (18)	2.78
RD 15 (28)	2.96
RD 20 (38)	2.61
RD 27 (52)	2.79
RD 30 (58)	2.74
RD 35 (80)	2.61
RD 45 (120)	3.11
Core 55 (0)	3.29
Core 55 (8)	3.05
Core 55 (10)	2.50
Core 55 (12)	2.84
Core 55 (16)	2.91
Core 55 (20)	3.22
Core 55 (26)	2.75
Core 55 (28)	2.79
Core 55 (32)	2.87
Core 55 (38)	2.84
Core 55 (44)	2.90
Core 55 (50)	2.85
Core 55 (54)	2.57
Core 55 (58)	2.72
Core 55 (68)	2.23
Core 55 (76)	
Core 55 (94)	1.89
Core 55 (96)	2.57
Core 55 (100)	1.80

Appendix 2. Supplemental information to Chapter 4

Core photos

On board ship, each core is cut in half, sectioned, and photographed. The photographs are archived in an online database that is available to researchers and the public at *http://iodp.tamu.edu/janusweb/imaging/photo.shtml*. Core photographs for Leg 160, Site 969, hole D, cores 4H (Fig. A1) and 5H (Fig. A2), which were used in this study, are reproduced here with the permission of the International Ocean Drilling Program. To identify the specific location of a sample on these photos, identify the section number of interest along the top margin. Then, locate the cm core depth along the left hand margin.

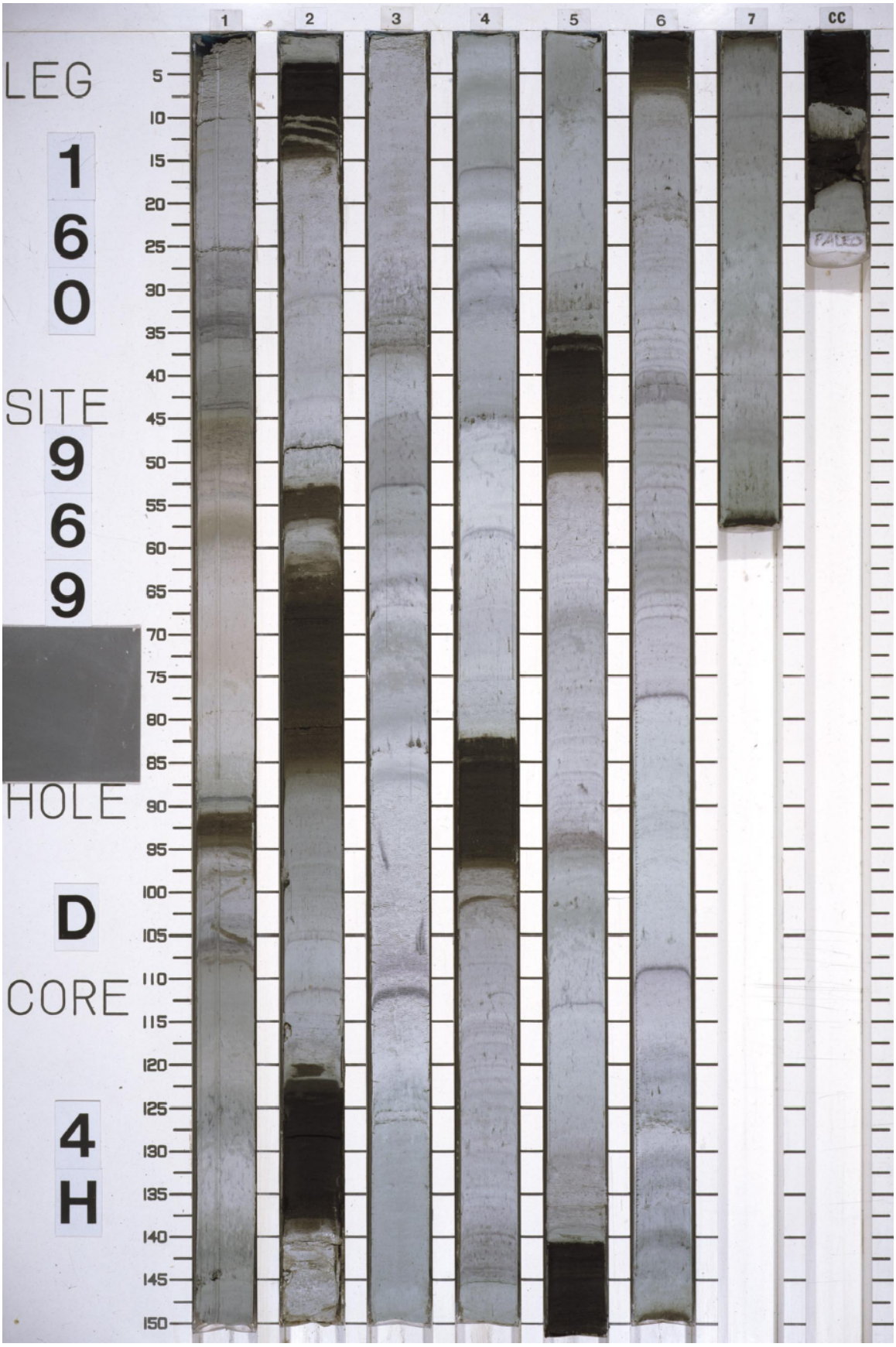
LEG
160
SITE
969
HOLE
D
CORE
4
H
1
2
3
4
5
6
7
CC

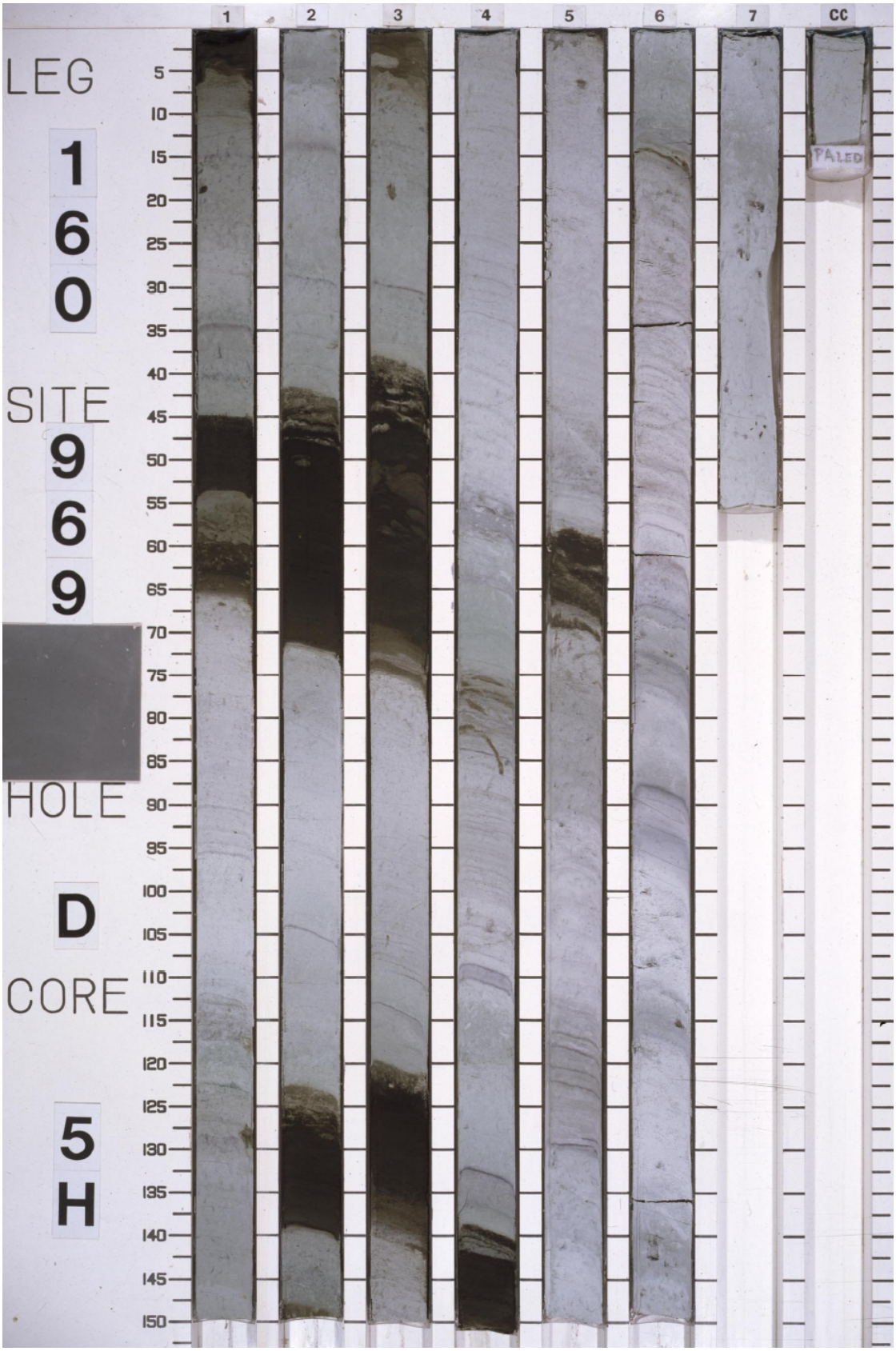
LEG
160
SITE
969
HOLE
D
CORE
5
H
1
2
3
4
5
6
7
CC
PALEO

Duplicate Samples

Table A3: Molybdenum isotope data for samples that were processed twice. In some cases more than one measurement was made of the sample solution.

Duplicate samples	δ^{98}Mo
4H-2, 131 (A)	1.317 [a]
4H-2, 131 (B)	1.237
4H-2, 61 (A)	0.919
4H-2, 61 (B)	0.966
5H-1, 50 (A)	0.579
5H-1, 50 (B)	0.516
5H-3, 100 (A)	2.369
5H-3, 100 (B)	2.519 [b]

[a] 4H-2, 131(A) was measured 4 times, averaging 1.317±0.03.
[b] Average of two measurements (2.556, 2.481)

Sample preparation for sulfur isotope analysis

A small subset of the Mediterranean samples (both sapropels and hemipelagic) was processed for multiple sulfur isotope analysis. Sediment powders were first boiled in 5M HCl to release acid volatile sulfur (AVS), then treated with a hot chrome(II)-reduction solution to reduce pyrite (Canfield et al., 1986). No AVS was produced in any of the samples. The H_2S evolved in each CRS reaction was captured as Ag_2S in a solution of 10% $AgNO_3$. Ag_2S was cleaned with 250 mL of Milli Q water and 50 mL of 1 M NH_4OH and dried. For fluorinations, samples were reacted in Ni bombs with F_2 gas at ~250 ºC for ~8 hours. This quantitatively converts the Ag_2S to SF_6. Product SF_6 was then purified with several liquid N_2 distillations, and by gas chromatography on a 12' molecular sieve 5 Å/Haysep Q column with a thermal conductivity detector. The S isotopic abundances of the purified SF_6 was analyzed on a Finnigan MAT 253 dual inlet mass spectrometer at m/e- values of 127, 128, 129, and 131 ($^{32}SF_5^+$, $^{33}SF_5^+$, $^{34}SF_5^+$, and $^{36}SF_5^+$). Analytical uncertainties on S isotope measurements,

estimated from long-term reproducibility of Ag_2S fluorinations, are 0.14, 0.008, and 0.20 (1σ) for $\delta^{34}S$, $\Delta^{33}S$, and $\Delta^{36}S$, respectively (e.g., Zerkle et al., 2008).

The minor isotope compositions of sulfur species are presented using the $\Delta^{3X}S$ notation, which describes the deviation of a sample datum in ^{33}S or ^{36}S (in ‰) from a reference fractionation line:

$$\Delta^{33}S = \delta^{33}S - \left[\left({}^{34}R_{sample} / {}^{34}R_{H2Si}\right)^{0.515} - 1\right]$$

and

$$\Delta^{36}S = \delta^{36}S - \left[\left({}^{34}R_{sample} / {}^{34}R_{H2Si}\right)^{1.90} - 1\right]$$

The exponents 0.515 and 1.90 are reference values assigned to approximate mass-dependent fractionations during thermodynamic equilibrium isotope exchange at low temperature (Hulston and Thode, 1965; Farquhar et al., 2003; Farquhar and Wing, 2003; Johnston et al., 2007; Ono et al., 2007). Small deviations from these reference values occur in biogeochemical systems because the redistribution of mass between sulfur pools by, e.g., mixing or Rayleigh processes, results in the isotope ratios of sulfur pools evolving in a linear fashion, which differs from the exponential relationship calculated for reference fractionation arrays. For a more detailed explanation of how these signatures are produced in natural systems, see Farquhar et al. (2003, 2007) and Johnston et al. (2005, 2007).

Mass balance calculations

The primary source of fresh water to the Mediterranean Sea is the Nile River. It contributes ~5 x 10^{14} L/y of water, with an average Mo concentration of

0.6 µg/L (Archer and Vance, 2008). In a normal year, the Black Sea contributes slightly less water (4×10^{14} L/y), which averages 1.5 µg/L Mo (Nägler et al., 2005). The input of water from the Western Mediterranean is ~4×10^{16} L/y (Bethoux, 1980). Mediterranean surface water has a slightly higher Mo concentration than seawater, 13.6 µg/L, because of evaporation (van der Weijden et al., 1990). The volume of the Eastern Mediterranean is 2.5×10^{18} L, the area 1.65×10^{6} km^2. The area used for the calculation is 2/3 of the total (1×10^{6} km^2).

Simple conservative linear mixing calculations were performed to test whether dilution of ambient seawater with Nile freshwater of a different isotopic composition could affect the δ^{98}Mo of the Mediterranean, using the following equations (Fry, 2002):

$$Conc_{mix} = fConc_{river} + (1-f)Conc_{EM}$$

$$\delta_{mix} = [fConc_{riv}\delta_{riv} + (1-f)Conc_{EM}\delta_{EM}]/Conc_{mix}$$

In these equations, *f* is the fraction of freshwater; subscripts refer to Mo concentrations and isotopic compositions (δ^{98}Mo) of a river freshwater source, the Eastern Mediterranean, and the mix. Several solutions are given for $\delta^{98}Mo_{mix}$ that assume different starting compositions for the Nile, based on measurements from Archer and Vance (2008). In order to significantly change the isotopic composition of the Eastern Mediterranean through freshwater addition alone, unreasonably large fractions of freshwater input are required (>80%), because the concentration in river water is so low.

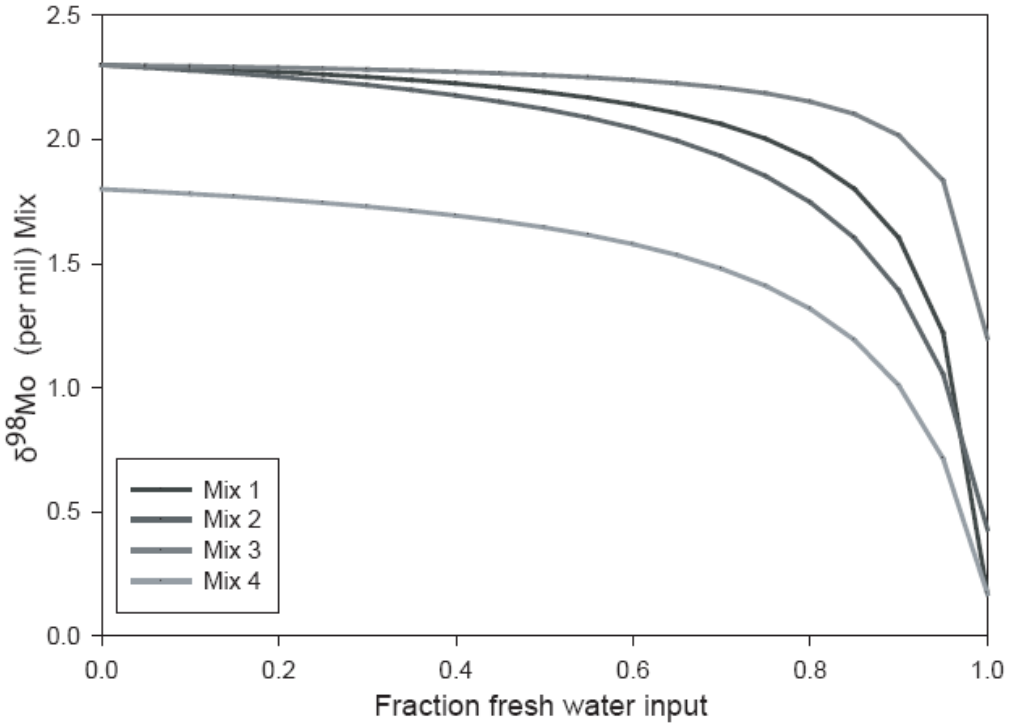

Figure A3: Isotope mixing model for the Eastern Mediterranean with Nile fresh water. The upper three mixes all assume a starting δ^{98}Mo of modern seawater. Mix 4 changes the starting δ^{98}Mo to 1.8‰. The parameters that change are the Mo concentration of Nile water, and the δ^{98}Mo (Archer and Vance, 2008). Mix 1 has (1.4 µg/L, 0.2‰), mix 2 has (1.4 µg/L, 0.4‰), mix 3 has (0.5 µg/L, 1.2‰), mix 4 has (1.4 µg/L, 0.2‰).

Some major element ratios can be useful when attempting to identify a source location for the elements (e.g., Nijenhuis et al., 1998). One major source of dust to the Mediterranean is the Sahara desert, and one sample of North Saharan Dust, collected in Cairo (Linke et al., 2006), does appear to have an elemental composition very similar to the Mediterranean sapropels. However, Nile particulate matter (Krom et al., 1999), which could potentially reach Site 969, is not compositionally similar (Fig. A.4). The problem with dust as a source of

trace elements is two-fold: 1.) sapropel deposition took place during wetter periods, when dust transport and deposition would be reduced (Wehausen and Brumsack, 1998), and 2.) calculations suggest that the trace element budget in dust is not high enough to supply sapropels with the requisite quantities (e.g., Nijenhuis et al., 1998). Based on these calculations, we suggest that seawater was indeed the source of Mo, V, and Re to the sediments. In order to avoid a drawdown scenario, seawater was probably circulating between the Eastern and Western Mediterranean.

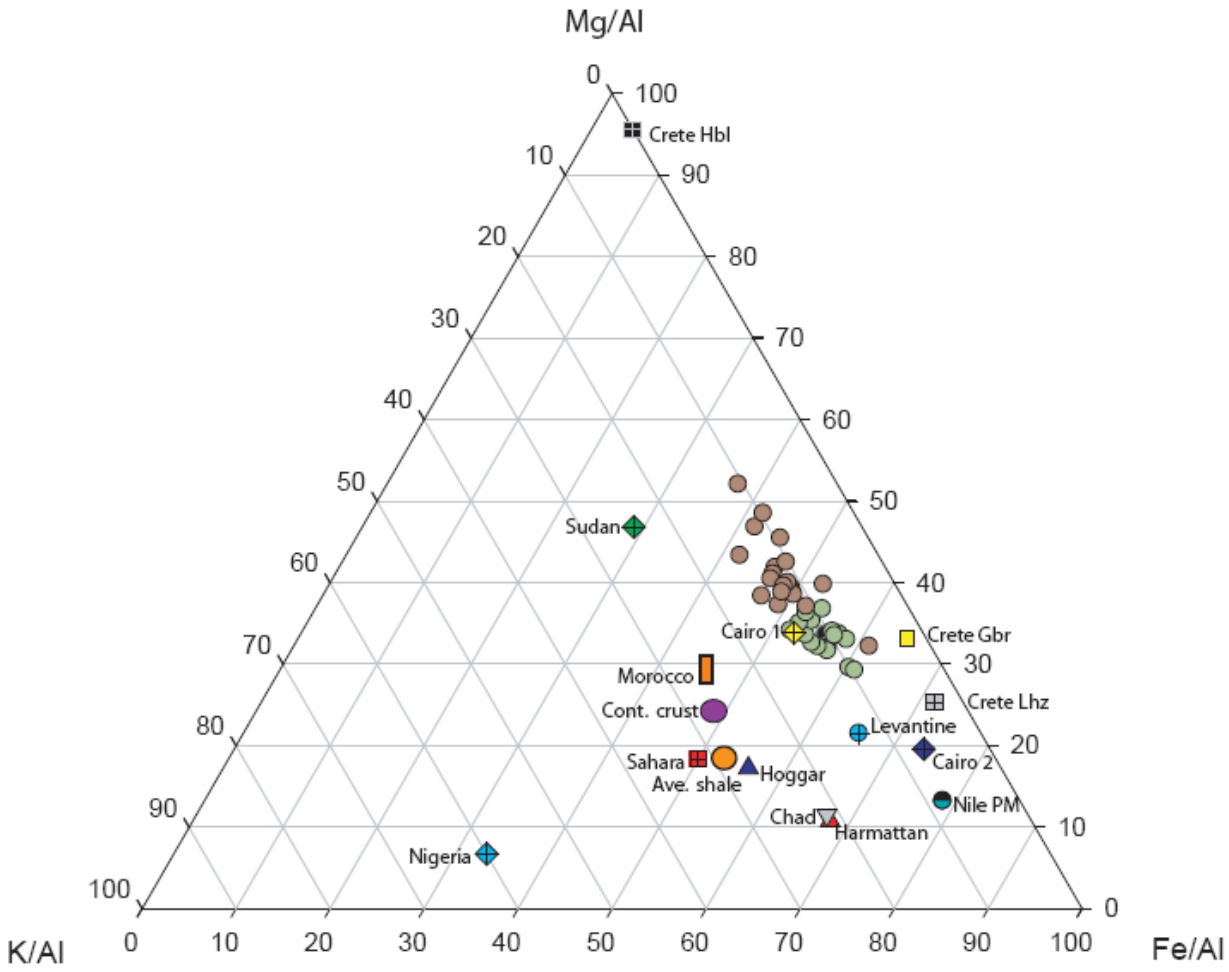

Figure A4: Ternary diagram of Al-normalized K, Fe, and Mg compositions from Mediterranean sapropels (green circles) and hemipelagic sediment (brown circles), and from a variety of possible sources of aeolian or particulate matter from rivers.
Average shale: Taylor and McLennan, 1985.
Continental crust: Rudnick and Gao, 2003.
Crete hornblende, gabbro, lherzolite: Koepke et al., 2002.
Nile particulates, Levantine, Sudan, Sahara: Krom et al., 1999.
Cairo 1 and 2, Niger, Morocco: Linke et al., 2006.
Chad, Harmattan, Hoggar: Castillo et al., 2008.

Bibliography

Adelson, J.M., Helz, G.R., Miller, C.V., 2001. Reconstructing the rise of recent coastal anoxia: Molybdenum in Chesapeake Bay sediments. Geochim. Cosmochim. Acta. 65, 237-252.

Albarede, F., Beard, B.L., 2004. Analytical methods for non-traditional stable isotopes. In: Johnson, C.M., Beard, B.L., Albarede, F., (Eds.) Geochemistry of non-traditional stable isotopes. Rev. Mineral. Geochem. 55, 113-152.

Albarède, F., Telouk, P., Blichert-Toft, J., Boyet, M., Agranier, A., Nelson, B., 2004. Precise and accurate isotopic measurements using multiple-collector ICPMS. Geochim. Cosmochim. Acta. 68, 2725-2744.

Algeo, T.J, 2004. Can marine anoxic events draw down the trace element inventory of seawater? Geology. 32, 1057-1060.

Algeo, T.J., Lyons, T., W., 2006. Mo-TOC covariation in modern anoxic marine environments: Implications for analysis of paleoredox and paleohydrographic conditions. Paleoceanograpy. 12, PA1016, doi:10.1029/2004PA001112.

Algeo, T.J., Lyons, T.W.,. Blakey, R.C., Over, D.J., 2007. Hydrographic conditions of the Devono-Carboniferous North American Seaway inferred from sedimentary Mo-TOC relationships, Palaeogeogr. Palaeoclimatol. Palaeoecol. 256, 204–230.

Anbar A.D., Creaser, R.A., Papanastassiou, D.A., Wasserburg, G.J., 1992. Rhenium in seawater: confirmation of generally conservative behavior. Geochim. Cosmochim. Acta 56, 4099-4104.

Anbar, A.D., Knab, K.A., Barling, J., 2001. Precise determination of mass-dependent variations in the isotopic composition of molybdenum using MC-ICPMS. Anal. Chem. 73, 1425-1431.

Archer, C., Vance, D., 2008. The isotopic signature of the global riverine molybdenum flux and anoxia in the ancient oceans. Nature Geosci. 1, 597-600.

Arnold, G.A., Anbar, A.D., Barling, J., Lyons, T.W., 2004. Molybdenum isotope evidence for widespread anoxia in Mid-Proterozoic oceans. Science. 304, 87-90.

Barling, J., Anbar, A.D., 2004. Molybdenum isotope fractionation during adsorption by manganese oxides. Earth Planet. Sci. Lett. 217, 315-329.

Barling, J., Arnold, G.L., Anbar, A.D., 2001. Natural mass-dependent variations in the isotopic composition of molybdenum. Earth Planet Sci. Lett. 193, 447-457.

Belshaw, N.S., Freedman, P.A., O'Nions, R.K., Frank, M., Guo, Y., 1998. A new variable dispersion double-focusing plasma mass spectrometer with performance illustrated for Pb isotopes. Int. J. Mass Spectrom. 181, 51-58.

Bermin, J., Vance, D., Archer, C., Statham, P.J., 2006. The determination of the isotopic composition of Cu and Zn in sea water. Chem. Geol. 226, 280-297.

Bertine, K.K., Turekian, K.K., 1973. Molybdenum in marine sediments, Geochim. Cosmochim. Acta. 37, 1415–1434.

Béthoux, J.P., 1980. Mean water fluxes across sections in the Mediterranean Sea evidenced on the basis of water and salt budget and of observed salinities. Oceanol. Acta. 9, 79–88.

Biggs, R.B., 1970. Sources and distribution of suspended sediment in northern Chesapeake Bay. Mar. Geol. 9, 187-201.

Boothman, W.S., Coiro, L.L., 2009. Laboratory determination of molybdenum accumulation rates as a measure of hypoxic conditions. Estuaries and Coasts. 32, 642-653.

Bostick, B.C., Fendorf, S., Helz, G.R., 2003. Differential adsorption of molybdate and tetrathiomolybdate on pyrite (FeS2), Environ. Sci. Technol. 37, 285-291, 2003.

Böttcher, M. E., Rinna, J., Warning, B., Wehausen, R., Howell, M. W., Schnetger, B., Stein, R., Brumsack, H. -J., Rullkötter J., 2003. Geochemistry of sediments from the connection between the western and the eastern Mediterranean Sea (Strait of Sicily, ODP Site 963). Palaeogeog., Palaeoclim., Palaeoecol. 190, 165-194

Boyd, F.R., Mertzman, S.A., 1987. Composition and structure of the Kaapvaal lithosphere, Southern Africa, in: Mysen, B.O. (Ed.), Magmatic Processes. Geochem. Soc. Spec. Publ., 13–24.

Bruland, K., 1983. Trace metals in seawater. Chem. Oceanog. 8, 157-220.

Brumsack, H.-J., 1986. The inorganic geochemistry of Cretaceous black shales (DSDP Leg 41) in comparison to modern upwelling sediments from the Gulf of California. In: Shackleton, N.J., Summerhayes, C.P., (Eds): North Atlantic Paleoceanography. Geol. Soc. Spec. Publ. 21, 447–462.

Brumsack, H.-J., 1989. Geochemistry of recent TOC-rich sediments from the Gulf of California and the Black Sea. Geolog. Rundschau. 78, 851-882.

Brunner, B., Bernasconi, S.M., 2005. A revised isotope fractionation model for dissimilatory sulfate reduction in sulfate reducing bacteria. Geochim. Cosmochim.Acta. 69, 4759–4771.

Calvert, S.E., Pedersen, T.F., 1993. Geochemistry of Recent oxic and anoxic marine sediments: Implications for the geological record, Mar. Geol. 113, 67-88.

Calvert, S.E., Price, N.B., 1977. Chemical variation in ferromanganese nodules and associated sediments from the Pacific Ocean, Mar. Chem. 5, 43-74.

Camerlenghi, A., 1990. Anoxic basins of the Eastern Mediterranean: Geological framework. Mar. Chem. 31, 1–19.

Camerlenghi A., Cita, M.B., 1987. Setting and tectonic evolution of some Eastern Mediterranean deep-sea basins. Mar.Chem. 75, 31–56.

Candela, P.A., 1989. The calculation of magmatic contributions to porphyry-type ore systems: Predicting fluid inclusion chemistries. Geochemical Journal. 23**,** 295-305.

Candela, P.A., Holland, H.D., 1984. The partitioning of copper and molybdenum between silicate melts and aqueous fluids. Geochim. Cosmochim. Acta. 48, 373-380.

Candela, P.A., Piccoli, P., 2005. Magmatic processes in the development of porphyry-type ore systems, in Hedenquist, J.W., Thompson, J.F.H., Goldfarb, R.J., Richards, J.R., eds., Society of economic geologists 100th Anniversary Volume, 25-38.

Canfield, D.E., 1989. Reactive iron in marine sediments, Geochim. Cosmochim. Acta. 53, 619–632.

Canfield, D.E., Raiswell, R., Westrich, J.T., Reaves, C.M., and Berner, R.A., 1986. The
use of chromium reduction in the analysis of reduced inorganic sulfur in sediments and shales: Chem. Geol. 54, 149-155.

Casford, J.S.L., Rohling, E.J., Abu-Zeid, R.H., Fontanier, C., Jorissen, F.J., Leng, M.J., Schmiedl, G., Thomson, J., 2003. A dynamic concept for eastern Mediterranean circulation and oxygenation during sapropel formation. Paleogeog., Paleoclim., Paleoecol. 190, 103-119.

Castillo, S., Moreno, T., Querol, X., Alastuey, A., Cuevas, E., Herrmann, L., Mounkaila, M., Gibbons W., 2008. Trace element variation in size-fractionated African desert dusts. J. Arid Envir. 72, 1034-1045.

Collier, R.W., 1985. Molybdenum in the Northeast Pacific Ocean. Limnol. Oceanogr. 30, 1351-1354.

Colodner, D., Sachs, J., Ravizza, G., Turekian, K., Edmond, J., Boyle, E., 1993. The geochemical cycle of rhenium: a reconnaissance. Earth Planet. Sci. Lett. 117, 205-221.

Colodner, D., Edmond J., Boyle, E., 1995. Rhenium in the Black Sea: comparison with molybdenum and uranium. Earth Planet. Sci. Lett. 131, 1–15.

Compston, W., Oversby, V.M., 1969. Lead isotopic analysis using a double-spike. J. Geophys. Res. 74, 4338-4348.

Coplen, T.B., Böhlke, J.K., De Bievre, P., Ding, T., Holden, N.E., Hopple, J.A., Krouse, H.R., Lamberty, A., Peiser, H.S., Revesz, K., Rieder, S.E., Rosman, K.J.R., Roth, E., Taylor, P.D.P, Vocke Jr., R.D., Xiao, Y.K., 2002. Isotope-abundance variations of selected elements (IUPAC Technical Report, and references therein). Pure Applied Chem. 74, 1987 - 2017.

Cooper, S.R., Brush, G.C., 1993. A 2,500-Year history of anoxia and eutrophication in Chesapeake Bay. Estuaries. 16, 617-626.

Cramp, A., O'Sullivan, G.O., 1999. Neogene sapropels in the Mediterranean: a review. Mar. Geol. 153, 11-28.

Cronan, D.S., 1976. Basal metalliferous sediments from the eastern Pacific. Geol. Soc. Am. Bull. 87, 929-934.

Cronin, T.M., Vann, C.D., 2003. The sedimentary record of climatic and anthropogenic influence on the Patuxent estuary and Chesapeake Bay ecosystems. Estuaries. 26, 196-209.

Crusius, J., Calvert, S., Pederson, T., Sage, D., 1996. Rhenium and molybdenum enrichments in sediments as indicators of oxic, suboxic, and sulfidic conditions of deposition, Earth Planet Sci. Lett. 145, 64-78.

Crusius, J., Thomson, J., 2000. Comparative behavior of authigenic Re, U, and Mo during reoxidation and subsequent long-term burial in marine sediments. Geochim. Cosmochim. Acta. 64, 2233-2242.

Crusius, J., Thomson, J., 2003. Mobility of authigenic rhenium, silver, and selenium during post-depositional oxidation in marine sediments. Geochim. Cosmochim. Acta. 67, 265–273.

Dahl, T.W., Anbar, A.D., Gordon, G.W., Rosing, M.T., Frei, R., Canfield, D.E., 2009. The behavior of molybdenum and its isotopes across the chemocline and

in the sediments of sulfidic Lake Cadagno, Switzerland. Geochim. Cosmochim. Acta. 74, 144-163.

Daskalakis, K.D., O'Connor, T.P., 1995. Normalization and elemental sediment contamination in the coastal United States. Environ. Sci. Technol. 29, 470-477.

Dauphas, N. Davis, A.M., Marty, B., Reisberg, L., 2004. The cosmic molybdenum-ruthenium isotope correlation. Earth Planet. Sci. Lett. 226, 465-475.

De Lange, G.J., Middelburg, J.J., Van der Weijden, C.H., Catalano, G., Luther III, G.W., Hydes, D.J., Woittiez, J.R.W., Klinkhammer, G.P., 1990. Composition of anoxic hypersaline brines in the Tyro and Bannock Basins, eastern Mediterranean. Mar. Chem. 31, 63-88.

Dideriksen, K., Baker, J.A., Stipp, S.L.S., 2006. Iron isotopes in natural carbonate minerals determined by MC-ICP-MS. Geochim. Cosmochim. Acta. 70, 118-132.

Dodson, M.H., 1963. A theoretical study of the use of internal standards for precise isotopic analysis by the surface ionization technique: Part I: General first-order algebraic solutions. J. Sci. Instrum. 40, 289-295.

Dodson, M.H., 1969. A theoretical study of the use of internal standards for precise isotopic analysis by the surface ionization technique: Part II: Error relationships. J. Phys. E. 2, 490-498.

Dolor, M.K., Helz, G.R., McDonough, W.F., 2009. Sediment profiles of less commonly determined elements measured by laser ablation ICP-MS.. Marine Pollution Bull. 59, 182-192.

Duggen, S., K. Hoernle, P. van den Bogaard, L. Rüpke, J.P.Morgan, 2003. Deep roots of the Messinian salinity crisis. Nature 422, 606-606.

Eaton, A., 1979. Impact of anoxia on Mn fluxes in Chesapeake Bay. Geochim. Cosmochim. Acta. 43, 429-432.

Emeis, K.-C., Robertson, A.H.F. and Richter, C., 1996. In: Proc. ODP, Init. Repts. 160. College Station, TX (Ocean Drilling Program).

Emeis, K.-C., Sakamoto, T., 1998. The sapropel theme of Leg 160. In: Robertson, A.H.F., Emeis, K-C., Richter, C., Camerlenghi A., (Eds). Proc. ODP Sci. Res., 160, 29-36. Ocean Drilling Program, College Station, TX.

Emeis, K.-C., Sakamoto, T., Wehausen, R., Brumsack, H.-J., 2000. The sapropel record of the eastern Mediterranean Sea- Results of Ocean Drilling Program Leg 160. Paleogeog., Paleoclim., Paleoecol. 158, 371-395.

Emerson, S.R., Huested, S.S., 1991. Ocean anoxia and the concentrations of molybdenum and vanadium in seawater, Mar. Chem. 34, 177-196.

Erickson, B.E., Helz, G.R., 2000. Molybdenum(VI) speciation in sulfidic waters: Stability and lability of thiomolybdates. Geochim. Cosmochim. Acta. 64, 1149-1158.

Eugster, O., Tera, F., Wasserburg, G.J., 1969. Isotopic analysis of barium in meteorites and in terrestrial samples. J. Geophys. Res. 74, 3897-3908.

Farges, F., Siewert, R., Ponader, C.W., Brown Jr., G.E., Guesdon, A., and Morin, G., 2006. Structural environments around molybdenum in silicate glasses and melts. I. Influence of composition and oxygen fugacity on the local structure of molybdenum. The Canadian Mineralogist. 44, 731-753.

Farges, F., Siewert, R., Ponader, C.W., Brown Jr., Pichavant, M., Behrens, H., 2006. Structural Environments around molybdenum in silicate glasses and melts. II. Effect of temperature, pressure, H_2O, halogens, and sulfur. The Canadian Mineralogist. 44, 755-773.

Farquhar, J., Johnston, D.T., Wing, B.A., Habicht, K.S., Canfield, D.E., Airieau, S., Thiemens, M.H., 2003. Multiple sulfur isotopic interpretations of biosynthetic pathways: Implications for biological signatures in the sulfur isotope record. Geobiology. 1, 27-36.

Farquhar, J., Johnston, D.T., Wing., B.A., 2007. Influence of network structure on sulfur isotope phase space of dissimilatory sulfate reduction: Implications of conservation of mass effects on mass-dependent isotope fractionations. Geochim. Cosmochim. Acta. 71, 5862-5875.

Farquhar, J., Wing, B.A., 2003. Multiple Sulfur Isotope analyses: Applications in geochemistry and cosmochemistry. Earth Planet. Science Lett. 213, 1-13.

Frausto da Silva, J.J.R., Williams, R.J.P., 2000. The biological chemistry of the elements: The inorganic chemistry of life. Oxford University Press, Oxford, UK.

Fry, B., 2002. Conservative mixing of stable isotopes across estuarine salinity gradients: a conceptual framework for monitoring watershed influences on downstream fisheries production. Estuaries. 25, 364-271.

Fry, B., Jannasch, H.W., Molyneaux, S.J., Wirsen, C., Muramoto, J., King, S., 1991. Stable isotope studies of the carbon, nitrogen and sulfur cycles in the Black Sea and the Cariaco Trench. Deep-Sea Res. Part II. 38, S1003–S1019.

Galer, S.J.G., 1999. Optimal double and triple spiking for high precision lead isotopic measurement. Chem. Geol. 157, 255-274.

Georgiadis, M. M., Komiya, H., Chakrabarti, P., Woo, D., Kornuc, J.J., Rees, D.C., 1992. Crystallographic Structure of the Nitrogenase Iron Protein from Azotobacter vinelandii.
Science 257, 1653-1659.

Glasby, G.P., 2000. Manganese; predominant role of nodules and crusts. In: Marine Geochemistry. Schulz, H., Zabel, M. (Eds.). 335-372. Springer-Verlag, Berlin, DE.

Goldberg, S., Su, C., Foster, H.S., 1998. Sorption of molybdate on oxides, clay minerals and soils. In: Jenne, E.A. (Ed.). Adsorption of metals by geomedia. P. 410. Academic Press, Amsterdam, NL.

Goldberg, T., Archer, C., Vance, D., Poulton, S.W., 2009. Mo isotope fractionation during adsorption to Fe (oxyhydr)oxides. Geochim. Cosmochim. Acta. 73, 6502-6516.

Gordon, G.W., Lyons, T.W., Arnold, G.L., Roe, J., Sageman, B.B., Anbar, A.D., 2009. When do black shales tell molybdenum isotope tales? Geology. 37, 535-538.

Gross, M.G., Karweit, M., Cronin, W.B., Schubel, J.R., 1978. Suspended sediment discharge of the Susquehanna River to Northern Chesapeake Bay, 1966 to 1976. Estuaries. 1, 106-110.

Gustafsson, J.P., 2003. Modelling molybdate and tungstate adsorption to ferrihydrite. Chem. Geol. 200, 105-115.

Hagy, J.D., Boynton, W.R., Keefe, C.W., Wood, K.V., 2004. Hypoxia in Chesapeake Bay, 1950-2001: Long-term change in relation to nutrient loading and river flow. Estuaries. 27, 634-658.

Hannah., J.L., Stein, H.J., Wieser, M.E., de Laeter, J.R., Varner, M.D., 2007. Molybdenum isotope variations in molybdenite: Vapor transport and Rayleigh fractionation of Mo. Geology. 35, 703-706.

Helly, J.J., Levin L. A., 2004. Global distribution of naturally occurring marine hypoxia on continental margins. Deep Sea Res. Part 1: Ocean.Res. Papers. 51, 1159-1168.

Helz, G.R., Adelson, J.A., Miller, C.V., Cornwell, J.C., Hill, J.M., Horan, M., Walker, R.J., 2000. Osmium isotopes demonstrate distal transport of contaminated sediments in Chesapeake Bay. Environ. Sci. Technol. 34, 2528-2534.

Helz, G.R., Miller, C.V., Charnock, J.M., Mosselmans, J.F.W., Patrick, R.A.D., Garner, C.D., Vaughn, D.J., 1996. Mechanism of molybdenum removal from the sea and its concentration in black shales: EXAFS evidence. Geochim. Cosmochim. Acta. 60, 3631-3642.

Helz, G.R., Setlock, G.H., Cantillo, A.Y., Moore, W.S., 1985a. Processes controlling the regional distribution of Pb-210, Ra-226, and anthropogenic zinc in estuarine sediments. Earth Planet. Sci. Lett. 76, 23-34.

Helz, G.R., Sinex, S.A., Ferri, K.L., Nichols, M., 1985b. Processes controlling Fe, Mn, and Zn in sediments of Northern Chesapeake Bay. Estuarine Coastal and Shelf Sci. 21, 1-16.

Herbel, M.J., Johnson, T.M., Oremland, R.S., Bullen, T. D., 2000. Fractionation of selenium isotopes during bacterial respiratory reduction of selenium oxyanions. Geochim. Cosmochim. Acta. 64, 3701-3709.

Hilgen, F.J., Astronomical calibration of Gauss to Matayuma sapropels in the Mediterranean and implication for the Geomagnetic Polarity Time Scale, 1991. Earth Planet. Sci. Lett., 104, 226-244.

Hille, R. Molybdenum and tungsten in biology. 2002. Trends in Biochemical Sciences 27, 360-367.

Hobbs, C.H. III, Halka, J.P., Kerhin R.T., Carron, M.J., 1992. Chesapeake Bay sediment budget. J. Coastal Res. 8, 292-300.

Hofmann, A., 1971. Fractionation corrections for mixed-isotope spikes of Sr, K, and Pb. Earth Planet. Sci. Lett. 10, 397-402.

Houk, R.S., 1986. Mass spectrometry of Inductively coupled plasmas. Anal. Chem. 58, 97A-105A.

Hsü, K.J., Ryan, W.B.F., Cita, M.B., 1973. Late Miocene desiccation of the Mediterranean. Nature 242, 240-244.

Hsü, K. J., Cita, M. B., Ryan, W. B. F, 1973. The origin of the Mediterranean evaporites. Init. Reports Deep Sea Drilling Proj., 13, 1203-1231. Washington, D.C. (U.S. Government Printing Office).

Huerta-Diaz, M., Morse, J.W., 1992. Pyritization of trace metals in anoxic marine sediments. Geochim. Cosmochim. Acta. 56, 2681-2702.

Hulston, J.R., Thode, H.G., 1965. Variations in the ^{33}S, ^{34}S, and ^{36}S contents of meteorites and their relation to chemical and nuclear effects. J. Geophys. Res. 70, 3475–3484.

Johnson, C.M., Beard, B.L., 1999. Correction of instrumentally produced mass fractionation during isotopic analysis of Fe by thermal ionization mass spectrometry. Int. J. Mass Spectrom. 193, 87-99.

Johnson, C.M., Beard, B.L., Albarede, F. (Eds.). Geochemistry of non-traditional stable isotopes: Reviews in Mineralogy and Geochemistry, 55. Min. Soc. Am., Washington, D.C.

Johnson, T.M., Bullen, T.D., 2004. Selenium, Iron, and Chromium stable isotope ratio measurements by the double spike TIMS method. In: Handbook of stable isotope analytical techniques, V 1. De Groot, P. (Ed.). Elsevier, Amsterdam, NL. 1258 pp.

Johnson, T.M., Herbel, M.J., Bullen, T.D., Zawislanski, P.T., 1999. Selenium isotope ratios as indicators of selenium sources and oxyanion reduction. Geochim. Cosmochim. Acta. 63, 2775-2783.

Johnston, D.T., Farquhar, J., Canfield, D.E., 2007. Sulfur isotope insights into microbial sulfate reduction: when microbes meet models, Geochim. Cosmochim. Acta. 71, 3929–3947.

Johnston D. T., Farquhar J., Habicht K. S., Canfield D. E., 2008. Sulphur isotopes and the search for life: strategies for identifying sulphur metabolisms in the rock record and beyond. Geobiology. 6, 425-435.

Johnston, D. T., Farquhar, J., Wing, B. A., Kaufman, A., Canfield, D. E., and Habicht, K. S., 2005a. Multiple sulfur isotope fractionations in biological systems: A case study with sulfate reducers and sulfur disproportionators. Am. J.of Sci. 305, 645-660.

Jongsma, D., Fortiun, A.R., Huson, W., Troelstra, S.R., Klaver, G.T., Peters, J.M., Van Harten, D., De Lange, G.J., Ten Haven, L., 1983. Discovery of an anoxic basin within the Strabo Trench, Eastern Mediterranean. Nature. 305, 795-797.

Jung, M., J. Ilmberger, A. Mangini, K.-C. Emeis, Why some Mediterranean sapropels survive burn-down (and others do not). 1997. Mar. Geol. 141, 51-60, 1997.

Kaback, D. S. , Runnells, D. D., 1980. Geochemistry of molybdenum in some stream sediments and waters. Geochim. Cosmochim. Acta. 44, 447-456.

Kane, J.S., Arbogast, B., Leventhal, J., 1990. Characteristics of Devonian Ohio shale SDO-1 as a USGS Geochemical Reference Sample. Geostandards Newsletter. 14, 169–196.

Kastens, K.A., 1981. Structural causes and sedimentological effects of the 'cobblestone topography' in the Eastern Mediterranean. Ph.D. dissertation, Scripps Inst. Of Oceanography, Univ. California San Diego, 207 pp.

Keyes, W.R., Turnlund, J.R., 2002. Determination of Molybdenum and enriched Molybdenum stable isotope concentrations in human blood plasma by isotope dilution ICP-MS. J. Anal. Atom. Spectrom. 17, 1153-1156.

Kingston, H.M., Greenberg, R.R., Beary, E.S., Hadas, B.R., Moody, J.R., Rains, T.C., Liggett, W.S., 1983. The characterization of the Chesapeake Bay: A systematic analysis of toxic trace elements, National Bureau of Standards report # NBSIR 83-2698, Washington DC.

Koepke, J., Seidel, E., Kreuze, H., 2002. Ophiolites on the Southern Aegean islands Crete, Karpathos and Rhodes: composition, geochronology and position within the ophiolite belts of the Eastern Mediterranean. Lithos 65, 183-203.

Krijgsman W., Hilgen, F. J., Raffi, I., Sierro, F. J., Wilson D. S., 1999. Chronology, causes and progression of the Messinian salinity crisis. Nature 400, 652-655.

Krom, M.D., Cliff, R.A., Eijsink, L.M., Herut, B., Chester, R., 1999. The characterization of Saharan dusts and Nile particulate matter in surface sediments from the Levantine basin using Sr isotopes. Mar. Geol. 155, 319-330.

Kroon et al., 1998 D. Kroon, I. Alexander, M. Little, J.L. Lourens, A. Matthewson, A.H.F. Robertson and T. Sakamoto, Oxygen isotope and sapropel stratigraphy in the Eastern Mediterranean during the last 3.2 million years, Proc. ODP Sci. Res. 160 (1998), pp. 181–190.

Larrasoaña, J.C., Roberts, A.P., Stoner, J.S., Richter, C., Wehausen, R., 2003. A new proxy for bottom-water ventilation in the eastern Mediterranean based on diagenetically controlled magnetic properties of sapropel-bearing sediments. Paleogeog., Paleoclim., Paleoecol. 190, 221-242.

Laskar, J., Joutel, F., Boudin, F., 1993. Orbital, precessional, and insolation quantities for the Earth from -20 Myr to +10 Myr. Astron. Astrophys. 270, 522-533.

Lee, D.-C., Halliday A. N., 2003. High precision W and Mo isotope compositions for iron meteorites, Geochim. Cosmochim. Acta. 67, A246.

Lehmann, B., Naegler, T.F. Holland, H.D., Wille, M., Mao J., Pan J., Ma D., Dulski, P., 2007. Highly metalliferous carbonaceous shale and Early Cambrian seawater. Geology. 35, 403-406.

Lewis, B.L., Glazer, B.T., Montbriand, P.J., Luther, G.W. III, Nuzzio, D.B., Deering, T., Ma, S., Theberge, S., 2007. Short-term and inter-annual variability of redox-sensitive chemical parameters in hypoxic/anoxic bottom waters of the Chesapeake Bay. Mar. Chem. 105, 296-308.

Liermann, L.J., R.L. Guynn, A. Anbar, S.L. Brantley, Production of a molybdophore during metal-targeted dissolution of silicates by soil bacteria, Chem. Geol. 220, 285-302, 2005.

Linke, C., Möhler, O., Veres, A., Mohacsi, Bozoki, Z., Szabo., G., Schnaiter, M., 2006. Optical properties and mineralogical composition of different Saharan mineral dust samples: A laboratory study. Atmos. Chem. Phys. 6, 3315-3326.

Lourens, L.J., Hilgen, F.J., Raffi, I., Base of large *Gephyrocapsa* and astronomical calibration of Early Pleistocene sapropels in Site 967 and Hole 969D: Solving the chronology of the Vrica Section (Calabria, Italy). Proc. Ocean Drill. Prog. Vol 160, 191-197.

Lu-Qi, Masuda, A., 1992. High accuracy measurements of isotope ratios of molybdenum in some terrestrial molybdenites, J. Am. Soc. Mass Spectrom. 3, 10-17.

Lyons, T.W., Severmann, S., 2006. A critical look at iron paleoredox proxies: New insights from modern euxinic marine basins. Geochim. Cosmochim. Acta. 70, 5698.

Lyons, T.W.,. Werne, J.P., Hollander, D.J., Murray, R.W., 2003. Contrasting sulfur geochemistry and Fe/Al and Mo/Al ratios across the last oxic-to-anoxic transition in the Cariaco Basin, Venezuela. Chem. Geol. 195, 131-157.

Malanotte-Rizzoli, P., Robinson, A.R., and the POEM group., 1992. (POEM: Physical Oceanography of the Eastern Mediterranean). General circulation of the Eastern Mediterranean," Earth Science Rev. 32, 285-309.

Malinovsky, D., D. Hammarlund, B. Ilyashuk, O. Martinsson, J. Gelting, 2007. Variations in the isotopic composition of molybdenum in freshwater lake systems, Chem. Geol. 236, 181-198, 2007.

Mann, J.L., Shuman, C. A., Kelly, W. R., Kreutz, K.J. 2008. Seasonal $\delta^{34}S$ variations in two high elevation snow pits measured by ^{33}S-^{36}S double spike thermal ionization mass spectrometry. Geochim. Cosmochim. Acta. 72, 3907-3927.

Marcantonio, F., Zimmerman, A., Xu, Y., Canuel, E., 2002. A Pb isotope record of Mid Atlantic US atmospheric Pb isotope emissions in Chesapeake Bay sediments. Mar. Chem. 77, 123-132.

Marechal, C.N., P. Telouk, F. Albarede, Precise analysis of copper and zinc isotopic compositions by plasma-source mass spectrometry, Chem. Geol. 156, 251-273, 1999.

Markey, R., Hannah, J.L., Morgan, J.W., Stein, H.J., 2003. A double spike for osmium analysis of highly radiogenic samples. Chem. Geol. 200, 395-406.

Marques, J.J., Schulze, D.J., Curi, N., Mertzman, S.A., 2004. Trace element geochemistry in Brazilian Cerrado soils. Geoderma. 121, 31-43.

Mason, R.P., Kim, E.-H., Cornwell, J., 2004. Metal accumulation in Baltimore Harbor: current and past inputs. Applied Geochem. 19, 1801-1825.

Mathur, R., Brantley, S., Anbar, A., Munizaga, F., Maksaev, V., Newberry, R., Vervoort, J., Hart, G., 2009. Variation of Mo isotopes from molybdenite in high-temperature hydrothermal ore deposits. Miner. Deposita. DOI 10.1007/s00126-009-0257-z.

Martin, J.M., Maybeck, M., 1979. Elemental mass balance of material carried by major world rivers. Mar. Chem. 7, 173–206.

McCrea, J.M., 1950. On the isotopic chemistry of carbonates and a paleotemperature scale. J. Chem. Phys. 18, 849-857.

McManus, J., Berelson, W. M. Severmann, S. Poulson, R. L., Hammond, D. E. Klinkhammer, G. P., Holm, C., 2006. Molybdenum and uranium geochemistry in continental margin sediments; paleoproxy potential. Geochim. Cosmochim. Acta. 70, 4643-4662.

McManus, J., Nägler, T.F., Siebert, C., Wheat, C.G., Hammond, D.E., 2002. Oceanic molybdenum isotope fractionation: Diagenesis and hydrothermal ridge-flank alteration, Geochem., Geophys., Geosyst. 3, 1078, doi:10.1029/2002GC00356, 2002.

Mendel, R., Bittner, F., 2006. Cell biology of molybdenum. Biochim. Biophys. Acta. (Molecular Cell Res.). 1763, 621-635.

Mendel, R., Schwarz, G., 1999. The mononuclear molybdenum enzymes. Crit. Rev. Plant Sci. 18, 33-69.

Meyers, P.A., M. Arnaboldi, Trans-Mediterranean comparison of geochemical paleoproductivity in a mid-Pleistocene interrupted sapropel. Paleogeog., Paleoclim., Paleoecol. 222, 313-328, 2005.

Millot C., Taupier-Letage, I., 2005. Circulation in the Mediterranean Sea, The Handbook of Environmental Chemistry, Volume K, 29 - 66.

Moffett, J.W., 1994. A radiotracer study of cerium and manganese uptake onto suspended particles in Chesapeake Bay. Geochim. Cosmochim. Acta. 58, 695-703.

Morford, J.L., Emerson, S., 1999. The geochemistry of redox-sensitive trace metals in sediments, Geochim. Cosmochim. Acta 63, 1735-1750.

Morford, J.L., Emerson, S.R., Breckel, E.J., Kim, S.H., 2005. Diagenesis of oxyanions (V, U, Re, and Mo) in pore water and sediments from a continental margin. Geochim. Cosmochim. Acta. 69, 5021-5032.

Morford, J.L., Martin, W.R., Kalnejais, L., Francois, R., Bothner, M., Karle I.-M., 2007. Insights on geochemical cycling of U, Re, and Mo from seasonal sampling in Boston Harbor. Geochim. Cosmochim. Acta. 71, 895-917.

Morford, J.L., Martin, W.R., Francois, R., Carney, C.M., 2009. A model for uranium, rhenium, and molybdenum diagenesis in marine sediments based on results from coastal locations. Geochim. Cosmochim. Acta. 73, 2938-2960.

Morgan J.W., Walker R.J., 1989. Isotopic determinations of rhenium and osmium using fusion, distillation and ion exchange separations, as applied to meteorites. Anal. Chim. Acta 222, 91-93.

Morse J.W., Luther III, G.W., 1999. Chemical influences on trace metal-sulfide interactions in anoxic sediments, Geochim. Cosmochim. Acta. 63, 3373–3378.

Murthy, R.V., 1962. Isotopic anomalies of molybdenum in some iron meteorites. J. Geophys. Res. 67, 905-907.

Murthy, V. R., 1963. Elemental and isotopic abundances of molybdenum in some meteorites, Geochim. Cosmochim. Acta. 27, 1171-1178.

Nägler, T. F., Eisenhauer, A., Müller, A., Hemleben, C., Kramers, J., 2000. The δ^{44}Ca temperature calibration on fossil and cultured *Globigerinoides sacculifer*; new tool for reconstruction of past sea surface temperatures. Geochem. Geophys. Geosyst. 2000, 1052, doi:10.1029/2000GC000091.

Nägler, Th.F., Siebert, C., Lüschen, H., Böttcher, M.E., 2005. Sedimentary Mo isotope record across the Holocene fresh-brackish water transition of the Black Sea. Chem. Geol. 219, 283-293.

Nakagawa, Y., Firdaus, M.L., Norisuye, K., Sohrin, K., Irisawa, K., Hirata, T., 2008. Precise Mo isotopic analysis of Pacific and Antarctic seawater. Geochim. Cosmochim. Acta. 72-S1, A670.

Nameroff, T.J., Balistrieri, L.S., Murray, J.W., Suboxic trace metal geochemistry in the eastern Tropical North Pacific, 2002. Geochim. Cosmochim. Acta. 66, 1139-1158.

Neretin, L.N., Volkov, I.I., Böttcher, M.E., Grinenko, V.A., 2001. A sulfur budget for the Black Sea anoxic zone. Deep Sea Res. Part I: Ocean. Res. Papers. 48, 2569-2593.

Neubert, N., Nägler, Th.F., Böttcher, M.E. , 2008. Sulfidity controls molybdenum isotope fractionation in euxinic sediments: Evidence from the modern Black Sea. Geology. 36, 775-778.

Nicolussi, G.K, Pellin, M.J., Lewis, R.S., Davis, A.M., Amari, S., Clayton R.N., 1998. Molybdenum isotopic composition of individual presolar silicon carbide grains from the Murchison Meteorite, Geochim. Cosmochim. Acta. 62, 1093-1104.

Nijenhuis, I.A., Bosch, H.-J., Sinninghe-Damste, J.S., Brumsack, H.-J.,. De Lange, G.J., 1999. Organic matter and trace element rich sapropels and black shales: a geochemical comparison. Earth Planet. Sci. Lett. 169, 277-290.

Nijenhuis, I.A., Brumsack, H.-J.,. de Lange, G.J., 1998. The trace element budget of the eastern Mediterranean during Pliocene sapropel formation, Proc. Ocean Drill. Prog. Sci. Res. 160, 199-206.

Officer, C.G., Biggs, R.B., Taft, J.L., Cronin, L.E., Tyler, M.A., Boynton, W.R., 1984. Chesapeake Bay anoxia: origin, development and significance. Science. 23, 22-27.

Ono, S. Shanks, W.C. Rouxel, O., Rumble, D., 2007. ^{33}S constraints on the seawater sulfate contribution in modern seafloor hydrothermal vent sulfides. Geochim. Cosmochim.Acta. 71, 1170–1182.

Passier, H.F., Bosch, H.J., Nijenhuis, I.A. , Lourens, L.J., Boettcher, M.E., Leenders, A., Sinninghe Damsté, J.S., de Lange, G.J., de Leeuw, J.W., 1999. Sulphidic Mediterranean surface waters during Pliocene sapropel formation. Nature 397, 146–149.

Passier, H.F., Böttcher, M.E., de Lange, G.J., 1999. Sulphur enrichment in organic matter of eastern Mediterranean sapropels: A study of sulphur isotope partitioning. Aquat. Geochem. 5, 99–118.

Passier, H.F., Middelburg, J.J., de Lange, G.J., Böttcher, M.E., 1997. Pyrite contents, microtextures, and sulfur isotopes in relation to formation of the youngest eastern Mediterranean sapropel. Geology. 25, 519-522.

Passier, H.F., Middelburg, J.J., van Os, B.J.H, de Lange, G.J., 1996. Diagenetic pyritisation under eastern Mediterranean sapropels caused by downward sulphide diffusion. Geochim. Cosmochim. Acta. 60, 751–763.

Pearce, C.R., Cohen, A.S., Coe, A.L., Burton, K.W., 2008. Molybdenum isotope evidence for global ocean anoxia coupled with perturbations to the carbon cycle during the Early Jurassic. Geology. 36, 231-234.

Pietruszka, A.J., Reznik, A.D., 2008. Identification of a matrix effect in the MC-ICP-MS due to sample purification using ion exchange resin: An isotopic case study of molybdenum.
International J. Mass Spectrom. 270, 23-30.

Pietruszka, A., Walker, R.J., Candela, P., 2006. Determination of mass-dependent molybdenum isotopic variations by MC-ICP-MS: an evaluation of matrix effects. Chem. Geol. 225, 121-136.

Poulson, R.L., Siebert, C., McManus, J., Berelson, W.M., 2006. Authigenic molybdenum isotope signatures in marine sediments. Geology. 34, 617-620.

Poulson-Brucker, R., McManus, J., Severmann, S., Berelson, W.M., 2009. Molybdenum behavior during early diagenesis: Insights from Mo isotopes. Geochem., Geophys., Geosyst. 10, doi:10.1029/2008GC002180.

Poulton, S.W., Raiswell, R., 2002. The low-temperature geochemical cycle of iron: from continental fluxes to marine sediment deposition, Am. J. Sci. 302, 774–805.

Raiswell, R., Canfield, D.E. , 1998. Sources of iron for pyrite formation in marine sediments, Am. J. Sci. 298, 219-245.

Rajagopalan, K.V., Johnson J.L., 1992. The pterin molybdenum cofactors. J. Biol. Chem. 267, 10199–10202.

Ravizza, G., Turekian, K.K., Hay, B.J., 1991. The geochemistry of rhenium and osmium in recent sediments from the Black Sea, Geochim. Cosmochim. Acta. 55, 3741-3752.

Rees, C.E., 1973. Steady-state model for sulfur isotope fractionation in bacterial reduction processes. Geochim. Cosmochim.Acta. 37, 1141–1162.

Reitz, A., Wille, M., Nägler, T.F., de Lange, G.J., 2007. Atypical Mo isotope signatures in eastern Mediterranean sediments. Chem. Geol. 245, 1-8.

Rempel, K.U., Migdisov, A.A., Williams-Jones, A.E., 2006. The solubility and speciation of molybdenum in water vapor at elevated temperatures and pressures: Implications for ore genesis. Geochim. Cosmochim. Acta. 70, 687-696.

Rempel, K.U., Williams-Jones, A. E., Migdisova, A., 2009. The partitioning of molybdenum(VI) between aqueous liquid and vapour at temperatures up to 370 ℃. Geochim. Cosmochim. Acta. 73, 3381-3392.

Rinna, J., Warning, B., Meyers, P. A., Brumsack, H. -J., Rullkötter, J., 2002. Combined organic and inorganic geochemical reconstruction of paleodepositional conditions of a Pliocene sapropel from the eastern Mediterranean Sea. Geochim. Cosmochim. Acta. 66, 1969-1986.

Ripperger, S., Rehkämper, M., 2007. Precise determination of cadmium isotope fractionation in seawater by double spike MC-ICPMS. Geochim. Cosmochim. Acta. 71, 631-642.

Robinson, A.R., W.G. Leslie, A. Theocharis and A. Lascaratos, 2001. Mediterranean Sea Circulation Encyclopedia of Ocean Sciences, Academic Press, 1689-1706.
Roether, W., Well, R., 2001. Oxygen consumption in the Eastern Mediterranean. Deep Sea Res. Part 1: Oceanographic Res. Papers 48, 1535-1551.

Rohling, E.J., 1994. Review and new aspects concerning the formation of eastern Mediterranean sapropels. Mar. Geol. 122, 1-28.

Rohling, E.J., Gieskes, W.W.C., 1989. Late Quaternary changes in Mediterranean intermediate water density and formation rate. Paleoceanography. 4, 531-545.

Rohling, E.J., Hilgen, F.J., 1991. The eastern Mediterranean climate at times of sapropel formation: A review. Geologie en Mijnbouw. 70, 253-264.

Rohling, E.J., Hopmans, E.C., Sinninghe Damste, J.S., 2006. Water column dynamics during the last interglacial anoxic event in the Mediterranean (sapropel S5). Paleoceanography. 21, PA2018, doi:10.1029/2005PA001237.

Rossignol-Strick, M., African monsoons, an immediate response to orbital insolation, Nature 304, 46-49, 1983.

Rossignol-Strick, M., W. Nesteroff, P. Olive, C. Vergnaud-Grazzini, After the deluge: Mediterranean stagnation and sapropel formation, Nature 295, 105-110, 1982.

Rudnick, R.L., Gao, S., 2003. The Composition of the Continental Crust, 1-64. In: The Crust. R.L. Rudnick, ed. Vol. 3, Treatise on Geochemistry (eds. H.D. Holland and K.K. Turekian), Elsevier-Pergamon, Oxford.

Russell, W.A., Papanastassiou, D.A., Tombrello, T.A., 1978. Ca isotope fractionation on the Earth and other solar system materials. Geochim. Cosmochim. Acta. 42, 1075-1090.

Ryan, W.B.F., Pitman III, W.C., Major, C.O., Shimkus, K., Moskalenko, V., Jones, G., Dimitrov, P., Gorür, N., Sakinç, M., Yüce, H., 1997. An abrupt drowning of the Black Sea shelf. Mar. Geol. 138, 119-126.

Ryan, W.F.B., Kastens, K.A., Cita, M.B., 1982. Geological evidence concerning compressional tectonics in the eastern Mediterranean. Tectonophys. 86, 213-242.

Ryan, W.B.F., Stanley, D.J., Hersey, J.B., Fahlquist, J.B., Allen, T.D., 1971. The tectonics and geology of the Mediterranean Sea. In: Maxwell E.A. (Eds), The Sea, 4. 387-492. Wiley, N.Y.

Ryb, U., Erel, Y., Matthews, A., Avni, Y., Gordon, G.W., Anbar, A.,D., Large molybdenum isotope variations trace subsurface fluid migration along the Dead Sea , transform, 2009. Geology. 37, 463-466.

Sakamoto, T., Janecek., Emeis, K.-C., 1998. Continuous sedimentary sequences from the eastern Mediterranean Sea: composite depth sections. In: Robertson, A.H.F., Emeis, K-C., Richter, C., Camerlenghi A., (Eds). Proc. ODP Sci. Res., 160, 37-59. Ocean Drilling Program, College Station, TX.

Sancetta, C., 1999. The mystery of the sapropels. Nature. 398, 27-28.

Schauble, E.A., 2004. Applying stable isotope fractionation theory to new systems. In: Johnson, C.M., Beard, B.L., Albarede, F. (Eds) Geochemistry of non-traditional stable isotopes. Rev. Mineral. Geochem. 55, 65-111.

Scheiderich, K., Helz, G.R., Walker, R.J., 2010. Century-long record of Mo isotopic composition in sediments of a seasonally anoxic estuary (Chesapeake Bay). Earth Planet Sci. Lett. 289, 189-197.

Schlitzer, R., Roether, W., Oster, H., Junghans, H.-J., Hausmann, H., Johannsen, A.M, 1991. Chlorofluoromethane and oxygen in the Eastern Mediterranean. Deep Sea Res. Part A: Oceanogr. Res. Papers. 38, 1531-1551.

Schoenberg, R., Zink, S. Staubwasser, M. von Blanckenburg, F., 2008. The stable Cr isotope inventory of solid Earth reservoirs determined by double spike MC-ICP-MS. Chem. Geol. 249, 294-306.

Schubel, J.R., Pritchard, D.W., 1987. A brief physical description of the Chesapeake Bay. In: Majumdar, S.K., Hall, L.W., Austin, H.M. (Eds.). Contaminant Problems and Management of Living Chesapeake Bay Resources. Penn. Acad. Sci, 1-32.

Scott, C., Lyons, T.W., Bekker, A., Shen, Y., Poulton, S.W., Chu, X., Anbar, A.D., 2008. Tracing the stepwise oxygenation of the Proterozoic ocean. Nature, 452, 456-460.

Scrivner, A.E., Vance, D., Rohling, E.J., 2004. New neodymium isotope data quantify Nile involvement in Mediterranean anoxic episodes. Geology. 32, 565-568.

Shaw, I.J., Sholkovitz, E.R., Klinkhammer, E., 1994. Redox dynamics in the Chesapeake Bay: The effect on sediment/water uranium exhange. Geochim. Cosmochim. Acta. 58, 2985-2995.

Shimmield, G. B., Price, N. B., 1986. The behaviour of molybdenum and manganese during early sediment diagenesis — offshore Baja California, Mexico. Mar. Chem. 19, 261-280.

Shipboard Scientific Party, 1996. Site 969. In: Robertson, A.H.F., Emeis, K-C., Richter, C., Camerlenghi A., (Eds). Proc. ODP Init. Reports. 160, 335-375. Ocean Drilling Program, College Station, TX. Ocean Drilling Program, College Station, TX.

Siebert, C., Kramers, J.D., Meisel, T., Morel, P., Nägler, T.F., 2005. PGE, Re-Os, and Mo isotope systematics in Archean and early Proterozoic sedimentary systems as proxies for redox conditions of the early Earth. 69, 1787-1801.

Siebert C., McManus J., Bice, A., Poulsen, R., Berelson, W.M., 2006. Molybdenum isotope signatures in continental margin marine sediments. Earth Planet. Sci. Lett. 241, 723-733.

Siebert, C., Nägler, T.F., Kramers, J.D., 2001. Determination of Molybdenum isotope fractionation by double-spike multicollector inductively coupled plasma mass spectrometry. Geochem., Geophys., Geosyst. 2, 2000GC000124.

Siebert, C., Nägler, T.F., von Blankenburg, F., Kramers, J.D., 2003. Molybdenum isotope records as a potential new proxy for paleoceanography. Earth Planet Sci. Lett. 211, 159-171.

Siebert, C. Ross, A., McManus, J., 2006. Germanium isotope measurements of high temperature geothermal fluids using double spike hydride generation MC-ICP-MS. Geochim. Cosmochim. Acta. 70, 3986-3995.

Sievers, E., Dörner, K., Garbe-Schönberg, D., Schaub, J., 2001. Molybdenum metabolism: Stable isotope studies in infancy. J. Trace Elem. Med. Biol. 15, 185-191.

Sinclair, W.D., 2007. Porphyry deposits. In: Goodfellow, W.D., ed., Mineral deposits of Canada: A synthesis of major deposit types, district metallogeny, the evolution of geological provinces, and exploration methods. Geol. Assoc. Canada. Special publication 5, 223-243.

Sinex, S.A., Helz, G.R., 1981. Regional geochemistry of trace elements in Chesapeake Bay sediments. Environ. Geol. 3, 315-323.

Sinex, S.A., Helz, G.R., 1982. Entrapment of zinc and other trace elements in a rapidly flushed industrialized harbor. Environ. Sci. Tech. 16, 820-825.

Stirling, C. H., Andersen, M. B., Potter, E.-K., Halliday, A.N., 2007. Low-temperature isotopic fractionation of uranium. Earth Planet. Sci. Lett. 264, 208-225.

Stratford, K., Williams, R.G., Myers, P.G., 2000. Impact of the circulation on sapropel formation in the eastern Mediterranean. Glob. Biogeochem. Cycles. 14, 683-695.

Taylor, S.R., McLennan, S.M., 1985. The continental crust: its composition and evolution.

Thomson, J., Higgs., N.C., Wilson, T.R.S., Croudace, I.W., de Lange, G.J., Van Santvoort, P.J.M., 1995. Redistribution and geochemical behavior of redox-sensitive elements around S1, the most recent eastern Mediterranean sapropel. Geochim. Cosmochim. Acta. 59, 3487-3501.

Thunell, R.C., D.F. Williams, Glacial-Holocene salinity changes in the Mediterranean Sea: hydrographic and depositional effects, Nature 338, 493-496, 1989.

Tossell, J.A., 2005. Calculating the partitioning of the isotopes of Mo between oxidic and sulfidic species in aqueous solution. Geochim. Cosmochim. Acta. 69, 2981-2993.

Tribovillard, N., Algeo, T.J., Lyons, T., Riboulleau, A., 2006. Trace metals as paleoredox and paleoproductivity proxies: an update. Chem. Geol. 232, 12-32.

Tribovillard, N., Lyons, T.W., Riboulleau, A., Bout-Roumazeilles, V., 2008. A possible capture of molybdenum during early diagenesis of dysoxic sediments. Bulletin Societe Geologique de France. 179, 3-12.

Tribovillard, N., Riboulleau, A., Lyons, T., Baudin., F., 2004. Enhanced trapping of molybdenum by sulfurized marine organic matter of marine origin in Mesozoic limestones and shales. Chem. Geol. 231, 385-401.

Tuenter, E., Weber, S. L., Hilgen, F. J., Lourens, L. J., 2003. The response of the African summer monsoon to remote and local forcing due to precession and obliquity. Global Planet. Change 36, 219-235.

Turner, P.J., Mills, D.J., Schröder, E., Lapitajs, G., Jungm, G., Iacone, L., Haydar, D., Montaser, A., 1998. Instrumentation for low- and high-resolution ICP-MS. In: Inductively coupled plasma mass spectrometry. Montaser, A. (Ed.). Wiley-VCH. 421-499.

Turnlund, J.R., Peiffer, G.L., 1995. Molybdenum absorption, excretion, and retention studied with stable isotopes in young men at five intakes of dietary molybdenum. Am. J. Clinic. Nutr. 62, 790-796.

Turnlund, J.R., Keyes, W.R., Peiffer, G.L., 1993. Isotope ratios of molybdenum determined by thermal ionization mass spectrometry for stable isotope studies of molybdenum metabolism in humans. Anal. Chem. 65, 1717-1722.

Urey, H.C., 1947. The thermodynamic properties of isotopic substances. J. Chem. Soc. 562 - 581.

van den Berg, C.M.G., 1993. Complex formation and the chemistry of selected trace elements in estuaries. Estuaries. 16, 512-520.

van der Weijden, C.H., Middelburg, J.J., de Lange, G.J., van der Sloot, H.A., Hoede, D., Woittiez, J.R.W., 1990. Profiles of the redox-sensitive trace elements As, Sb, V, Mo and U in the Tyro and Bannock Basins (eastern Mediterranean). Mar. Chem. 31, 171–186.

Van Santvoort, P.M., de Lange, G.J., Thomson, J., Cussen, H., Wilson, T.R.S., Krom, M.D. and Ströhle, K., 1996. Active post-depositional oxidation of the most recent sapropel S1 in sediments of the eastern Mediterranean Sea. Geochim. Cosmochim. 60, 4007–4024.

Voegelin, A.R., Nägler, T.F., Samankassou, E., Villa, I.M., 2009. Molybdenum isotopic composition of modern and Carboniferous carbonates. Chem. Geol. 265, 488-498.

Vorlicek, T.P. and G.R. Helz, Catalysis by mineral surfaces: Implications for Mo geochemistry in anoxic environments, Geochim. Cosmochim. 66, 3679-3692, 2002.

Vorlicek, T.P., Kahn, M.D., Kasuya, Y., Helz, G.R., 2004. Capture of molybdenum in pyrite-forming sediments: role of ligand-induced reduction by polysulfides. Geochim. Cosmochim. Acta. 68, 547-556.

Walder, A.J., Platzner, I., Freedman, P.A., 1993. Isotope ratio measurement of lead, neodymium and neodymium–samarium mixtures, Hafnium and Hafnium–Lutetium mixtures with a double focusing multiple collector inductively coupled plasma mass spectrometer. J. Anal. At. Spectrom. 8, 19-24.

Warning, B., Brumsack, H.-J., 2000. Trace metal signatures of eastern Mediterranean sapropels. Palaeogeog., Palaeoclim., Palaeoecol. 158, 293-309.

Wasylenki, L.E., Anbar, A.D., Liermann, L.J., mathur, R., Gordon, G.W., Brantley, S.L., 2007. Isotope fractionation during microbial metal uptake measured by MC-ICP-MS. J. Anal. At. Spectrom. 22, 905-910.

Wasylenki, L.E., Rolfe, B.A., Weeks, C.L., Spiro, T.G., Anbar, A.D., 2008. Experimental investigation of the effects of temperature and ionic strength on Mo isotope fractionation during adsorption to manganese oxides. Geochim. Cosmochim. Acta. 72, 5997-6005.

Wehausen, R., Brumsack, H.-J., 1998. The formation of Pliocene Mediterranean sapropels: constraints from high-resolution major and minor element studies, Proc. Ocean Drill. Prog. Sci. Res. 160, 207-216.

Werne, J.P., Sageman, B.B., Lyons, T.W., Hollander, D.F., 2002. An integrated assessment of a "type euxinic" deposit: evidence for multiple controls on black shale deposition in the middle Devonian Oatka Creek formation. Am. J. Sci. 302, 110-143.

Wetherill, G.W., 1964. Isotopic composition and concentration of Molybdenum iron meteorites, J. Geophys. Res. 69, 4403-4408.

Wieser, M.E., de Laeter, J.R., 2003. A preliminary study of isotope fractionation in molybdenites. International J. Mass Spectrom. 225, 177-183.

Wieser, M.E, De Laeter, J.R., 2007. Absolute isotopic composition of molybdenum and solar abundances of the p-process nuclides ^{92,94}Mo. Phys. Rev. C. 75, 055802-1-055802-8.

Wieser, M.E, De Laeter, J.R., 2009. Molybdenum isotope fractionation in iron meteorites. Int. J. Mass Spectrom. 286, 98-103.

Wilde, P., Lyons, T.W., Quinby-Hunt, M.S., 2004. Organic carbon proxies in black shales: molybdenum. Chem. Geol. 206, 167-176.

Wille, M., Kramers, J.D., Nägler, T.F., Beukes, N.J., Schröder, S., Meisel, Th., Lacassie, J.P., Voegelin, A.R., 2007. Evidence for a gradual rise of oxygen between 2.6 and 2.5 Ga from Mo isotopes and Re-PGE signatures in shales. Geochim. Cosmochim. Acta. 71, 2417-2435.

Wille, M., Nägler, T.F., Lehmann, B., Schröder, S., Kramers, J.D., 2008. Hydrogen sulphide release to surface waters at the Precambrian/Cambrian boundary. Nature. 453, 767-769.

Wombacher, F., Rehkämper, M., 2003. Investigation of the mass discrimination of multiple collector ICP-MS using neodymium isotopes and the generalized power law. J. Anal. At. Spectrom. 18, 1371-1375.

Yin, Q. Z., Jacobsen, S. B., 1998. The ^{97}Tc- ^{97}Mo chronometer and its implications for timing of terrestrial accretion and core formation. Lunar Planet. Sci. Conf. Abs. 29.

Zerkle, A.L., Farquhar, J., Johnston, D.T., Cox, R.P., Canfield, D. E., 2008. Fractionation of multiple sulfur isotopes during phototrophic oxidation of sulfide and elemental sulfur by a green sulfur bacterium. Geochim. Cosmochim. Acta. 73, 291-306.

Zheng, Y., Anderson, R.F., van Geen, A., Fleisher, M. Q., 2000. Authigenic molybdenum formation in marine sediments: a link to pore water sulfide in the Santa Barbara Basin. Geochim. Cosmochim. Acta. 64, 4165-4178.

Zimmerman, A.R., Canuel, E.A., 2002. Sediment geochemical records of eutrophication in the mesohaline Chesapeake Bay. Limnol. Oceanog. 47, 1084-1093.